



University of Zagreb

Faculty of Graphic Arts

Tamara Tomašegović

**FUNCTIONAL MODEL  
OF PHOTOPOLYMER PRINTING PLATE  
PRODUCTION PROCESS**

DOCTORAL THESIS

Supervisor:  
Assoc. Prof. Dr. Sc. Sanja Mahović Poljaček

Zagreb, 2016



Sveučilište u Zagrebu

Grafički fakultet

Tamara Tomašegović

**FUNKCIONALNI MODEL  
PROCESA IZRADE  
FOTOPOLIMERNE TISKOVNE FORME**

DOKTORSKI RAD

Mentorica:  
Izv. prof. dr. sc. Sanja Mahović Poljaček

Zagreb, 2016

## ACKNOWLEDGEMENTS

This Thesis would have not been able to come to life without the help and support of a number of colleagues, friends and the cooperation with extraordinary people from several academic institutions and companies.

I would like to offer my special gratitude to my mentor, Assoc. Prof. Dr. Sc. Sanja Mahović Poljaček, for all the help, advice and encouragement whenever I needed them. Thank you for believing in me and always being there for me.

To the Committee for the evaluation and the defense of this Thesis – Prof. Dr. Sc. Branka Lozo, Assoc. Prof. Dr. Sc. Lidija Mandić and Prof. Dr. Sc. Mirela Leskovac – your constructive comments and suggestions upgraded this Thesis to a new level. I am thankful for your time and efforts.

Furthermore, I would like to thank Prof. Dr. Sc. Vedran Mudronja and Asst. Prof. Dr. Sc. Suzana Jakovljević for provided help with the measurements, and colleagues from Rotoplast d.o.o. for providing printing plates and prints analysed in this research, together with some very helpful suggestions.

My special thanks are extended to the colleagues from institutions outside the University of Zagreb: my dear colleagues from Swansea University, Welsh Centre for Printing and Coating: Prof. Tim Claypole, Dr. David Beynon, Dr. Davide Deganello, Dr. Youmna Mouhamad, Ms. Sakulrat Foulston, Ms. Christine Hammet, Dr. Zari Tehrani, Dr. Tatyana Korochkina and the members of the research team – an important part would have been missing from the following pages if it weren't for you. My special thanks are extended to Prof. Dr. Sc. Mladen Lovreček for connecting me with these amazing people.

To my colleagues from University of Pardubice, Faculty of Chemical Technology and to my dear friends from University of Novi Sad, Faculty of Technical Sciences – thank you for the help with preliminary experiments that enabled me to pull the threads of the matter and focus.

To my dear colleagues and friends: Prof. Dr. Sc. Miroslav Gojo, Dr. Sc. Tomislav Cigula and Prof. Dr. Sc. Diana Milčić – thank you for inviting me to the world of printing plates and helping me along the way.

Finally – to my family: mom, dad and Daniel, to my friends and loved ones – thank you for the help, support and tolerance (not necessarily in this order). Daslav, Paula, Sandra, Dalia, Martina – needless to say that without you, this would have been a fruitless victory.

## Summary

Characterization of the effects of UVA and UVC exposures in the post-treatment process of photopolymer flexographic printing plate production was performed by various measurement-and-analysis methods. Samples used in this research were solvent-washable and water-washable Computer to Plate (CtP), Laser Ablation Mask Layer (LAMS) flexographic printing plates. Analysis of the chemical, thermal, mechanical and surface properties of photopolymer samples was performed in order to define and quantify the influence of the post-treatment process on the properties of printing plates and corresponding prints. Chemical changes in the material were analysed by means of Fourier transform infrared spectroscopy – attenuated total reflectance method, energy dispersive X-ray spectroscopy and swelling experiments. Thermal analysis (differential scanning calorimetry and thermogravimetric analysis) displayed the influence of the duration of post-treatments on the thermal stability and degradation process of the material, as well as the influence on the crosslinking completion. Mechanical analysis provided the information about the changes in hardness of the printing plate due to the post-treatment process. Surface properties of the photopolymer printing plate samples were analysed by calculating the components of surface free energy and roughness parameters. Obtained results were integrated via correlations, as well as least squares fitting and neural network modelling in order to define the functional model of flexographic printing plate production in relation to influencing parameters in the definition of printing plate's properties in the reproduction process. Prints obtained by UVA and UVC post-treated printing plates displayed significant changes in ink layer thickness and the deformation of fine lines on the prints, as well as the changes in optical density and surface coverage in low and high coverage areas.

Results obtained in this research proved that UVA and UVC exposures in the post-treatment process of flexographic printing plate production can be used as a simple and quick tool for modification of the properties of photopolymer material. This modification is useful in adjusting printing plate's surface and mechanical properties to a specific value, therefore tailoring the flexographic reproduction system for specific applications in conventional and functional printing.

**Keywords:** flexography, photopolymer material, UV post-treatment, crosslinking, surface properties, functional printing

## Sažetak

Analiza utjecaja UVA i UVC post-ekspozicija u procesu izrade fotopolimerne tiskovne forme za fleksotisak u ovom doktorskom radu provedena je pomoću različitih metoda mjerenja i analize. Fotopolimerni uzorci korišteni u ovom istraživanju bili su *Computer to Plate (CtP) Laser Ablation Mask Layer (LAMS)* tiskovne forme za fleksotisak sa vodenim i solventnim razvijanjem. Analiza njihovih kemijskih, toplinskih, mehaničkih i površinskih svojstava provedena je s ciljem definiranja i kvantificiranja utjecaja procesa post-ekspozicije na tiskovnu formu i otisak dobiven pomoću tiskovnih formi s varijacijama u post-ekspoziciji.

Kemijske promjene u materijalu uzrokovane UV post-ekspozicijom analizirane su pomoću Fourier transform infracrvene spektroskopije – postupkom prigušene totalne refleksije, energijski razlučujuće/disperzivne rentgenske spektrometrije i metode bubrenja. Toplinska analize (diferencijalna pretražna kalorimetrija i termogravimetrijska analiza) prikazale su utjecaj trajanja UVA i UVC post-ekspozicija na toplinsku stabilnost i razgradnju materijala. Mehanička analiza dala je podatke o promjenama u tvrdoći tiskovne forme tijekom različitih vremena post-ekspozicije. Površinska svojstva fotopolimernog materijala analizirana su pomoću izračuna polarne i disperzne faze slobodne površinske energije te parametra hrapavosti. Dobiveni rezultati su integrirani putem korelacije, kao i robusne metode najmanjih kvadrata i modeliranja neuronskom mrežom kako bi se definirao funkcionalni model procesa izrade tiskovne forme u odnosu na parametre koji utječu na definiciju njenih površinskih svojstava. Otisci dobiveni modificiranim tiskovnim formama pokazali su značajne promjene u debljini nanosa bojila, gustoći zacrnjenja, pokrivenosti površine svjetlih i tamnih tonova te deformaciji tankih linija.

Rezultati dobiveni u ovom istraživanju dokazali su da se UVA i UVC post-ekspozicije u procesu izrade tiskovnih formi za fleksotisak mogu koristiti kao jednostavan i brz alat za modifikaciju svojstava njihove površine. Ova modifikacija može se koristiti za prilagodbu površinskih svojstava tiskovne forme specifičnim zahtjevima, odnosno stvaranje “personalizirang” fleksotiskarskog reprodukcijskog sustava za posebne primjene u konvencionalnom i funkcionalnom tisku.

**Ključne riječi:** fleksotisak, fotopolimerni materijal, UV post-ekspozicija, umrežavanje, površinska svojstva, funkcionalni tisak

## **Content**

<b>1. INTRODUCTION</b>	<b>1</b>
1.1. Objective of the research	2
1.2. Assignment of the research	4
1.3. Hypotheses of the research	7
<b>2. BACKGROUND</b>	<b>8</b>
2.1. Flexography – now and before	9
2.2. Flexographic printing plate production process	11
2.3. Qualitative properties of flexographic printing plate	16
<b>3. EXPERIMENTAL</b>	<b>19</b>
3.1. Systematic approach to the research	20
3.1.1. Requirement for expanded research of photopolymer printing plates	20
3.1.2. Preliminary research	22
3.1.2.1. Changes of surface and mechanical properties of photopolymer material by UV post-treatments	22
3.1.2.2. Chemical changes in photopolymer material caused by UVC post-treatment	25
3.1.2.3. Formation of printing elements in the photopolymer material	29
3.1.3. Research plan	35
3.2. Materials and devices	36
3.2.1. Preparation of samples	36
3.2.2. Equipment and devices	39
3.3. Measurement and analysis methods	44
3.3.1. Chemical methods for photopolymer material analysis	44
3.3.2. Thermal analysis of photopolymer material	47
3.3.3. Measurement and analysis methods of photopolymer surface properties	48
3.3.4. Roughness measurement and display of photopolymer surface	50
3.3.5. Optical methods for printing plate and print evaluation	51
3.3.6. Modelling methods	53
<b>4. RESULTS AND DISCUSSION</b>	<b>56</b>
4.1. Thermal, chemical and mechanical properties of photopolymer materials	57
4.1.1. DSC analysis	58
4.1.2. TGA analysis	65

4.1.3. Hardness of printing plates	69
4.1.4. Swelling properties of photopolymer materials	70
<b>4.2. Surface properties of photopolymer printing plates</b>	<b>78</b>
4.2.1. Roughness of printing plate surface	79
4.2.2. Surface free energy of printing plates	81
4.2.3. FTIR-ATR analysis of photopolymer surface layer	84
4.2.4. EDS analysis of photopolymer surface layer	90
<b>4.3. Quality of prints and photopolymer printing plates related to reproduction process</b>	<b>92</b>
4.3.1. Topography of printing elements on printing plates	93
4.3.2. Microscopic displays of prints	96
4.3.3. Coverage values on prints	100
4.3.4. Optical density on prints	103
4.3.5. Thickness of printed ink layer	105
<b>5. MODELLING THE PROPERTIES OF PRINTING PLATES AND PRINTS</b>	<b>107</b>
<b>5.1. Analysis of the influencing parameters on <math>\gamma^d</math> and <math>\gamma^p</math> of photopolymer material</b>	<b>108</b>
5.1.1. Weight loss of photopolymer material in relation to $\gamma^d$	109
5.1.2. Relation of oxygen ratio in the surface layer of photopolymer material and $\gamma^p$	119
<b>5.2. Qualitative properties of prints in relation to modified printing plate surface properties</b>	<b>124</b>
5.2.1. Relation of the properties of printing plates and coverage values on prints	125
5.2.2. Relation of the properties of printing plates and optical density on prints	128
5.2.3. Relation of the properties of printing plates and thickness of printed ink layer	130
<b>5.3. LS model fitting of the influencing parameters for printing plate and print properties</b>	<b>132</b>
5.3.1. LS fitting of the printing plate parameters	133
5.3.2. LS fitting of the print properties	139
<b>5.4. Neural network as a functional model for estimation of surface properties of photopolymer printing plate</b>	<b>145</b>
<b>6. CONCLUSIONS</b>	<b>154</b>
<b>7. REFERENCES</b>	<b>160</b>
<b>Appendix 1</b>	<b>171</b>
List of figures	172
List of tables	178

List of equations	180
List of identifications	181
List of abbreviations	182
<b>Appendix 2</b>	183
ACE Digital printing plate – material safety data sheet	184
Digital MAX printing plate – material safety data sheet	186
Cosmolight QS printing plate – material safety data sheet	190
<b>Appendix 3</b>	195
Printed elements in highlight area (1% and 10% nominal coverage value)	196
<b>Appendix 4</b>	199
Modification of surface properties of photopolymer printing plate by UV-ozone treatment	200
<b>CURRICULUM VITAE</b>	228
<b>LIST OF PUBLISHED SCIENTIFIC RESEARCH</b>	229



# **1. INTRODUCTION**

**1.1. Objective of the research**

**1.2. Assignment of the research**

**1.3. Hypotheses of the research**

## 1.1. Objective of the research

In the fast-paced technology development in graphic industry, modern flexography has found its domain mostly in the packaging and functional printing. Due to the new qualitative requirements, workflows and materials used in flexography had to be updated and improved. The application of digitally controlled processes and procedures has taken the place of the analogue production, together with the new methods for processing of the material and improvements of the materials themselves.

This thesis focuses on the functional modification of photopolymer material used as a flexographic printing plate with the aim of achieving optimal output quality. During the transfer of the printing ink from the anilox to the printing plate and then to the printing substrate, surface properties of the photopolymer printing plate highly influence the quality of the print. Therefore, surface properties of the printing plate should be compatible with the used printing ink and the printing substrate, which is especially important when using new formulations of functional inks and for the implementation of different printing substrates and applications.

Workflow of Computer to Plate (CtP) flexographic printing plate production includes exposures of the photopolymer material to ultraviolet radiation, 365 nm (UVA exposure) and 255 nm (UVC exposure), rinsing and drying. UVA exposures have a role of initiation and conduction of the photo-initiated crosslinking process, while UVC exposure terminates the crosslinking in the post-treatment process and significantly affects the surface and mechanical properties of finished printing plate.

Although the composition of photopolymer printing plates, besides copolymers and photoinitiators, includes functional components such as plasticizers and UV stabilizers, surface and mechanical properties of printing plates are subject to change due to the variation of UV exposure, especially in the post-treatment. Furthermore, the process of the printing element formation is dependent on several factors, such as the type of the photopolymer material and the process of the crosslinking, chemical and mechanical parameters during the rinsing cycle and processes of drying and stabilization. Final surface and mechanical properties of printing plate have to be exactly defined, since the quality of the reproduced graphic product depends on the quality of the transfer of the printing ink to the printing substrate.

Since the parameters of the printing plate production are often adjusted to the specific workflow and therefore deviate from those recommended from the manufacturer, it is necessary to precisely define the influence of the processing parameters in the printing plate production system, specifically in the post-treatment which includes additional UVA and UVC exposures and defines printing plate's surface properties.

The object of this doctoral thesis is to define influence of the processing, specifically post-treatment parameters, on the changes of printing element's surface, mechanical and chemical properties, and their behaviour in the reproduction process. Relation of the influencing parameters and the printing plate's properties, as the main objective of this thesis, was presented by means of the functional model of photopolymer printing plate production process.

## 1.2. Assignment of the research

The parameters primarily examined in this thesis were UVA and UVC exposures in the post-treatment process. In order to form printing elements in the photopolymer material, all steps in the printing plate production workflow, beginning with back exposure, must be conducted following the manufacturer's recommendation in order to obtain correctly shaped printing elements in the first place.

However, with post-treatment process, there is a window of the recommended duration for the UVA and UVC exposures, and since it is the last step in the flexographic printing plate production workflow, it actually determines and defines its final surface properties which are of crucial importance in the reproduction process. Furthermore, as a last step in the production process which is also easily alterable regardless of the type of photopolymer material used, its variation is convenient in the real graphic reproduction systems.

Optical, spectroscopic and other analytic methods used for the characterization of (polymeric) surfaces and chemical composition of the compounds were applied in this research. The combination of these methods will provide the insight in the mechanism of changes in the photopolymer material which could influence the behaviour of the printing element and its functional properties important in the reproduction process.

Methods chosen for the characterization of the photopolymer material caused by the UV post-treatments:

- Mechanical and topographic properties of the photopolymer printing plate surface significant for the process of graphic reproduction ( $R_a$  roughness parameter of the printing plate surface and Shore A hardness) was calculated. Variation in the surface roughness may have a direct influence on the changes of the printing plate's surface properties and on the adsorption of the printing ink during the printing process. Hardness of the printing plate is a parameter that has to be defined and adjusted to the specific printing substrate and the reproduction system due to its significant influence on deformation of the image information in the printing process.
- For the analysis of printing plate's physicochemical properties, measurements of contact angles of probe liquids and calculations of surface free energy and its polar and

dispersive component were performed. These changes could influence the graphic reproduction process during the transfer of the specific type of printing ink to the printing plate and from the printing plate to the printing substrate. By establishing the correlation with the results of other analysis methods, the character of the physicochemical changes in the photopolymer material was defined;

- Since the UV radiation causes the chemical changes in the photopolymer material, several methods for this type of analysis were performed. Energy-dispersive X-ray spectroscopy (EDS) is a method used to determine the elementary composition of the material and the ratio of elements in the surface layer of material. This method was used as an indicator of changes in the surface layer composition by monitoring mass portion of the oxygen in the surface of the printing plate. In order to detect the changes in chemical bonds in the photopolymer material, Fourier transform infrared spectroscopy – attenuated total reflectance method (FTIR-ATR) was used. Changes in crosslinking dynamics of the photopolymer material (influenced by the UV post-treatments), were monitored by means of the swelling method;

- Thermal characterization of the photopolymer material was performed by differential scanning calorimetry (DSC) and thermogravimetry (TGA) in order to define thermal behaviour and stability of the material, as well as to define the influence of the post-treatment process on the crosslinking in the photopolymer material;

- Formation of the printing element and its shape, which depends on the duration of the main UV exposure and the type of the photopolymer material, was monitored by means of optical methods – microscopies. Changes of the shape of the printing element in three dimensions, depending on the photopolymer material type, were detected;

- In order to perform the control measurements of the printing element properties significant for the reproduction system, test prints were produced. The information about the surface coverage, optical density, ink layer thickness and the shape of fine printed elements on prints were used to define the qualitative changes of the graphic product in the reproduction process.

- For the purpose of expanding the research about the influence of UV-treatments on the properties of photopolymer materials and prints obtained by treated printing plates, the UV-ozone treatment of the photopolymer surface was performed in collaboration with Welsh

Centre for Printing and Coating. Properties of treated flexographic printing plates and obtained test prints were analysed. However, since this type of treatment is not a part of standard flexographic printing plate production workflow, the results have not been incorporated in this thesis' presentation of the results. The report on the influence of the UV-ozone treatment on the photopolymer printing plates is given in Appendix 4 in this thesis, due to its significance in expanding the knowledge and understanding the behaviour of the photopolymer materials exposed to UV treatments, specifically to treatments of energy higher than in regular production process.

The term „functional model“ in the title of this thesis applies to the fitting of the influencing parameters on photopolymer material and the properties of printing plate by applying robust LS method, as well as modelling the prediction of the printing plate's surface properties with variable durations of the UVA and UVC exposures in the post-treatment process. Applied modelling methods will provide the weight coefficients for photopolymer material properties regarding their influence on the surface properties of printing plate and the prints, therefore enabling more precise control of the flexographic reproduction process quality. They also enabled quantitative prediction of printing plate's surface properties with the random durations of UVA and UVC exposures in the post-treatment process.

### 1.3. Hypotheses of the research

The object of the thesis is to define influence of the processing parameters (specifically, post-treatment process) on the changes in surface, mechanical and chemical properties of printing elements on the printing plates.

According to the object of the research, two hypotheses are defined:

- It is possible to characterize and quantify the influence of the parameters in flexographic printing plate production process by means of spectroscopic, mechanical and optical methods;
- It is possible to define the functional model of flexographic printing plate production by determination of the significant parameters in printing plate production.

*Functional model of photopolymer printing plate production process* has been defined and completed at University of Zagreb Faculty of Graphic Arts in collaboration with the following institutions and companies:

- University of Zagreb Faculty of Chemical Engineering and Technology, Zagreb
- University of Zagreb Faculty of Mechanical Engineering and Naval Architecture, Zagreb
- College of Engineering, Welsh Centre for Printing and Coating, Swansea
- University of Pardubice, Faculty of Chemical Technology, Pardubice
- University of Novi Sad, Faculty of Technical Sciences, Novi Sad
- Rotoplast d.o.o., Zagreb

## **2. BACKGROUND**

**2.1. Flexography – now and before**

**2.2. Flexographic printing plate production process**

**2.3. Qualitative properties of flexographic printing plate**



## 2.1. Flexography – now and before

Flexography is a printing technique of high complexity. In the 1960s, used mostly for printing on the corrugated board, this technique has developed and is nowadays applied in printing of various packaging materials and printed electronics [1, 2]. In the beginning of flexographic printing application, printing plates for flexography were produced of rubber by means of mechanical methods (Figure 1.).



Figure 1. Flexographic printing plates:

a) rubber flexographic printing plate, b) photopolymer CtP flexographic printing plate

Due to the properties of rubber material, these types of printing plates were applied in production of low-quality and long-run prints used in the packaging printing, specifically transport packaging [3].

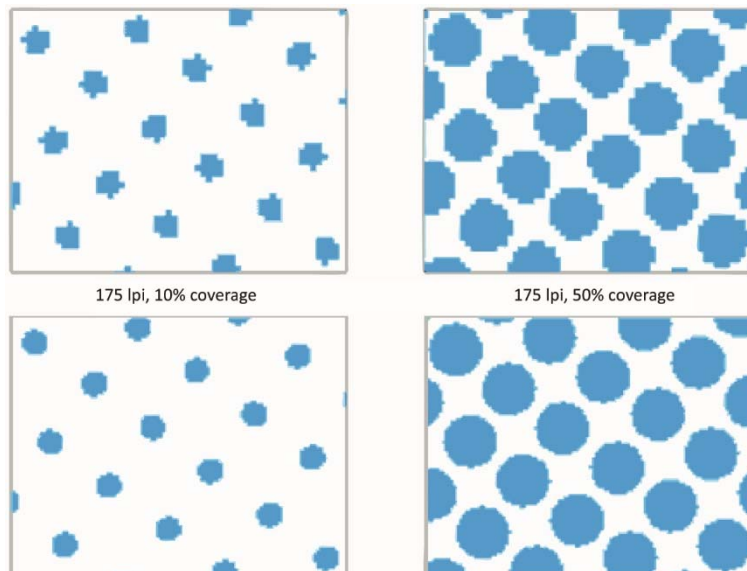


Figure 2. Top line – conventional flexographic digital file - 2540 ppi, bottom line – *HD flexo* digital file – 4000 ppi

After the technological advancement and development of synthetic polymeric materials around 1960., the quality of flexography started to ascend. In past 10 years, the term High-definition (*HD flexo*) (Figure 2.) became a new quality standard in the area of reproduction in flexography, competing with offset printing.

Modern flexographic printing plates can be solvent-washable or water-washable and are based on the effect of crosslinking of certain organic compounds under the exposure to UVA wavelengths that initiate crosslinking and UVC wavelengths that terminate it, thus giving large and stable molecular structures insoluble in the defined developing solution. Composition of this type of printing plates includes different types of copolymers, most common styrene-butadiene-styrene (SBS) and styrene-isoprene-styrene (SIS) block copolymers, photoinitiators sensitive to UV radiation, plasticizers which provide elastic properties, colorants and other additives [4].

With the development of new photopolymer materials for printing plate production, boundaries of the printing plate qualitative properties were pushed even further. Nowadays, optimal surface properties of the flexographic printing plate can be achieved by number of technologies such as Asahi's pinning top technology, flat-top printing elements first presented by Kodak, sharp edges of micro-elements on the printing plate (Kodak's DigiCap technology) and various types of photopolymer's surface micro-patterning and shaping (Figure 3.). The purposes of these technologies are to reduce the dot gain, obtain sharply formed printing elements on the printing plate and to enhance the adsorption of the ink on the printing plate. In this thesis, purposeful modification of the surface free energy of the printing plate will be applied in order to optimize the dot gain and the adsorption of the printing ink.

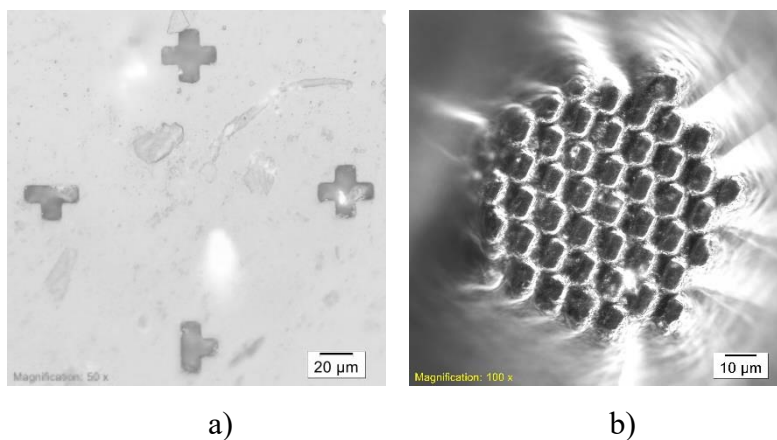


Figure 3. Printing elements on printing plate: a) printing elements at 75% coverage (Kodak's SQUARESPOT technology), b) micro-pattern on flexographic printing element (Kodak's DigiCap technology)

## 2.2. Flexographic printing plate production process

The baseline for production of printing elements in the photopolymer materials used in modern flexography, is radical photo-initiated crosslinking. Specifically, when exposed to UV wavelengths, photoinitiator activates, and the process of radical crosslinking occurs [5]:

Initiation:



Propagation:



Termination:



where  $R$  presents radical,  $M$  monomer, while  $n$  and  $m$  present the numbers of repeating units. UVA radiation initiates (1) while UVC carries out and completes (4).

Printing plates in flexography can be divided based on the type of the rinsing agent: solvent-washable and water-washable. Solvents used in the washing process are organic-based volatile solutions. Ecologically, water-washable printing plates are more acceptable and do not require stabilization period as solvent-washable plates. They do not swell significantly in the water, such as solvent-washable plates do in the developing agents [6]. However, since water-washable printing plates are relatively new to the market, they have not been integrated in the commercial workflows as much as solvent-washable plates. Furthermore, their properties can differ from the solvent-washable printing plates to some extent. Therefore, their application would require certain adjustments in the digital file workflow and the printing process.

Second possible division of flexographic printing plates is related to their application in the printing process. Softer and thicker printing plates are usually used in printing on corrugated board and rough surfaces, while harder and thinner printing plates have an application for prints of high quality and functional printing, such as printed electronics.

Third division of flexographic printing plates is based on the technology used for the transfer of the digital information onto the surface of the printing plate. Most common methods of image transfer from the computer file to the printing plate are based on Laser Ablation Mask Layer (LAMS) and Thermal Imaging Layer (TIL) technology. When producing printing plates with various types of LAMS technology, the black mask layer - LAMS - must be ablated by means of a laser on the image area of the printing plate. After ablation process, printing plate is exposed to UV wavelengths [7]. However, during the period between the laser ablation and UV radiation, photopolymer material is exposed to the destructive influence of the oxygen, resulting with round-top printing elements on the printing plate. TIL technology overcomes this problem by imaging TIL layer separately and laminating it on the printing plate after the imaging process, starting the exposures to UV radiation immediately. The barrier layer, which is a part of the TIL layer, disables the influence of the oxygen on the printing plate [8].

LAMS technology is the most common and widely adopted principle used in the printing houses for production of flexographic printing plates. It was the first Computer to Plate (CtP) technology applied in flexography. The process of flexographic printing plate production based on LAMS is presented in Figure 4.

The base of the photopolymer flexographic printing plates is made of PET, on which the photopolymer material has been applied (Figure 4.a). LAMS mask covers the whole surface of the printing plate. It enables the transfer of the image to the plate by ablation process. After the back exposure performed in order to create the base layer for the printing elements (Figure 4.b), LAMS is removed by laser ablation from the image parts of the photopolymer material (Figure 4. c). Figure 4. d) presents the main exposure to UVA radiation, where printing and nonprinting areas are formed. Exposed parts crosslink and become insoluble in the defined rinsing solution (organic solvent or water).

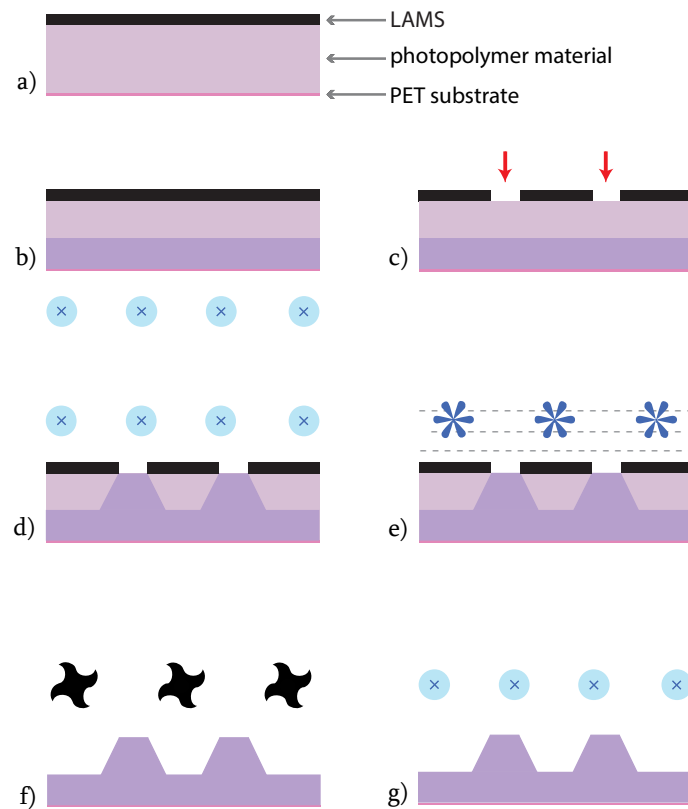


Figure 4. Production of the LAMS-based flexographic printing plate: a) photopolymer sheet prepared for the image transfer, b) back exposure, c) ablation of the LAMS, d) main exposure, e) rinsing, f) drying, g) post-treatment

After the main exposure, follow the rinsing of the unexposed parts in the photopolymer material (Figure 4. e) and drying (Figure 4. f). Printing plate is finished after the post-treatment when it is exposed to UVC radiation (Figure 4. g) in order to terminate the crosslinking process and obtain the optimal surface properties [8, 9].

However, during the period of laser ablation and the period of UV radiation, photopolymer material is exposed to the destructive influence of the oxygen. Oxygen disables the crosslinking, which results with the solubility of the tops of printing elements in the rinsing solution [10]. The consequence can mostly be seen in the whole tonal range, but it is detectable primary in the highlights. The results are poorly and incompletely formed small printing elements which will be unable to transfer the printing ink to the printing substrate correctly.

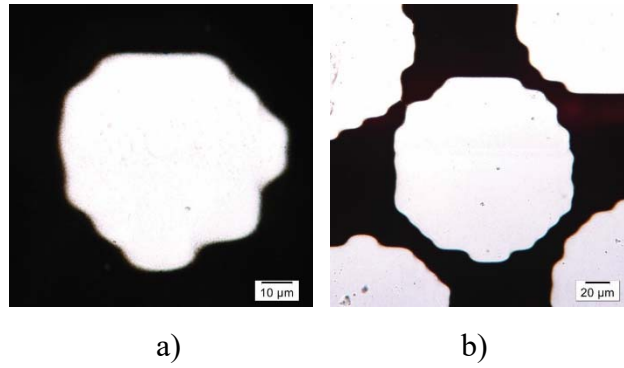


Figure 5. Areas opened on LAMS for: a) 5% and b) 50% nominal coverage value

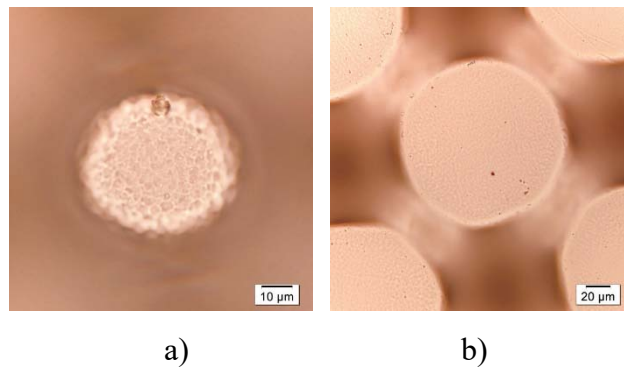


Figure 6. Printing elements on the flexographic printing plate for: a) 5% and b) 50% nominal coverage value, corresponding to Figure 5.a) and 5.b), respectively

Figure 5. and Figure 6. display the differences in the shape ablated in LAMS and the corresponding printing element on the printing plate. It is visible that the area of printing element, especially in the low coverage area of 5%, is smaller than the one ablated in LAMS. Therefore, corrections of the coverage values in the highlight area in the digital file must be performed in order to make those printing elements reproducible (*bump curves*) [2].

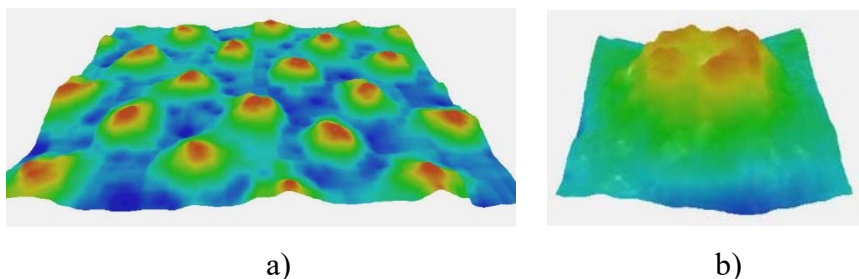


Figure 7. 3D display of printing elements of 5% coverage value on flexographic printing plate for: a) magnification of 40x and b) magnification of 200x

Figure 7. presents 3D displays of printing elements on flexographic printing plate. One can see that they are not uniformly and therefore not correctly formed. Their inadequate height

can cause absence of highlights, and the round top may result as excessive dot gain due to the deformation and the ink travelling down the shoulders of the element.

Therefore, it is important to be well acquainted with the formation of the printing elements in a specific photopolymer material and apply necessary corrections of the digital information to be transferred to the printing plate surface.

### 2.3. Qualitative properties of flexographic printing plate

Flexographic printing process depends on a number of parameters which should be controlled and defined in the reproduction workflow. Surface properties of the printing substrate and printing ink should be defined and characterised. Furthermore, quality of the digital file adjustment, type of the anilox roller and type of the base placed under the printing plate to adjust the pressure during the printing process have a significant influence on the quality of the final product [11]. Photopolymer material used for the printing plate production and all processing steps in platemaking workflow have a significant influence, as well [12].

When starting the process of flexographic printing plate production, one should, apart from following the instructions from the plate manufacturer, adjust several different parameters. For example, power of the UV tubes, pressure of the scrubber in the chemical processing, temperature and saturation of the developing agent, drying temperature, stabilisation period for solvent-washable plates and post-treatment duration must be adjusted to the specific system and workflow. Considering the fact that a number of parameters has to be defined, it is obvious that this kind of reproduction process is of high complexity.

Properties of flexographic printing plate are influenced by the type of printing plate material (photopolymer material), crosslinking process and duration of UV exposures [2, 11]:

- **Hardness** of flexographic printing plate is a parameter influencing the deformation of the printing plate during the engagement in printing process and is related to elastic deformation of the plate. The softer the plate, the more expressed the deformation [13]. When exposed to UV radiation, exposed parts of the printing plate undergo the crosslinking process and become insoluble in the defined processing solution. However, after the last step of flexographic printing plate making process, the plate structure can still be incompletely crosslinked. This can result with stickiness and/or reduced hardness of the printing plate and thus more expressed deformation in the printing process. Post-treatment process increases the plate's hardness to a certain level and can be used as a tool for achieving the optimal hardness value. Furthermore, hardness of the printing plate has to be adjusted to the specific printing substrate in order to achieve optimal results.

- **Elastic deformation** of flexographic printing plate can be characterized as plate's advantage and weakness. It enables printing on the wide range of materials because the



printing plate is able to adjust to various rough surfaces due to its deformation when engaged [14]. On the other hand, the images transferred to the printing substrate could thus be deformed. The level of deformation of the flexographic printing plate has to be a known parameter in the reproduction process, and, together with the height of the printing plate, used to calculate plate's distortion during the printing process.

- **Roughness** of the flexographic printing plate is a property which is connected to the physicochemical surface properties of the photopolymer material, specifically dispersive component of surface free energy. Increased roughness of the printing plate's surface generally results with better adsorption of the printing ink on the plate's surface. Sometimes, roughness of the photopolymer material, due to its low value (commonly,  $R_a$  of up to 1.2  $\mu\text{m}$ ), can be increased by applying micro-pattern on the surface of printing elements [15]. This procedure is commonly used in high coverage value area in order to enhance the ink transfer and result with more vivid print. However, changes in roughness of the photopolymer material due to certain outer influence (specifically, UV treatments), can be used as an indicator of changes in the material structure.

- **Surface free energy (SFE)** - duration of UV post-treatments affects the surface free energy of the photopolymer material. With prolonged exposure, UV radiation causes crosslinking of compounds in the material structure. By increasing the duration of exposure, molecular weight of the photopolymer would increase. The surface tension of polymers tends to increase with increasing molecular weight (however, this is dependable on the type of photopolymer material). Therefore, surface free energy value also increases. Polar and dispersive components of the surface energy change as a result of physicochemical changes that occur on the photopolymer surface under the influence of the UV radiation. These changes can affect the adsorption of the printing ink on the printing plate in the graphic reproduction process. [16]

- **Durability** of flexographic printing plate is an important feature, not only in long run lengths. Upon the use, flexographic printing plates are often stored and used again, if the job is repeated (for example packaging, electronic components). Most flexographic printing plates are declared as being able to produce one million copies before mechanical wear. However, the type of the ink used in the printing process and washing process after printing have a significant impact on the photopolymer material [17, 18]. UV-curable flexographic inks are

known to act destructively on the printing plate’s surface, and can decrease the plate durability considerably, up to 50% compared to water-based inks. Furthermore, washing agents for flexographic printing plates often contain solvents such as ethyl acetate, which causes the swelling of the photopolymer material and can even cause the dissolution of the photopolymer to certain extent. Therefore, careful adjustment of the materials used in the flexographic reproduction process is needed.



Figure 8. Influencing parameters in flexography related to printing plate

Figure 8. presents graphic display of the influencing parameters in connection with the printing plate in flexographic reproduction process.

Since standards in flexography are mainly focused on the process control concerning screen ruling and parameters connected to process colors [19], printing substrates and dot gain (ISO standard 12647-6), further analysis and experiments are yet to be performed when considering the influences of the printing plate quality on the graphic reproduction process.

Previous research in the area of flexographic printing plates and the UVC post-treatment in the printing plate making process pointed out the influence of the duration of the exposure on the printing plate's performance in the printing process [13], and the changes which occur on the printing plate surface when prolonging the post-treatment process [20]. However, the character of these changes and their importance for the graphic reproduction should be systematically defined. Therefore, the connection between the surface phenomena, chemical changes in the photopolymer material and the potential influence on the reproduction process need to be studied and elaborated.

# **3. EXPERIMENTAL**

## **3.1. Systematic approach to the research**

**3.1.1.** Requirement for expanded research of photopolymer printing plates

**3.1.2.** Preliminary research

*3.1.2.1. Changes of surface and mechanical properties of photopolymer material by UV post-treatments*

*3.1.2.2. Chemical changes in photopolymer material caused by UVC post-treatment*

*3.1.2.3. Formation of printing elements in the photopolymer material*

**3.1.3.** Research plan

## **3.2. Materials and devices**

**3.2.1.** Preparation of samples

**3.2.2.** Equipment and devices

## **3.3. Measurement and analysis methods**

**3.3.1.** Chemical methods for photopolymer material analysis

**3.3.2.** Thermal analysis of photopolymer material

**3.3.3.** Measurement and analysis methods of photopolymer surface properties

**3.3.4.** Roughness measurement and display of photopolymer surface

**3.3.5.** Optical methods for printing plate and print evaluation

**3.3.6.** Modelling methods

### **3.1. Systematic approach to the research**

#### **3.1.1. Requirement for expanded research of photopolymer printing plates**

After analysing available literature, an overview of the research performed in the field of flexography pointed out the need for more detailed research in the area of photopolymer printing plates used in flexography.

Existing defined standards in the area of flexography refer to the process control regarding the screening, process colors, printing substrates and dot gain values on the imprint [19]. Research referring to the reproduction possibilities in flexography have been performed [21], but the influence of the printing plates and their processing on the quality of the printed product has not been defined. Therefore, this research will be directed to the processes in flexographic printing plate production in order to define the optimal functional model of the printing plate production process.

Research of the screen quality influence on the formation and shape of printing elements in flexography has been performed [22]. The emphasis in this research was on the changes which occur in tonal value due to the scattering of the light during the exposure. Methods applied in mentioned analysis proved to be of significant importance and are therefore applied in this research, as well.

Prepress process of graphic reproduction regarding printing plate production, which includes series of adjustments considering dimensions of screen elements on the printing plate [23] sets the important guidelines regarding the process of the printing element formation, which will enable the functionality of the printing plate in graphic reproduction process.

Research of the influence of UV radiation in the flexographic printing plate production process (ageing of the printing plate) on the quality of graphic reproduction has been performed [20], but the physicochemical changes in photopolymer material have not been considered. Some researches discuss the impact of the back exposure and main exposure on the formation of printing elements and physicochemical properties of the printing plate [24]. However, the influence of the post-treatment, which proved to be a significant influencing parameter in the preliminary research of this thesis [25], has not been defined. Furthermore, in the research with the aim of analysing the changes in flexographic printing plate's surface

structure due to the post-treatment, no direct relation to the other printing plate's surface and mechanical properties exists. Therefore, the emphasis in this thesis will be addressed to the connection between structural, mechanical and surface changes in the photopolymer material as a result of UV post-treatment.

Method of material swelling [26] has been used for the analysis of the photopolymer material's crosslinking properties. This method is not commonly applied in the research of flexographic printing plates. However, since it has proven to be applicable for the experiment performed in this research, it will be applied in order to characterize changes in the ratio of non crosslinked compound in the material and as a control method for testing the resistance of the material to the washing solution.

Several methods for the analysis of the structures and composition of polymer materials and surfaces exist; for example FTIR-ATR spectroscopy - Fourier transform infrared spectroscopy – total attenuated reflectance (FTIR-ATR), Energy-dispersive X-ray spectroscopy (EDS), Differential scanning calorimetry (DSC). By applying mentioned methods, one can precisely define the structures and surfaces of the photopolymer material used in flexographic printing plate production, as well as determine the changes which occur in the material due to the treatment of the printing plate in the production process.

### 3.1.2. Preliminary research

Overview of the performed and existing research in the area of flexography, specifically flexographic printing plates, and potential analysis and measurement methods, was used as a starting point for the preliminary experiments and formation of the research plan.

#### *3.1.2.1. Changes of surface and mechanical properties of photopolymer material by UV treatment*

Quality of flexographic printing depends on several parameters, such as the ability of printing plate to adsorb printing ink from the anilox roller and ability of printing substrate to assimilate printing ink from the printing plate. Hardness of printing plate and pressure in the printing process are the influencing parameters, too. Therefore, in order to monitor changes in flexographic printing plate's quality, changes in hardness and surface free energy of flexographic printing plates produced under different main exposure conditions were examined.

For that purpose, five samples of full-tone liquid photopolymer printing plate with variations in main exposure were prepared. Liquid photopolymer TRODAT i40 was used. Back exposure time was set at 32 seconds, post-treatment at 900 seconds, and main exposure was varied (126, 153, 180, 207 and 234 seconds). The duration of exposures was defined according to the manufacturer's recommendations [27].

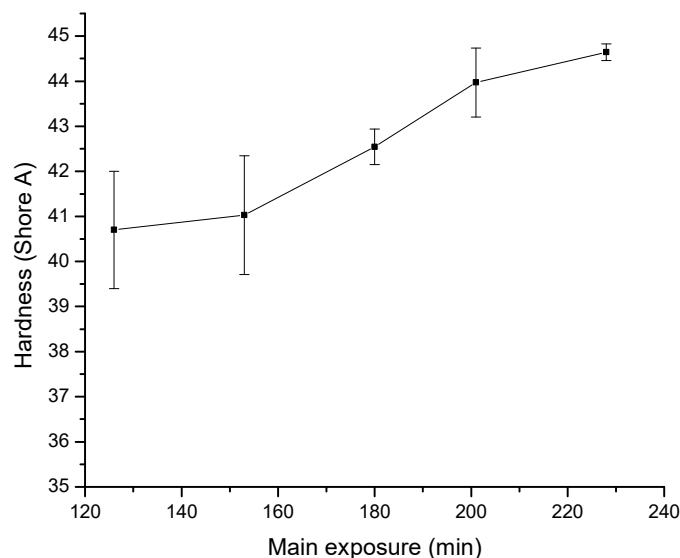


Figure 9. Dependence of hardness of printing plate on main exposure

In Figure 9. one can see the relation between the hardness of flexographic printing plate and the main exposure. With prolonged main exposure, printing plate hardness increases. Overall, 90% increase of main exposure time results with 10% increase of printing plate's hardness for this photopolymer material. That relation is probably a result of higher degree of monomer space-bounding due to the longer exposure which results with more compact and solid material structure.

Dependence of contact angle of probe liquids on the main exposure can be seen in Figure 10. Contact angle values of glycerol are highest and vary from 91° to 98°. For water, contact angle values vary from 66° to 76°, and contact angle values of diiodomethane are lowest, with variations from 65° to 77°. One can also see that all contact angle values show decreasing tendency with prolonged main exposure.

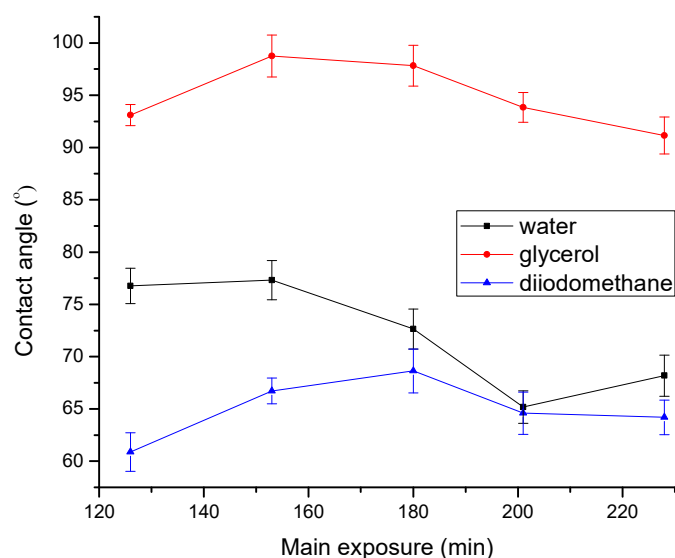


Figure 10. Dependence of contact angle on main exposure

Obtained results indicate that changes occur in the physicochemical properties of photopolymeric surface, which could be the result of the increased degree of crosslinking caused by main exposure, and chemical changes in the surface layer of the photopolymer material.

Results of surface free energy ( $\gamma$ ) calculations (Eq. 6), obtained from the average values of contact angles are presented in Figure 11.

Based on obtained surface free energy results, one can conclude that the overall increase of surface free energy is caused by increase of the polar component ( $\gamma^p$ ) which is a consequence

of the polar interactions in the compound, while the dispersive component ( $\gamma^d$ ) as a consequence of the weak intermolecular forces such as van der Waals forces does not change significantly. This type of surface free energy changes in dependence on main exposure time can be caused by the increased amount of polar bonds in the material's molecular structure.

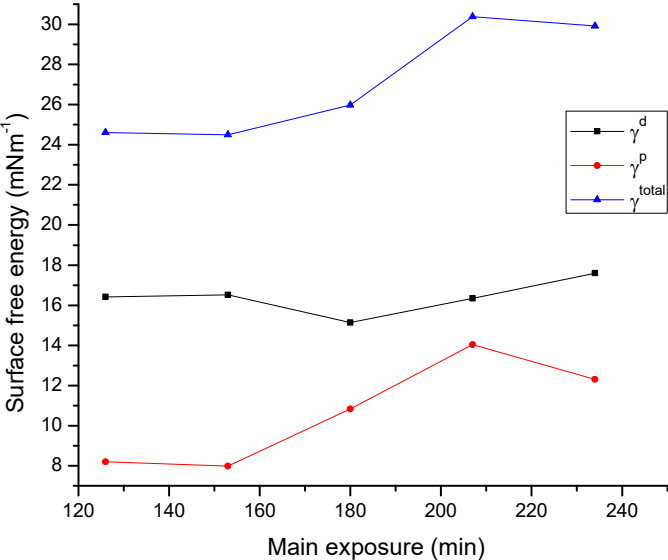


Figure 11. Dependence of surface free energy of printing plate on main exposure

Increase of the polar component of surface free energy influences the adsorption of the printing ink on the flexographic printing plate [28]. Therefore, the changes that occur in the surface layer of the photopolymer material caused by UV radiation need to be examined and analysed in detail.

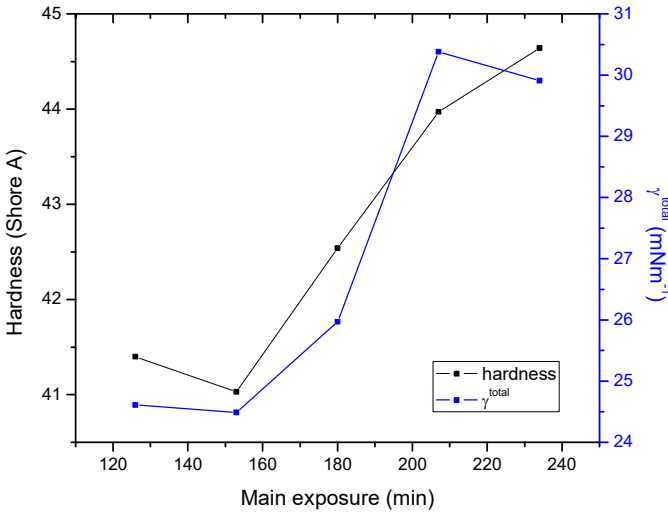


Figure 12. Relation between printing plate's hardness and surface free energy



Figure 12. presents the diagram of correlation between flexographic printing plate's average hardness values and calculated surface free energy. Pearson's correlation coefficient is 0.953. Same trend of hardness and surface free energy values on the printing plate indicates that crosslinking process has uniform impact on both properties.

In the reproduction process, the transfer of the printing ink from the anilox roller to the printing plate and finally to the imprint depends on the surface properties of all used materials. Since the printing plate is in the middle of that reproduction chain, its surface energy must be adequate to achieve the optimal transfer of the tonal values from the anilox roller to the printing substrate [29, 30].

### *3.1.2.2. Chemical changes in photopolymer material caused by UVC post-treatment*

The next step in the research was to determine the influence of the printing plate's post-treatment process on the functional characteristics of flexographic printing plates. The influence of the UVC post-treatment on the contact angle of different probe liquids and surface free energy of the printing plate were observed. Due to its higher energy compared to the UVA radiation, it was expected to have a significant influence on the changes of photopolymer material's properties.

For that purpose, samples of solvent washable CtP flexographic printing plates MacDermid Digital MAX with thickness of 1.14 mm were used. Back and main exposures were conducted in conditions defined for the specific workflow considering the UV tubes power and the duration of the exposure. Developing process, stabilization and UVA post-treatment were also performed in the standard conditions, but duration of the UVC post-treatment was varied.

In order to define the influence of different duration of UVC post-treatment on the surface characteristics of the printing plate, samples used in this research varied from lower UVC post-treatment duration (1 minute) to the extreme of 14 minutes with the step of 1 minute. In order to define the changes in surface structure of the photopolymer material, FTIR and EDS spectroscopy were used.

Results of the contact angle measurements, surface free energy calculations and energy-dispersive X-ray spectroscopy indicated that UVC post-treatment causes noticeable changes in the chemical structure of the photopolymer surface, which results with the changes of the

surface free energy and distribution of its polar and dispersive component. Figure 13. presents the influence of different UVC post-treatment duration on the contact angle by application of probe liquids.

In Figure 13. one can see that by prolonging the UVC post-treatment, contact angle of both water and glycerol decrease, with the final difference between first (1 minute of UVC post-treatment) and last sample (14 minutes of UVC post-treatment) of approximately 8°. Water is a liquid of primary polar character, and glycerol is a liquid of both polar and non-polar (dispersive) characteristics. The contact angles of both water and glycerol are relatively high, with values from 77° to 86°.

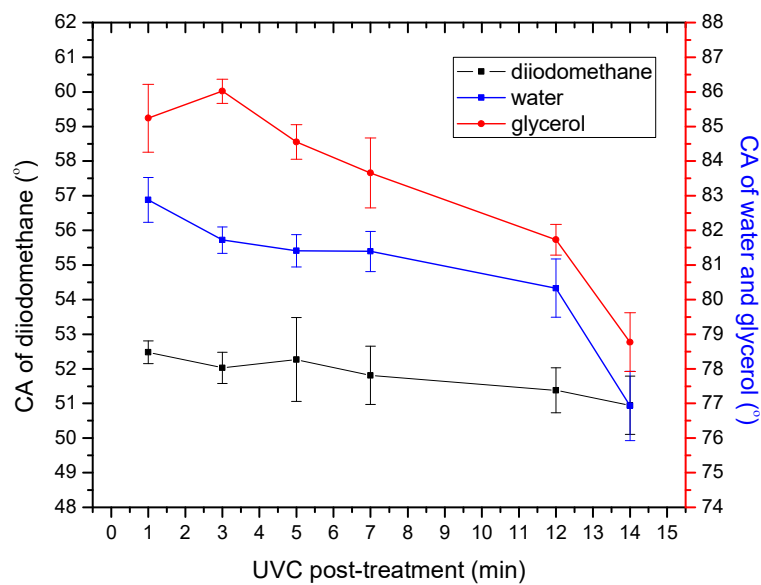


Figure 13. Contact angle (*CA*) of probe liquids on the examined flexographic printing plate samples

Obtained values were highly stable and reproducible with deviations not greater than 3%. Contact angle of diiodomethane amounts approximately 52° with changes of maximally 1° through UVC post-treatment variation.

In Figure 14. one can see the differences between the surface free energy of different variations of UVC post-treated samples. With prolonged UVC post-treatment, total surface free energy and both its polar and dispersive components increase, with more emphasized increase of the dispersive component.

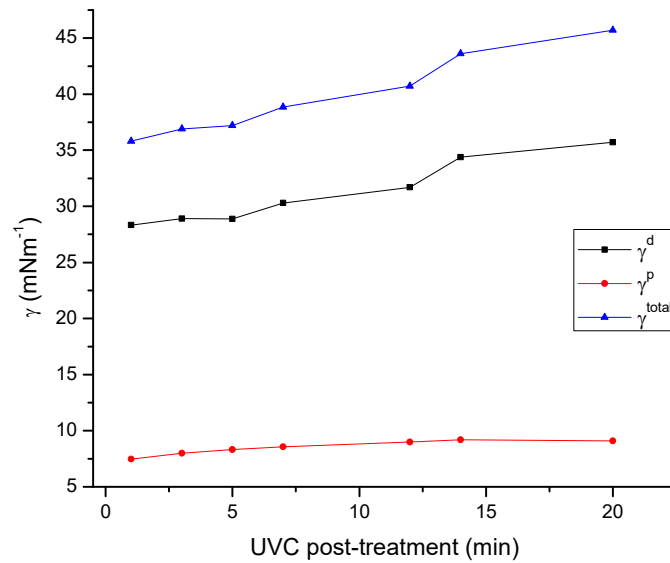


Figure 14. Surface free energy components of the examined flexographic printing plate samples

After surface free energy calculation, the EDS analysis method was applied in order to define and characterize the changes of the surface free energy.

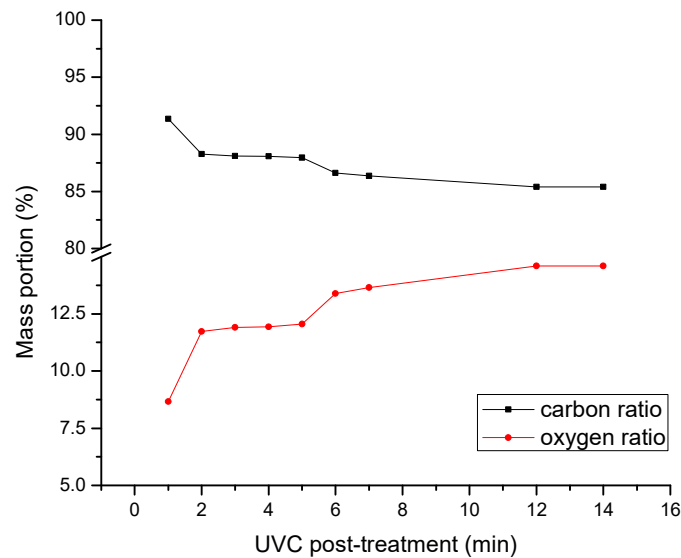


Figure 15. EDS analysis of the samples with mass portion of carbon (C) and oxygen (O)

EDS analysis showed that the increased duration of UVC post-treatment results with higher mass portion of oxygen in the photopolymer surface (Figure 15.). One can see that mass ratio of oxygen increases from 8.66% for 1 minute to 14.60% for 12 and 14 minutes of UVC post-treatment. EDS analysis indicated that prolonged UVC post-treatment causes placement of the structures containing oxygen in the photopolymer surface structure, therefore increasing the polar component of the surface free energy. Therefore, the changes in contact angle of the

polar liquid (water) and the liquid with the share of polar phase (glycerol) are caused by the increase of the oxygen concentration in the surface layer of the photopolymer [9]. In addition, the increase of the dispersive component of the surface free energy was probably caused by further crosslinking process in the photopolymer material structure.

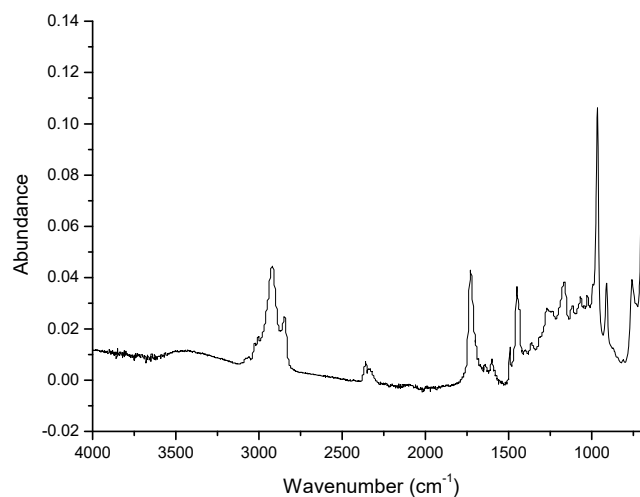


Figure 16. FTIR analysis of the printing plate sample exposed to UVC radiation for 1 minute

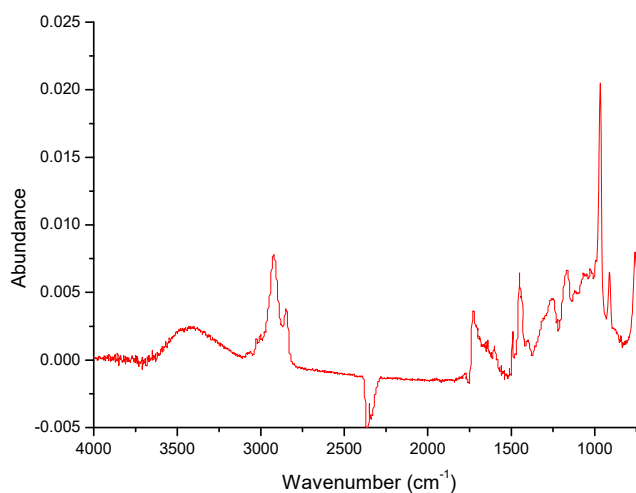


Figure 17. FTIR analysis of the printing plate sample exposed to UVC radiation for 14 minutes

In Figure 16. and Figure 17. one can see the FTIR spectra of samples exposed to shortest and longest UVC exposure, respectively. FTIR analysis supports the results obtained by means of the EDS analysis. The main difference in spectra is visible in the region of 3200 to 3500  $\text{cm}^{-1}$  and 1650 to 1750  $\text{cm}^{-1}$ . The areas of interest correspond to vibrations of hydroxyl (OH) and carbonyl (C=O) bonds, respectively [31]. Therefore, the origin of increased mass portion of the oxygen in EDS analysis can be explained by increased portion of hydroxyl and carbonyl

bonds in the sample with UVC exposure of 14 minutes. Both groups increase the polarity of the surface, resulting with lower contact angle of applied polar liquid and increased polar component of the surface free energy. This could result with inadequate adsorption of the printing ink with surface properties adapted to the flexographic printing process and printing substrates, to the printing plate, and therefore cause problems in the graphic reproduction process [32]. Furthermore, chemical changes which occur in the photopolymer structure as a result of prolonged UVC post-treatment appear to have the similar effect as the oxidation process.

In addition, chemical changes in photopolymer related to UV-induced progression and/or termination of the crosslinking process could affect the hardness and roughness of the printing plate. Therefore, in further research in this thesis, the impact of both UVA and UVC post-treatments will be studied with the aim of defining not only the changes in the chemical and surface properties of the photopolymer material, but also the changes of mechanical properties which occur in the material.

### *3.1.2.3. Formation of printing elements in the photopolymer material*

In flexographic reproduction process, the limitations caused by the photopolymer material are mostly visible in the highlight area. Due to the small area opened in LAMS layer, insufficient amount of the UV energy interacts with the photopolymer material, combined with the destructive influence of the oxygen. It results with incorrectly formed small printing elements of inadequate height, which are not able to transfer printing ink to the printing substrate. The correction which should be applied in order to overcome the influence of the crosslinking process and the influence of oxygen on the printing plate is performed on the digital image file. It is called the *bump curve*. The bump curve increases the coverage value of the highlights in order to make the smallest printing element correctly formed. For example, it is possible to enlarge the opening in LAMS (to e.g. 7%) in order to obtain 1% of coverage value on the printing plate [33].

In order to analyse the connection between different bump curves and the improvement of the printing element formation, solvent-washable MacDermid Digital MAX LAMS-based printing plate was used. Two types of samples were prepared: five samples of unfinished printing plate with different bump curves, where only ablation of the LAMS on the image

area was performed, and five samples of finished printing plate corresponding to the LAMS samples. The differences between bump curves can be seen in Table 1.

Samples of finished printing plates were processed in standard conditions proposed by the printing plate manufacturer. The image transferred to the samples was a control strip with fields of coverage values from 1% to 100%, with step of 10% coverage value between the fields. Additionally, fields in highlight area had a smaller step: coverage values of 1, 3, 5, 8, 10 and 15 % were represented on the control strip in order to examine the formation of the small printing elements in detail.

Table 1. Coverage values on the printing plate and size of openings on LAMS for different bump curve

Sample	Opening on LAMS for the smallest printing element	Coverage value of the smallest printing element on the printing plate
2BU	6 pixels	2%
4BU	12 pixels	4%
6BU	18 pixels	6%
8BU	24 pixels	8%
10BU	29 pixels	10%

In order to monitor the formation of the small printing elements (highlights), the areas of the openings on LAMS and the percentage of the image elements on the observed area of the printing plate were measured. Also, topography and cross-section of printing elements were captured and displayed by means of AniCAM 3D microscope (Figure 18.) [34].

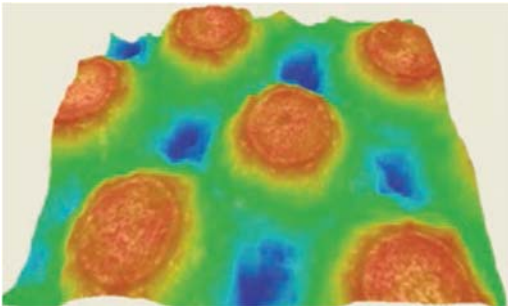


Figure 18. Topography of flexographic printing elements of 50% coverage value displayed by AniCAM 3D microscope

In Figure 19, one can see the differences in areas of openings on LAMS for different bump curves in the highlight area. The area of openings on LAMS for 1% coverage value on 2BU curve is cca. 800  $\mu\text{m}^2$ , and cca. 3200  $\mu\text{m}^2$  for 10BU curve. As the nominal coverage value increases, the difference between highest and lowest bump curve decreases. For the 20% nominal coverage value it equals cca. 1500  $\mu\text{m}^2$ .

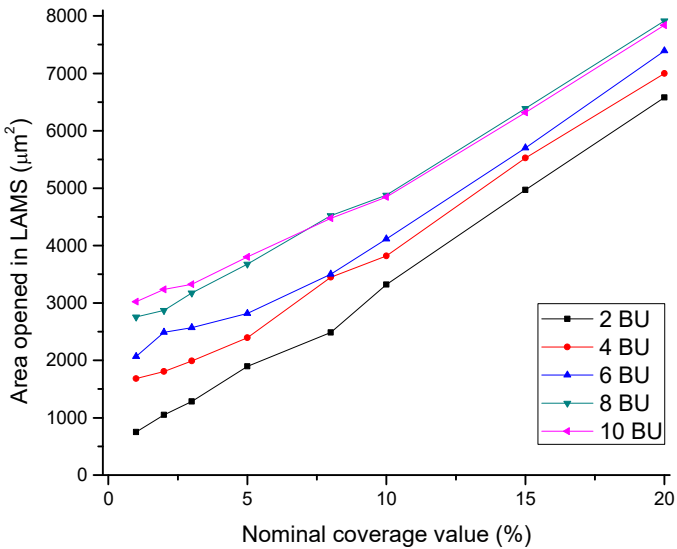


Figure 19. Comparison of the area of openings on LAMS for different bump curves applied in highlights

Figure 20, presents the differences between area of printing elements produced with different bump curves in highlights. It shows the increase in the area difference in higher coverage value area (15% - 20%), which is opposite of the area trend in Figure 19.

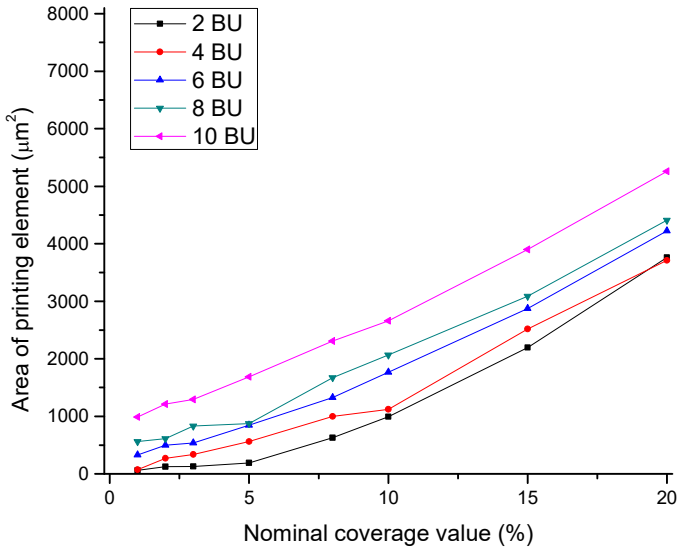


Figure 20. Comparison of the area of the printing elements for different bump curves applied in highlights

This indicates that the formation of the printing elements is not in linear correlation to the openings on LAMS, as with the increase of the coverage value the undercopying starts to impact the printing element formation [33]. Therefore, when applying a bump curve type, one should also consider its influence on the formation of printing elements of higher coverage value.

Cross-sections from right and left side of the smallest printing element produced on the printing plate samples (1% coverage value) are displayed in the Figures 21. - 23.

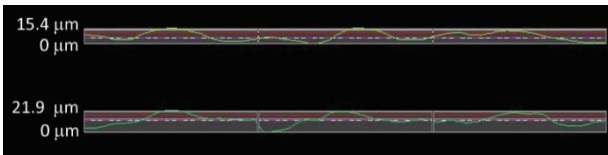


Figure 21. Cross-section of printing elements at 1% coverage value with application of bump curve 2BU

The cross-section of the printing element of 1% coverage value presented in Figure 21. shows that printing elements have not been formed. Printing area cannot be clearly distinguished from the nonprinting area, and therefore the elements will not have the necessary functional properties. Also, the height of the relief is only between 15.4 μm and 21.9 μm, which is not enough to achieve optimal printability in the reproduction process.

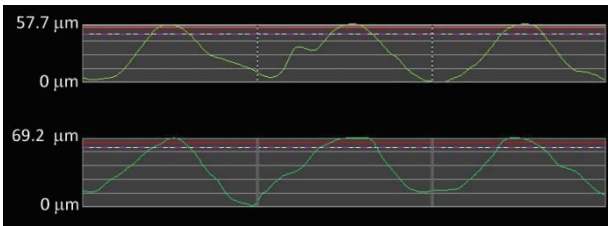


Figure 22. Cross-section of printing elements at 1% coverage value with application of bump curve 6BU

In Figure 22. one can see the cross-section of printing elements produced by application of 6BU curve. Although the printing elements have the sufficient height to achieve optimal printability, their formation is not completely correct. The difference in the height of two sides of the element is 12.5 μm, which could result with the deformations of the printed element on the printing substrate. Since the shapes of the printing elements are not correct (printing elements are too narrow), it could result with the instability in the reproduction



process due to the pressure during the printing. The outcome would be deformed screen elements on the print [21, 22].

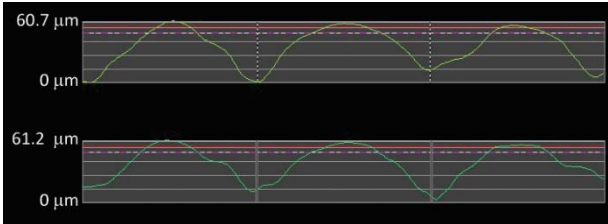


Figure 23. Cross-section of printing elements at 1% coverage value with application of bump curve 10BU

Correctly formed printing elements of 1% coverage value are produced by application of the bump curve 10BU (Figure 23.). The heights of both profile sides of printing elements are similar, and the base of the printing element is wide, which ensures the stability in the reproduction process. The influence of the oxygen is still visible, since the printing area at the 1% coverage value of the printing plate sample 10BU is similar to the printing area of printing plate sample 6BU. Nevertheless, printing elements produced by application of the bump curve with highest value are optimally formed.

The topographies of printing elements of 1% coverage value produced by application of 2BU, 6BU and 10BU (Figure 24.) confirm presented results and show the difference in the formation of the printing elements.

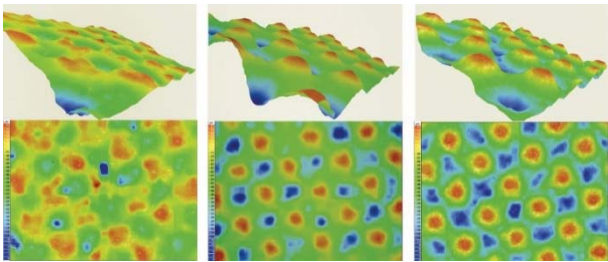


Figure 24. 3D display of printing elements of 1% coverage value with application of bump curve 2BU, 6BU and 10BU, respectively

The application of 2BU curve does not result with functional printing elements. As it is visible in Figure 22. and Figure 23., the main difference between the 6BU and 10BU printing plate samples is in the base of the printing element. In the flexographic reproduction process printing elements are deformed because of the pressure. If the printing element base is not

wide enough (printing plate sample 6BU), the deformation will be more expressed causing the transfer of the excessive ink amount to the printing substrate. On the other hand, the shape of the printing elements on 10BU sample will result with their stability in the printing process and the deformation of the screen element on the print will be minor. Therefore, when applying the bump curve to the digital file, one should, besides the correct formation of the printing element's top, also consider the shape and stability of the whole printing element. This would result in the optimal coverage value transfer throughout the graphic reproduction process [35].

Performed research pointed out the importance of the correct application of the bump curves on the printing plate samples. However, the formation of the printing elements has to be highly dependent on the type of photopolymer material as well. Therefore, having in mind the correct application of the bump curve, one of the research points in this thesis will be analysis of the printing element quality in the highlight area with correct application of the bump curve, but with the usage of different photopolymer materials.

### 3.1.3. Research plan

After the overview of the results obtained in the preliminary research, it became evident that the properties of the photopolymer material used in flexography can significantly change due to the UV post-treatment. Furthermore, it was apparent that chemical, mechanical and surface properties need to be analysed on different types of photopolymer materials exposed to varied UV post-treatments. Prints obtained with printing plates modified in this way needed to be analysed, as well. Therefore, the following research plan was defined (Figure 25.):

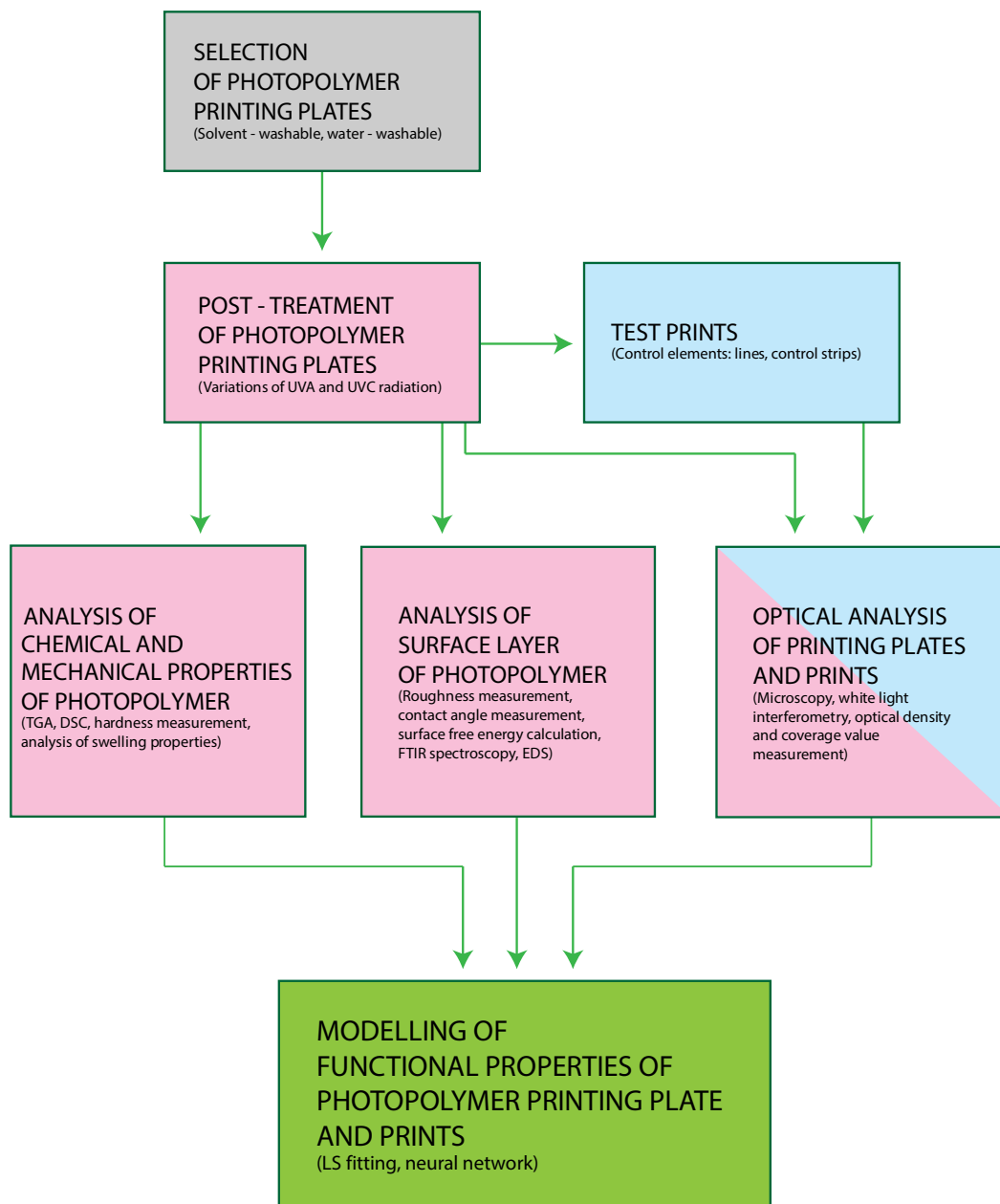


Figure 25. Research plan

### 3.2. Materials and devices

In this chapter, materials, preparation of samples, devices and methods used in this study to measure, calculate and analyse the changes of the properties photopolymer material's due to the variations of UVA and UVC post-treatments are listed and described. Modelling methods used to quantitatively identify the influencing parameters and predict the behavior of properties of flexographic printing plate during the UV post-treatment (least square fitting and application of neural network) will be demonstrated in discussion.

#### 3.2.1. Preparation of samples

In this thesis, three different photopolymer materials were tested in terms of their chemical, surface and mechanical properties which are subject to change due to the variations in the post-treatment process. All types of printing plates were LAMS-based, with digital (CtP) production procedure. Two types of printing plates were more commonly used solvent-washable, and one type was water-washable printing plate (Figure 26).

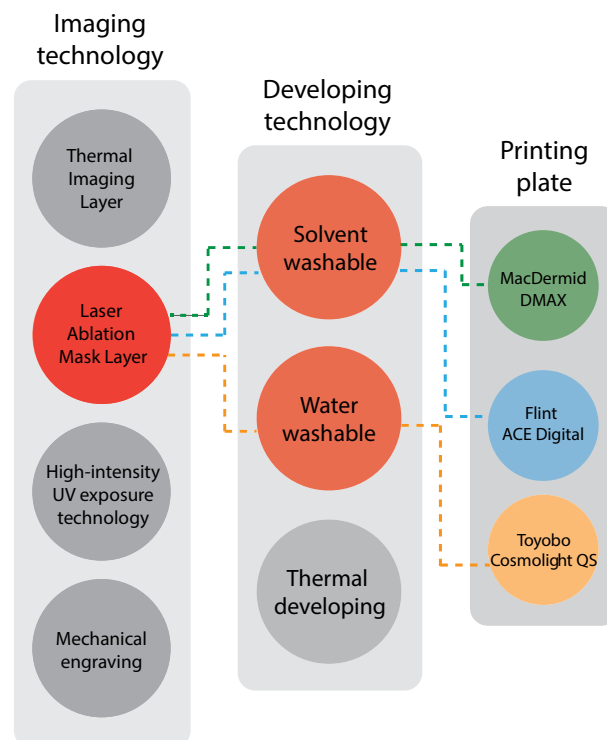


Figure 26. Types of flexographic printing plates

All samples of printing plates were produced by the standard procedure recommended by their manufacturer [36-38], up to the post-treatment process. The test image transferred to the printing plate surface consisted of the control strip and the fine lines (Figure 27.). The variations of the post-treatments are listed in Table 3.

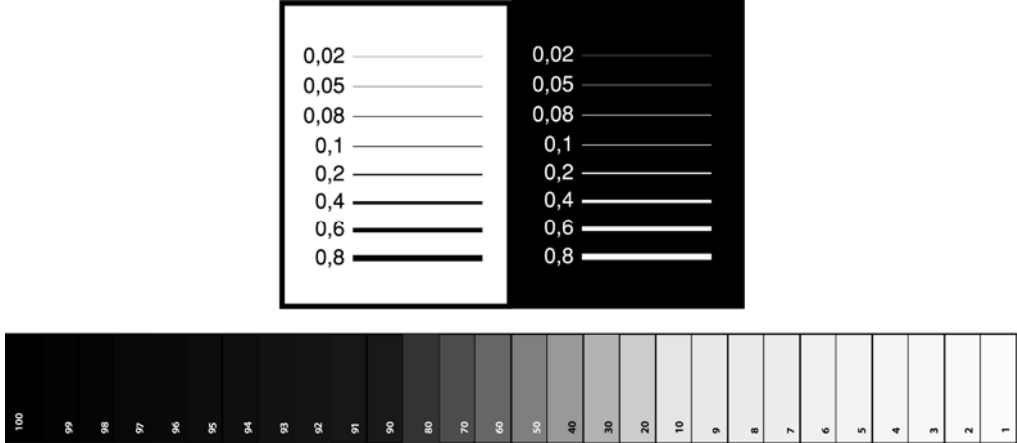


Figure 27. Test image transferred from the digital file to the printing plate

After the stabilisation period, produced printing plate samples were exposed to different durations of UVA and UVC post-treatments. The duration of the post-treatments was varied from 0 to 20 minutes, with the step of 1 minute.

Table 2. shows the two sets of samples with combinations and the durations of the performed exposures.

Table 2. Variations of the post-treatments on the samples

	Duration of the post-treatments (min)
<b>SET 1</b>	<b>Variations of UVA post-treatment</b>
UVA	0, 0, 1, 2, 3, ... , 18, 19, 20
UVC	0, 10, 10, 10, 10, ... , 10, 10, 10
<b>SET 2</b>	<b>Variations of UVC post-treatment</b>
UVA	10, 10, 10, 10, ... , 10, 10, 10
UVC	0, 1, 2, 3, ... , 18, 19, 20

The purpose of this research was to maintain the necessary functional properties of the flexographic printing plate. Therefore, both post-treatments were performed on the samples (except the first, referent sample without any post-treatment), but the duration of one of them was varied. The duration of the post-treatment that was kept constant was an optimal duration recommended by the manufacturers (10 minutes of UVA and UVC radiation for ACE Digital and Digital MAX printing plate and 10 minutes of UVA and 5 minutes of UVC for Cosmolight QS printing plate).

Samples of test prints obtained by means of the printing plate samples listed in Table 2. were produced in Rotoplast d.o.o. under their standard production conditions. ISO 9001:2008 and ISO 14001:2004 standards were respected [39-40]. The characteristics of used anilox were  $400 \text{ lcm}^{-1}$ , with cell volume of  $4.5 \text{ cm}^3\text{m}^{-2}$ . Printing speed was  $200 \text{ mmin}^{-1}$ .

### 3.2.2. Equipment and devices

In this work, several types of materials, devices and softwares were used in order to perform detailed analysis of the modern photopolymer materials used in flexographic printing plate production. They are listed in Table 3.

Table 3. List of materials, devices and software used in the research

<p><b>Flexographic printing plate samples (photopolymer materials)</b></p>	<p><b><i>Solvent-washable elastomeric photopolymer printing plate:</i></b></p> <ul style="list-style-type: none"> <li>• MacDermid Digital MAX (1.14 mm);</li> <li>• Flint ACE Digital (1.14 mm);</li> </ul> <p><b><i>Water-washable elastomeric photopolymer printing plate:</i></b></p> <ul style="list-style-type: none"> <li>• Toyobo Cosmolight QS (1.14 mm)</li> </ul>
<p><b>Equipment for printing plate production</b></p>	<p><b><i>Imagesetter: Esko Spark 4835:</i></b></p> <ul style="list-style-type: none"> <li>• External drum design</li> <li>• Max. plate format 48"x 35" / 1200 mm x 900 mm</li> <li>• Solid granite machine base High power Fiber Laser source</li> <li>• Class 1 laser Image quality Screen rulings: up to 200 lpi, depending on imaging resolution</li> <li>• Halftone 1-99% Resolutions: fully variable from 2000 to 4000 ppi on job-to-job base</li> </ul> <p><b><i>Exposure unit: Cyrel 1000 ECDLF:</i></b></p> <ul style="list-style-type: none"> <li>• Max. nominal plate width: 900 mm – 36 inch</li> <li>• Max. nominal plate length: 1,200 mm – 48 inch</li> <li>• UVA tubes wave length: 360 nm – 380 nm</li> <li>• UV-C tubes wave length: 254 nm</li> <li>• Plate thickness: 0.5 mm to 7.0 mm</li> <li>• Electrical (field configurable): 370 / 440 Volt – 50 / 60hz</li> <li>• Power (nominal): 9.5 kW</li> </ul> <p><b><i>Rinsing unit: BASF Combi Fill:</i></b></p> <ul style="list-style-type: none"> <li>• Processor + EDLF (Exposure, Dryer and Light-Finisher combination)</li> <li>• Punch and pinbars with external heater</li> <li>• Max. plate size: 90 x 120 cm</li> <li>• Length: 395 cm</li> <li>• Hight: 135 cm</li> <li>• Width: 157 cm</li> <li>• Weight net: 1000 kg</li> <li>• Weight gross: 1400 kg</li> <li>• Power requirements: 5 kW</li> </ul>
<p><b>Materials and equipment for the production of the prints</b></p>	<p><b><i>Printing press: Miraflex CM:</i></b></p> <ul style="list-style-type: none"> <li>• Printing decks: 8 / 10</li> <li>• Printing width: 820 – 1450 mm</li> <li>• Repeat length: max. 800 mm</li> </ul>

	<ul style="list-style-type: none"> <li>• Speed: 500 m/min. / 600 m/min</li> </ul> <p><b>Printing substrate:</b> PE LD white, 60 µm</p> <p><b>Printing ink: Gecko ® Base:</b></p> <ul style="list-style-type: none"> <li>• Solvent (ethanol) based printing ink for flexible packaging</li> <li>• High-intensity pigment concentrate color</li> </ul>
<p><b>Equipment for optical analysis</b></p>	<p><b>Olympus BX 51 microscope:</b></p> <ul style="list-style-type: none"> <li>• UIS optical system</li> <li>• Focus vertical stage movement: 25mm stage stroke with coarse adjustment limit stopper</li> <li>• Illuminator built-in Koehler illumination for transmitted light 12V100W halogen bulb (pre-centered)</li> <li>• Light intensity LED indicator</li> <li>• Abbe (N.A. 1.1), for 4×—100×</li> <li>• Swing out Achromatic (N.A. 0.9), for 1.25×—100× (swing-out: 1.25×—4×)</li> <li>• Achromatic aplanatic (N.A. 1.4), for 10×—100×</li> <li>• Universal (N.A. 1.4/0.9), for 2×—100× (swing-out: 2×—4×, with oil top lens: 20×—100×)</li> </ul> <p><b>Troika AniCAM 3D microscope:</b></p> <ul style="list-style-type: none"> <li>• Chrome and copper gravure cylinders (20 - 200 lpcm   50 - 500 lpi)</li> <li>• Ceramic anilox cylinders (40 - 475 lpcm   100 - 1200 lpi)</li> <li>• Flexo plates &amp; sleeves (22 - 80 lpcm   55 - 200 lpi)</li> <li>• Minimum roll diameter: 2.5" / 63 mm</li> <li>• Digital zoom range 1:1 up to 6:1</li> <li>• Flexo plate readings: .fcp format (incl. 2D/3D info)</li> <li>• Anilox readings: .acp format (incl. 2D/3D info)</li> <li>• Gravure readings: .gcp format (incl. 2D/3D info)</li> <li>• All readings: JPEG and BMP (bitmap export)</li> <li>• 1 co-axial and 2 x 9 radial white light LEDs (SW-controlled)</li> <li>• Three lenses (x04, x10 and x20)</li> </ul> <p><b>X-Rite vipFLEX II:</b></p> <ul style="list-style-type: none"> <li>• Functions: dot area (%), dot size (dot diameter), screen ruling (lines/cm or lines/inch), line Width, edge factor, dot void factor, mottle, visual analysis, digital zoom (2x), characteristic curve</li> <li>• Measurement samples: flexo plates, masked plates, offset plates (positive and negative), paper, film, foil</li> <li>• Sensor RGB camera 640 x 480</li> <li>• Resolution sensor 10'000 ppi</li> <li>• Target size approx. 1.5 x 1.1 mm, (0.6 x 0.43 inch)</li> <li>• Illumination RGB (Auto Selection)</li> <li>• Screen ruling range (AM) 32-60 l/cm, 80 - 150 lpi</li> <li>• Repeatability +/- 0.5%</li> <li>• Measurement time &lt; 1 sec.</li> </ul>
<p><b>Equipment for chemical</b></p>	<p><b>Thermogravimetric unit TA instrument Q500:</b></p>



<p><b>characterization</b></p>	<ul style="list-style-type: none"> <li>• Temperature Range: Ambient to 1000 C</li> <li>• Isothermal Temperature Accuracy: 1 C</li> <li>• Isothermal Temperature Precision: 0.1 C</li> <li>• Continuous Weighing Capacity: 1.0 g</li> <li>• Sensitivity: 0.1 ug</li> <li>• Weighing Precision: 0.1 ug</li> <li>• Heating Rate: 0.1-100 C/min</li> <li>• 30-position autosampler</li> </ul> <p><b>Differential scanning calorimeter Mettler Toledo DSC 823e:</b></p> <ul style="list-style-type: none"> <li>• Ceramic sensor plate guarantees robustness and design flexibility</li> <li>• Measurement with 56 (FRS5) or 120 (HSS7) thermocouples for high resolution and unsurpassed sensitivity</li> <li>• Digital resolution of 16 million points</li> <li>• Circular thermocouple arrangement for excellent baseline stability without mathematical data manipulation</li> <li>• Modular design ensures future access to entire range of product options</li> <li>• Broadest dynamic measurement range for safety investigations</li> <li>• Various cooling options and choice between two furnace options to match application needs</li> </ul> <p><b>FTIR spectrometer Perkin Elmer Spectrum One:</b></p> <ul style="list-style-type: none"> <li>• Wavelength range 7,800 – 350 cm<sup>-1</sup> with KBr beamsplitter</li> <li>• Resolution: 0.5 cm<sup>-1</sup> to 64 cm<sup>-1</sup></li> <li>• Wavelength accuracy: 0.1 cm<sup>-1</sup> at 1,600 cm<sup>-1</sup></li> <li>• Signal to noise ratio: 30,000/1 rms, 6,000/1 p-p for a 5 second measurement and 100,000/1 rms, 20,000/1 for a 1 minute measurement</li> <li>• Available OPD velocities: 0.1, 0.2, 0.5, 1 and 2 cms<sup>-1</sup></li> <li>• Used crystal: Diamond/ZnSe</li> </ul> <p><b>EDS unit:</b></p> <ul style="list-style-type: none"> <li>• Quorum Technologies Sputter Coater SC7620</li> <li>• TESCAN SEM VEGA TS 5136 MM Oxford Instruments Si(Li)EDS INCA 250 device</li> </ul>
<p><b>Device for measurement and calculation of surface properties</b></p>	<p><b>Goniometer Dataphysics OCA 30:</b></p> <ul style="list-style-type: none"> <li>• Sample table dimensions: 100 x 100 mm</li> <li>• Traversing range of x-y-z sample table: 100 x 100 x 50 mm</li> <li>• Measuring range for contact angles: 0...180 °; ± 0.1 ° measuring precision of video system</li> <li>• Measuring range for surface and interfacial tensions: 1·10<sup>-2</sup>... 2·10<sup>3</sup> mN/m, resolution: min. ± 0.05 mN/m</li> <li>• Electronic positioning accuracy: ± 0.01 mm in the sample plane, ± 0.005 mm perpendicular to the sample plane</li> <li>• Max. sample weight: 3.0 kg</li> <li>• Optics: 6-fold zoom lens (0.7 - 4.5 magnification) with integrated continuous fine focus (± 6 mm)</li> <li>• Video system: CCD camera with a resolution of max.</li> </ul>

	<p>1600x1240 pixels (768x576 pixels standard), FOV 1.75 x 1.4–11.7 x 9 mm, image distortion &lt; 0.05%</p> <ul style="list-style-type: none"> <li>• High-performance image processing system with 132 MB/s data transfer rate (compatible with Euronorm CCIR and US standard RS-170), 50 images per second</li> <li>• Measuring techniques: sessile and captive drop method, tilting table/base method, pendant and oscillating drop method, lamella method on test spheres and rods</li> </ul>
<b>Equipment for the quality analysis of test prints</b>	<p><b>Plate reader ICPlate II:</b></p> <ul style="list-style-type: none"> <li>• Functions: dot area ( % ), visual analysis</li> <li>• Measurement samples: standard offset plates, processless plates, polyester plates, positive and negative plates, AM screening, FM screening, hybrid screening</li> <li>• Ring illumination</li> <li>• Illumination colors R</li> <li>• Screen ruling range (AM): 26 – 147, 65 – 380 lpi</li> <li>• Dot size range (FM): 10 µm – 50 µm</li> <li>• Repeatability: ± 0.5% (typ.)</li> <li>• Measurement time: 3 sec (typ.)</li> </ul> <p><b>X-Rite 939 SpectroDensitometer:</b></p> <ul style="list-style-type: none"> <li>• Measuring geometry and area: 0/45°, DRS spectral engine, choice of aperture: 4mm, 8mm, 16mm</li> <li>• Receiver: blue enhanced silicon photodiodes</li> <li>• Light source: gas-filled tungsten lamp, approx. 2856°K (corrected for D65 illuminant)</li> <li>• Illuminant types: A, C, D50, D65, D75, F2, F7, F11, &amp; F12</li> <li>• Standard observers: 2° &amp; 10°</li> <li>• Measurement range: 0 to 200% reflectance, 0 to 2.5D</li> <li>• Spectral range: 400nm – 700nm</li> <li>• Spectral interval: 10nm – measured, 10nm – output</li> </ul> <p><b>SaluTron D4-Fe:</b></p> <ul style="list-style-type: none"> <li>• Continuous measuring range: 0 - 5000 µm</li> <li>• Display of measured values: 0 - 999 in µm</li> <li>• Digital display resolution: <ul style="list-style-type: none"> <li>0.1 µm in the range of 0.0 - 99.9 µm</li> <li>1 µm in the range of 100 - 999 µm</li> <li>0.01 mm in the range of 1.00 - 5.00 mm</li> </ul> </li> </ul>
<b>Software support for modelling of flexographic printing plate properties</b>	Matlab R2014b with neural network toolbox
<b>Other equipment</b>	<p><b>White light interferometer Wyko NT 2000:</b></p> <ul style="list-style-type: none"> <li>• Range of objectives: 2X-50X with an additional zoom from 0.5-2X (the field-of-view (FOV) objective)</li> <li>• Measurement techniques: phase-shift interferometry (PSI),</li> </ul>

vertical-scanning interferometry (VSI)

- Tungsten halogen lamp (user-replaceable)
- Manual filter selection
- Integrated illuminator
- Interchangeable discrete field-of-view lenses
- Closed – loop precision vertical scanning assembly
- Vertical measurement range > 0.1 nm to 1 mm
- Vertical resolution: < 1 Å Ra
- RMS repeatability: 0.01 nm

***Durometer Zwick Roell:***

- Shore A and Shore D range
- Test stand with loading weight for Shore A
- Test table diameter: 90 mm, projection 70 mm
- Specimen thickness: max. 120 mm
- Contact force: 10 N/12.5 N
- Suitable for determining hardness of plastics and rubber to ISO 7619-1, ASTM D 2240, ISO 868, NFT 51109 and BS 903 Part A26

***OHAUS MB 45 moisture analyser:***

- 6 shut off criteria (manual, timed, 3 pre-defined auto settings, or user-set auto), 4 heating profiles (standard, ramp, step, fast), 50° to 200° C heating range (1°C increments)
- Display backlit dot matrix display
- Communication RS232 with GLP/GMP data output
- Halogen heat source, metal and ABS housing, metal pan support, metal pan handler, level indicator, in-use cover

***Chemicals used for swelling tests:***

- acetone (capillary GC grade), ethyl acetate (ACS grade), toluene (ACS reagent)

### 3.3. Measurement and analysis methods

#### 3.3.1. Chemical methods for photopolymer material analysis

- Fourier transform infrared spectroscopy - attenuated total reflectance (FTIR-ATR)

FTIR-ATR spectroscopy is a technique used to identify the presence of certain functional groups in the molecule [41, 42]. IR radiation does not have enough energy to induce electronic transitions in a sample. Therefore, absorption of IR is restricted to compounds with small energy differences in the possible vibrational and rotational states which are specific for different functional groups and bonds. Vibrations and rotations at a certain wavelength in the IR area are detected by IR spectrometry and can help in determining molecular composition and impurities in the sample [43]. FTIR-ATR is a characterization technique which can be used to obtain an infrared spectrum of a solid, liquid or gas, with the specific frequencies at which the chemical bonds in the sample vibrate due to the IR radiation.

In this research, FTIR-ATR was used in order to primarily identify the changes in the representation of the oxygen-containing and CH<sub>2</sub> and CH<sub>3</sub> bonds of the photopolymer material exposed to UV post-treatments. The interpretation of FTIR-ATR spectra was used to back up, explain and integrate the results obtained by other measurement and analysis techniques used in this work.

- Energy dispersive X-ray spectroscopy (EDS)

EDS is a technique for detecting X-rays that are produced by a sample exposed to electron beam and analyses the elemental composition of the sample. EDS has a sensitivity of > 0.1% for elements heavier than carbon and is joined with scanning electron microscopy (SEM) [44]. Electron beams which enter the sample cause the ejection of the electrons from the atoms. The resulting electron vacancies are filled by electrons from a higher state, and an X-ray is emitted to balance the energy difference between the two electrons' states (Figure 28.). Each element has characteristic emitted X-ray energy (peaks). Moreover, elements can have more than one characteristic peak, and some peaks from different elements can overlap. The spectrum of X-ray energy is used to determine the elemental composition of the sampled volume [45].

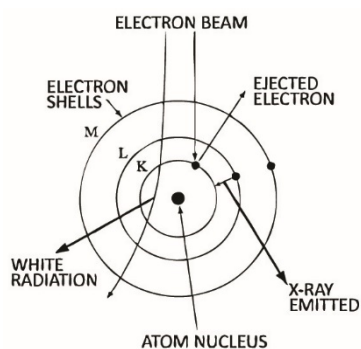


Figure 28. Principle of energy-dispersive X-ray spectroscopy

EDS was used to identify the ratio of carbon to oxygen in tested printing plate samples. After coating the samples with platinum and gold dust in Quorum Technologies Sputter Coater SC7620 in order to make them responsive to electron beam, they were put in the TESCAN SEM VEGA TS 5136 MM unit, where the Vega program support was used to obtain the results of the carbon and oxygen mass portions in order to support the FTIR analysis and identify the influence of the UV treatments on the photopolymer material.

- Normalized degree of swelling of photopolymer material

Swelling measurements were performed by gravimetric method [46], in a controlled environment with a constant temperature of 25 °C. Ethyl acetate (ACS grade), toluene (ACS grade) and acetone (ACS grade) were used as a swelling agents due to the different types and strengths of their molecular bonds, and therefore different impact on the photopolymer material. Named swelling agents cause swelling and partial dissolving of the photopolymer material used in the printing plate production. Furthermore, ethyl acetate has a regular application in flexography, specifically in the composition of printing inks and as a solution for cleaning the ink from the printing plate [17]. Its usage needs to be therefore regulated in terms of the concentration in the pigments and washing agents. Swelling properties of the photopolymer material in acetone and toluene were used to gain more detailed insight in the photopolymer swelling behaviour.

Photopolymer samples were immersed in the ethyl acetate, toluene and acetone for periods up to 420 minutes, after which the weighing showed that the equilibrium of swelling was reached. Normalized swell ratio ( $M_t$ ) for control periods of 5, 15, 30, 60, 90, 120, 180, 300 and 420 minutes of immersion were calculated using Eq. 5:

$$M_t = \frac{m_t - m_0}{m_0} \cdot 100\% \quad (5)$$

where  $m_t$  stands for the mass of the swollen polymer at a time  $t$ , and  $m_0$  for the mass of the dry polymer sample before the immersion. After immersions, samples were dried at 80 °C by means of OHAUS MB 45 moisture analyser, after which the solvent ratio in the sample decreased to 0.23% and stabilised. Samples were then weighted again to determinate the mass loss after the swelling.

### 3.3.2. Thermal analysis of photopolymer material

- Thermogravimetric analysis (TGA)

TGA is used as a technique to characterize materials used in various applications. It is a technique in which the weight of a specimen is monitored as a function of temperature or time [47-49]. The sample specimen is subjected to a controlled temperature program in a controlled atmosphere [50-52]. Thermogravimetric analysis (TGA) was carried out on TA Q500 instrument at a temperature range from 25 °C to 900 °C at a heating rate of 10°Cmin<sup>-1</sup> under the nitrogen atmosphere (50 cm<sup>3</sup>min<sup>-1</sup>). The weight of the specimens was about 10 mg. The rate of mass loss of the photopolymer material was displayed in thermal curves enabling the analysis of the amount of the residue after the heating and thermal stability and degradation of the photopolymer material exposed to various durations of UV post-treatments.

- Differential scanning calorimetry (DSC)

In DSC analysis, a sample of known weight is heated or cooled, and the changes in its heat capacity are tracked as changes in the heat flow. This enables the detection of transitions such as melts, glass transitions, phase changes, and curing [53, 54].

In this thesis, DSC was used to display changes of photopolymer material's heat capacity in dependence on temperature [55]. DSC measurements were performed using a Mettler Toledo DSC 823e. Specimens of the weight of ca. 10 mg were put in the DSC unit and analysed in order to characterize transitions in photopolymer material and detect potential changes in those transitions caused by variations of UV post-treatments (cross-linking, degradation). Heat effects as a function of temperature were detected in the interval between 140 °C and 340 °C.

### 3.3.3. Measurement and analysis methods of photopolymer surface properties

- Contact angle measurement

On the printing plate samples contact angles of different probe liquids and surface free energy were analysed by means of goniometer Data Physics OCA 30 [56]. Contact angle and surface free energy of the probe liquids are the parameters which are then used to calculate the surface energy of the printing plate samples. Three probe liquids of known surface energy were used for the measurements: water, glycerol and diiodomethane (Table 4).

Contact angle was measured using Sessile drop method, ten times on each sample, on the different parts of the printing plate (Figure 29.).

Table 4. Surface free energy ( $\gamma_{lv}$ ) and their dispersive ( $\gamma_{lv}^d$ ) and polar ( $\gamma_{lv}^p$ ) components for probe liquids

Liquid	Surface free energy ( $\text{mNm}^{-1}$ )		
	$\gamma_{lv}$	$\gamma_{lv}^d$	$\gamma_{lv}^p$
Diiodomethane (Ström et al.)	50.8	50.8	0.0
Glycerol (van Oss et al.)	64.0	34.0	30.0
Water (Ström et al.)	72.8	21.8	51.0

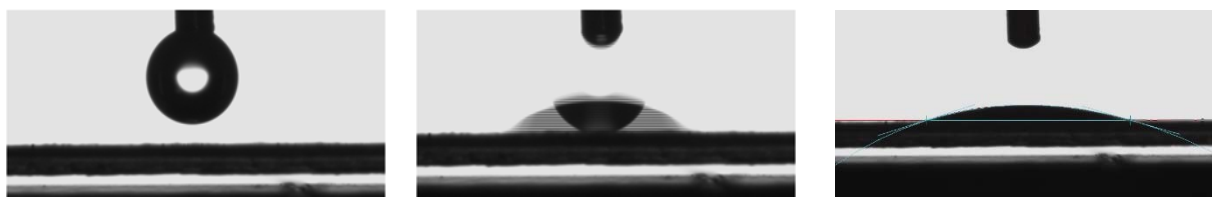


Figure 29. Contact angle measurement using sessile drop method

The shape of the probe liquid drops was a spherical cap, and the volume of the drops was  $1 \mu\text{m}^3$ . All measurements of the contact angle on the samples were performed in the same moment after the drop touched the photopolymer surface - with delay of 10 frames, and average value was calculated [57].



- Surface free energy calculation

Surface free energy was calculated using OWRK method, applicable for polymer, aluminium and coatings characterization [57]. After obtaining the values of contact angles for each probe liquid, mean values of contact angle for each sample were calculated. Results of the contact angle measurements enable calculation of the surface free energy, its polar and dispersive component (Eq. 6):

$$\frac{(1 - \cos \theta) \cdot \gamma_s}{\sqrt[2]{\gamma_l^D}} = \sqrt{\gamma_s^P} \sqrt{\frac{\gamma_l^P}{\gamma_l^D}} + \sqrt{\gamma_s^D} \quad (6)$$

where  $\gamma_s$  is surface tension of the solid,  $\gamma_l$  is the surface tension of the liquid,  $\gamma^d$  dispersive part of surface tension,  $\gamma^p$  polar phase of surface tension, and  $\theta$  is the contact angle [58].

### 3.3.4. Roughness measurement and display of photopolymer surface

- White light interferometry

Roughness measurements on the samples were performed by means of the white light interferometry on WYKO NT - 2000 White Light Interferometer. WYKO NT- 2000 is used to profile objects (structures) by using interferometry. The profiles and surfaces of the structures can be measured without the physical contact with the sample, which can greatly minimize the chance of destroying the fragile structures [59]. Software support for WYKO NT – 2000 can be used for the analysis of samples which requires optical or other methods (calculation of coverage value, dimensions of the elements, approximation of the film thicknesses, etc.).

White light interferometry was used for roughness measurements in this thesis, because of its advantage of the non-contact measurement and therefore increased precision compared to the mechanical roughness measurement. Mechanical roughness measurement was not suitable for the photopolymer surface due to the flexibility of the photopolymer material.

Furthermore, white light interferometry can be used to obtain a vivid display of the examined surface. Therefore, it was also used in order to visually examine photopolymer samples exposed to UV-ozone radiation and check if any damage appeared on the surface, which was expressed after prolonged UV-ozone treatment (Appendix 4).

### 3.3.5. Optical methods for printing plate and print evaluation

- Microscopy

Images of the fine lines and screen elements on test prints were observed by Olympus BX51 microscope (Figure 30.) [60].

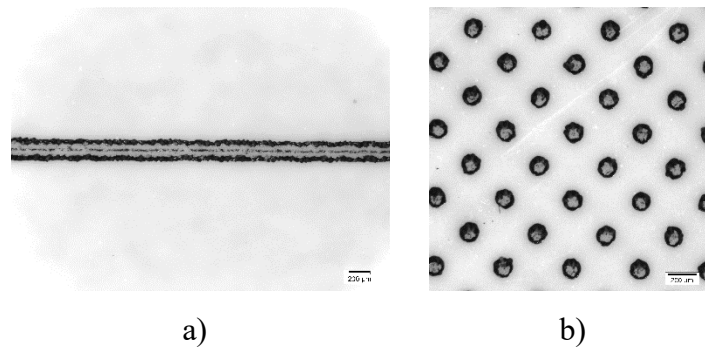


Figure 30. Images with magnification of 50x obtained by Olympus BX51 of:  
a) fine lines and b) screen elements of 10% nominal coverage value on prints

By using its program support for image adjustment and analysis, widths of the fine lines on prints were compared in order to analyse the influence of UV treatments on the quality of the prints. Furthermore, screen elements on test prints were observed in order to examine their regularity and shape as a consequence of different durations of UV treatments.

For the analysis of the printing elements' formation, 3D microscope AniCAM was used. AniCAM microscope can be used for the flexographic printing plate, gravure printing cylinder and the anilox roller analysis. It was used to display the 3D image of the surface by capturing its layers based on changes in focus, and then merge them.

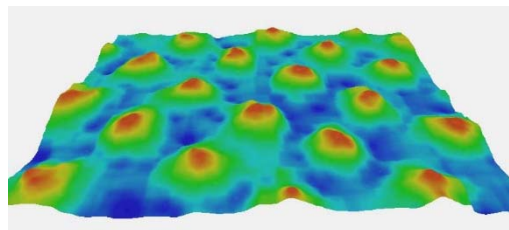


Figure 31. 3D image of the photopolymer printing plate  
with elements of 5% coverage value

Figure 31. presents the 3D display of the flexographic printing plate surface. Different colors are assigned to different height (red – highest area of the surface, blue – deepest area).

AniCAM can also display the cross-section of the selected area. The obtained images were used to compare formed printing elements on different types of photopolymer material, and the topography of different printing plates in general.

- Coverage value and optical density measurements on printing plates ad prints

Covearge value measurements of the control strips on the printing plate samples were performed by means of X-Rite vipFLEX device. Due to its transparency mode, vipFLEX is effective in analysis of both flexographic printing plates and prints on the transparent foils [61]. However, due to the algorithm for the coverage value calculation, it was not as effective for the flexographic prints evaluation, specifically in low or high coverage area.

Therefore, IC Plate II was used for the measurement of coverage values on the prints [62]. Although it is a portable device primarily intended for the offset printing plate measurements, it has an integrated mode for measurement on the printing substrate as well. Its precise measurement of coverage values on test prints examined in this thesis enabled obtaining precise results even in the coverage area higher than 95%.

Optical density was calculated by X-Rite 939 SpectroDensitometer [63] in order to detect the changes caused by variations of UV post-treatments which could affect the visual impression of the print.

Printed ink layer thickness was measured by means of SaluTron D4-Fe device. The gauge SaluTron D4-Fe based on the magnetic induction principle measures all nonmagnetic coatings such as synthetics, lacquers, enamels, copper, chromium, zinc, etc. on steel or iron.

Coverage values, optical density and ink layer thickness on prints were measured on differents spots 20 times to ensure correct calculations of the error.

Results of the measurements were used to identify the influence of printing plate parameters, subjected to change during variations of the UV post-treatment process, on the quality of prints.

### 3.3.6. Modelling methods

- Least squares in matrix form

In this thesis, least squares were used to form a model of influencing parameters in the post-treatment process related to printing plate and print properties. Least squares are often used as a robust fitting model for one or more parameters which influence the dependent variable [64]. In practice, the situation is often more involved in the sense that there exists more than one variable that influences the dependent one. In these situations a simple regression may be misleading. This is the case in modelling the influence of the UV post-treatments on the surface free energy components of photopolymer material and the quality of test prints, as well. The results of the research show that influencing parameters on the observed samples include hardness, roughness, carbon/oxygen ratio and changes in the dynamics of the crosslinking process. However, due to the complexity and synergy of these parameters, just by observing the diagrams, it is hard to perceive the „weight“ of each changing parameter in order to get a detailed and complete insight into the process. Therefore, least squares in matrix form will be applied for modelling the functional parameters of the printing plate's post-treatment process and the parameters of test print quality.

The system for the application of least squares [65]:

Let the predetermined system  $Ax = b$ , be composed of  $m$  equations with  $n$  unknowns, where  $m > n$ . As the norm of the vector  $x$  is defined as  $\|x\|^2 = x^T x$ , the problem of least squares  $\|Ax - b\|^2 \rightarrow \min$  can be written as  $(Ax - b)^T (Ax - b) \rightarrow \min$ .

Let  $Q$  be defined by Eq. 7:

$$Q(x) = \|Ax - b\|^2 = (Ax - b)^T (Ax - b) \quad (7)$$

$$= x^T A^T A x - b^T A x - x^T A^T b + b^T b$$

$$= x^T B x - 2x^T c + \beta,$$

$$\text{where } B = A^T A, c = A^T b, \beta = \|b\|^2$$

In the multidimensional case, this corresponds to  $x = B^{-1} c$ , hence  $x$  is the solution to system  $Bx = c$ , respectively  $A^T A x = A^T b$

This equation is called the normal equation. Furthermore, vectors  $Ax$  and  $Ax-b$  are perpendicular to each other (Eq. 8):

$$(Ax) \cdot (Ax - b) = (Ax)^T(Ax - b) = x^T A^T(Ax - b) = 0 \quad (8)$$

Geometrically it means that vector  $Ax$  is an orthogonal projection of vector  $b$  on set  $\{Ay: y \text{ is arbitrary}\}$ . Furthermore, vectors  $Ax$ ,  $b$  and  $Ax-b$  form a right triangle with hypotenuse  $b$ .

The solution to least square problem  $x$  is also called the quadratic approximation of the  $Ax = b$  system in terms of the least squares. The quality of adjustment is given by Eq. 9:

$$q = \sqrt{\frac{Q(x)}{Q(0)}} = \frac{\|Ax-b\|}{\|b\|} \quad (9)$$

Since  $b$  is hypotenuse of the right triangle with sides  $Ax$ ,  $Ax-b$  and  $b$ , thus  $q$  is always in the interval  $[0, 1]$ .

If  $q = 0$ , then the adjustment is the best possible, and  $x$  is the exact solution to the system  $Ax = b$ . If  $q$  has a small value, the adjustment is fine, and if the value of  $q$  is near 1, the adjustment is poor.

- Neural network

Neural networks (Figure 32.), with their ability to derive meaning from complicated or imprecise data, can be used to extract patterns and detect trends too complex to be noticed by conventional methods (2D and 3D diagrams, observation). A trained neural network can be thought of as an "expert" in the category of the information given to analyse. Neural network can then be used to provide projections given new situations of interest and predict the behaviour of a complex system [66].

Neural networks are very good at function fitting problems. A neural network with enough elements (called neurons) can fit the data with arbitrary accuracy. Neural networks are particularly well suited for solving non-linear problems. Given the non-linear nature of the most system behaviours in the real world, neural networks are a good tool applicable in solving many types of problems [67].

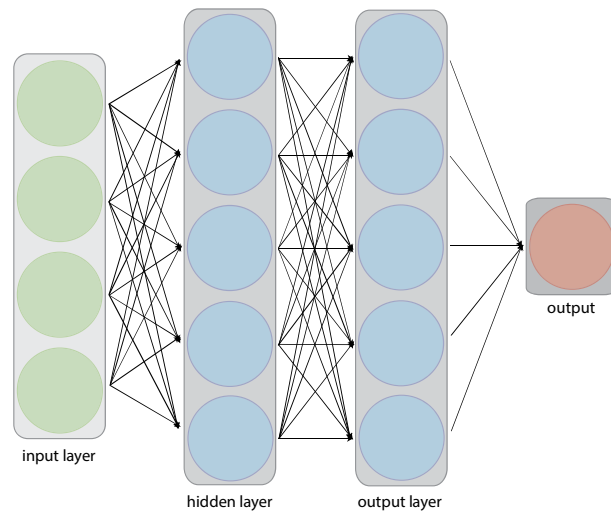


Figure 32. Neural network with two hidden layers

In this thesis, a neural network that can estimate the surface free energy of the photopolymer material in dependence on the UVA and UVC post-treatment will be applied. Neural network will be defined as a fitting problem, where known inputs are matched up to associated target outputs, and generated network will be able to generalize and accurately estimate outputs for inputs that were not used to design the solution.

# **4. RESULTS AND DISCUSSION**

## **4.1. Thermal, chemical and mechanical properties of photopolymer materials**

- 4.1.1. DSC analysis
- 4.1.2. TGA analysis
- 4.1.3. Hardness of printing plates
- 4.1.4. Swelling properties of photopolymer materials

## **4.2. Surface properties of photopolymer printing plates**

- 4.2.1. Roughness of printing plate surface
- 4.2.2. Surface free energy of printing plates
- 4.2.3. FTIR-ATR analysis of photopolymer surface layer
- 4.2.4. EDS analysis of photopolymer surface layer

## **4.3. Quality of prints and photopolymer printing plates related to reproduction process**

- 4.3.1. Topography of printing elements on printing plates
- 4.3.2. Microscopic displays of prints
- 4.3.3. Coverage values on prints
- 4.3.4. Optical density on prints
- 4.3.5. Thickness of printed ink layer



#### **4.1. Thermal, chemical and mechanical properties of photopolymer materials**

Thermal, chemical and mechanical properties of photopolymer materials are presented in a joint chapter of this thesis because they display the changes which occur both in the surface layer and in the core of photopolymer material. Changes occurring only in the surface layer of the printing plate are presented in chapter 4.2. Interpretation of the results and the discussion will show that prolonged UV post-treatment of photopolymer material results with two-phase system: surface and core of the photopolymer flexographic printing plate. This is important for separating the surface properties of the printing plate which will influence the ink transfer in the reproduction process from the properties which will influence printing plate's behavior during the engagement and its durability.

#### 4.1.1. DSC analysis

Results obtained by DSC analysis of different photopolymer materials pointed to the changes in the crosslinking process related to the duration of UVA and UVC post-treatment. DSC curves for different photopolymer materials have different number of onsets at different temperatures (Figures 33. – 38.).

Figures 33. and 34. present DSC curves for ACE Digital photopolymer material samples. One can see that the exothermic peak for the sample before UV post-treatments occurs at 203.77 °C, and the temperatures for the peaks of UVA and UVC post-treated samples show similar values. Occurred peaks can be related to the further heat-induced crosslinking in the material [68]. The energy of the first exotherm for sample treated with 10 minutes of UVA and UVC post-treatments (Figure 33.) equals 161.83% of the energy corresponding to the not treated sample, 23.04% for the sample treated with 20 minutes of UVA post-treatment, and 127.23% for the sample treated with 20 minutes of UVC post-treatment (Figure 34.).

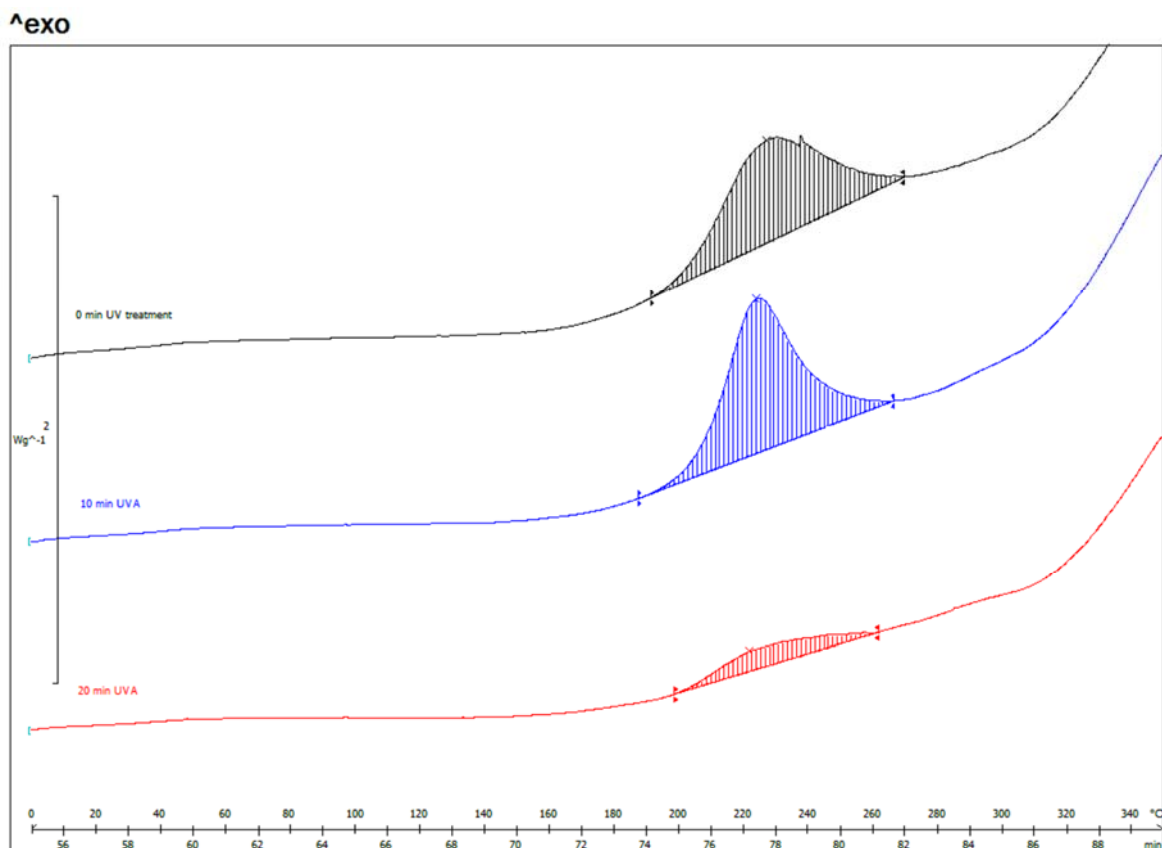


Figure 33. DSC curves for ACE Digital samples exposed to varied UVA post-treatment

Energies released in the exothermic reactions, as well as their onsets, peaks and endsets for ACE Digital samples are given in Table 5.

The maximal energy release for ACE Digital samples is present for the sample treated for 10 minutes of UVA and UVC post-treatments. This indicates that the crosslinking reactions take maximal effect for that sample. Figures 33. and 34. show that UVA and UVC post-treatments with prolonged duration (20 minutes) have different influences on ACE Digital photopolymer material samples.

Longest UVA post-treatment results with lower energy released in exothermic reaction compared to sample treated for 10 minutes of UVA and UVC post-treatments, while the longest UVC post-treatment results with minor decrease in the exothermic reaction energy. This was expected, since UVA radiation causes crosslinking in the photopolymer network and therefore leaves the sample with less crosslinkable compounds, while UVC radiation terminates the crosslinking reaction and could therefore enable secondary reactions involving radicals [69].

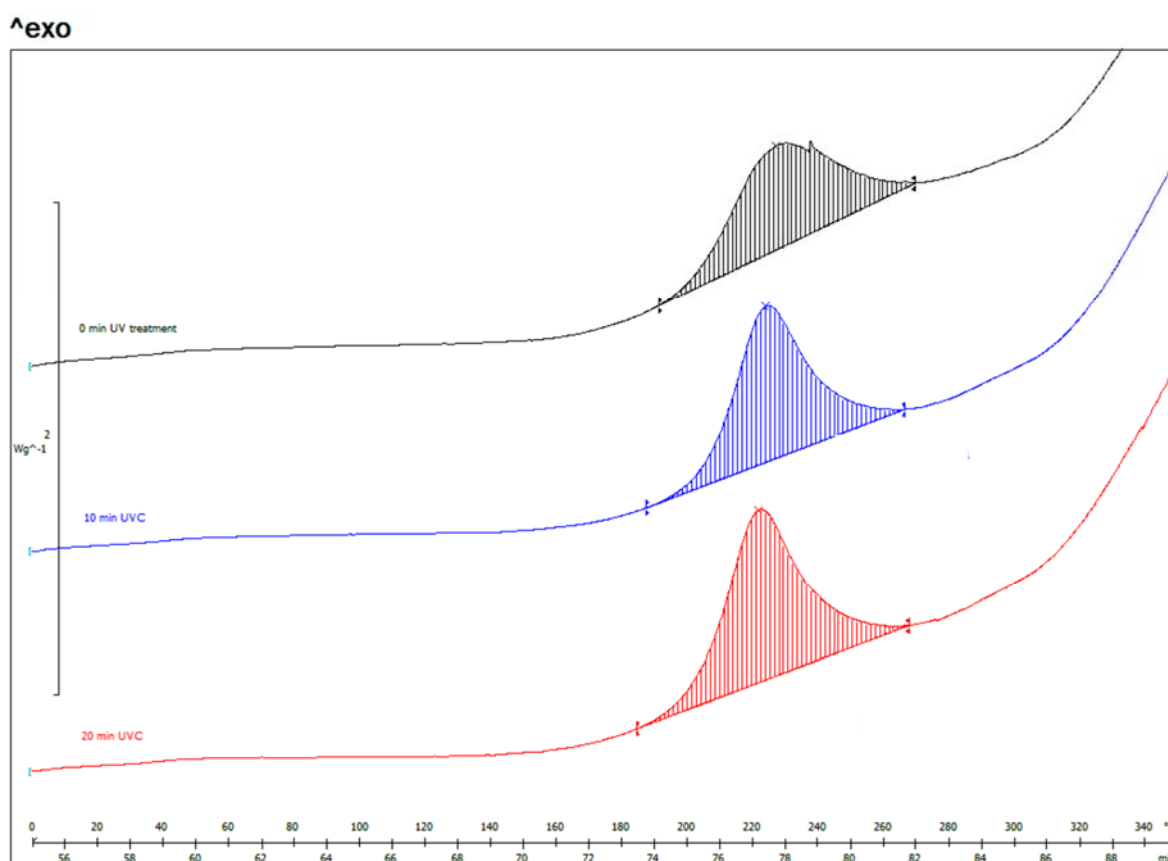


Figure 34. DSC curves for ACE Digital samples exposed to varied UVC post-treatment

Table 5. Characteristics of DSC curves for UV post-treated ACE digital photopolymer material

	0 min UV	10 min UV	20 min UVA	20 min UVC
<b>Integral (mJ)</b>	565.12	914.58	130.21	719.01
<b>Onset (°C)</b>	203.77	207.35	203.50	203.87
<b>Peak (°C)</b>	227.65	224.48	222.22	222.30
<b>Endset (°C)</b>	262.08	247.83	257.09	245.62

Figures 35. and 36. display the temperature shift of exothermic reactions in Digital MAX photopolymer flexographic printing plate exposed to various durations of UVA and UVC post-treatments. Photopolymer material not treated with any UVA and UVC post-treatments displays one peak at 235.30 °C, which points to the further heat-induced crosslinking reaction in the sample. However, with prolonged UV post-treatments separation to two exothermic peaks occurs.

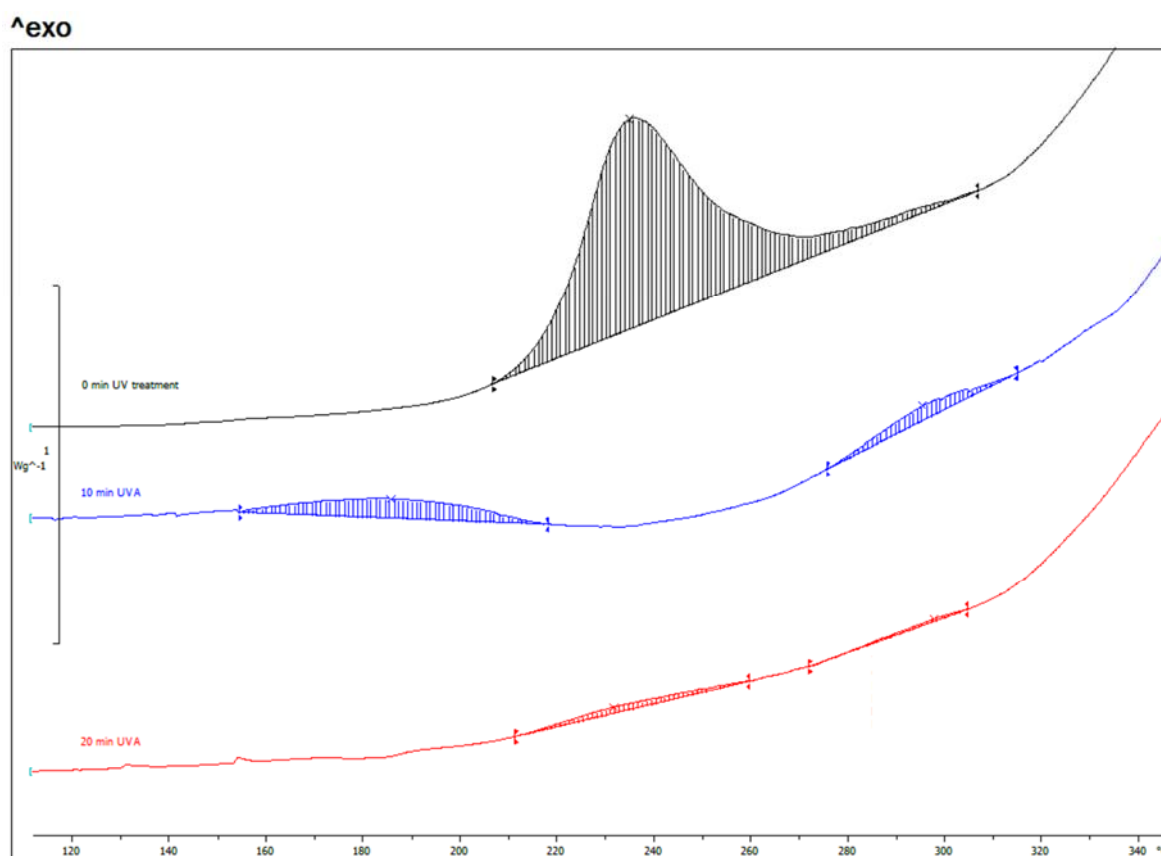


Figure 35. DSC curves for Digital MAX samples exposed to varied UVA post-treatment

The energy released in the exothermic reaction decreases, corresponding to the increase of the crosslinking degree in the samples. Energies of reactions, peaks, onsets and endsets are given in Table 6.

The first peak after 10 minutes of UVA and UVC post-treatments occurs at 185.96 °C, and at 232.10 °C after 20 minutes of UVA post-treatment (Figure 35. and Table 6). After 20 minutes of UVC post-treatment, the first exothermic peak occurs at 189.58 °C (Figure 36. and Table 6.). Significant shift of the first exothermic peak to higher temperature is displayed after 20 minutes of UVA post-treatment, while the second exothermic peak does not display significant shift. The energy for the first peak released in the exothermic reaction for sample treated with 10 minutes of UV post-treatments equals 13.28% of the energy corresponding to the not treated sample. The energy for the first peak released in the exothermic reaction for sample treated with 20 minutes of UVA post-treatments equals 2.98% of the energy corresponding to the not treated sample. Finally, the energy for the first peak released in the exothermic reaction for sample treated with 20 minutes of UVC post-treatment equals 12.64% of the energy corresponding to the not treated sample.

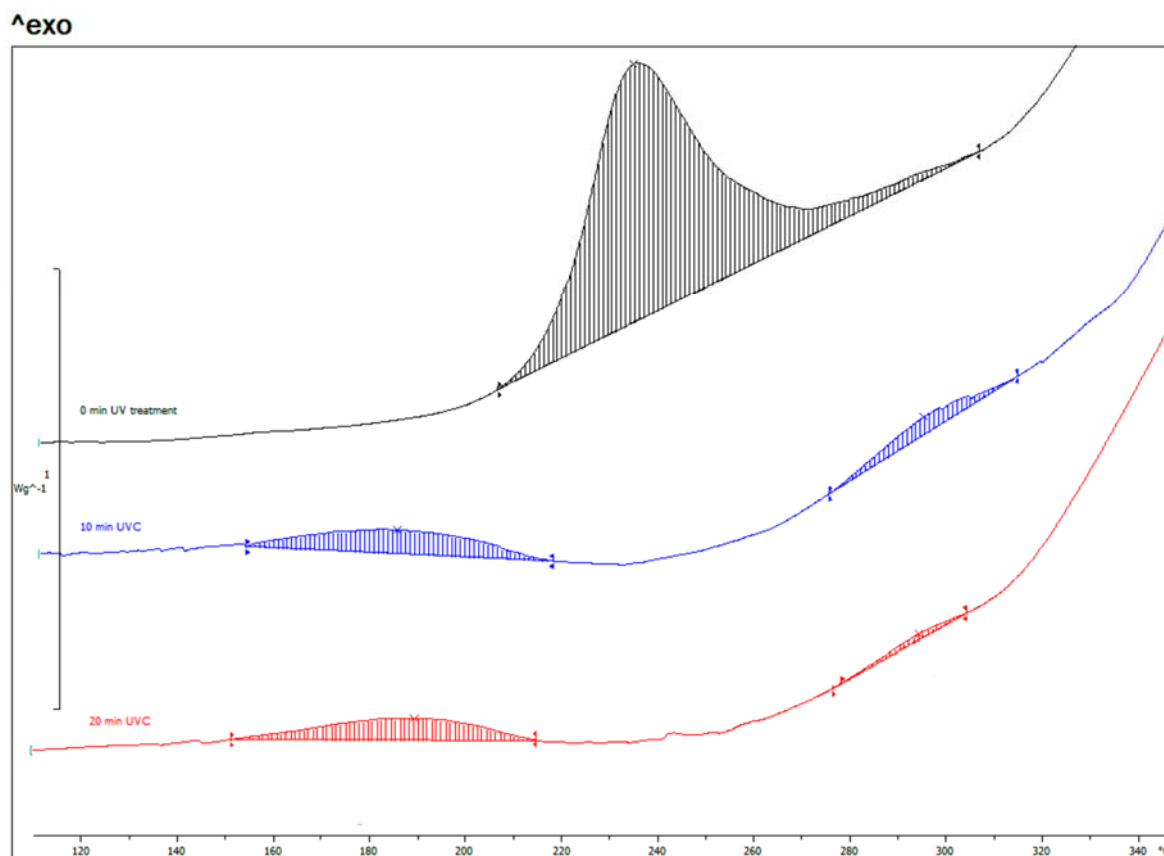


Figure 36. DSC curves for Digital MAX samples exposed to varied UVC post-treatment

The decrease of the released energy for 10 and 20 minutes of UVA post-treatment (Figure 35.) indicates that the smaller amount of non-crosslinked compounds remain in the photopolymer material after UVA post-treatments, since UVA radiation induces cross-linking in the sample and triggers the reaction of crosslinkable parts.

As the UVC post-treatment terminates the cross-linking reaction, there is no significant difference between first peaks for 10 and 20 minutes of UVC post-treatment (Figure 36.).

Table 6. Characteristics of DSC curves for UV post-treated Digital MAX photopolymer material

	0 min UV	10 min UV (1 <sup>st</sup> peak)	10 min UV (2 <sup>nd</sup> peak)	20 min UVA (1 <sup>st</sup> peak)	20 min UVA (2 <sup>nd</sup> peak)	20 min UVC (1 <sup>st</sup> peak)	20 min UVC (2 <sup>nd</sup> peak)
<b>Integral (mJ)</b>	785.13	104.28	39.65	23.41	5.11	99.21	10.28
<b>Onset (°C)</b>	218.62	154.65	278.62	211.47	272.19	186.82	283.38
<b>Peak (°C)</b>	235.30	185.96	295.67	232.10	297.97	189.58	294.65
<b>Endset (°C)</b>	262.78	211.36	306.72	260.16	305.28	213.38	304.62

Second peaks for Digital MAX samples occurring on DSC curves of UV post-treated samples around 295 °C point to the conclusion that UV post-treatment results with forming of the two-phase system: the surface and the core of the photopolymer material [41]. The second exothermic peaks visible at 10 and 20 minutes for both UV post-treatments could therefore correspond to the reaction involving the hydroxyl group, which is the only new bond appearing in the surface layer of the photopolymer material of UV-treated samples and is visible in FTIR-ATR spectra of the samples, as will be presented in 4.2.3.

Finally, DSC curves of Cosmolight QS samples show similar behavior as Digital MAX to a certain degree (Figures 37. and 38.). In Figure 36., it is shown that prolonged UVA post-treatment results with the decrease in the exothermic area, pointing to the higher crosslinking degree in the sample, with main exothermic peaks in range from 155.73 °C to 192.25 °C.

The energy released for the crosslinking in the exothermic reaction for sample treated for 10 minutes of UVA and UVC post-treatments equals 35.69% of the energy corresponding to the not treated sample and 10.14% for the sample treated for 20 minutes of UVA post-treatment; peaks, onsets and endsets being presented in Table 7.

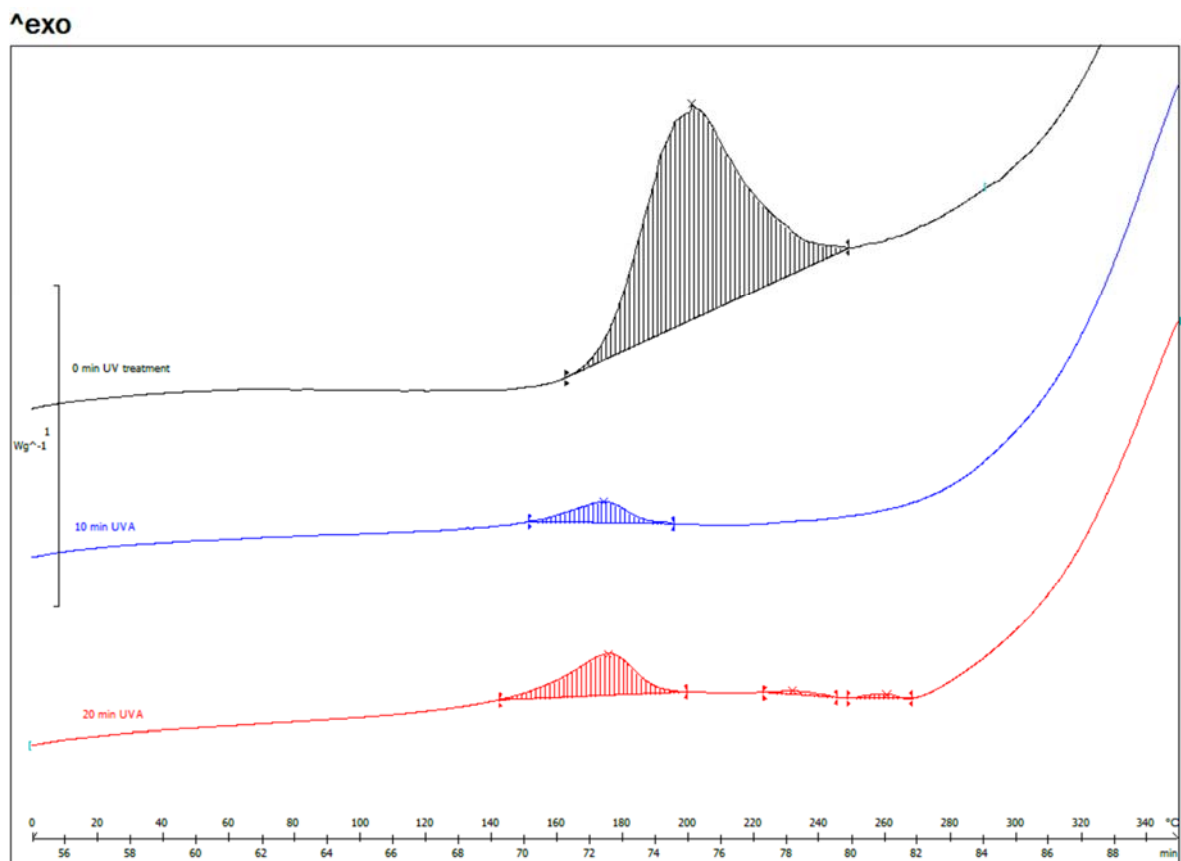


Figure 37. DSC curves for Cosmolight QS samples exposed to varied UVA post-treatment

Two additional low-energy exothermic reactions occur in the sample treated with 20 minutes of UVA post-treatment point to the secondary reactions. They could correspond to the formulation of photopolymer material of Cosmolight QS printing plate. Cosmolight QS, compared to two main components in the composition of the other two tested photopolymer materials, consists of three compounds which make the majority of the formulation: two types of synthetic rubbers and polyurethane methacrylate (Appendix 2).

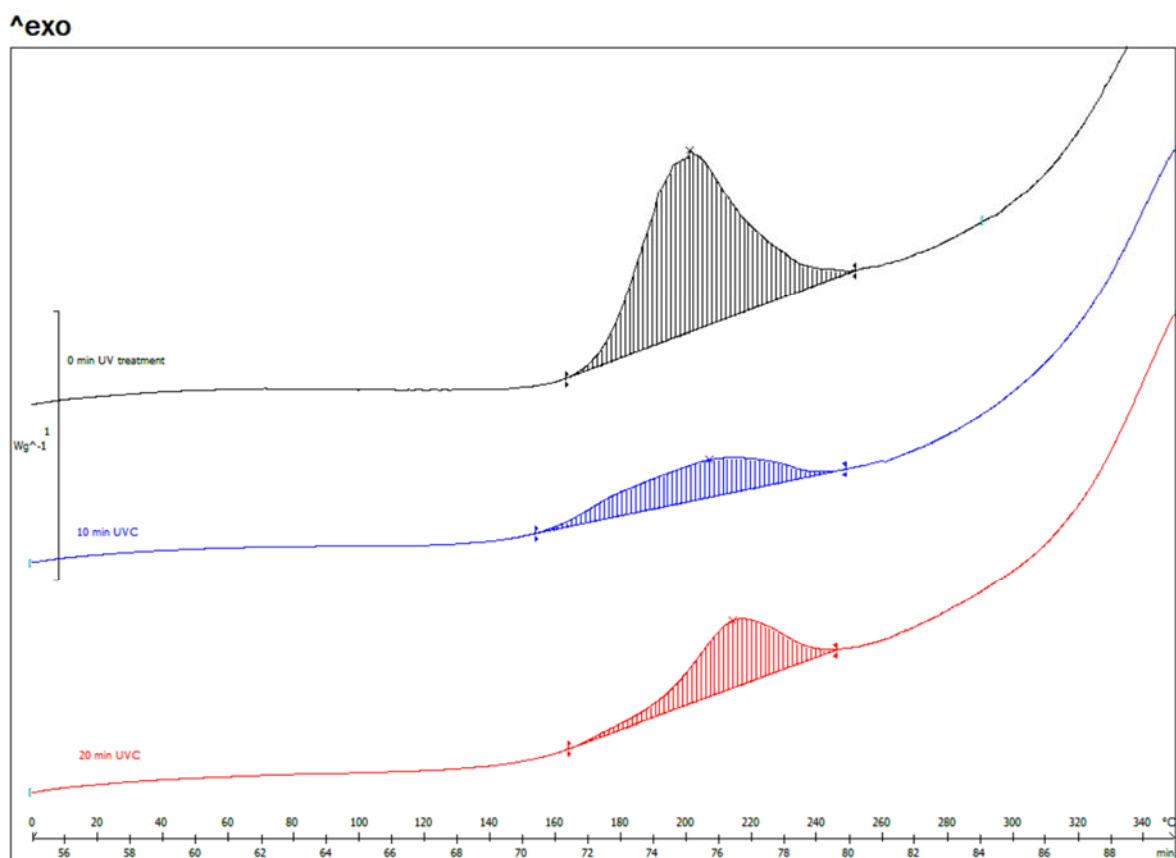


Figure 38. DSC curves for Cosmolight QS samples exposed to varied UVC post-treatment

DSC curves presented in Figure 38. show the decreased intensity of exotherms when UVC post treatment is prolonged. The energy released for the crosslinking in the exothermic reaction for sample treated for 10 minutes of UV post-treatment equals 35.69% of the energy corresponding to the not treated sample and 34.92% for the sample treated for 20 minutes of UVC post-treatment. This result confirms that prolonged UVC post-treatment has no considerable effect on the further process of crosslinking in the photopolymer material.

Table 7. Characteristics of DSC curves for UV post-treated Cosmolight QS photopolymer material

	0 min UV	10 min UV	20 min UVA (1 <sup>st</sup> peak)	20 min UVA (2 <sup>nd</sup> peak)	20 min UVA (3 <sup>rd</sup> peak)	20 min UVC
<b>Integral (mJ)</b>	1088.36	388.44	110.44	9.77	6.10	380.15
<b>Onset (°C)</b>	181.31	161.72	155.73	221.03	250.54	192.25
<b>Peak (°C)</b>	201.51	207.38	176.09	232.13	260.82	215.16
<b>Endset (°C)</b>	230.70	239.41	189.95	243.90	266.14	241.70



#### 4.1.2. TGA analysis

TGA analysis was performed in order to detect potential changes in thermal stability and thermal degradation rates [70] of photopolymer materials exposed to UVA and UVC post-treatments. Results are displayed in Figures 39. – 41.

In Figure 39. one can see TG (green) and DTG (blue) curves of ACE Digital samples which have been exposed to varied durations of UVA and UVC post-treatments. It is visible in TG curves that ACE Digital photopolymer material degrades in two stages [71] with maximal weight loss rate (DTG curves) at  $\sim 430\text{ }^{\circ}\text{C} - 435\text{ }^{\circ}\text{C}$ .

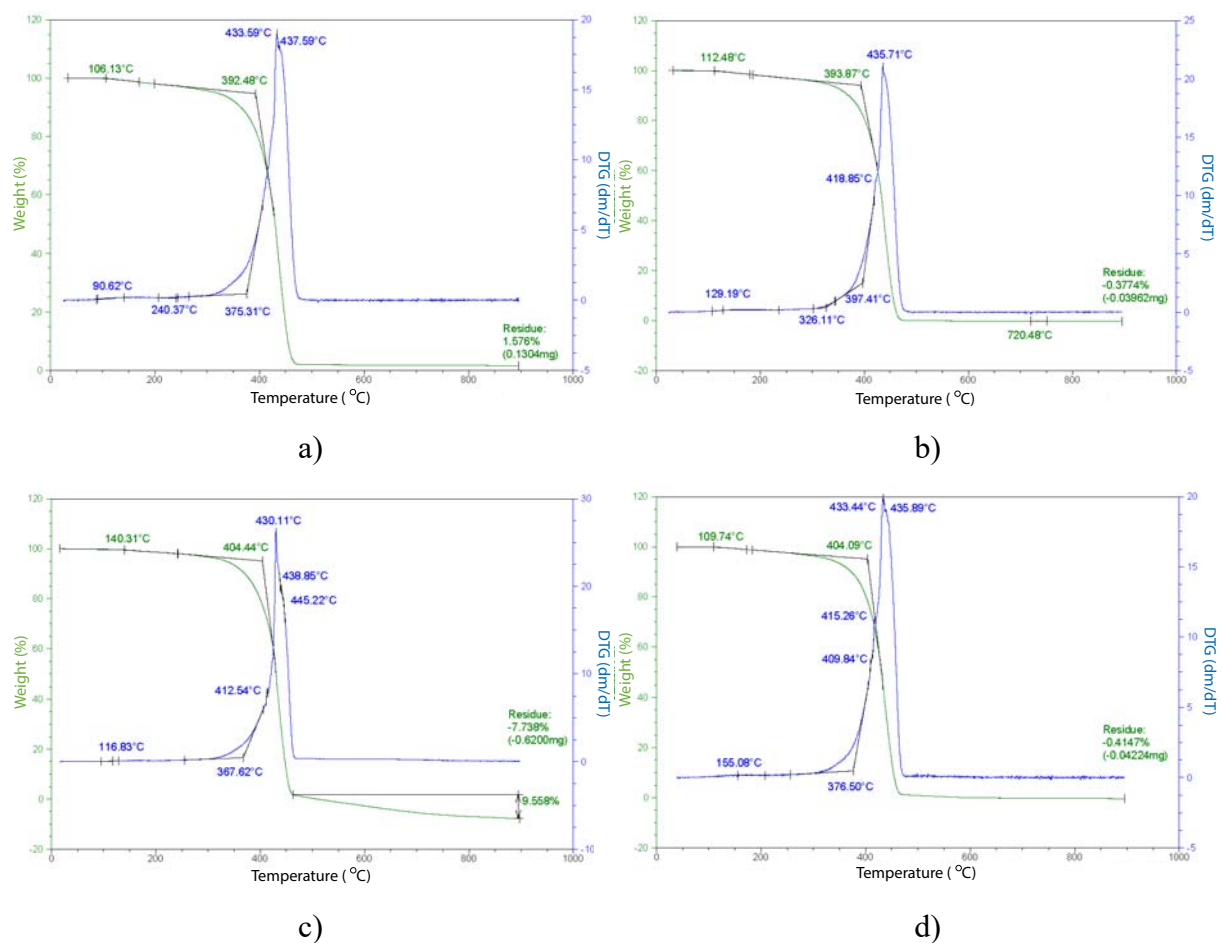


Figure 39. TG and DTG curves for ACE Digital photopolymer samples:

- a) non UV post-treated sample, b) 10 min UV post-treatment,
- c) 20 min UVA post-treatment, d) 20 min UVC post-treatment

Residual after thermal degradation is present only in the non post-treated sample (Figure 39.a), which could be the consequence of impurities present on/in the sample.

Furthermore, there is no trend shift of degradation temperatures to lower values with prolonged UV post-treatments, indicating that thermal stability of the material remains undiminished. Moreover, sample treated for 20 minutes of UVA post-treatment starts to degrade on higher temperature (140 °C compared to ~109 °C – 112 °C for other samples), which points to a higher crosslinking degree and higher network density in that sample, since volatile components, monomers and plasticizers can cause weight loss in that temperature range [72].

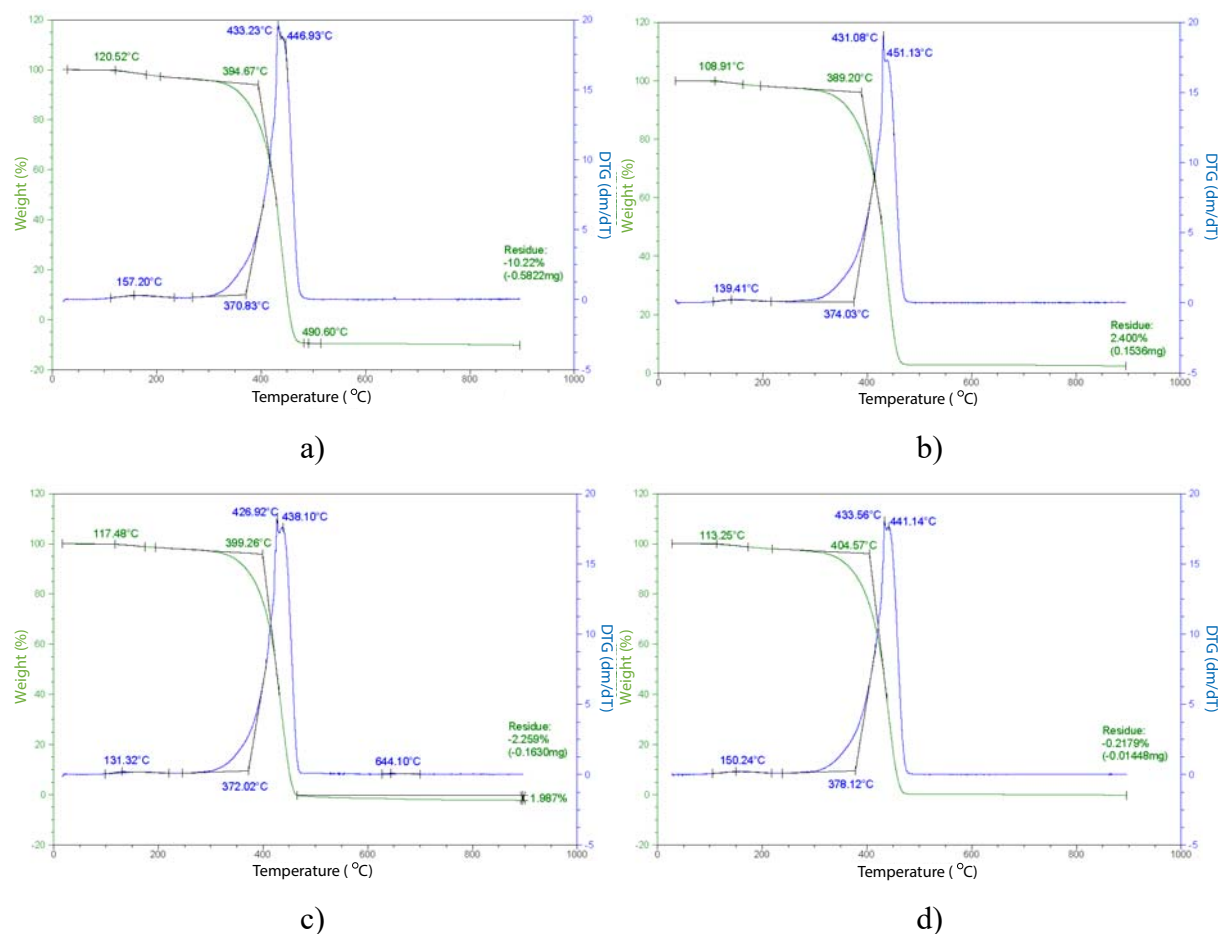


Figure 40. TG and DTG curves for Digital MAX photopolymer samples:

- a) non UV post-treated sample, b) 10 min UV post-treatment,
- c) 20 min UVA post-treatment, d) 20 min UVC post-treatment

Figure 40. presents TG and DTG curves of Digital MAX samples which have been exposed to varied durations of UVA and UVC post-treatments. Similar behavior compared to ACE Digital samples can be observed regarding maximal weight loss rate at ~ 427 °C – 433 °C and two-stage degradation, as well. The first stage of degradation starting at ~ 108 °C – 120 °C can, like in ACE Digital samples, be assigned to plasticizers and other thermally unstable

components that are not dependent on the crosslinking process and the duration of the UV post-treatment.

Figure 41. presents TG and DTG curves of Cosmolight QS samples which have been exposed to varied durations of UVA and UVC post-treatments. As a water-washable plate composed of water-dispersive system, TGA analysis of Cosmolight QS samples shows a bit different results than other two analysed types of photopolymer materials.

The degradation of Cosmolight QS samples occurs in three stages (TG curves), which can be assigned to differences in composition compared to ACE Digital and Digital MAX printing plates. ACE Digital and Digital MAX photopolymer materials are primarily composed of styrene-diene copolymer and acrylate phase, while Cosmolight QS consists primarily of synthetic rubber, liquid rubber and polyurethane methacrylate presenting a water-dispersive system [73].

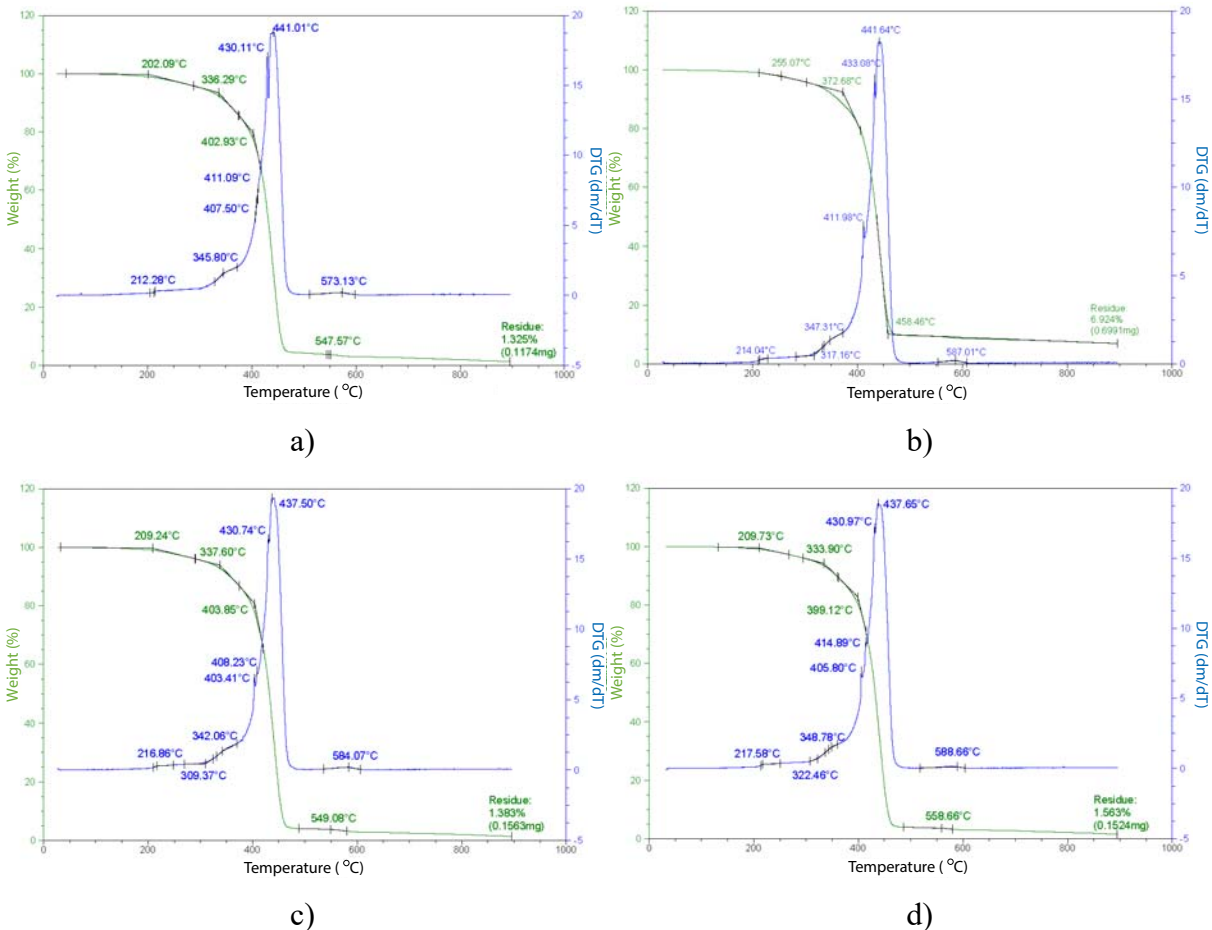


Figure 41. TG and DTG curves for Cosmolight QS photopolymer samples:  
 a) non UV post-treated sample, b) 10 min UV post-treatment,  
 c) 20 min UVA post-treatment, d) 20 min UVC post-treatment

Maximal weight loss rate occurs at ~ 437 °C - 440 °C for all samples.

The weight loss of Cosmolight QS samples, unlike the weight loss of ACE Digital and Digital MAX, starts above 200 °C which could be assigned to the fact that there is no plasticizer listed in the composition of Cosmolight QS, probably because of the liquid rubber present in the formulation. The structure of Cosmolight QS is therefore more thermally stable compared to other two types of printing plates.

### 4.1.3. Hardness of printing plates

Results of hardness measurements of photopolymer printing plates are displayed in Figure 42. Results show the increasing trend, which was expected due to the further crosslinking in the material volume and therefore increased network density [74]. Increased hardness of the printing plates will result with lower deformation of the printed elements during the engagement in the reproduction process. Specifically, UVC post-treatment causes more expressed increase in printing plate's hardness than UVA post-treatment.

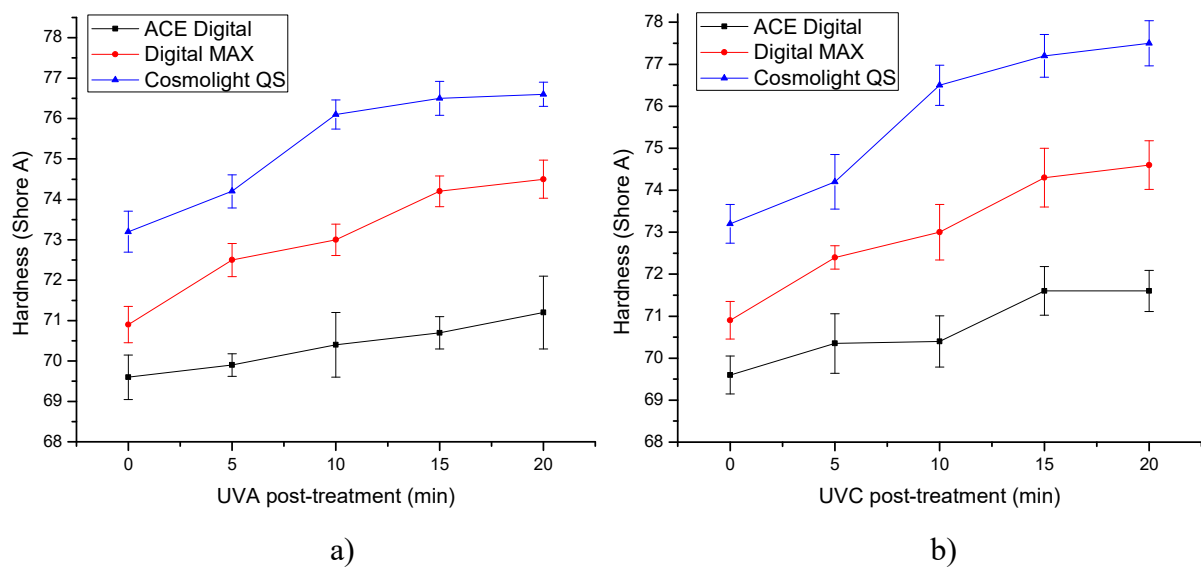


Figure 42. Changes of printing plate hardness in dependence on the duration of  
a) UVA post-treatment, b) UVC post-treatment

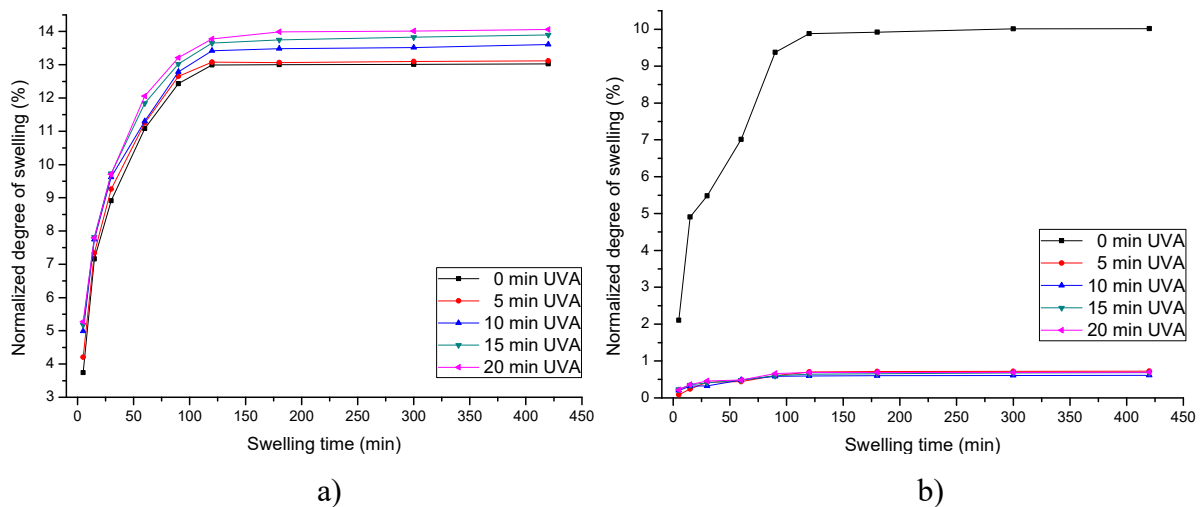
ACE digital printing plate displays the highest resistance to UV post-treatments in relation to changes in hardness, with maximal increase of 1.4 according to Shore A scale. This result supports the results obtained by DSC analysis and the statement that excessive UV radiation causes the migration of protective waxes to the surface, which will minimize the influence of the post-treatment on the core of the material.

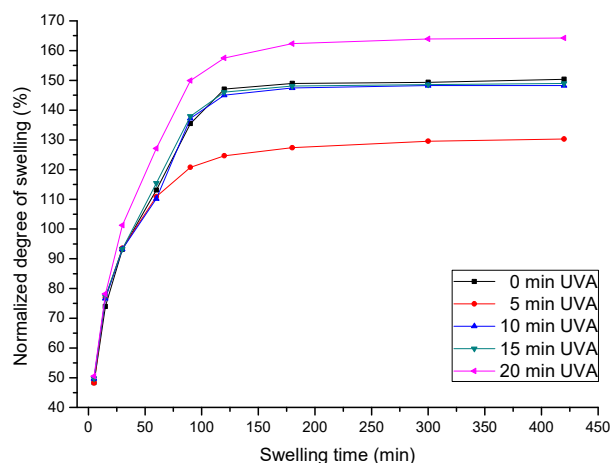
Maximal increase of the hardness for Digital MAX is 3.9 on Shore A scale, and for Cosmolight QS 4.2 on Shore A scale. Changes in hardness of the photopolymer material are relevant because they could, together with the changes of the printing plate's surface properties, have an effect on the quality of fine printed elements. Obtained results point to the conclusion that prolonged UV post-treatments, although causing different types of changes in photopolymer surfaces, have a similar impact on the core of the material.

#### 4.1.4. Swelling properties of photopolymer materials

Swelling experiments on photopolymer samples were performed in order to get an insight into the changes of photopolymer's cohesion parameters as a result of the UV post-treatments. When immersing the sample in the solvents of known solubility parameters, normalized degrees of swelling (Eq. 5) provide the information about the “compatibility” of the material and the specific solvent. Similar cohesion parameters of the immersed material with solubility parameters of solvent result in higher swelling degree and possible partial dissolving [75]. Results of swelling experiments are presented in Figures 43.- 48.

Normalized swelling degrees for UV post-treated ACE Digital samples can be observed in Figures 43. and 44. One can see that prolonged UVA post-treatment causes increase of swelling degree in acetone (Figure 43.a), which points to the increased compatibility of forces in the material and the forces in the acetone, and is an indicator of the changes in strength of chemical bonds in photopolymer material. The highest value of swelling degree in acetone is 14.06%, and is visible for the sample treated for 20 minutes of UVA post-treatment.





c)

Figure 43. Normalized degrees of swelling for UVA post-treated ACE Digital samples immersed in different solvents: a) acetone, b) ethyl acetate, c) toluene

Swelling degree in ethyl acetate (Figure 43.b) decreases with prolonged UVA post-treatment compared to the not treated sample, which is a valuable information if using inks and plate washing agents with ethyl acetate in their composition. Maximal normalized swelling degree in ethyl acetate depending on the duration of UVA post-treatment is 10.02% for not treated sample.

Swelling behavior in toluene (Figure 43.c) shows the most expressed swelling degree. Until 5 minutes of UVA post-treatment, swelling degree decreases, and then starts to increase, reaching 164.20% for 20 minutes of UVA post-treatment. This specific behavior can be related to the decrease of surface free energy, presented in 4.2.2.

UVC post-treatment has a similar influence on the changes of ACE Digital's swelling degrees (Figure. 44.). The difference in swelling dynamics compared to the samples treated with varied UVA post-treatment is visible for sample treated for 5 and 20 minutes of UVC post-treatment immersed in toluene (Figure 44.c).

Compared to the samples treated for 5 and 20 minutes of UVA post-treatment, there is no significant difference in swelling degrees of UVC post-treated samples with longer time of immersion. Obtained results are dependent on the solubility parameters of used solvents [76], presented in Table 8. They are specific for each solvent and predict if the observed material will form a solution with another material. The closer the solubility parameters of observed material and solvent, the more that material is likely to dissolve in that solvent.

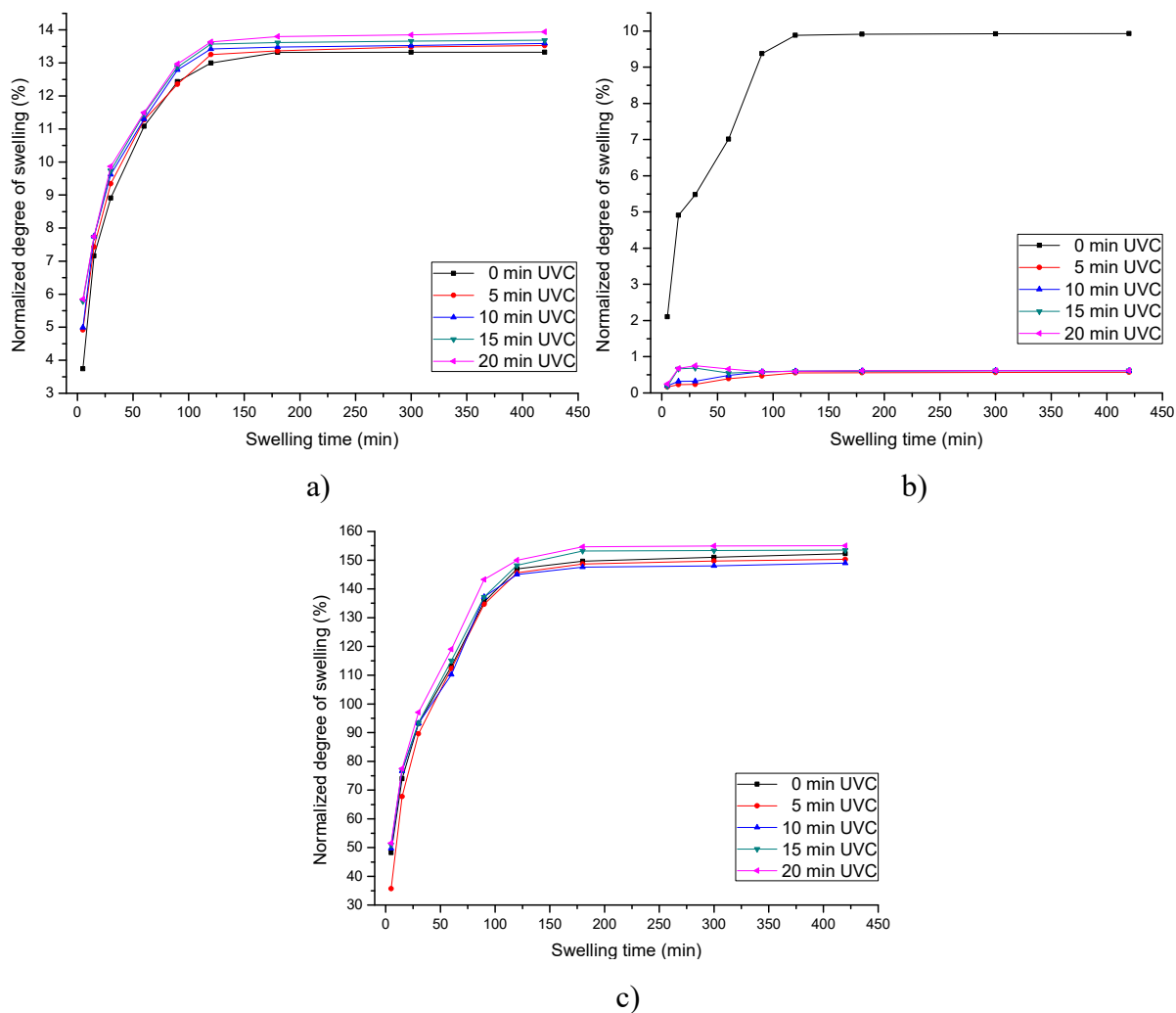


Figure 44. Normalized degrees of swelling for UVC post-treated ACE Digital samples immersed in different solvents: a) acetone, b) ethyl acetate, c) toluene

Table 8. Hansen solubility parameters for solvents used in swelling experiments

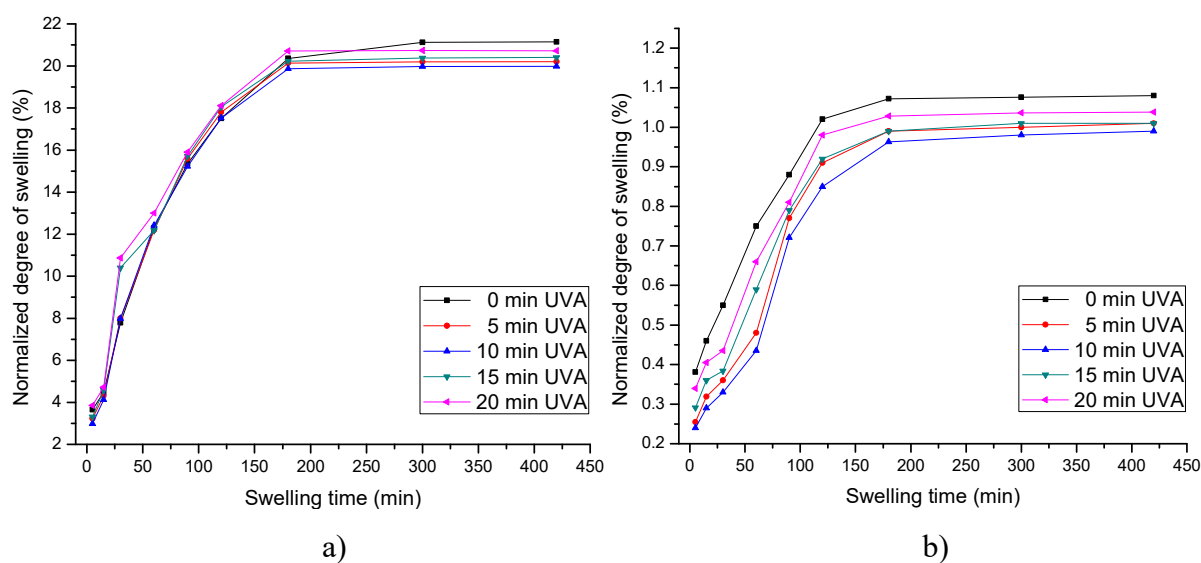
Hansen parameters for solvents at 25 °C (MPa <sup>1/2</sup> )	Acetone	Ethyl acetate	Toluene
<b>Total Hildebrand parameter (<math>\delta_t</math>)</b>	20	18.1	18.2
<b>Dispersion component (<math>\delta_d</math>)</b>	15.5	15.8	18
<b>Polar component (<math>\delta_p</math>)</b>	10.4	5.3	1.4
<b>Hydrogen bonding component (<math>\delta_h</math>)</b>	7.0	7.2	2.0

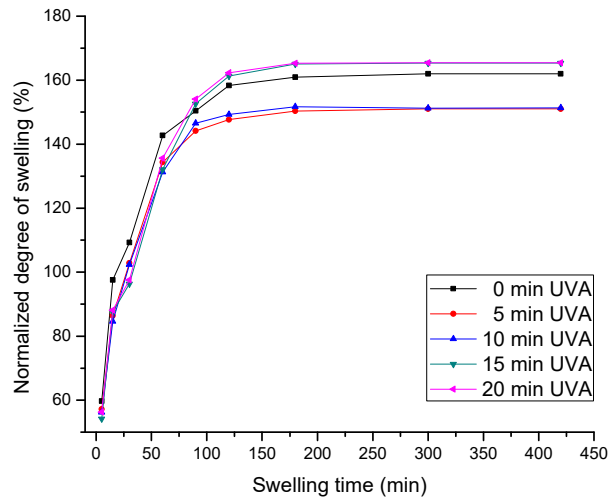
Specifically, samples with highest swelling degree in particular solvent have the closest value of their cohesion parameters to solubility parameters of that solvent. Obtained results indicate that there is the highest compatibility of the forces inside the ACE Digital photopolymer material and toluene due to the expressed swelling degree. This is true for the other tested



photopolymer materials, as well (Figures 45. and 46.). Observing Table 8., one can conclude that this compatibility manifests due to the highest dispersion forces in toluene, and weak hydrogen bonding capability, which is in consonance with the flexographic photopolymers' basic composition. Furthermore, acetone's and ethyl acetate's solubility parameters differ primarily in the polar component, which indicates that the polar forces in the ACE Digital photopolymer material have more similarity in their strength to acetone's.

Figures 45. and 46. present the normalized degrees of Digital MAX photopolymer swelling in different solvents depending on durations of UV post-treatments. It is worth noticing that the general behavior of photopolymer swelling shows the similar trend for immersion in all solvents, but with different normalized swelling degree. Generally, the degree of swelling decreases with UVA and UVC post-treatments of durations up to 5 -10 minutes and then increases, reaching the equilibrium. Normalized degree of swelling in acetone (Figure 45.a) reaches a maximum of 15.66% for 20 minutes of UVA post-treatment and a value of 15.23% for 20 minutes of UVC post-treatment (Figure 46.a). On the other hand, swelling in ethyl acetate (Figure 45.b) is less expressed, with maximum of 1.08% for non UV post-treated sample and 1.19% for sample treated with UVC post-treatment for 20 minutes (Figure 46.b).

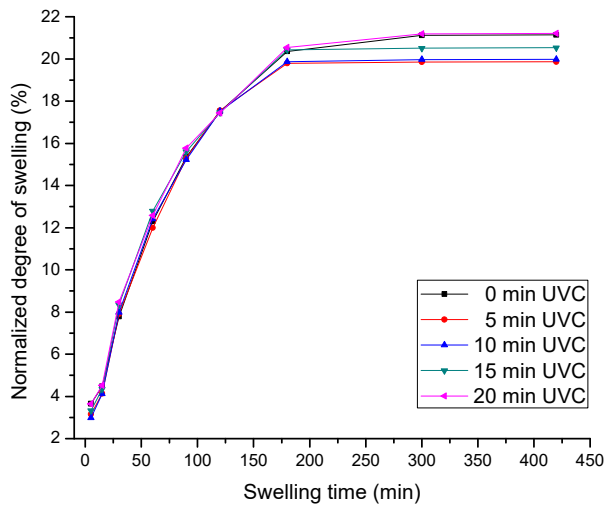




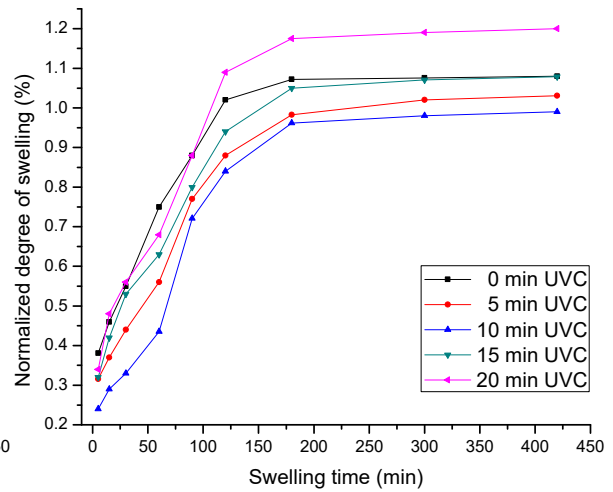
c)

Figure 45. Normalized degrees of swelling for UVA post-treated Digital MAX samples immersed in different solvents: a) acetone, b) ethyl acetate, c) toluene

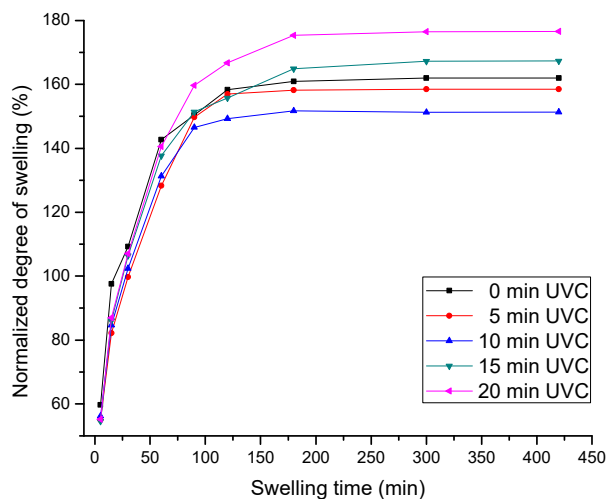
General increase of the normalized degree of swelling after 10 minutes of UV post-treatments can be associated with the changes in the surface free energy caused by UV radiation, since the solvent first needs to penetrate the surface of the photopolymer material. However, the maximal normalized degree of swelling in toluene is, similar to other tested photopolymer materials, 10.78 times higher than in acetone and 142.48 times higher than in ethyl acetate.



a)



b)



c)

Figure 46. Normalized degrees of swelling for UVC post-treated Digital MAX samples immersed in different solvents: a) acetone, b) ethyl acetate, c) toluene

This indicates, analogue to the behavior of ACE Digital samples, that swelling of Digital MAX photopolymer material in toluene shows the highest values due to the similar cohesion parameter of soluble component of photopolymer material in relation to the dispersion force of toluene, and that the Digital MAX photopolymer material does not display the hydrogen bonding capability [77].

Figures 47. and 48. display the results of swelling experiments for Cosmolight QS samples. Both UVA and UVC treatments have similar influence on swelling behavior in different solvents, with maximal values obtained for samples treated with longest durations of post-treatments.

Maximal swelling degrees in acetone are 14.15% for sample treated with UVA post-treatment (Figure 47.a) and 13.80% for sample treated UVC post-treatment (Figure 48.a). Ethyl acetate causes the maximal swelling degree of 2.08% for UVA post-treatment, and 2.02% for UVC post-treatment. Swelling degrees in toluene display the highest values of 157.32% for UVA post-treatment, and 149.87% for UVC post-treatment. A trend that is not generally increasing is present in the swelling degrees of samples immersed in ethyl acetate. The exceptions are the not treated sample, and the sample treated with 5 minutes of UVA post-treatment, which obtains a lower energy compared to UVC post-treatment.

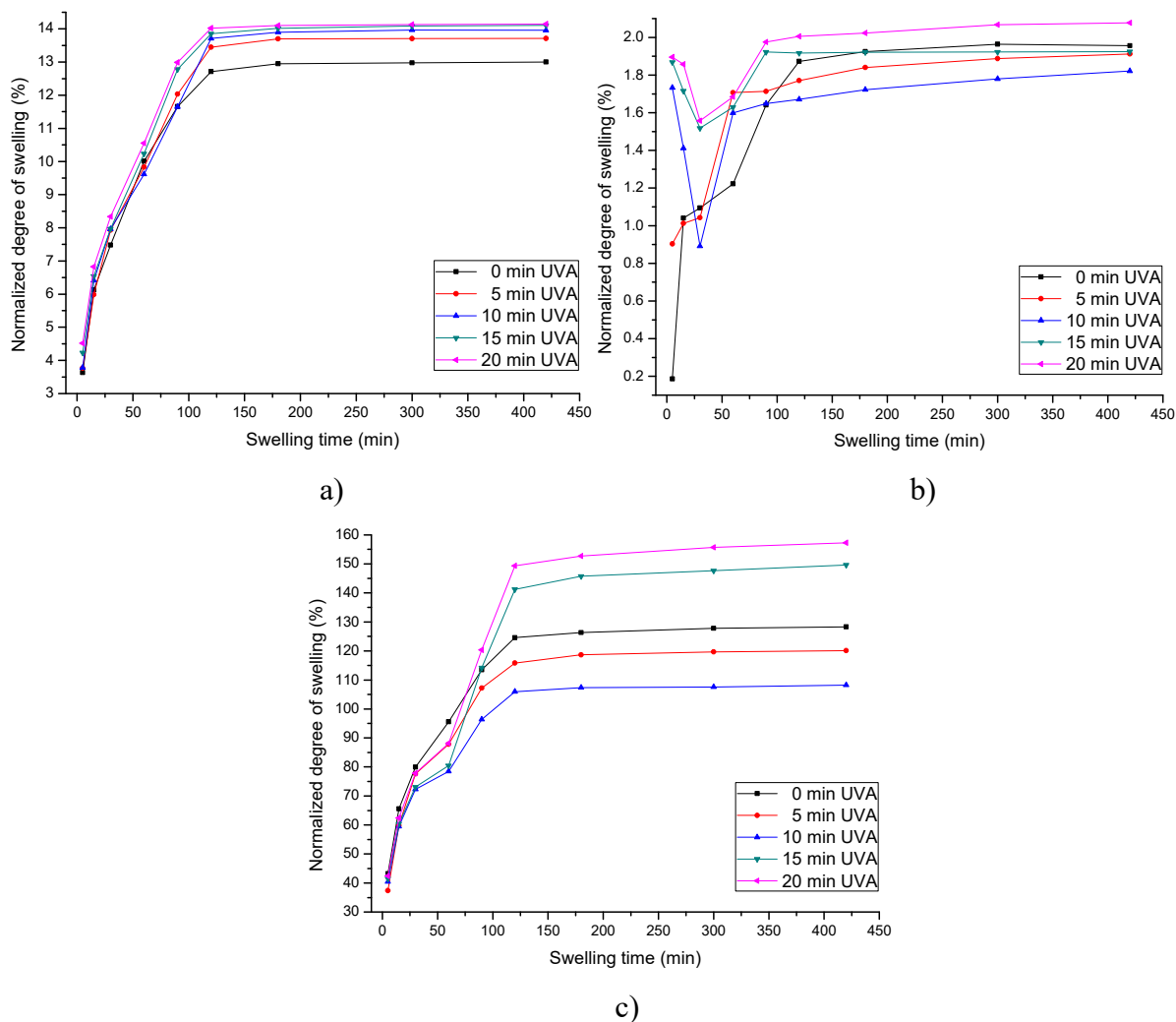


Figure 47. Normalized degrees of swelling for UVA post-treated Cosmolight QS samples immersed in different solvents: a) acetone, b) ethyl acetate, c) toluene

For all other samples immersed in ethyl acetate, there is an initial decrease of the swelling degree up to 30 minutes of the immersion period. Analogue to the explanation of the solvent penetration in other tested photopolymer materials and by observing Table 8., the compatibility of Cosmolight QS samples and ethyl acetate is not expressed up to the first 30 minutes of immersion. After 30 minutes of immersion, swelling degree increases.

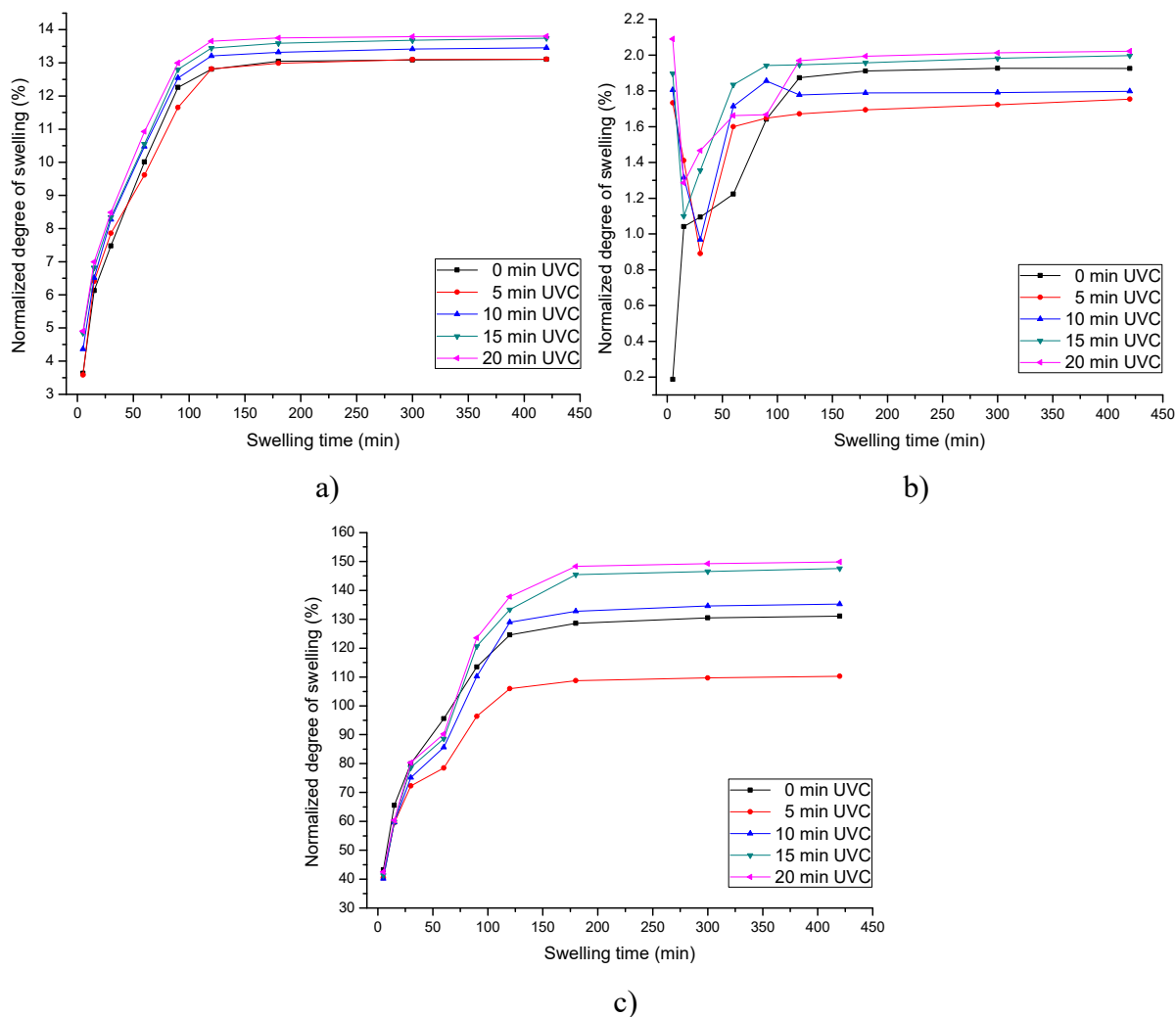


Figure 48. Normalized degrees of swelling for UVC post-treated Cosmolight QS samples immersed in different solvents: a) acetone, b) ethyl acetate, c) toluene

This dynamic of ethyl acetate's penetration in Cosmolight QS samples indicates that in the first 30 minutes, solvent slowly penetrates the surface layer of the material, which is affected by UV post-treatments. Changed surface properties of the photopolymer material after 5 minutes of UVA post-treatment, and in the whole duration range of UVC post-treatment, modifies the cohesion parameters in the photopolymer surface layer drastically, compared to the volume of the material [78]. This points to the conclusion of the formation of two-phase system: surface and the core of material, with expressed differences in their physicochemical properties.

## **4.2. Surface properties of photopolymer printing plates**

Results of experiments related to measurement and analysis of photopolymer materials' surface properties are primarily important because of their influence on the adsorption of the printing ink and its transfer to and from the printing plate in the reproduction process. UVA and UVC post-treatment are specifically used to modify the surface of the photopolymer materials. As a main aim of this research, this modification needed to result with as expressed changes in surface properties of the printing plates as possible. At the same time, the functional properties of the material needed to be retained. Changes in chemical and physicochemical properties of photopolymer materials are displayed as results of roughness measurements, calculation of surface free energy, and the results of chemical changes in the surface layer obtained by FTIR-ATR and EDS analysis.

#### 4.2.1. Roughness of printing plate surface

Results of photopolymer surface roughness measurements are presented in Figure 48. One can notice that values of  $R_a$  parameters of examined photopolymer materials have generally low values. Maximal  $R_a$  of 0.1575  $\mu\text{m}$  was measured on ACE Digital sample treated with 20 minutes of UVA post-treatment (Figure 49.a). It is obvious that the trend of changes in  $R_a$  depends on the type of photopolymer material.

For ACE Digital samples,  $R_a$  decreases up to 5 minutes of UVA and up to 15 minutes of UVC post-treatment (Figure 49.b) and after that starts to increase towards the value of non UV post-treated sample. Digital MAX samples show the similar behavior, but the initial decrease of  $R_a$  for UV post-treated samples is present up to 15 minutes of UVA and 10 minutes of UVC post-treatment, after which  $R_a$  starts to increase. Cosmolight QS samples, on the other hand, show the constant increase of  $R_a$ , mostly expressed between 10 and 15 minutes of UVC post-treatment.

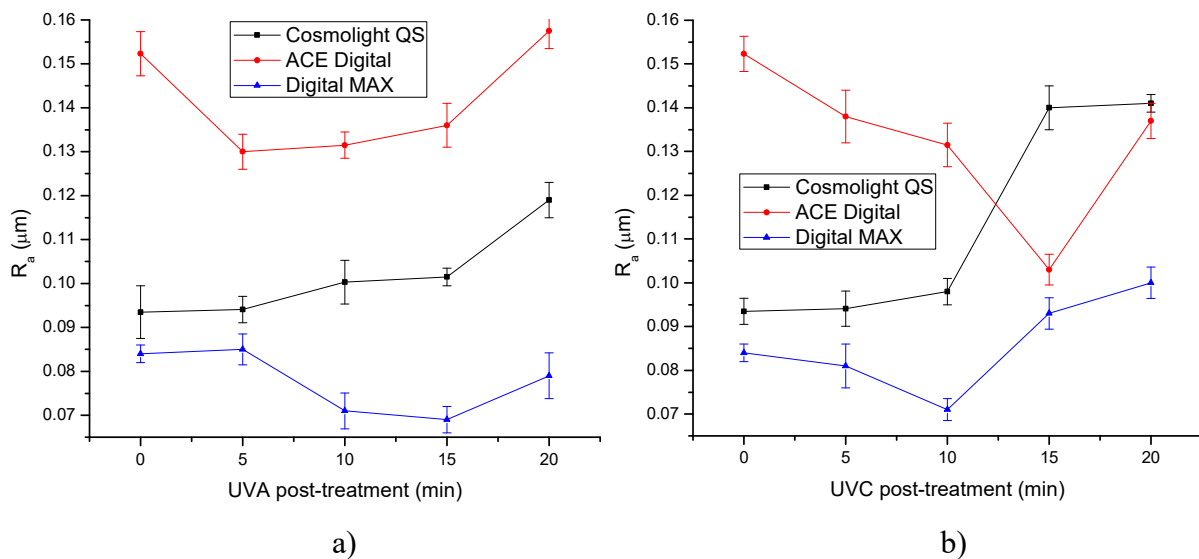


Figure 49.  $R_a$  parameters of printing plate samples exposed with: a) varied UVA post-treatment, b) varied UVC post-treatment

Although the changes in the roughness of photopolymer materials are not significant in terms of their numerical values, they could be used as an indicator of the other, not as easily measurable changes in the materials.

Specifically, changes of the photopolymeric surface roughness can be assigned to the changes in the crosslinking degree in the material [79] and the changes in the types of bonds in the surface layer [80], caused by the UV post-treatments.

Surface roughness is one of the parameters influencing the surface free energy of the material [81]. However, complex changes that occur in the flexographic photopolymer material as a result of UV post-treatments and the trends of changes of  $R_a$  which are not constant, disable the direct interpretation of roughness results in relation to printing plate's surface properties. Therefore, to quantify the influence of the surface roughness on material's properties,  $R_a$  results will be included in the fitting model described in the discussion chapter.



#### 4.2.2. Surface free energy calculation

calculations of the surface free energy ( $\gamma^{\text{total}}$ ) and its dispersive ( $\gamma^{\text{d}}$ ) and polar ( $\gamma^{\text{p}}$ ) components showed that the variations in UVA and UVC post-treatments have a similar trend of the effect on the photopolymer material samples, except for the Cosmolight QS sample (Figures 50. – 52.). However, changes in components of  $\gamma$  caused by prolonged UVC post-treatment are more expressed than changes caused by UVA radiation, since UVC radiation carries more energy.

Setting the duration of the UVA post-treatment of the photopolymer material from 0 to 20 minutes causes the increase of  $\gamma^{\text{total}}$  from 33.5 mNm<sup>-1</sup> to 40.08 mNm<sup>-1</sup> for Digital MAX samples, and from 23.9 mNm<sup>-1</sup> to 32.56 mNm<sup>-1</sup> for Cosmolight QS samples (Figure 50.a). However,  $\gamma^{\text{total}}$  for ACE Digital samples reaches maximal value of 32.27 mNm<sup>-1</sup> at 5 minutes of UVA post-treatment and then decreases to 28.63 mNm<sup>-1</sup> for 20 minutes of UVA post-treatment.

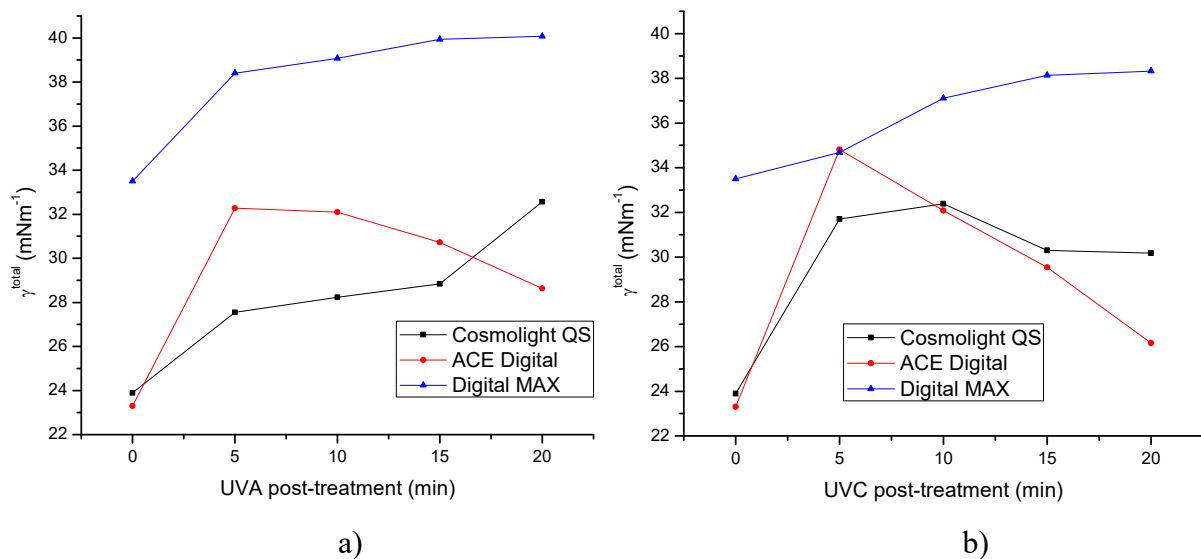


Figure 50. Total surface free energy of printing plate samples exposed with:  
a) varied UVA post-treatment, b) varied UVC post-treatment

Specifically, the trends of changes of  $\gamma^{\text{total}}$  with prolonged UVA radiation are primarily caused by the changes of  $\gamma^{\text{d}}$  (Figure 51.a). The increase of  $\gamma^{\text{d}}$  and  $\gamma^{\text{total}}$  of photopolymer material can be explained by further crosslinking which occurs in the photopolymer material and indicates that, even after the printing plate is considered to be finished in its production process, further crosslinking caused by UVA radiation takes place. The inflexion point at 5 minutes of UVA

post-treatment for  $\gamma^{\text{total}}$  and  $\gamma^{\text{d}}$  for ACE Digital sample can be explained by the weaker intermolecular forces in the polymer network with prolonged UVA post-treatment due to the possible start of the material degradation [82].

Furthermore, changes of  $\gamma^{\text{p}}$  are not as expressed as changes of  $\gamma^{\text{d}}$  (Figure 52.a). Therefore, UVA radiation can be used as a tool to adjust  $\gamma^{\text{d}}$  of ACE Digital photopolymer material, but not as a tool to enhance significantly the adsorption of polar inks and coatings.

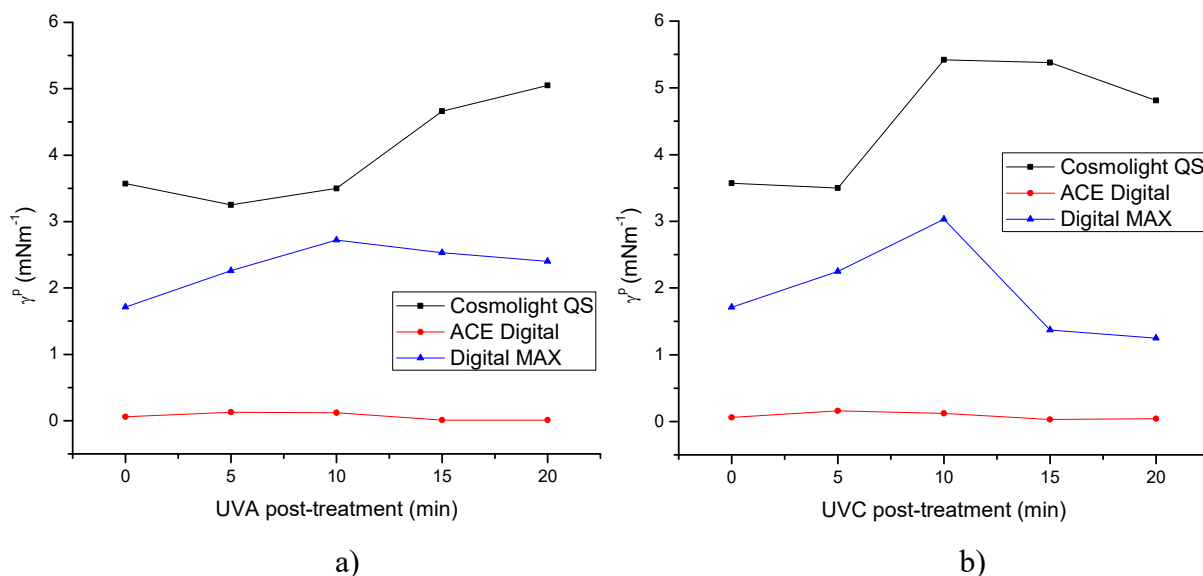


Figure 51. Polar component of surface free energy of printing plate samples exposed with:  
a) varied UVA post-treatment, b) varied UVC post-treatment

UVC post-treatment (Figures 50.b), 51.b) and 52.b) has a more distinct effect on all components of  $\gamma$ .

When performing the variation of UVC radiation from 0 to 20 minutes,  $\gamma^{\text{total}}$  of the photopolymer surface for ACE Digital samples reaches maximal value of 34.81 mNm<sup>-1</sup> at 5 minutes of UVC post-treatment and then decreases to 26.16 mNm<sup>-1</sup> for 20 minutes of UVC post-treatment. Cosmolight QS samples display similar behavior, reaching maximal value of  $\gamma^{\text{total}}$  of 32.39 mNm<sup>-1</sup> at 10 minutes of UVC post-treatment and then decreasing to 30.18 mNm<sup>-1</sup> for 20 minutes of UVC post-treatment. Digital MAX samples display the constant increase of  $\gamma^{\text{total}}$  from 33.5 mNm<sup>-1</sup> to 41.2 mNm<sup>-1</sup>.

These changes, just like the increases of  $\gamma^{\text{total}}$  and its components caused by UVA post-treatment, are significant for the graphic reproduction process because of the changes in the adsorption of the printing ink on the printing plate. Furthermore, even though  $\gamma^{\text{d}}$  is a dominant

component influencing  $\gamma^{\text{total}}$ , changes in  $\gamma^{\text{p}}$  have an interesting trend.  $\gamma^{\text{p}}$  for all samples displays an inflexion point after initial increase after which it decreases to a certain level, depending on the photopolymer material. Initial increase of  $\gamma^{\text{p}}$  is caused by the integration of the oxygen in the surface layer of photopolymer material. However, the decrease of  $\gamma^{\text{p}}$  after the certain duration of UV post-treatment can be explained by the process of migration of non-polar carbohydrate compounds of low molecular weight (such as protective waxes added to these types of photopolymers) to the surface of the material [4].

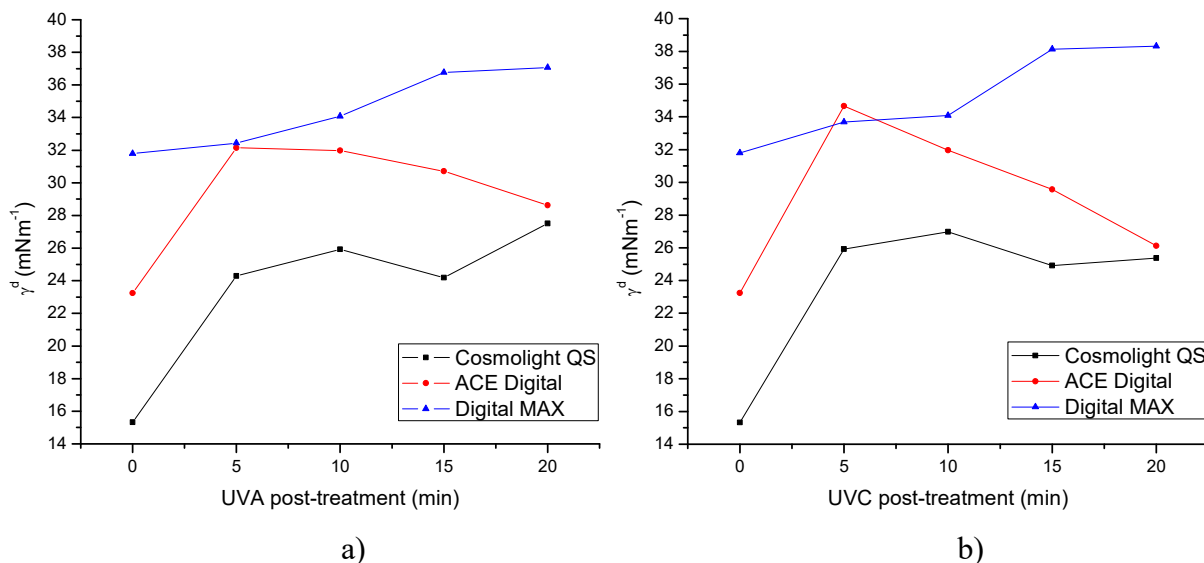


Figure 52. Dispersive component of surface free energy of printing plate samples exposed with: a) varied UVA post-treatment, b) varied UVC post-treatment

Therefore, when needing to adjust  $\gamma^{\text{p}}$  of the flexographic printing plate surface, initial test needs to be performed in order to detect the inflexion point with maximal  $\gamma^{\text{p}}$ .

However, since UVA radiation initiates the crosslinking reaction, and UVC terminates it due to the higher energy and generation of ozone, one should use both post-treatments and combine their duration in order to achieve desired  $\gamma$ , but at the same not diminish the functionality of the photopolymer printing plate in the reproduction process [83, 84].

#### 4.2.3. FTIR-ATR analysis of photopolymer surface layer

FTIR-ATR analysis of the photopolymer materials treated with varied durations of UV post-treatments displayed the changes in the area of oxygen bonds and in the area of CH<sub>2</sub> and C=C vibrations for all analysed samples (Figures 53. – 58.).

Figures 53. and 54. display FTIR-ATR spectra of ACE Digital samples with varied UV post-treatments. There are similar changes in bonds present with variations of both UV post-treatment durations, differing in intensity.

The changes present in the peak at 1650 cm<sup>-1</sup> can be assigned to changes in C=C stretching and present the increased saturation of the system due to the crosslinking process, since the peak intensity decreases for UV post-treated samples. Furthermore, the increased amount of oxygen bonds is visible in the area of 1750 cm<sup>-1</sup> with increased duration of both UV post-treatments and in area from 3200 cm<sup>-1</sup> - 3500 cm<sup>-1</sup> for prolonged UVC post-treatment. These areas correspond to the vibrations of C=O bond and OH bond, respectively [85].

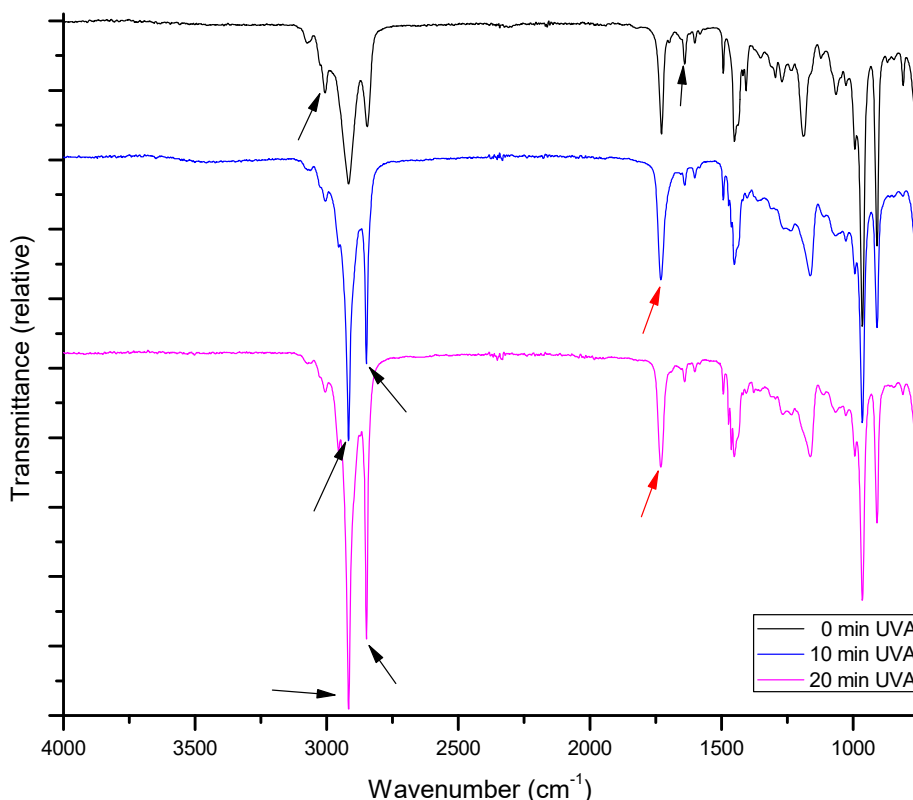


Figure 53. FTIR-ATR spectra of ACE Digital samples exposed to varied UVA post-treatment

The increased portion of oxygen bonds in the samples point to the integration of the oxygen in the surface layer of photopolymer material and to oxidative termination of the crosslinking process, which is a usual mechanism in termination of the radical crosslinking [41, 86]. Oxygen levels in the surface of the material will influence  $\gamma^p$ .

However, oxygen, together with ozone generated by UVC tubes, can have a destructive influence to the photopolymer material causing photooxidative degradation [87]. Therefore, prolonged exposures to the UV radiation, especially to UVC post-treatment, has to be adjusted according to the material sensitivity.

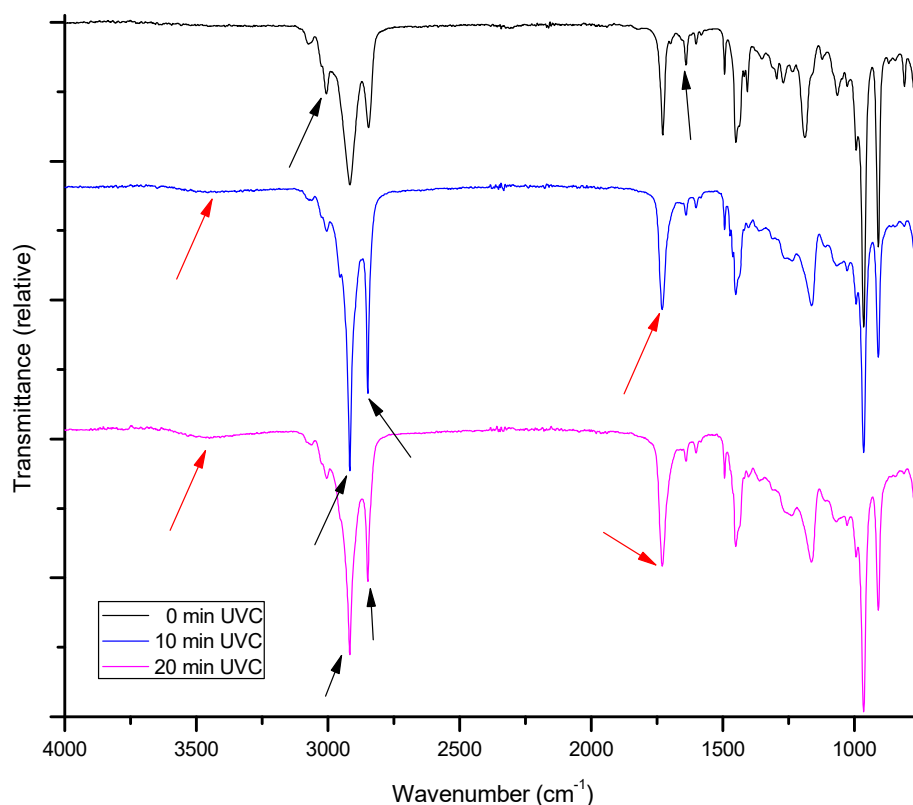


Figure 54. FTIR-ATR spectra of ACE Digital samples exposed to varied UVC post-treatment

Other changes connected to the crosslinking process of the photopolymer material are visible in areas of saturated C-H stretching at 2850 cm<sup>-1</sup> and 2950 cm<sup>-1</sup>. Their decreased transmittance (meaning, increased intensity of the bond vibration) is visible for all UV post-treated samples, and is more expressed with prolonged UVA post-treatment. These changes can be assigned to the migration of low molecular weight compounds, such as oxygen protective waxes added to the photopolymer structure, onto the surface of the material.

Increased transmittance of the peak at  $3010\text{ cm}^{-1}$  with prolonged UV post-treatments belongs to the unsaturated C-H stretching and can be interpreted as a confirmation of the unsaturation in the sample not treated with any UV post-treatment [88].

Figures 55. and 56. display FTIR-ATR spectra for Digital MAX samples with varied UV post-treatments. It is visible that types of changes in the intensity of peaks are similar to ACE Digital samples, but they are not as expressed. Furthermore, there are no significant changes in the intensity of peaks corresponding to C-H stretching below  $3000\text{ cm}^{-1}$ , which points to the conclusion that there is no migration of the compounds to the surface layer present in this photopolymer material.

Dominant change in FTIR-ATR spectra for Digital MAX samples is visible in the area corresponding to O-H stretching (from  $3200\text{ cm}^{-1}$  to  $3500\text{ cm}^{-1}$ ). Specifically, with prolonged UVA, and especially with UVC post-treatment, the ratio of O-H bonds increases.

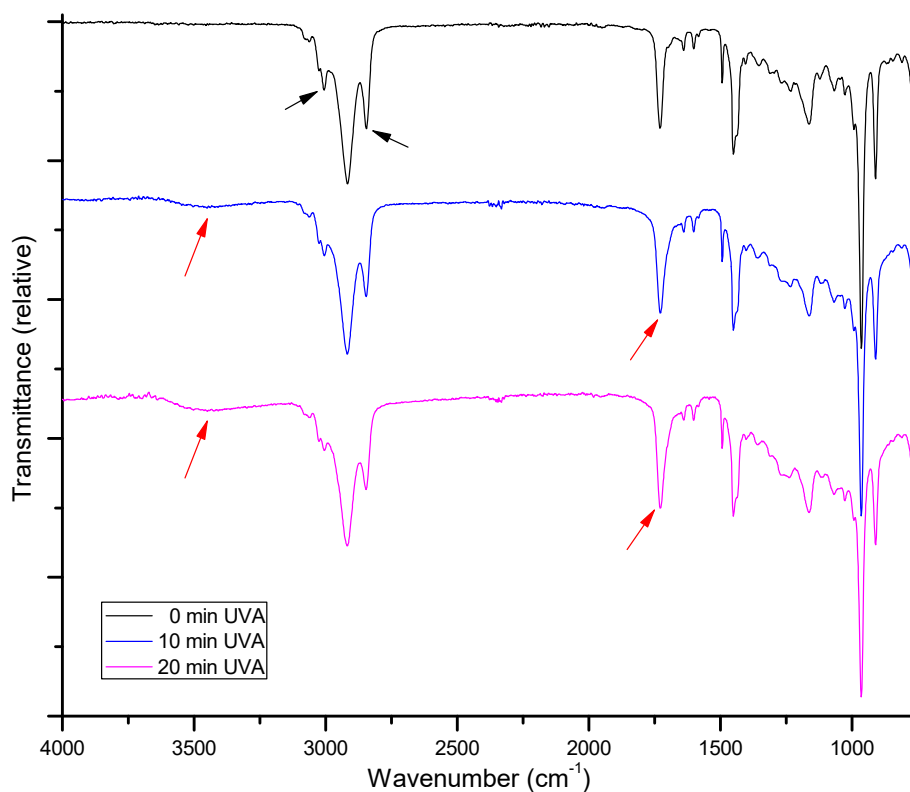


Figure 55. FTIR-ATR spectra of Digital MAX samples exposed to varied UVA post-treatment

The decreased transmittance of C=O bonds ( $1750\text{ cm}^{-1}$ ) appears with the prolonged UVC post-treatment. This indicates that oxygen will have a major influence on the changes of surface properties of this type of photopolymer material.

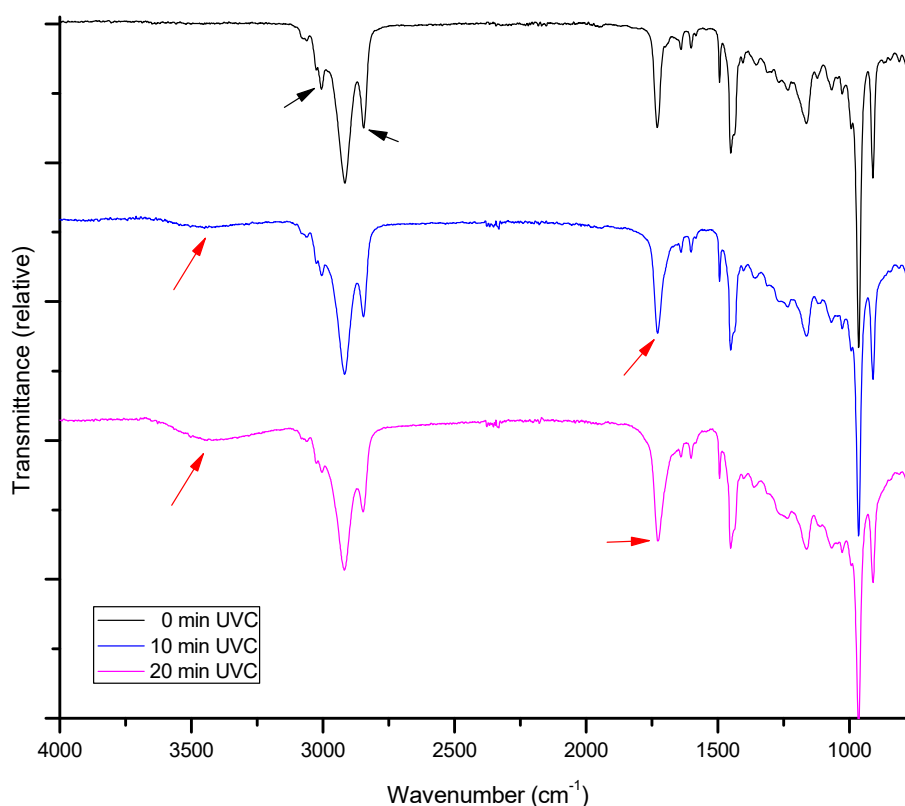


Figure 56. FTIR-ATR spectra of Digital MAX samples exposed to varied UVC post-treatment

There is no significant change in C-H stretching area, except for slightly increased peak at  $2850\text{ cm}^{-1}$  and  $3010\text{ cm}^{-1}$  compared to the UV post-treated samples. The transmittance in this area increases with longer exposures to UVA and UVC post-treatment. This points to the changes in the structure of photopolymer network, which could be a consequence of the crosslinking termination/oxidation process.

In Figures 57. and 58. one can see the differences in FTIR-ATR spectra for UV post-treated Cosmolight QS samples. Although Cosmolight QS is a water-washable printing plate with different basic composition than ACE Digital and Digital MAX, FTIR-ATR analysis displayed the similar changes as ones detected in other two photopolymer materials.

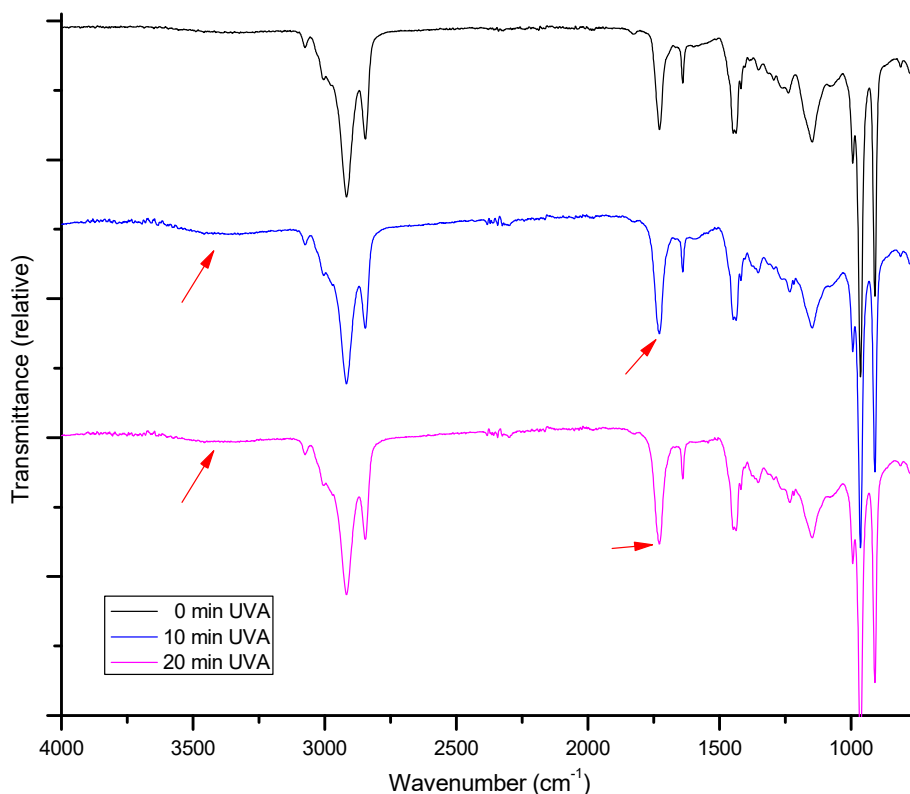


Figure 57. FTIR-ATR spectra of Cosmolight QS samples exposed to varied UVA post-treatment

Prolonged UV post-treatment, specifically UVC post-treatment, causes the increased ratio of C=O bond ( $1750\text{ cm}^{-1}$ ) and OH bond ( $3200\text{ cm}^{-1} - 3500\text{ cm}^{-1}$ ). This points to the increased amount of the oxygen in the surface layer.

Moreover, similar change in peak intensity as for the Digital MAX sample is visible at  $2850\text{ cm}^{-1}$  for sample treated for 20 minutes of UVC post-treatment. Increased transmittance in this area with prolonged UVC post-treatment belongs to the stretching of saturated C-H bond and points to the changes in the network structure which could be a part of the photooxydation process.

It is also important to notice that peak at  $3010\text{ cm}^{-1}$ , which belongs to the unsaturated C-H stretching, almost disappears after 20 minutes of UVC post-treatment, pointing to the highest crosslinking degree in the material [88].



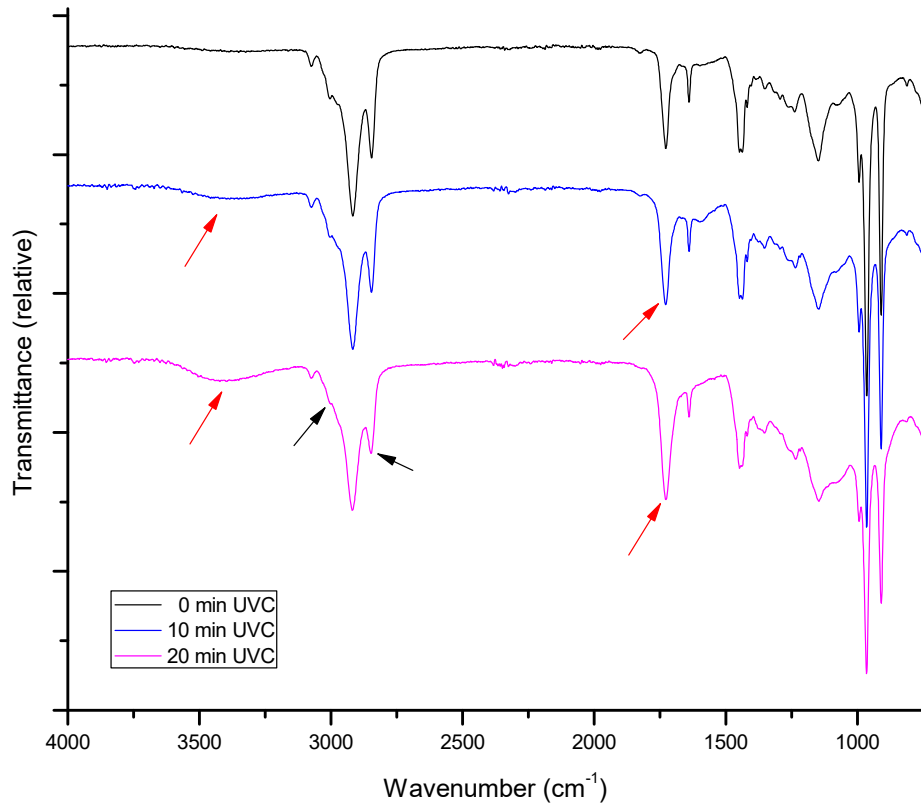


Figure 58. FTIR-ATR spectra of Cosmolight QS samples exposed to varied UVC post-treatment

#### 4.2.4. EDS analysis

EDS analysis of photopolymer material samples was performed in order to confirm the results obtained by FTIR-ATR analysis and to quantify the oxygen ratio in photopolymer materials exposed to varied UV post-treatments. EDS analysis performed in this research enables the assessment of the material sensitivity to oxygen related to the duration of the exposure to UVA and UVC post-treatments [89].

Observing Figure 59.a), one can conclude that Digital MAX printing plate is most subject to the formation of oxygen bonds in the surface layer compared to other tested printing plates when exposed to UVA post-treatment. The maximal ratio of oxygen for Digital MAX material is 15.13% at 20 minutes of UVA post-treatment.

ACE Digital samples showed the highest resistivity to oxygen with prolonged UVA post-treatment, reaching maximal value of 12.58% oxygen ratio at 5 minutes of the UVA post-treatment, after which the oxygen ratio in the material surface decreases. These results confirm the conclusion reached by FTIR-ATR analysis about the migration of non-polar oxygen protective waxes to the surface layer of photopolymer material.

Cosmolight QS samples displayed the initial decrease of oxygen ratio, pointing to the similar mechanism of the oxygen protection as for ACE Digital photopolymer material.

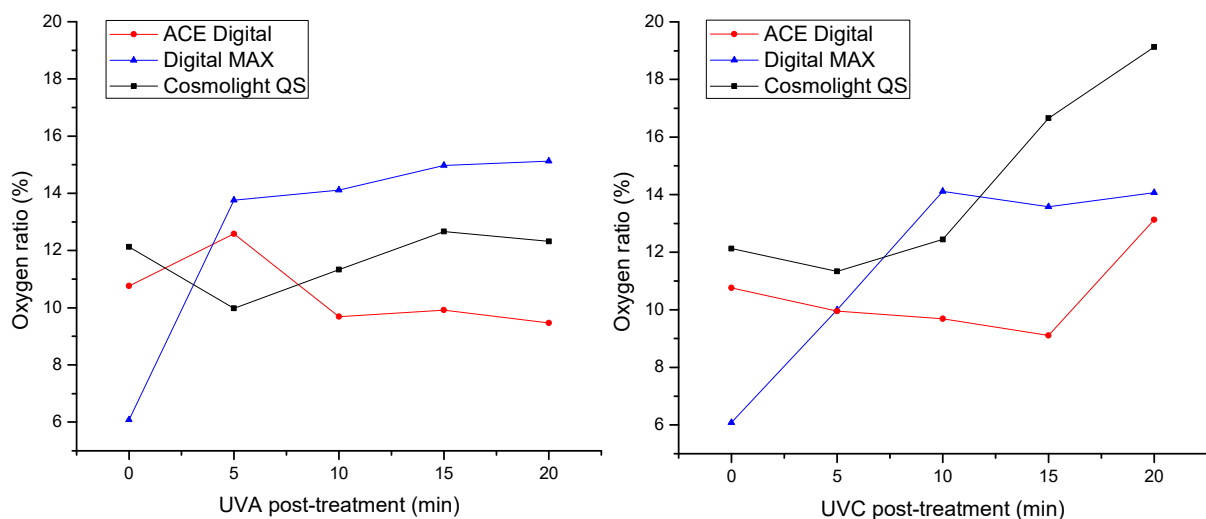


Figure 59. Oxygen ratios in the surface layer of photopolymer samples exposed to:  
a) varied UVA post-treatment, b) varied UVC post-treatment

However, decreasing trend of oxygen ratio was not expressed in Cosmolight QS samples after 5 minutes of UVA post-treatment, when oxygen ratio started to increase up to 12.66%.

UVC post-treatment, caused more expressed and rapid increase in oxygen ratio for Digital MAX and Cosmolight QS samples than for ACE Digital samples (Figure 59.b). Oxygen ratio increased from 6.08% to 14.07% for Digital MAX samples, and from 12.12% to 19.13% for Cosmolight QS samples after 20 minutes of UVC post-treatment.

Even ACE Digital photopolymer material displayed the increase of the oxygen ratio after 15 minutes of UVC post-treatment. Specifically, portion of oxygen in ACE Digital surface layer initially decreases from 10.76% for the sample not exposed to any UV post-treatment to 9.11% at 15 minutes of UVC post-treatment, and then increases to 13.13% at 20 minutes of the UVC post-treatment.

It can be concluded that ACE Digital photopolymer material is the most resistant to oxygen during the exposure to UVA and UVC post-treatments: maximal increases in oxygen ratio were 7% for UVC post-treated Cosmolighth QS samples, and 7.99% for UVC post-treated Digital MAX samples.

Results obtained by EDS analysis will be used in modelling of the oxygen ratio influence on the surface free energy of printing plates and on the thickness of the printed layer.

### **4.3. Quality of prints and photopolymer printing plates related to reproduction process**

Variety of photopolymer materials are used in the composition of different flexographic printing plates. Results presented in this chapter are emphasizing the influence of the modified properties of printing plates used in this research on the quality of prints.

Before the results of measurements and analysis performed on prints obtained by UV post-treated printing plates, the formation of the printing elements in photopolymer material during the main exposure in the printing plate processing needed to be discussed, since different oxygen sensitivity of the material in the crosslinking process will cause different deformation of formed printing elements. Deformations of the shape of formed printing elements will result with differences on the prints.

In order to analyse the quality of the prints obtained by UV post-treated printing plates, microscopy of printed fine lines was performed, together with the calculations of coverage values, optical density and ink layer thickness on the prints.

#### 4.3.1. Topography of printing elements on printing plates

Images presented in Figures 60. - 62. were obtained by AniCAM 3D microscope. Fields of 5%, 50% and 95% surface coverage on printing plates treated with the optimal durations of the UV post-treatments (according to the manufacturer) were scanned in order to observe the surface of the halftones on different printing plates. Despite the same compensation curve applied to all printing plate samples, one can notice the differences in the shapes and sizes of the printing elements at 5% coverage value (Figures 60.a), 61.a) and 62.a). The shape of the printing element top is influenced by the oxygen in the main exposure process, and the size (area) of the printing element is then determined by the bump curve, adjusted to each type of photopolymer material specifically.

Furthermore, the difference in topography of the printing elements in the area of 50% coverage is visible as well (Figures 60.b), 61.b) and 62.b). With the increase of the coverage value, visual differences on the surface become less apparent (Figures 60.c), 61.c) and 62.c).

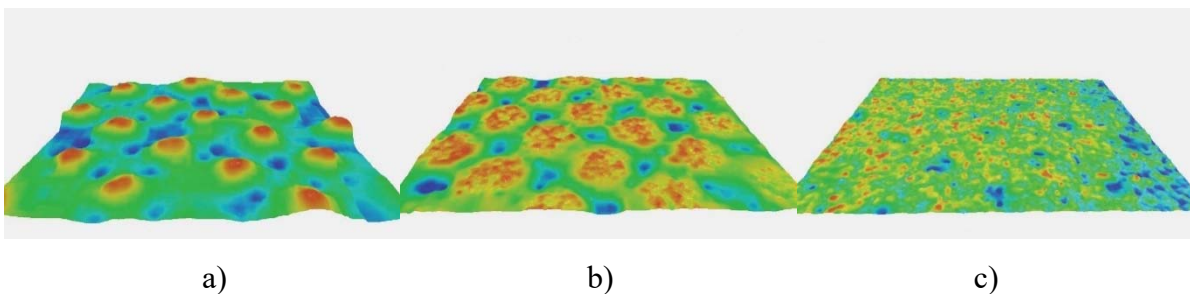


Figure 60. 3D scans of printing elements on ACE Digital printing plate at:  
a) 5% coverage value, b) 50% coverage value, c) 95% coverage value

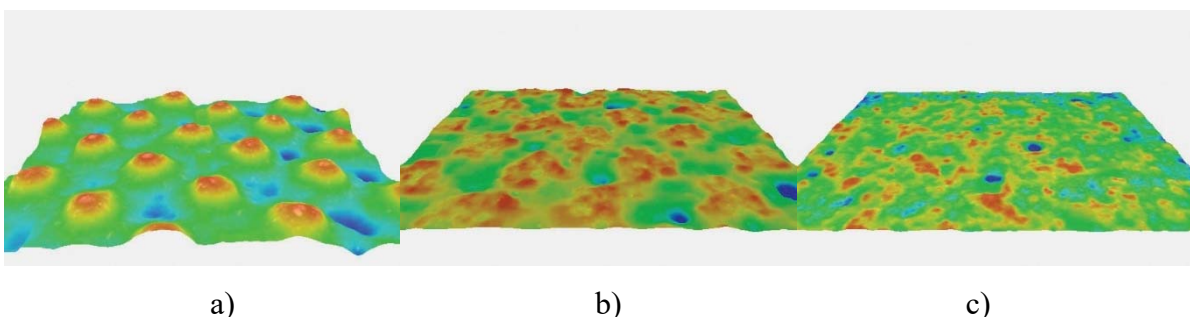


Figure 61. 3D scans of printing elements on Digital MAX printing plate at:  
a) 5% coverage value, b) 50% coverage value, c) 95% coverage value

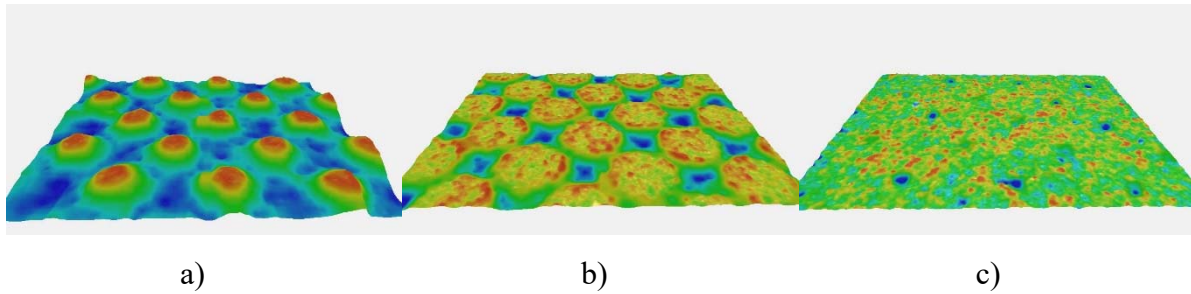


Figure 62. 3D scans of printing elements on Cosmolight QS printing plate at:  
 a) 5% coverage value, b) 50% coverage value, c) 95% coverage value

As a confirmation of results of roughness measurements, Digital MAX printing plate displays the lowest visual roughness, too.

In order to observe the printing elements formed in the highlight area, elements from the area of DFTA control strip used to analyse the shape of small elements were scanned with AniCAM 3D microscope as well (Figures 63. – 66.). Observed printing element areas in highlights on the printing plates were image areas of C, H and P fields transferred from the DFTA control strip (Figure 63.) to the printing plates' surfaces.



Figure 63. DFTA control strip

Field C corresponds to the area of 4 pixels ablated on the mask layer on the printing plate, field C to 14 pixels ablated on the mask layer on the printing plate, and field P to 30 pixels ablated on the mask layer on the printing plate.

Figures 64.a), 65.a) and 66.a) display printing elements on field C of DFTA strip, which was supposed to be the first field with stable and correctly formed printing elements after the application of correction curves. However, it is visible that not all the elements formed correctly. Some printing elements have formed with the higher edge than the inside area of the element top. This occurrence is often connected to the relaxation after the compression of the photopolymer material during the exposure on printing plates produced by technology that includes the oxygen-protection layer attached to the plate before and during the exposure (for example, Kodak NX technology with TIL film, MacDermid LUX ITP technology) [90, 91].

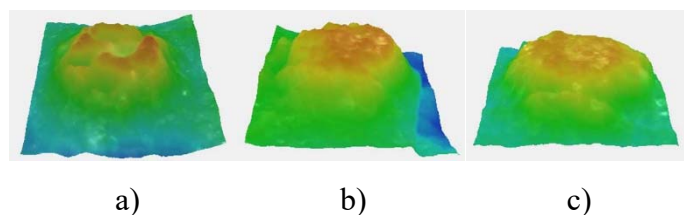


Figure 64. 3D scans of fields on DFTA strip transferred to ACE Digital printing plate:

a) field C – 4 px, b) field H – 14 px, c) field P – 30 px

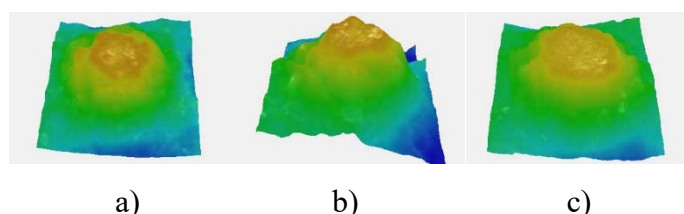


Figure 65. 3D scans of fields on DFTA strip transferred to Digital MAX printing plate:

a) field C – 4 px, b) field H – 14 px, c) field P – 30 px

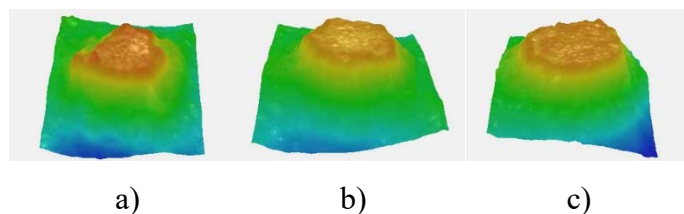


Figure 66. 3D scans of fields on DFTA strip transferred to Cosmolight QS printing plate:

a) field C – 4 px, b) field H – 14 px, c) field P – 30 px

However, printing plate samples in this research were not produced using that type of technology. Furthermore, in other figures (Figures 64. – 66., b) and c) correctly formed elements with (mostly) flat top are visible. Besides that, photopolymers usually contract during the crosslinking process due to the increased network density [92]. Therefore, the reason for the incorrectly formed elements on field C could be the diffraction of light passing through the ablated areas of small dimensions and different sensitivity of photopolymer materials to the UV radiation [93].

The differences in printing elements formed in different photopolymer materials for fields H and P are apparent in the printing elements' areas and surface roughness. Therefore, when choosing the printing plate for the specific purpose, especially in functional and/or high-quality printing, one should, beside the implicated physicochemical properties, have in mind the reproductive limitations of the material, as well.

#### 4.3.2. Microscopic displays of prints

The results of the microscopic analysis are displayed for the fine printed lines, with nominal width of 20  $\mu\text{m}$  (Figures 67. – 69.). Microscopic images of screen elements of different coverage values didn't display any significant visual changes in quality. This points to the conclusion that the variation of one type of UV post-treatment (UVA or UVC), while keeping the other one constant at optimal value, results with printing plate of functional properties which is able to perform correctly when printing halftones. Microscopic images of potentially most problematic coverage area in flexography – highlights [94], are presented in Appendix 3 (images of 1% and 10% coverage areas). Areas with 100% coverage have been analysed by calculations of the optical density and measurements of the printed ink layer thickness.

Images of printed lines obtained by UV post-treated ACE Digital samples are presented in Figure 67. It is visible that the print obtained by printing plate exposed to 2 minutes of UVA post-treatment (Figure 67.a) prints the inconsistent line, probably due to the insufficient hardness of the printing plate.

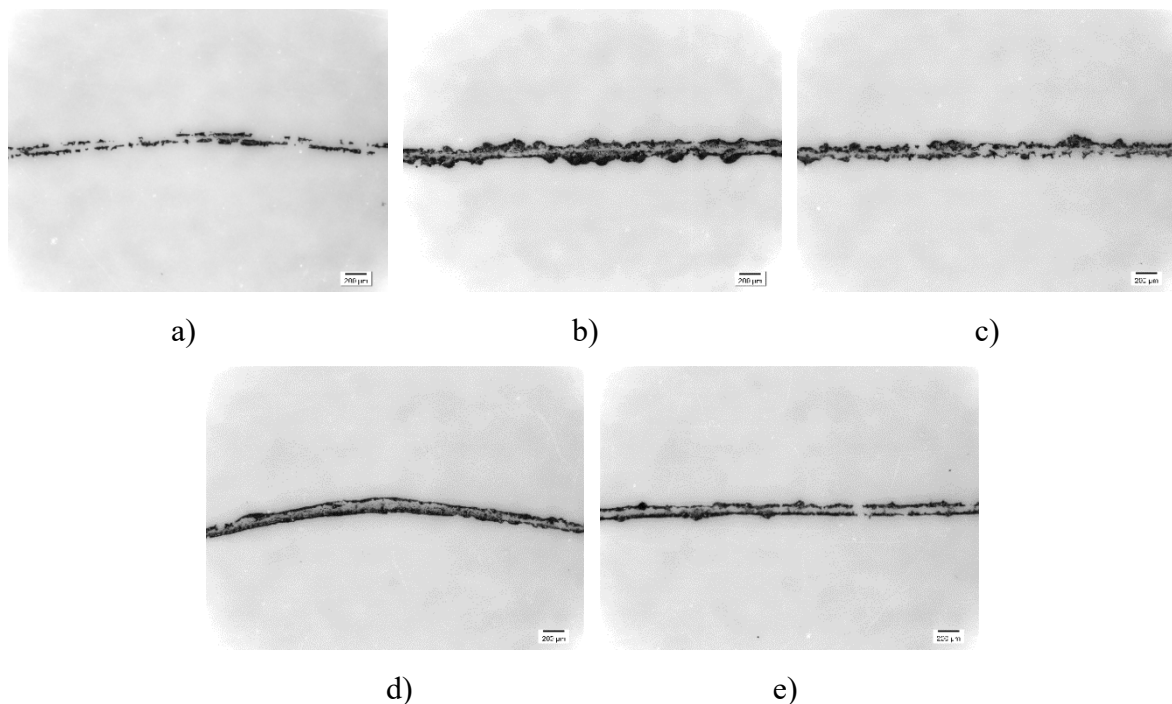


Figure 67. Lines with nominal width of 20  $\mu\text{m}$  (magnification of 50x) on prints obtained by ACE Digital printing plates exposed to varied UV post-treatments:

- a) 2 min UVA post-treatment, b) 10 min UV post-treatment, c) 20 min UVA post-treatment,
- d) 2 min UVC post-treatment, e) 20 min UVC post-treatment



10 minutes of UV post-treatment (Figure 67.b) results with thicker printed line, but its edges are not well defined, probably due to the poor wetting of the printing ink on the printing plate.

In general, ACE Digital printing plate does not enable the optimal quality of printed thin lines, since its  $\gamma$  decreases with prolonged UV post-treatments. However, increased hardness of the printing plate will improve the quality of the prints (Figure 67.e), but the end result is still not good enough for high-quality prints of specific motives.

In Figure 68. one can see the effect of the varied UV post-treatments on fine lines on prints obtained by Digital MAX printing plates. It is visible that the line printed by means of printing plate with 2 minutes of UVA post-treatment (Figure 68.a) results with poor ink transfer to the printing substrate. This indicates that  $\gamma$  of the photopolymer material is too low at that point in order to ensure the correct adsorption of the printing ink on the printing plate surface. Prolonging the UVA post-treatment results with better definition of the line shape (Figure 68.b), since the UV post-treatment increases the hardness of the photopolymer material, as well.

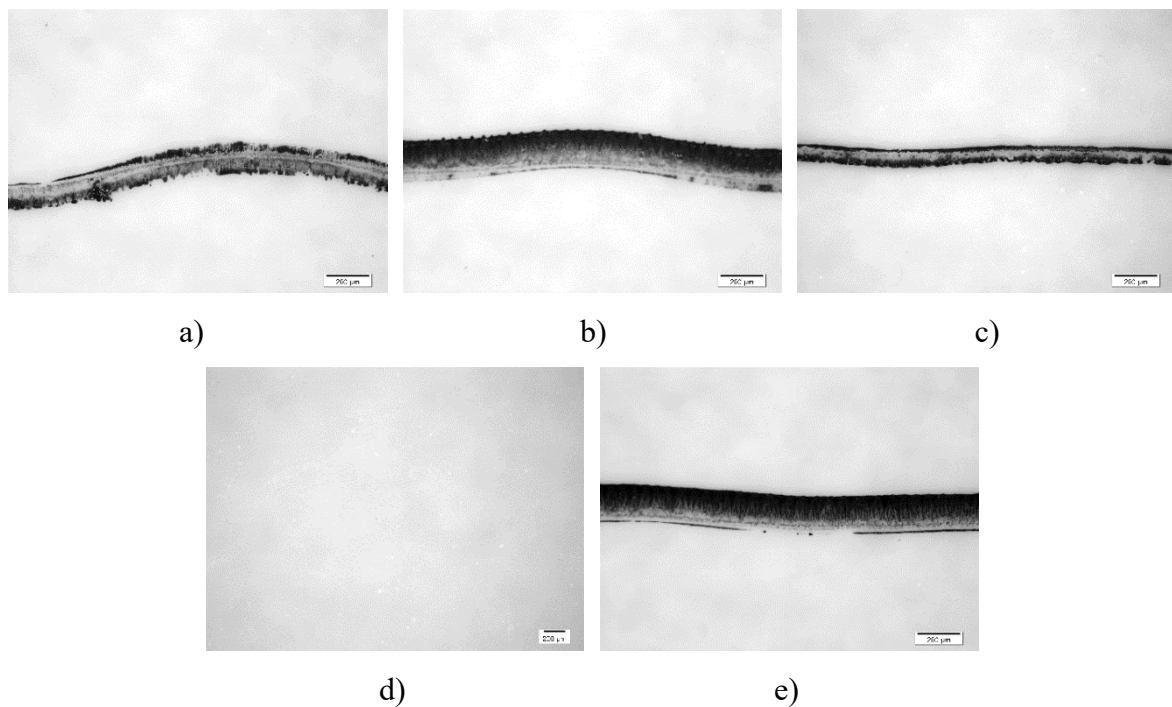


Figure 68. Lines with nominal width of 20  $\mu\text{m}$  (magnification of 50x) on prints obtained by Digital MAX printing plates exposed to varied UV post-treatments:

- a) 2 min UVA post-treatment, b) 10 min UV post-treatment, c) 20 min UVA post-treatment,
- d) 2 min UVC post-treatment, e) 20 min UVC post-treatment

However, as the hardness of the printing plate increases and ensures less elastic deformation of the printing plate during the engagement, and  $\gamma^p$  decreases at 20 minutes of UVA post-treatment, the line on the print becomes thinner with not as well defined edges (Figure 68.c). Therefore, UVA post-treatment can be used to decrease the width of the printed fine elements (in coordination with specific printing ink and printing substrate used) [95].

On the other hand, the absence of UVC post-treatment (Figure 68.d) results with mechanical damage on the fine element area on the printing plate during the engagement, and the loss of the ink transfer to the printing substrate. Prolonged UVC post-treatment of the Digital MAX photopolymer material (Figure 68.e) will ensure stable, correctly defined line on the print. Since  $\gamma$  of the photopolymer material increases with prolonged UVC treatment more than with prolonged UVA treatment, adsorption of printing ink on the printing plate becomes improved as well. Therefore, the width of the line will not be decreased significantly and ink uniformity and shape on the printed element will improve due to the increased hardness.

Figure 69. displays fine lines printed by Cosmolight QS printing plates. Printed fine lines are straight, regardless of the duration of UV post-treatments, pointing to the stable and correctly formed fine printing elements on the printing plate.

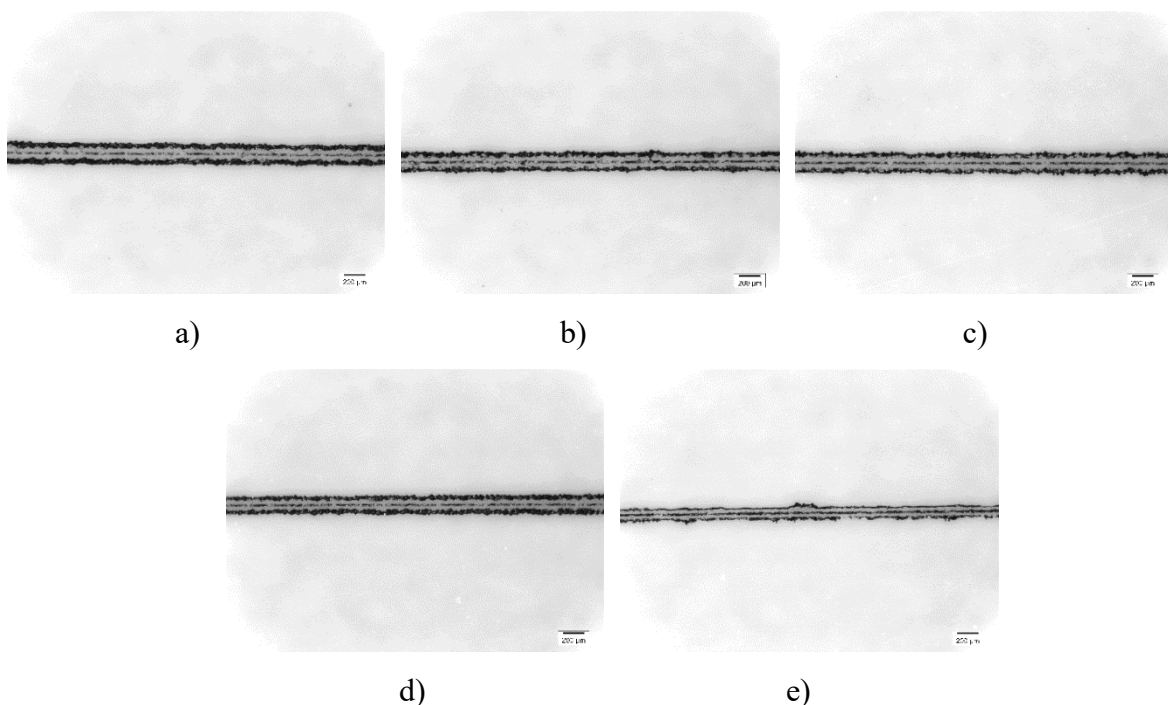


Figure 69. Lines with nominal width of 20  $\mu\text{m}$  (magnification of 50x) on prints obtained by Cosmolight QS printing plates exposed to varied UV post-treatments:

- a) 2 min UVA post-treatment, b) 10 min UV post-treatment, c) 20 min UVA post-treatment,
- d) 2 min UVC post-treatment, e) 20 min UVC post-treatment

It is visible that 5 minutes of UVA post-treatment (Figure 69.a) results with the increased ink amount on the print compared to prolonged UVA and UVC post-treatments. The reason is poorer wetting (because of lower  $\gamma$ ) than for printing plates exposed to prolonged UV post-treatments. Prolonged UVC post-treatment (Figure 69.e) can be used as a tool to decrease the width of the printed line.

Moreover, it is important to notice that neither ACE Digital, nor the Cosmolight QS printing plates give optimal results regarding the consistency of the fine printed line. The deformation specific for flexographic printing plate results in absence of the printing ink transfer in the center of the printed element (screen element, line, etc.). Therefore, if printing with conductive inks, where the uniformity and coverage of the whole line/element surface is of crucial importance, nominal width of the line must be adjusted to the specific printing plate if possible [96, 97]. Alternatively, the choice of different type of photopolymer flexographic printing plate must be made.

### 4.3.3. Coverage values on prints

Results of coverage values measured on prints obtained by UV post-treated printing plates are presented in Figures 70. – 72. Coverage area of highlights and mid-tones on prints did not display any significant difference in relation to the duration of UV post-treatments. However, noticeable changes were detected in high coverage area, where the deformation of the printing plate and excessive dot gain in the printing process can cause the loss of shadow area on the print, i.e. printing a solid tonal patch in the halftone area [98].

Figure 70. presents the changes in high coverage area on prints obtained by UV post-treated ACE Digital printing plates. There is no visible trend of UVA and UVC post-treatment influence on coverage values. ACE Digital is a printing plate with lowest hardness compared to two other printing plates tested in this research (maximal hardness of ACE Digital printing plate is 71.6 on Shore A scale, while Digital MAX's is 74.6, and Cosmolight QS's 77.5 on Shore A scale).

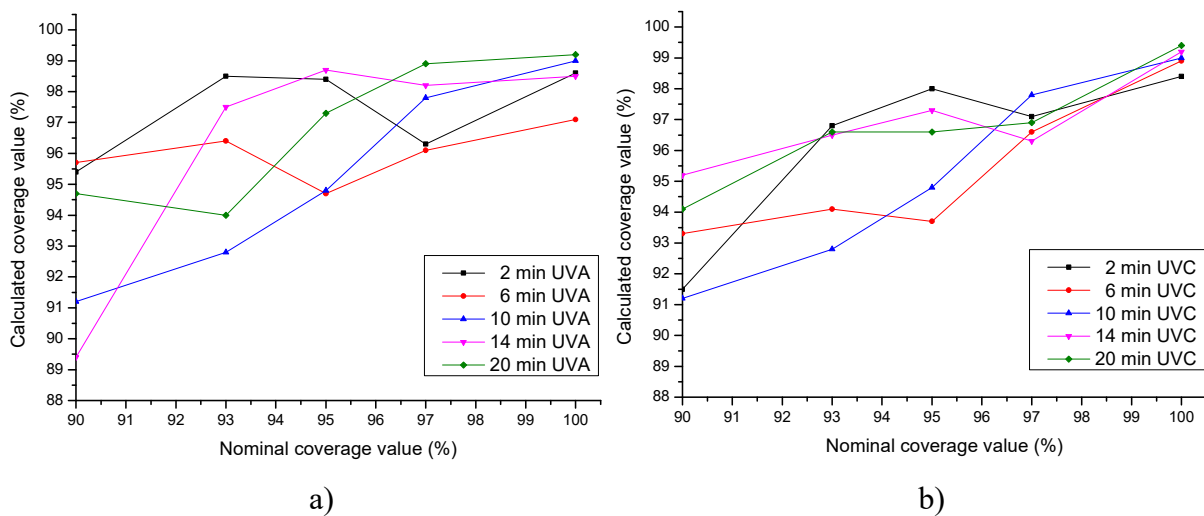


Figure 70. Changes in high coverage area on prints obtained by UV post-treated ACE Digital printing plates:

a) with variation of UVA post-treatment, b) with variation of UVC post-treatment

Higher hardness of Digital MAX and Cosmolight QS printing plates, and therefore increased stability in terms of elastic deformation in the printing process [99, 100], results with the visible effect of varied UV post-treatments on the halftones in high coverage area (Figures 71. and 72.).

Specifically, with prolonged UVA post-treatment (Figures 71.a) and 72.a), coverage values in the shadow area decrease, probably primarily because of the increasing hardness and less deformation of the printing plates.

This decrease in high coverage area on prints is significant (from 98% to 93.4% for Digital MAX printing plates and from 97.8% to 89.9% for Cosmolight QS printing plates, at nominal coverage value of 93%).

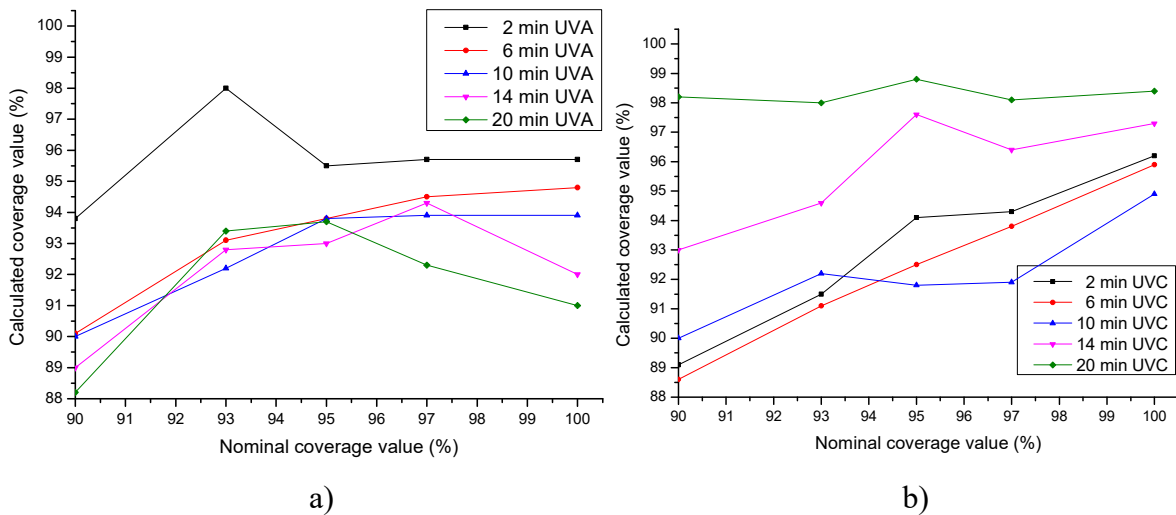


Figure 71. Changes in high coverage area on prints obtained by UV post-treated Digital MAX printing plates:

a) with variation of UVA post-treatment, b) with variation of UVC post-treatment

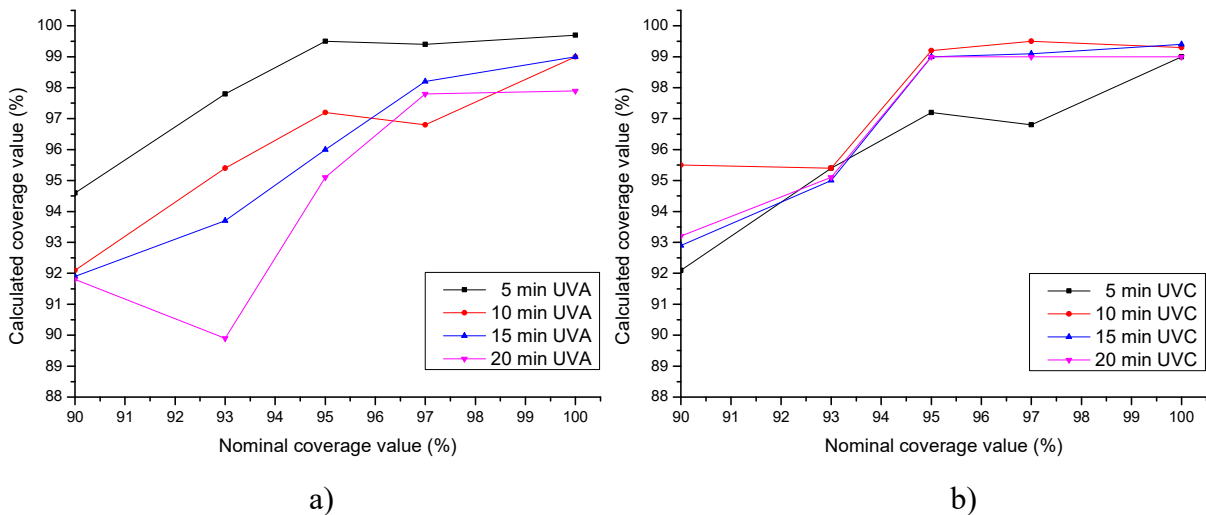


Figure 72. Changes in high coverage area on prints obtained by UV post-treated Cosmolight QS printing plates:

a) with variation of UVA post-treatment, b) with variation of UVC post-treatment

On the other hand, UVC post-treatment results with the opposite trend of changes in high coverage area (Figures 71.b) and 72.b).

For Digital MAX printing plates, coverage values on prints decrease slightly up to 10 minutes of UVC post-treatment duration. After that, coverage values increase considerably (from values of ~ 91% at 93% of nominal coverage to 94.6% and 98% for 14 and 20 minutes of UVC post-treatment, respectively). For Cosmolight QS printing plates, coverage values on prints increase after 5 minutes of UVC post-treatment (from 97.2% to 95% at nominal coverage of 93%).

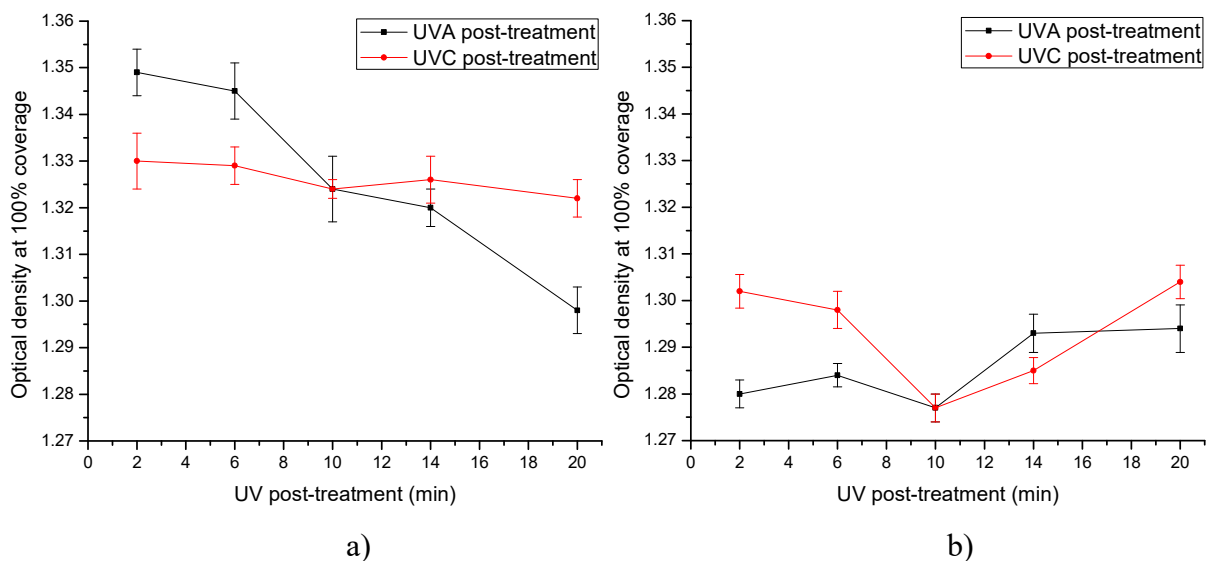
Trends of the changes in measured coverage values on prints obtained by Digital MAX and Cosmolight QS printing plates follow the trends of changes in printing plates'  $\gamma^p$  [101].

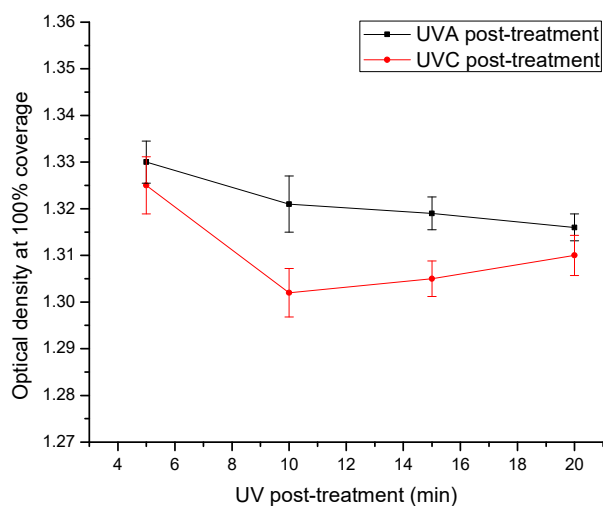
Therefore, if initial hardness of the printing plate is sufficient to eliminate excessive deformations during the engagement, duration of UVA post-treatment can be used to decrease the coverage values in shadow area due to the increasing hardness, while the duration of UVC post-treatment (adjusted to the application of the specific printing ink) can be used to decrease and increase coverage values on prints, adjusting them to the desired levels.

#### 4.3.4. Optical density on prints

Results of optical density of printed black ethanol-based printing ink by means of UV post-treated printing plates in this thesis has a significance for the detection of changes in visual impression of high-quality color prints, obtained by printing plates with modified surface properties due to the differences in the UV post-treatment duration. Optical density calculations are presented in Figure 73.

In Figure 73.a) one can notice the changes in optical density on prints obtained by ACE Digital printing plates. It is visible that optical density decreases with prolonged UVA post-treatment (from 1.349 to 1.298), affecting the visual impression of the print [102]. Varied UVC post-treatment has no significant influence on the changes of optical density on prints. This points to the complex mechanism of the influencing parameters on high-quality color prints obtained by UV-modified printing plates (since both UVA and UVC post-treatment have a similar impact on  $\gamma$  of ACE Digital photopolymer material), related to the adsorption and transfer of the printing ink on the printing plate and involving the chemical changes occurring on the printing plate surface. Therefore, if printing high-quality color reproductions with UV-modified ACE Digital printing plate and similar type of printing ink as the one used in this research, one should be aware of potential unwanted decrease of optical density on prints [103].





c)

Figure 73. Changes of optical density on prints obtained by UV post-treated printing plates:

a) ACE Digital, b) Digital MAX, c) Cosmolight QS

UVA and UVC post-treatment have a similar trend of influence on the optical density of printed ink layer obtained by Digital MAX printing plates. However, variation of UVC post-treatment causes more expressed changes than by ACE Digital (Figure 73.b). It is interesting to notice that the optimal duration of both UV post-treatments recommended by the manufacturer (10 minutes) results with lowest optical density on print. This could be the result of the highest  $\gamma^p$  at that duration of UV post-treatments, which is related to the amount of printing ink adsorbed on the printing plate in the reproduction process [104].

For UV-modified Cosmolight QS printing plates (Figure 73.c), varied UVA post-treatment causes the slight decrease of optical density (from 1.330 to 1.316), which is not a considerable change. Similar trend can be observed for printing plate samples exposed to varied UVC post-treatment, with an exception of the sample treated with 10 minutes of UVC post-treatment. This decrease of optical density can be connected to the peaked  $\gamma^p$  for that printing plate sample.

It can be concluded that the changed surface properties of flexographic printing plates will have an influence on the optical density on prints, depending on the type of the photopolymer material used for the printing plate production, as well as on the used printing ink and substrate. These potential changes could affect the quality of the print and should therefore be taken into account if modifying printing plate's surface properties by UV post-treatments.



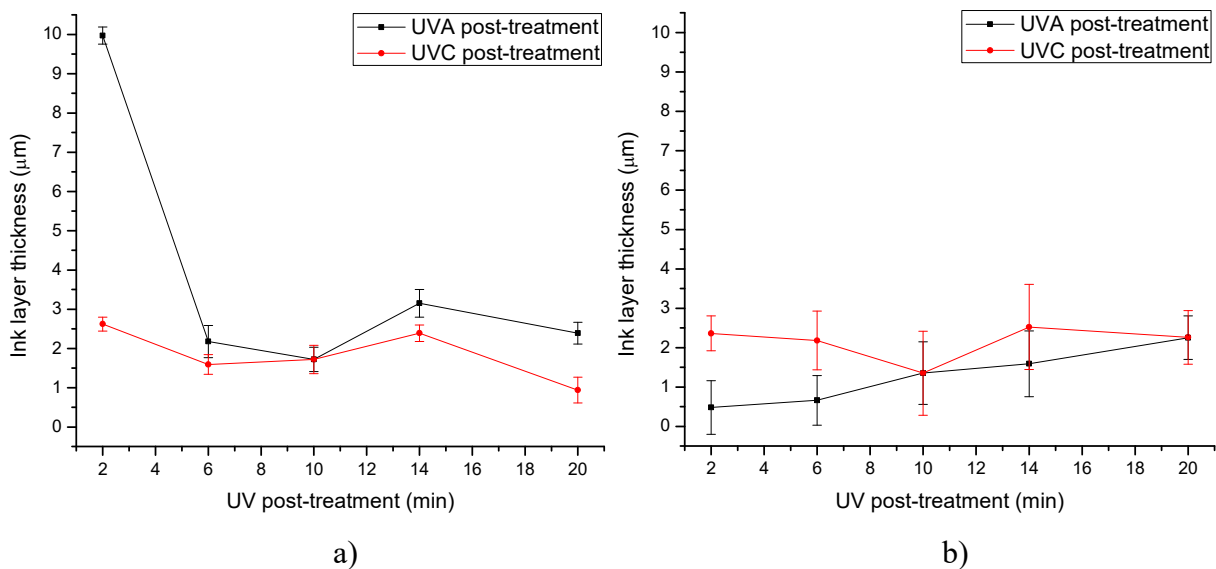
#### 4.3.5. Thickness of printed ink layer

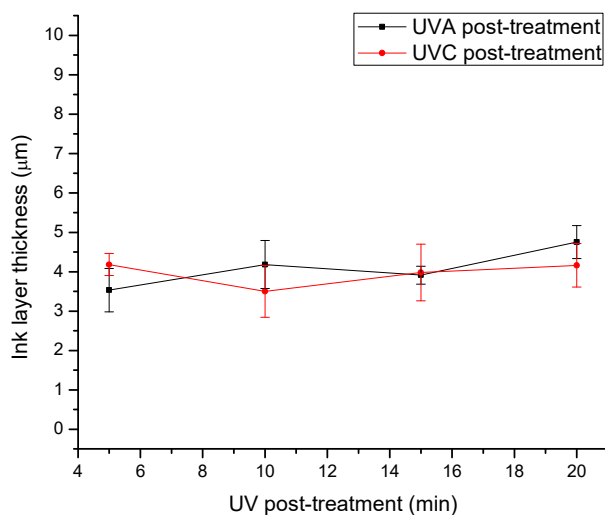
Thickness of the printed ink layer is one of the crucial features of printed functional layers [105]. Finer adjustment of the ink (or coating) thickness than can be achieved by anilox selection [106], could present a step forward in improved quality of flexographic-printed thin layers.

Figure 74. displays the effect of the UVA and UVC post-treatments on the thickness of the ink layer on prints.

Specifically, lower durations of UVA post-treatment for ACE Digital photopolymer material (Figure 74.a) results with the distinguished lower  $\gamma^d$  of the photopolymer material, therefore resulting with poor wetting of the ethanol-based type of printing ink used in this research and transfer of the lower amount of the printing ink to the printing substrate. Prolonged UVA post-treatment of ACE Digital printing plate results with the thicker layer of printing ink on the printing substrate. Analogue to the results of optical density calculations, this could be explained by dominant influence of the interaction between the printing plate surface and the black printing ink containing polar groups chemisorbed on pigments' surfaces [107].

UVC post-treatment of ACE Digital printing plate has no considerable effect on the ink layer thickness on prints, but the wide range of thickness achieved by UVA post-treatment (from 9.97  $\mu\text{m}$  to 2.39  $\mu\text{m}$ ) can be used to adjust the properties of the deposited ink/coating layer.





c)

Figure 74. Changes of ink layer thickness on prints obtained by UV post-treated printing plates:

a) ACE Digital, b) Digital MAX, c) Cosmolight QS

Changes of the ink layer thickness on prints obtained by Digital MAX printing plates (Figure 74.b) are not as expressed as on prints obtained by ACE Digital printing plates.

According to the trend of the changes in the ink layer thickness on prints obtained by printing plates treated with varied UV post-treatments, one can conclude that  $\gamma^p$  has the main influence on the definition of the ink layer thickness, which is specifically visible for sample treated for 10 minutes of UV post-treatments. Cosmolight QS printing plates (Figure 74.c) display lowest deviations in the ink layer thickness related to the duration of UV post-treatments.

Furthermore, beside the ACE Digital sample treated for 2 minutes of UVA post-treatment, printed ink layers obtained by Cosmolight QS obtain the highest thickness. The reason for that could be the highest  $\gamma^p$  of Cosmolight QS photopolymer material among the three photopolymer materials examined in this research. Specifically in this case, high  $\gamma^p$  of the printing plate will decrease the wetting of ethanol-based printing ink, ethanol being a liquid with  $\gamma^{lv}$  of 21.4 mNm<sup>-1</sup>  $\gamma^{d_{lv}}$  of 18.8 mNm<sup>-1</sup> and  $\gamma^{p_{lv}}$  of 2.6 mNm<sup>-1</sup> [108].

This proves that, although the changes of the surface properties of flexographic printing plates due to the UV post-treatments may not appear as significant at a first glance, they affect the quality of the ink/coating layer on the printing substrate.

# **5. MODELLING THE PROPERTIES OF PRINTING PLATES AND PRINTS**

## **5.1. Analysis of the influencing parameters on $\gamma^d$ and $\gamma^p$ of photopolymer material**

5.1.1. Weight loss of photopolymer material in relation to  $\gamma^d$

5.1.2. Relation of oxygen ratio in the surface layer of photopolymer material and  $\gamma^p$

## **5.2. Qualitative properties of prints in relation to modified printing plate surface properties**

5.2.1. Relation of the properties of printing plates and coverage values on prints

5.2.2. Relation of the properties of printing plates and optical density on prints

5.2.3. Relation of the properties of printing plates and thickness of printed ink layer

## **5.3. LS model fitting of the influencing parameters for printing plate and print properties**

5.3.1. LS fitting of the printing plate parameters

5.3.2. LS fitting of the print properties

## **5.4. Neural network as a functional model for estimation of surface properties of photopolymer printing plates**

## 5.1. Analysis of the influencing parameters on $\gamma^d$ and $\gamma^p$ of photopolymer material

After displaying all results obtained by different measurement and analysis methods in order to understand the changes that occur in the photopolymer materials due to the varied UVA and UVC post-treatments, it was necessary to integrate the influencing parameters in order to define the influence of the UV post-treatments on the surface properties ( $\gamma^d$  and  $\gamma^p$ ) of photopolymer materials.

Identified changes occurring in the core of the material (changes of the weight loss of swollen photopolymer samples) were important in order to get a better insight into the changes in composition and the crosslinking degrees of tested materials, and to assess the changes that influence the performance of the printing plate in the reproduction process. Changes in the surface properties of photopolymer printing plates are primarily the result of the changes in ratio of oxygen bonds in the surface layer.

However, primary context of discussion chapter in this thesis is the integration of parameters influencing the surface properties of the printing plate ( $\gamma^d$  and  $\gamma^p$ ) with varied durations of UV post-treatments, since they are mostly responsible for the process of the printing ink/coating transfer to and from printing plate and for tailoring the properties of the printed layer.

### 5.1.1. Weight loss of photopolymer material in relation to $\gamma^d$

Results of swelling properties of photopolymer materials enabled the comparison of the relative differences in the cohesion forces in photopolymer materials that were immersed in solvents of different solubility parameters (Figures 43. - 48.). Swelling in toluene was most expressed for all photopolymer material samples due to the highest dispersion forces in toluene and lowest hydrogen bonding component compared to other used solvents. Dynamics of swelling with prolonged UV post-treatments pointed to the possible expressed differences between the surface and the core of the photopolymer material. Hardness measurements (Figure 42.) and thermal analysis (Figures 33. - 38.) indicated that the crosslinking degree in the core of materials generally increases with prolonged UV post-treatments. Since the surface analysis (Chapter 4.2.) pointed to the possible start of the material degradation caused by photo oxydation, further analysis of obtained results needed to be performed.

The results of swelling experiments were used to calculate the weight loss of the samples after immersion in different solvents and drying. Segments in the core of photopolymer materials' composition which are soluble in used solvents would cause the weight loss after the immersion and drying. Increased crosslinking degree in the material should result with the decreased weight loss [109]. However, since the UV post-treatments affect differently the surface and the core of the material, changes in weight loss would differ for the samples treated with varied durations of UV post-treatments. In this way, degradation by erosion of the surface, expressed during the swelling experiments could be detected and analysed.

Figure 74. presents the weight loss of ACE Digital samples immersed in different solvents. After 5 minutes of both UVA and UVC post-treatments,  $\gamma^d$  of ACE Digital material reaches maximal values. Observing Figure 75., one can see that UV post-treated samples of ACE Digital material show the increasing trend of weight loss in toluene. This points to the expressed compatibility of cohesion forces in the material and solubility parameters of toluene.

Immersion of ACE Digital photopolymer material in acetone and ethyl acetate causes the similar weight loss behavior. It can be concluded that the unsaturation in not UV post-treated sample or compounds that haven't participated in the crosslinking reactions cause the partial dissolution. Weight loss then decreases up to 10-15 minutes of the UV post-treatment, but then increases again. This indicates that prolonged UV post-treatments results with breakage

of bonds in photopolymer structure and/or formation of residuals soluble in acetone and ethyl acetate.

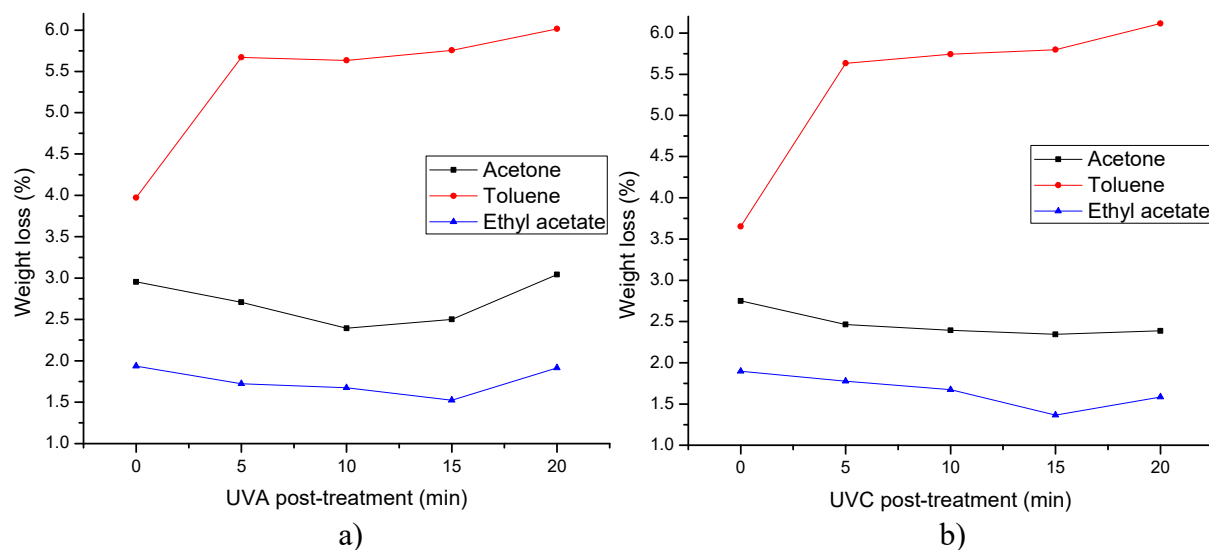


Figure 75. Weight loss of ACE Digital photopolymer material immersed in different solvents for varied: a) UVA post-treatment, b) UVC post-treatment

Based on DSC and TGA analysis results, one can conclude that these changes in the material network occur on the surface and could therefore influence the reproduction quality in the long run, since the degradation of ACE Digital material caused by UV post-treatments is obviously present.

Figure 76. displays weight loss of Digital MAX photopolymer materials after immersion in different solvents. The material shows the decreased weight loss in all used solvents with prolonged UV post-treatments.

The dynamics of changes in weight loss is similar for both types of UV post-treatments, but the decrease in weight loss is more expressed with prolonged UVC post-treatment. Expressed decrease of weight loss in toluene at prolonged UVC post-treatment points to the conclusion of both increased crosslinking degree and the positive changes in cohesion parameters in the material regardless of the incorporation of the oxygen in the surface with its presumably destructive influence. Weight loss in acetone and ethyl acetate decreases to approx. 0.3% with prolonged UVC post-treatment. Compounds containing oxygen bonds are not causing the degradation of Digital MAX photopolymer material, they are rather incorporated in the crosslinked structure.

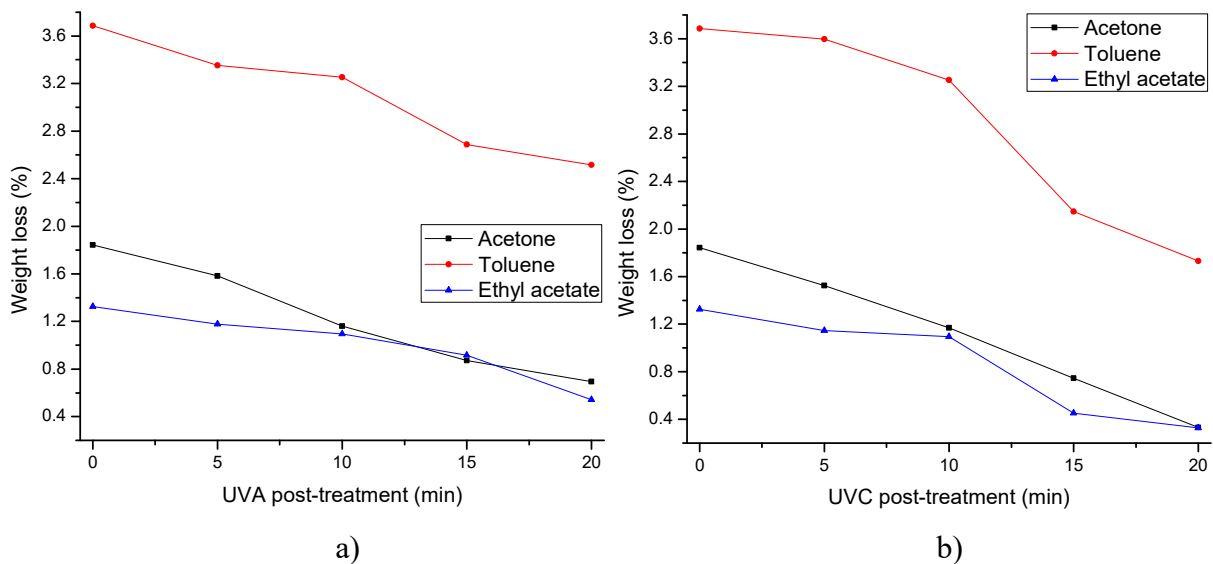


Figure 76. Weight loss of Digital MAX photopolymer material immersed in different solvents for varied: a) UVA post-treatment, b) UVC post-treatment

Weight loss of Cosmolight QS photopolymer material (Figure 77.) displays the decreasing trend for the samples immersed in acetone and ethyl acetate, pointing to the increased crosslinking degree in the material after prolonged UV post-treatments. However, since toluene showed the highest compatibility with tested photopolymer materials in terms of cohesion and solubility parameters, the increased weight loss after 10 minutes of UVC post-treatment is indicative. Since both  $\gamma^d$  and  $\gamma^p$  of Cosmolight QS material decrease after 10 minutes of UVC post-treatment (Figures 51. and 52.), cohesion parameters in the material would decrease, as well. This could be caused by both migration of the non-polar components to the surface of the material and the simultaneous start of the bond breakage in the photopolymer network, resulting with the dissolution of segments in toluene.

Trends of the changes in weight loss of photopolymer materials immersed in different solvents proved to follow the trends of changes in  $\gamma$ , specifically in relation to changes of  $\gamma^d$ . This proves that the increased weight loss of some samples in solvents is caused by degradation by erosion present in the surface layer as a result of the UV post-treatments.

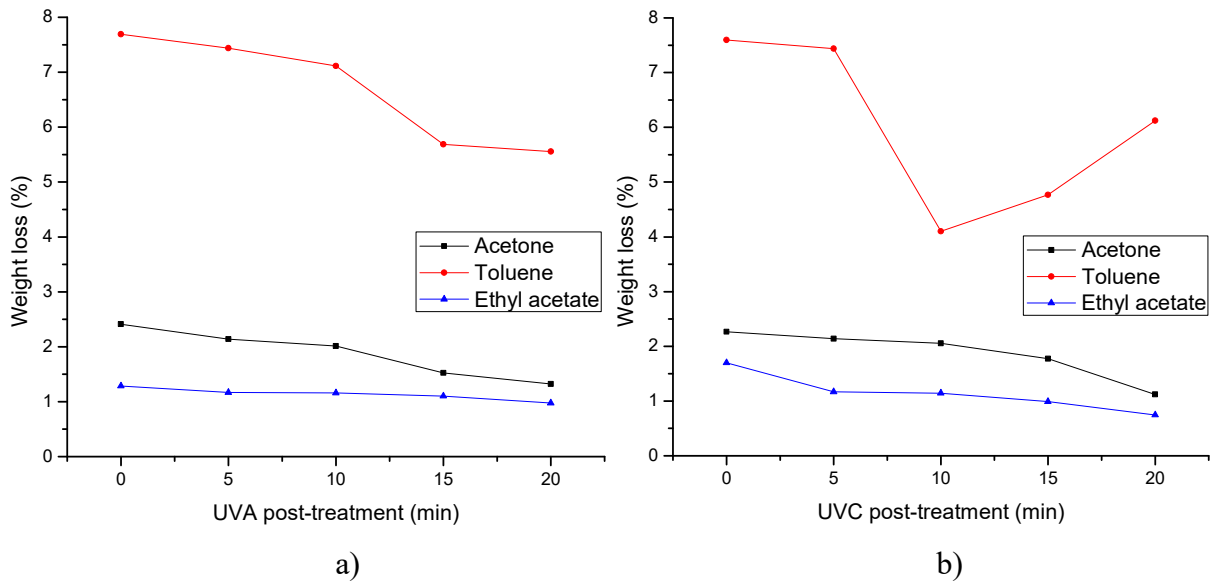


Figure 77. Weight loss of Cosmolight QS photopolymer material immersed in different solvents for varied: a) UVA post-treatment, b) UVC post-treatment

Figures 78. – 80. were displayed in order to compare weight loss of different photopolymer materials, due to the differences in their composition and  $\gamma$ .

Figure 78. presents the weight loss of tested photopolymer materials after immersion in acetone. It is visible that ACE Digital material is the only one showing increased solubility with prolonged UV post-treatments.

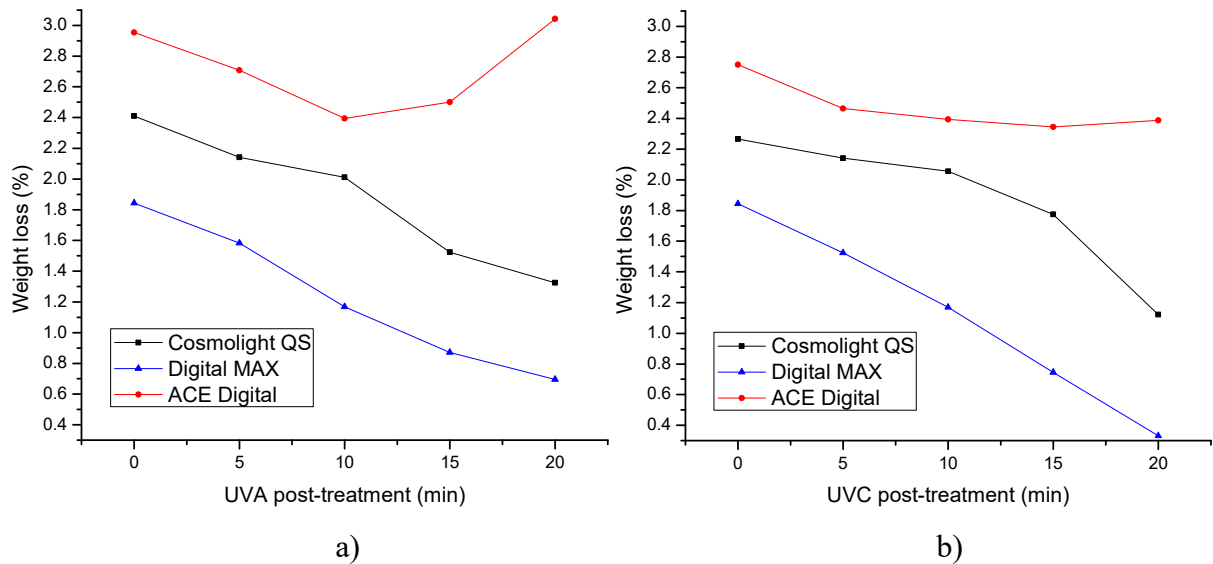


Figure 78. Weight loss of photopolymer materials immersed in acetone for varied: a) UVA post-treatment, b) UVC post-treatment



Since swelling experiments showed that solubility parameters of acetone are not particularly compatible with tested photopolymer materials, inflexion point of weight loss at 10 minutes of UV post-treatments for ACE Digital material points to more expressed changes in the chemical bonds of this material compared to other samples.

Weight loss in ethyl acetate for different photopolymer materials displays the similar trend as in acetone (Figure 79.). However, weight losses in ethyl acetate are significant if using printing ink or printing plate washing agent which contains ethyl acetate. Although the weight loss in ethyl acetate is not significant (between 1.1% and 1.7%) for samples treated with officially recommended duration of UV post-treatments, when varying the UV post-treatment duration, the partial dissolution of photopolymer materials in ethyl acetate could become more expressed.

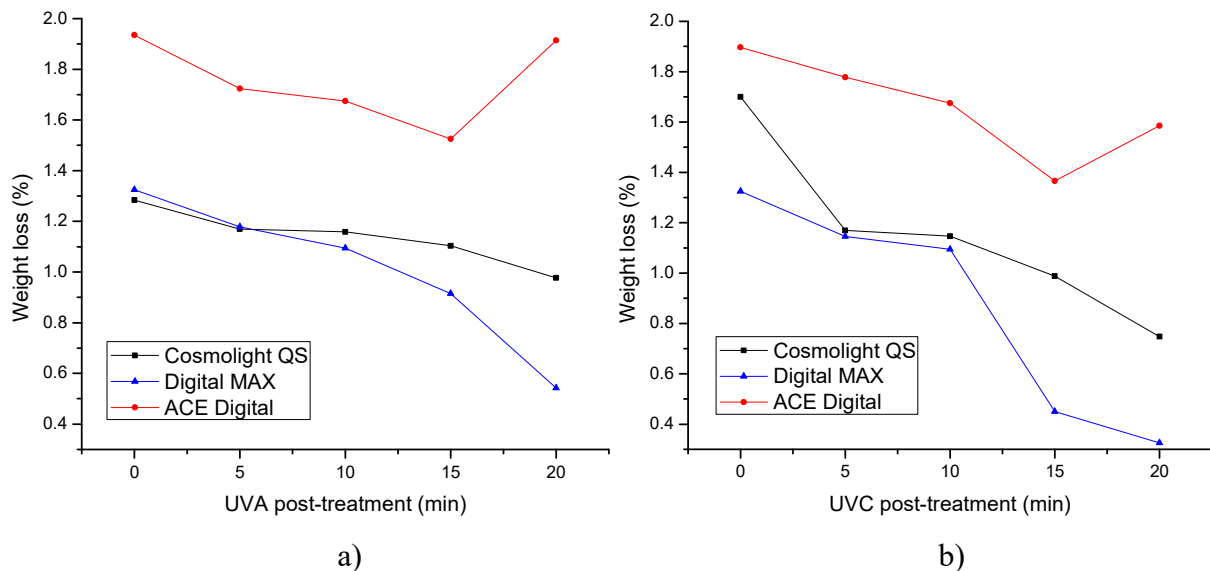


Figure 79. Weight loss of photopolymer materials immersed in ethyl acetate for varied:  
a) UVA post-treatment, b) UVC post-treatment

In Figure 80., one can see the compared weight loss of UV post-treated photopolymer materials after immersion in toluene. Swelling in toluene was most expressed for all samples and therefore most indicative in this research. Again, changes occurring in ACE Digital material result with increased dissolution after prolonged UVA post-treatment, while weight losses for other two materials decrease after prolonged UVA post-treatments.

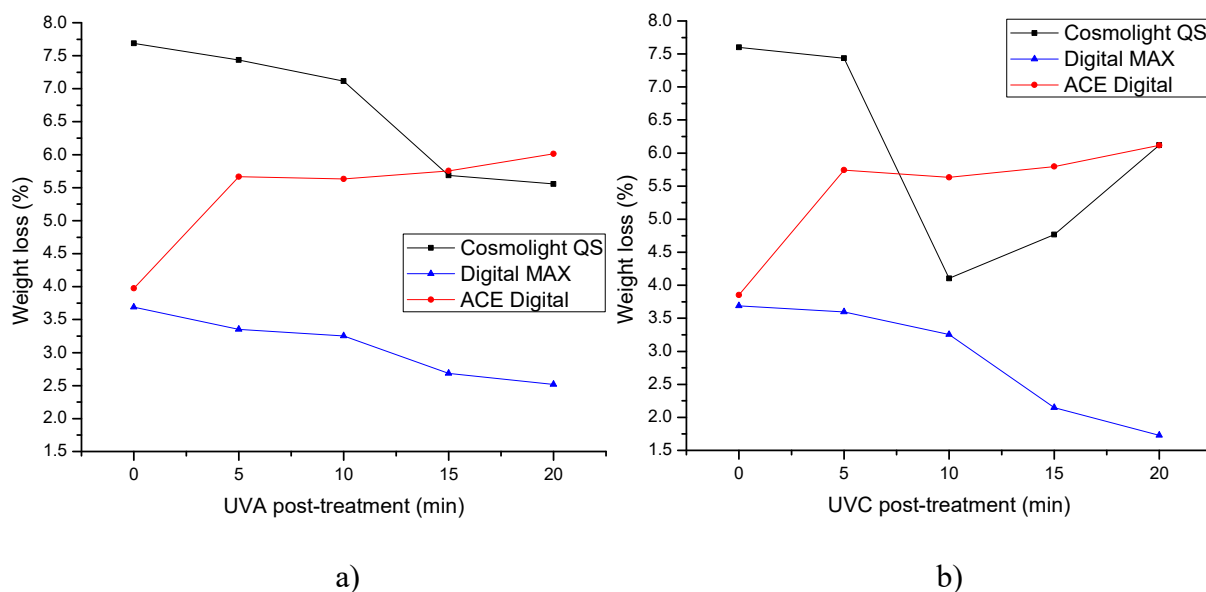


Figure 80. Weight loss of photopolymer materials immersed in toluene for varied:  
a) UVA post-treatment, b) UVC post-treatment

One can see that UVC post-treatment will have the same influence on Cosmolight QS material as on ACE Digital after immersion in acetone and ethyl acetate. If explaining this result in terms of the changes in  $\gamma$  and its components (Figures 50. - 52.), one can conclude that Digital MAX material is most stable in toluene due to its highest  $\gamma$  among three tested materials. This relation between  $\gamma$  and material's resistivity to solvent could be a valuable note when using particular solvent in ink/coating formulation and getting it in the contact with printing plate surface.

Finally, cohesion parameter of the photopolymer material itself is not an only indicator for printing plate's behavior in the contact with specific solvent: its (modified) surface properties will have a noticeable influence, as well.

Figure 81. is presented with the aim of comparing the dependence of  $\gamma^d$  on the UV post-treatment duration of different photopolymer materials and summarize the influence of UV post-treatments on  $\gamma^d$  as an indicator of the crosslinking degree in the material. It is visible (Figure 81.a) and b) that UVC post-treatment results with higher range of changes for ACE Digital and Digital MAX photopolymer materials than UVA post-treatment. For ACE Digital material, initial increase of  $\gamma^d$  is caused by the crosslinking in the material, which was confirmed directly by DSC analysis (Figures 33. and 34.) and indirectly by hardness measurements (Figure 42.).

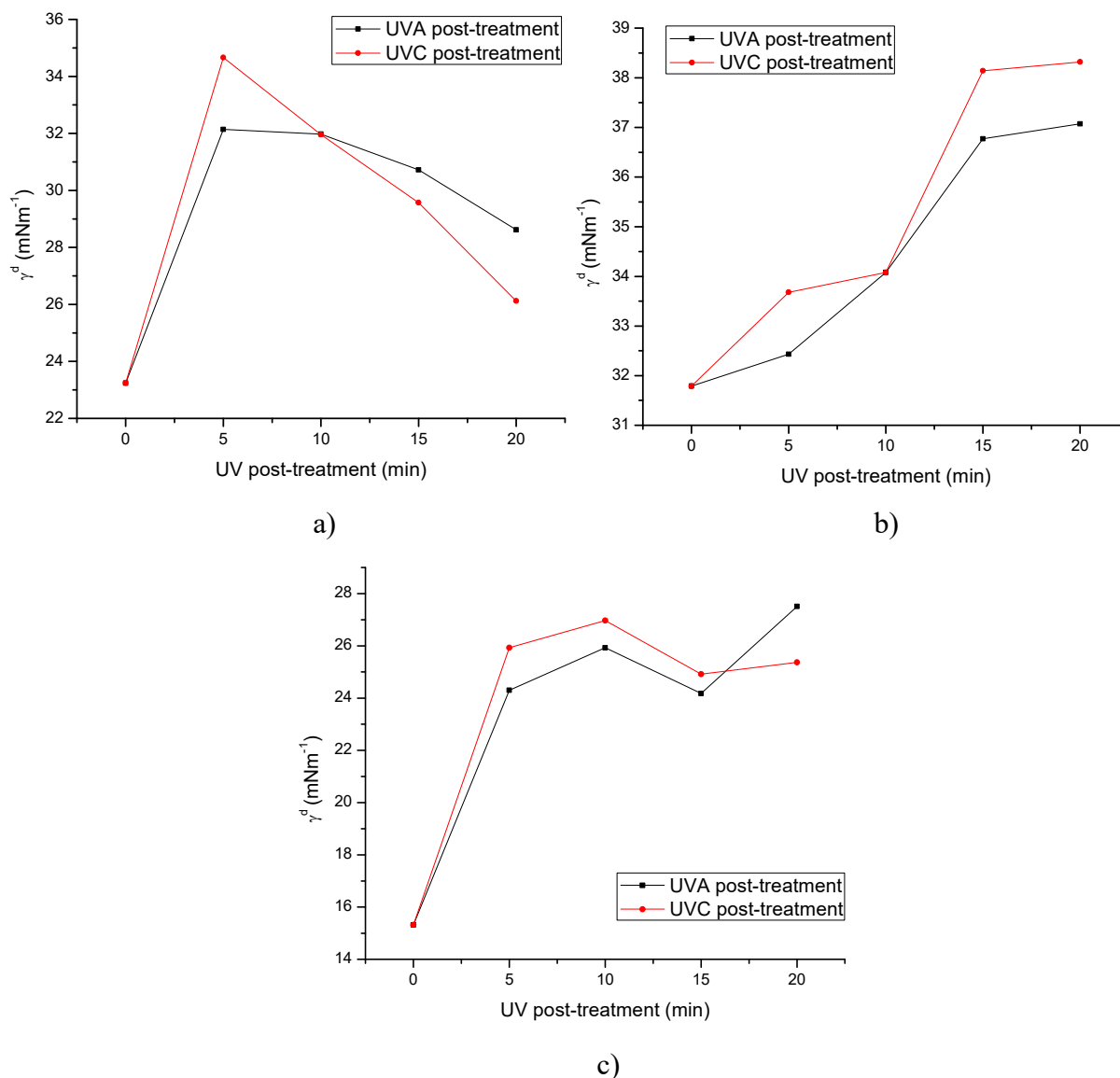


Figure 81. Dependence of  $\gamma^d$  and UV post-treatment durations for:

a) ACE Digital printing plate, b) Digital MAX printing plate, c) Cosmolight QS printing plate

Prolonged UV post-treatments result with changes in the types and strengths of bonds in the surface layer of the material, pointing to the possible start of the surface degradation.

For Digital MAX photopolymer material (Figure 81.b), changes in  $\gamma^d$  do not point to the start of degradation, but only to the increased crosslinking degree in the surface layer. For Cosmolight QS samples,  $\gamma^d$  increases with prolonged UV post-treatments as well, but with some inconsistencies after 10 minutes of UVA and UVC post-treatment. These inconsistencies can be the result of the migration processes in the surface layer, similar to ACE digital material, but with different dynamics and influence on  $\gamma^d$ , or the production of the residuals in the crosslinking process.

In order to define the influence of the changes of weight loss in solvents (and therefore changes in crosslinking degree of the materials) on  $\gamma^d$ , Pearson product-moment correlation coefficient (measure of the linear correlation between two variables -  $r$ ) for weight loss (Eq. 10) in different solvents and  $\gamma^d$  influenced by UVA and UVC post-treatment was calculated according to Eq. 10. and displayed in Table 9. and Table 10.

$$r = \frac{\sum_{i=1}^n (x_i - \bar{x})(y_i - \bar{y})}{\sqrt{\sum_{i=1}^n (x_i - \bar{x})^2 \sum_{i=1}^n (y_i - \bar{y})^2}}, \quad (10)$$

$\{x_1, \dots, x_n\}$  and  $\{y_1, \dots, y_n\}$  present the datasets containing  $n$  values, while  $\bar{x}$  and  $\bar{y}$  present the sample means.

It is visible that UVA post-treated ACE Digital material displays very good negative correlation between weight loss in acetone and  $\gamma^d$  as well as weight loss in ethyl acetate and  $\gamma^d$  (Table 9.). Therefore, decreased weight loss in these solvents is directly connected to the increased  $\gamma^d$  due to the decreased crosslinking degree in the material caused by UVA post-treatments, and vice versa. High  $r$  values prove that this interpretation on connection between crosslinking degree,  $\gamma^d$  and solubility in specific solvent is valid.

Table 9. Calculated  $r$  values for weight loss and  $\gamma^d$  of photopolymer materials for the set of samples exposed to varied UVA post-treatment

% weight loss	$\gamma^d$ (ACE Digital)	$\gamma^d$ (Digital MAX)	$\gamma^d$ (Cosmolight QS)
<b>Acetone</b>	<b>-0.88</b>	<b>-0.99</b>	<b>-0.73</b>
<b>Ethyl acetate</b>	<b>-0.85</b>	<b>-0.87</b>	<b>-0.54</b>
<b>Toluene</b>	0.54	<b>-0.95</b>	<b>-0.59</b>

However, there is no valuable correlation for  $\gamma^d$  and weight loss in toluene for ACE Digital material. This is probably due to the fact that ACE Digital has the lowest  $\gamma^p$  and  $\gamma^{\text{total}}$  among tested photopolymer materials (Figures 50. and 51.). Its solubility in toluene which has highest dispersion forces compared to acetone and ethyl acetate (Table 8.) is obviously not dependent on the changes of surface properties.

Digital MAX samples show very good, even excellent negative correlation of  $\gamma^d$  and weight loss in different solvents, pointing to the strong inversely proportional relation of these two values.

Cosmolight QS photopolymer material displays good negative correlation of  $\gamma^d$  and weight loss in acetone, but its solubility in other solvents is not directly related to its surface properties.

Table 10. displays similar trends as Table 9. in terms of  $r$  values for weight losses in solvents and  $\gamma^d$  of printing plates exposed to varied UVC post-treatments. Changes in  $\gamma^d$  occurring with varied UVC post-treatment are strongly related to weight loss in all solvents for Digital MAX photopolymer material.  $\gamma^d$  of ACE Digital displays very good correlation with weight loss in ethyl acetate, but not in acetone, pointing to different influences of UVA and UVC post-treatments in terms of the changes in types and strengths of chemical bonds in the material. This can be concluded because of the differences in polar and dispersion forces of acetone and ethyl acetate.

Table 10. Calculated  $r$  values for weight loss and  $\gamma^d$  of photopolymer materials for the set of samples exposed to varied UVC post-treatment

% weight loss	$\gamma^d$ (ACE Digital)	$\gamma^d$ (Digital MAX)	$\gamma^d$ (Cosmolight QS)
<b>Acetone</b>	-0.65	-0.96	-0.73
<b>Ethyl acetate</b>	-0.95	-0.98	-0.46
<b>Toluene</b>	0.52	-0.95	-0.67

In order to assess the potential influence of changes of surface roughness on  $\gamma^d$  of photopolymer materials due to the UV post-treatments, relations between  $\gamma^d$  of each printing plate and  $R_a$  parameters were studied.

Surface roughness of flexographic printing plates, if not increased by surface patterning (which has not been the case for printing plates used in this research), usually has low values (0.09  $\mu\text{m}$  – 0.19  $\mu\text{m}$  for samples in this research) and has not shown the substantial influence on  $\gamma^d$  at a first glance.

Despite that, although no correlation of  $R_a$  parameter and  $\gamma^d$  was found for ACE Digital and Cosmolight QS materials,  $R_a$  of Digital MAX material displayed good correlation with  $\gamma^d$  for samples treated with varied UVC post-treatment ( $r = 0.74$  - Figure 82.a), and very good correlation with  $\gamma^p$  for samples exposed to varied UVC post-treatment ( $r = -0.96$  – Figure 82.b).

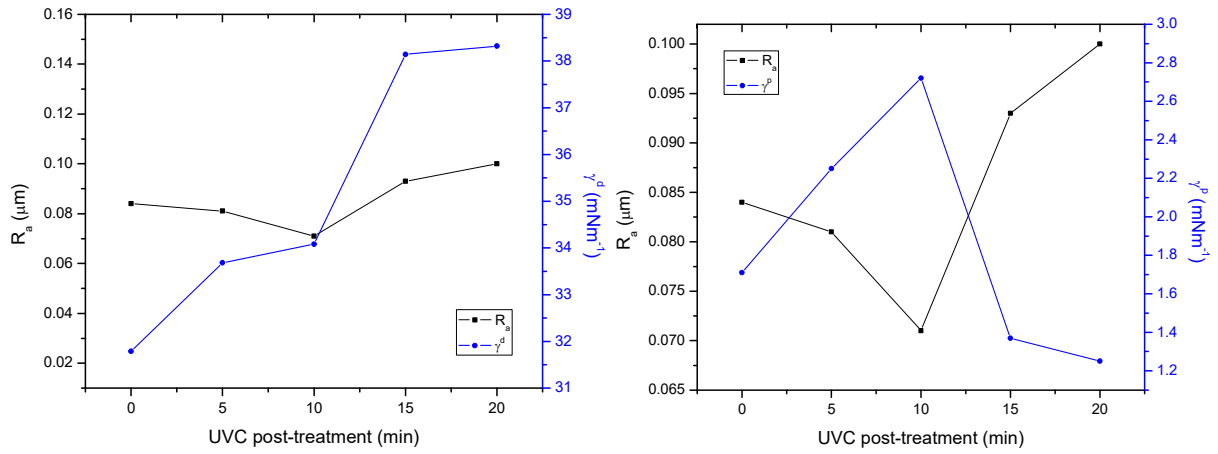


Figure 82. Relation between  $R_a$  and components of  $\gamma$  for UVC post-treated Digital MAX printing plate:

a) relation between  $R_a$  and  $\gamma^d$ , b) relation between  $R_a$  and  $\gamma^p$

This result showed that, although its values are too low to visibly influence  $\gamma$  of photopolymer printing plate, for some materials, changes in  $R_a$  are indicative and display the high correlation coefficients with the changes of the material's surface properties.

### 5.1.2. Relation of oxygen ratio in the surface layer of photopolymer material and $\gamma^p$

Relative absorbance ratios of chemical bonds in various polymer materials are important for the detection of changes in the representation of chemical bonds in relation to changes in composition, curing, diffusion of solvents or water in the polymer, treatments of the materials etc. [110, 111]. In this research, values of relative absorbance ratio for C=O and OH bonds were calculated from FTIR-ATR spectra in order to assess the influence of the ratio of oxygen bonds on  $\gamma^p$  of photopolymer materials. The calculation of the relative absorbance ratios for the chemical bond of interest  $\alpha(t)$  can be obtained from the FTIR-ATR spectra, by comparing the area under the peak of interest to the area of the peak that does not undergo any changes during the altering of material properties, in the absorbance mode of FTIR-ATR spectra.

$\alpha(t)$  values were calculated from FTIR-ATR spectra by means of Eq. 11.:

$$\alpha(t) = \frac{\left(\frac{P_a}{P_b}\right)_t - \left(\frac{P_a}{P_b}\right)_0}{\left(\frac{P_a}{P_b}\right)_0} \cdot 100, \quad (11)$$

$\alpha(t)$  presents the relative absorbance ratios of chemical bonds of interest,  $\left(\frac{P_a}{P_b}\right)_0$  is the ratio of the peak (bond) area of interest on FTIR-ATR spectra and reference peak (bond) area that does not display any changes in absorbance level when UV post-treatments are varied, for non UV post-treated sample.  $\left(\frac{P_a}{P_b}\right)_t$  is the ratio of the peak (bond) area of interest on FTIR-ATR spectra and reference peak (bond) area that does not display any changes in absorbance level when UV post-treatments are varied, for the sample treated with  $t$  minutes of UV post-treatment. In this analysis, chosen reference peak was at  $912 \text{ cm}^{-1}$ , corresponding to C=C vibrations in the styrene component present in all tested photopolymer materials [112].

Figure 83. presents  $\alpha(t)$  of C=O and OH bonds in ACE Digital photopolymer surface. It is visible that UVA post-treatment causes the decrease of  $\alpha(t)$  for C=O bond after the exposure longer than 15 minutes, which will directly affect  $\gamma^p$  of the material (Figure 83.a). The decreased oxygen inhibition is the result of the formation of protective layer on the material surface due to the migration of protective compounds added to these types of photopolymer materials.  $\alpha(t)$  for OH bond increases up to 175% for the sample treated with 10 minutes of UV post-treatment (Figure 83.b). In the period between 10 and 20 minutes of UVA post-treatment, it maintains the value between 160% and 200%.

On the other hand, oxidative degradation could take effect with prolonged UVC post-treatment, since both  $\alpha(t)$  of C=O and OH bond increase. This points to the sensitivity of UVC post-treated ACE Digital photopolymer material to oxygen environment, which is specifically represented in the increase of  $\alpha(t)$  of OH bond up to 400% for the sample treated for 20 minutes of UVC post-treatment.

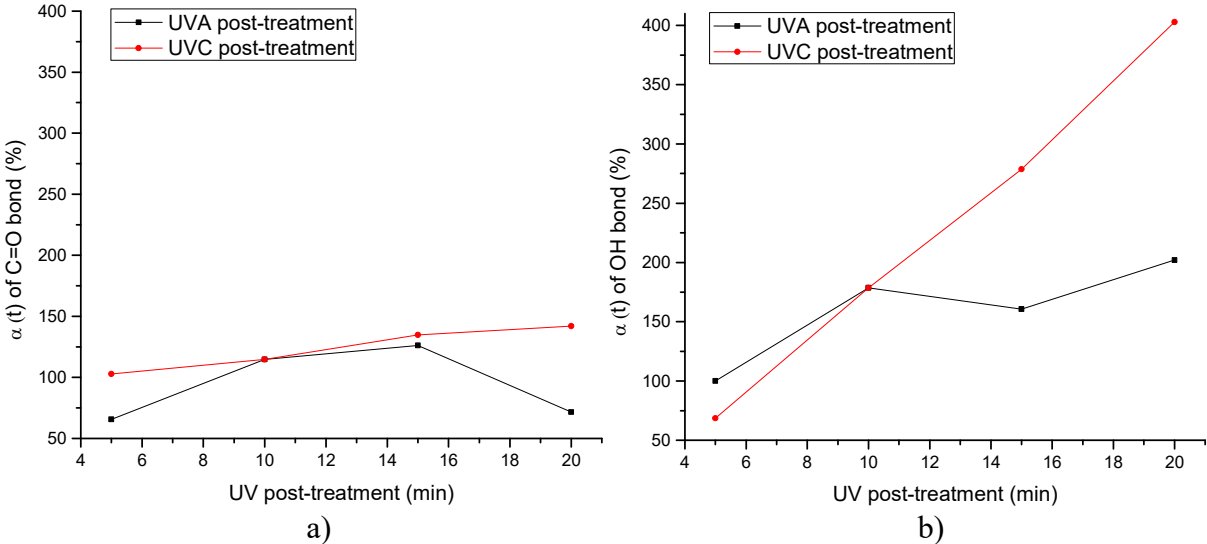


Figure 83.  $\alpha(t)$  for UV post-treated ACE Digital material for: a) C=O bond, b) OH bond

Figure 84. presents the  $\alpha(t)$  values of C=O and OH bonds for Digital MAX material. Digital MAX material displays the highest resistivity to oxygen among the three tested photopolymer materials. With the increased duration of UVA post-treatment,  $\alpha(t)$  values of C=O and OH bonds increase up to 51% and 43%, respectively, with the tendency of stabilization, or even the slight decrease between 15 and 20 minutes of the UVA post-treatment.

As expected, UVC post-treatment has more distinct effect on Digital MAX material than UVA post-treatment. It is visible that the exposure of the material to UVC post-treatment longer than 10 minutes causes the rapid increase of  $\alpha(t)$  of C=O and OH bonds. The increase of  $\alpha(t)$  for C=O bonds stabilizes after 15 minutes of UVC post-treatment, while  $\alpha(t)$  of OH bond continues to increase almost linearly. This signifies that C=O and OH bond display different behavior in the reactions in the photopolymer material. Specifically, the decreased  $\alpha(t)$  of OH bond with prolonged UVA post-treatment (Figure 84.b) can be due to the back-bending of OH groups that form the hydrogen bonding with the carbonyl groups in the polymer backbone which causes their decreased ratio in the surface of the material [113].



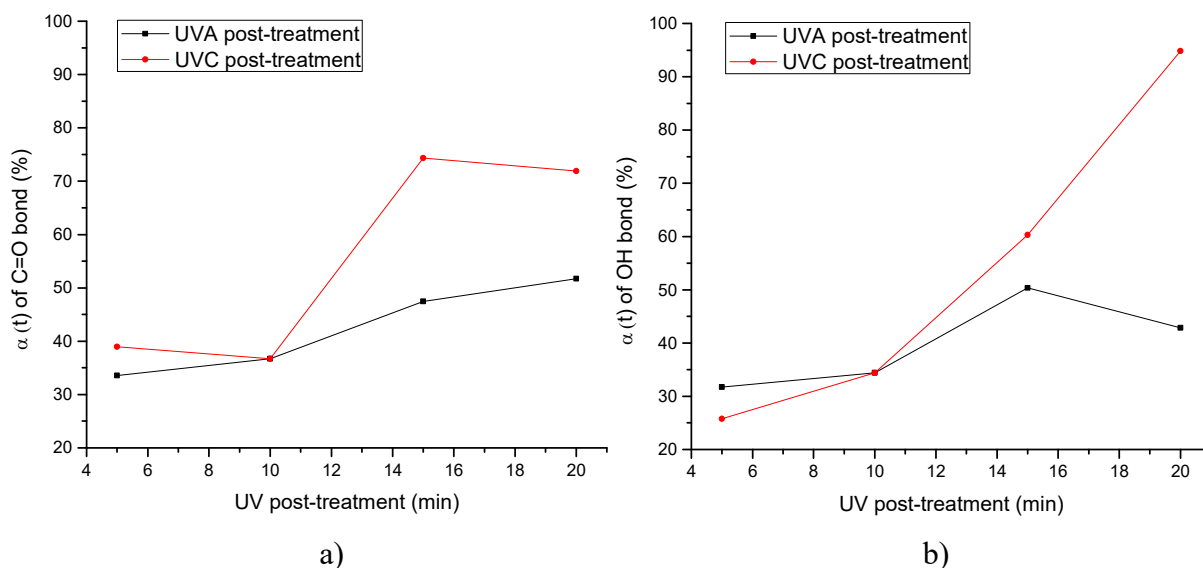


Figure 84.  $\alpha(t)$  for UV post-treated Digital MAX material for: a) C=O bond, b) OH bond

From the results obtained by other measurement and analysis methods, it can be concluded that  $\alpha(t)$  of C=O and OH bonds, with maximal value of 95% for OH bond at 20 minutes of UVC post-treatment, does not affect negatively functional properties of Digital MAX material.

Figure 85. presents  $\alpha(t)$  of C=O and OH bonds for Cosmolight QS photopolymer material.

Increases of  $\alpha(t)$  for C=O and OH bonds after prolonged UVA post-treatment are not significant, except that the decrease of  $\alpha(t)$  for OH bond as a result of UVA post-treatment longer than 10 minutes points to the possible migration process in the material surface and/or changed orientation of OH groups in the surface, similar as in Digital MAX material.

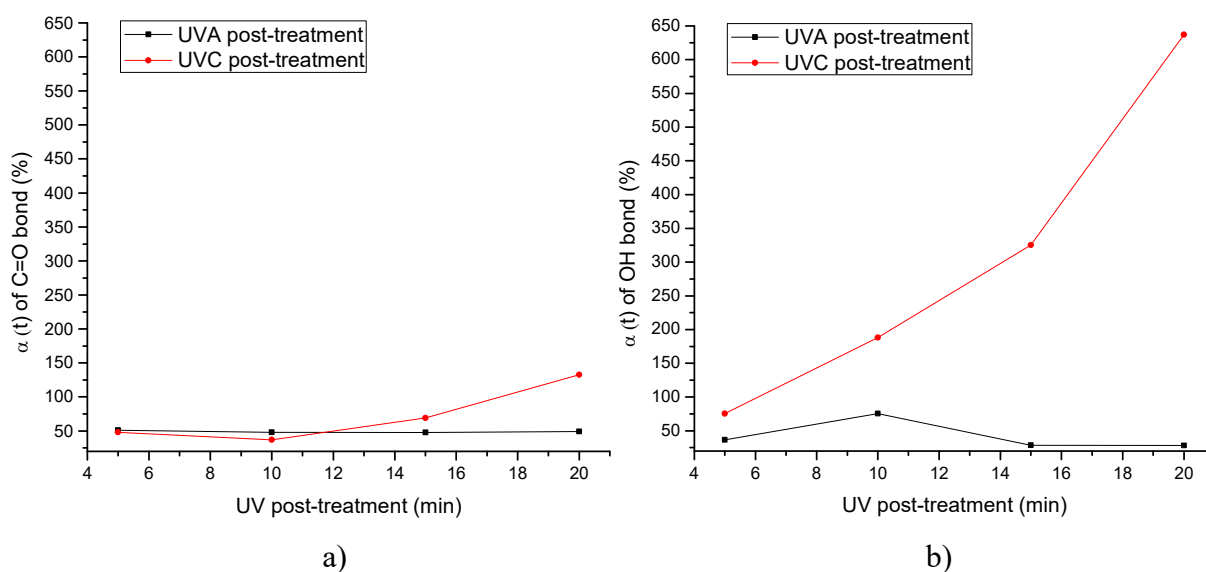


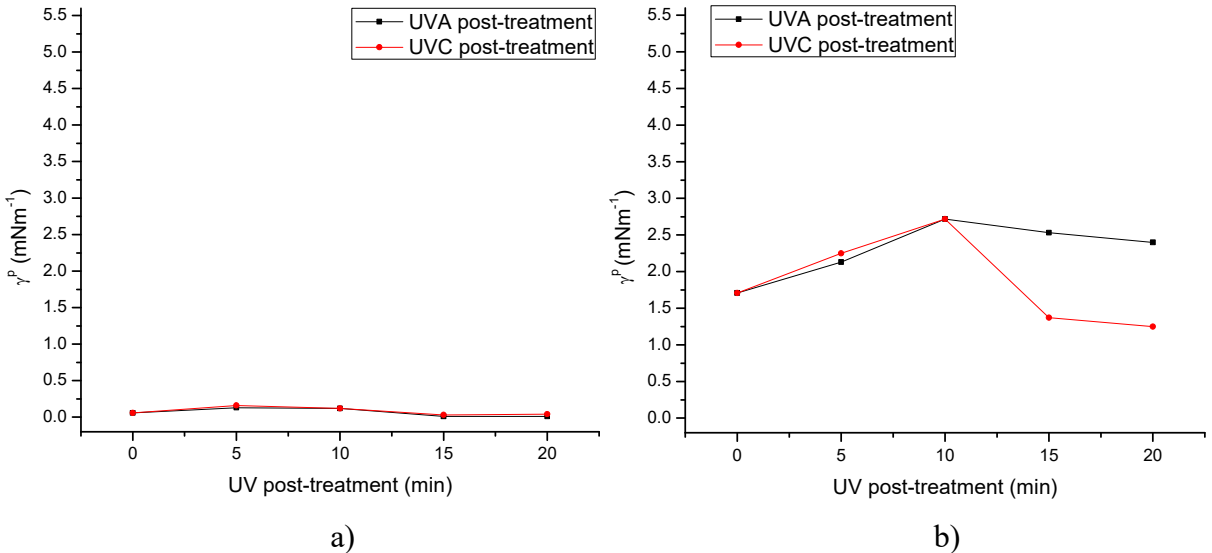
Figure 85.  $\alpha(t)$  for UV post-treated Cosmolight QS material for: a) C=O bond, b) OH bond

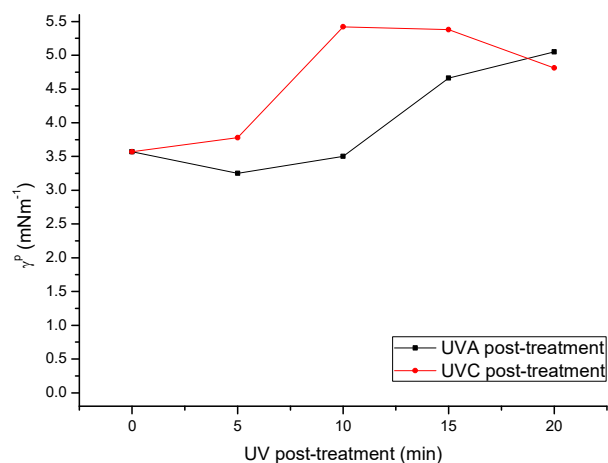
Furthermore, the material with high  $\alpha(t)$  of oxygen bonds caused by UV post-treatments, if its mechanical properties remain optimal, could be the most suitable candidate for applications where printing plate surface needs to be significantly modified.

Cosmolight QS material displays the highest values of  $\alpha(t)$  for OH bond at prolonged UVC post-treatment (up to 650%), with other  $\alpha(t)$  values under 150%.

Figure 86. displays the changes of  $\gamma^p$  of photopolymer materials in dependence on the duration of UV post-treatments.

Flexographic photopolymer materials have low initial  $\gamma^p$ . However, it is clearly visible in Figure 86. a) – c) that the effects of UVA and UVC post-treatments are different for each tested photopolymer material. Each material presents a different system in terms of the initial  $\gamma^p$  and the differences in the effects of UVA and UVC post-treatments on the oxygen inhibition. ACE Digital material (Figure 86.a) has the lowest  $\gamma^p$  among the tested materials, and UVA and UVC post-treatments have the similar impact on the changes of  $\gamma^p$ . Digital MAX material (Figure 86.b), with higher initial  $\gamma^p$  than ACE Digital, displays the expressed decrease of  $\gamma^p$  after UVC post-treatment longer than 10 minutes. The effect of UV post-treatments on Cosmolight QS material (Figure 86.c) is present in the increase of  $\gamma^p$  with the slight tendency of the decrease after 15 minutes of UVC post-treatment. Cosmolight QS material displays the highest values of  $\gamma^p$  among the tested materials.





c)

Figure 86. Dependence of  $\gamma^p$  and UV post-treatment durations for:

a) ACE Digital printing plate, b) Digital MAX printing plate, c) Cosmolight QS printing plate

The fact that the prolonged UVC post-treatment causes the decrease of  $\gamma^p$  of tested photopolymer materials, while  $\alpha(t)$  of OH bond significantly increases for all UVC post-treated samples points to the conclusion that OH bond does not generally contribute to the polarity of the surface. However, FTIR-ATR analysis reaches the depth of  $\sim 2 \mu\text{m}$  in the sample, which also points to the conclusion that the oxygen at the surface of the material causes different changes in the composition of the surface (photo oxydation, crosslinking termination) than in the deeper layer of the material.

Calculations of  $\alpha(t)$  for C=O and OH bonds for tested photopolymer materials displayed that these two types of chemical bonds that contain oxygen have a different influence on the oxygen ratio at the interface of the photopolymer materials. Since their impacts on the surface properties of tested printing plates is obviously complex and interconnected, this justifies the application of the fitting model in order to quantify their influence on the surface properties of photopolymer materials.

## **5.2. Qualitative properties of prints in relation to modified printing plate surface properties**

In order to define the influence of modified printing plate surfaces on the print quality, several parameters related to the quality of printed layer are discussed in this chapter.

The influence of UV post-treatments on print quality is discussed for coverage values in shadow area of prints obtained by printing plates exposed to varied UVA and UVC post-treatments. Furthermore, optical density on solid tonal patches on prints, as well as the changes in ink layer thickness are analysed. Calculation of  $r$  values for components of  $\gamma$  of the printing plates and the properties of prints have been chosen as a method for obtaining the relation between the surface properties of printing plates and the specific parameters of printed layer.

### 5.2.1. Relation of the properties of printing plates and coverage values on prints

In order to define the influences of changes in  $\gamma^d$  and  $\gamma^p$  of photopolymer materials caused by UV post-treatments and coverage values in shadow area (90% - 100%),  $r$  values for coverage values on prints and components of  $\gamma$  were calculated.

Since the trends of increases and decreases in coverage values ( $cv$ ) on prints caused by UV post-treatments were not monotonic due to the measurement deviations and the deviations in the printing process itself, for the correlation calculation, summed coverage values in the shadow area were used and  $\Delta cv$  for the correlation calculations were obtained.

Specifically,  $\Delta cv$  for ACE Digital and Digital MAX photopolymer materials was calculated by Eq. 12:

$$\Delta cv = \sum_{n=90}^{100} cv(n_2) - \sum_{n=90}^{100} cv(n_x), \quad (12)$$

$n = (90, 93, 95, 97, 100),$   
 $x = (6, 10, 14, 20),$

where  $cv$  presents coverage value,  $cv(n_2)$  presents the coverage value for the sample treated for 2 minutes of particular UV post-treatment,  $n$  presents the specific nominal coverage value at  $x$  minutes of UV post-treatment. For the prints obtained by Cosmolight QS printing plates, the same equation was applied, but with  $t_2$  replaced with  $t_5$ , and  $x = (10, 15, 20)$ .

Table 11. displays the  $r$  values for  $\Delta cv$  and the components of  $\gamma$  for tested printing plate samples exposed to varied UVA post-treatment.

It is visible that  $\Delta cv$  of prints obtained by all printing plates shows very good or excellent correlation with  $\gamma^d$ .

Table 11. Calculated  $r$  values for  $\Delta cv$  and components of  $\gamma$  of photopolymer materials for the set of samples with varied UVA post-treatment

$\Delta cv$	$\gamma^d$	$\gamma^p$
ACE Digital	0.81	0.82
Digital MAX	0.97	0.13
Cosmolight QS	0.99	0.41

This means that UVA post-treatment's influence on  $\gamma^d$  of photopolymer material can be directly used to modify the coverage values on prints in shadow area: the higher  $\gamma^d$ , the lower

coverage values. For ACE Digital printing plate, both  $\gamma^d$  and  $\gamma^p$  present a strong correlation with  $\Delta cv$ .

Coverage values in shadow area on prints obtained by Digital MAX and Cosmolight QS printing plates show excellent correlation with  $\gamma^d$ . It can be concluded that  $\gamma^d$  of these two types of printing plates with modified UVA post-treatment can be used as a precise tool to adjust the coverage values in shadows and enhance the visual appearance on prints.

Calculated  $r$  values for  $\Delta cv$  and  $\gamma^p$  display a good correlation only for ACE Digital printing plate, although  $\gamma^p$  values are lowest for that photopolymer material. The component  $\gamma^p$  of other photopolymer materials displayed no valuable correlation with  $\Delta cv$ .

It can be concluded that UVA post-treatment, which initially induces crosslinking in the photopolymer material, can be used as a precise tool to adjust high coverage values via modification of  $\gamma^d$  of printing plate of ethanol-based ink used in this research. The high  $r$  values proved  $\gamma^d$  as a direct and strong influencing parameter in tailoring the print properties.

Table 12. displays  $r$  values between  $\Delta cv$  on prints and components of  $\gamma$  with modified UVC post-treatment.

ACE Digital printing plate's  $\gamma^d$  displays positive correlation with  $\Delta cv$ , similar to UVA post-treatment. Digital MAX printing plate exposed to varied UVC post-treatment and  $\Delta cv$  show good negative correlation, but not good enough to use  $\gamma^d$  of printing plate treated with specific duration of UVC post-treatment to precisely adjust coverage values in shadow area.

Table 12.  $r$  values for  $\Delta cv$  and components of  $\gamma$  of photopolymer materials for the set of samples with varied UVC post-treatment

$\Delta cv$	$\gamma^d$	$\gamma^p$
ACE Digital	0.81	0.94
Digital MAX	-0.75	0.90
Cosmolight QS	-0.97	-0.57

On the other hand, Cosmolight QS printing plate's  $\gamma^d$  and corresponding prints display excellent negative correlation, offering an option of using modified  $\gamma^d$  of UVC post-treated printing plate as a tool for adjustment of high coverage values on prints, as well. Negative correlation in this case comes from the fact that increased  $\gamma^d$  caused negative differences between sum of coverage values for printing plate treated with shortest duration of UVC post-

treatment, and printing plate treated with longest duration of UVC post-treatment. Therefore, increased  $\gamma^d$  of Cosmolight QS printing plate will decrease high coverage values on prints of the printing ink used in this research.

Due to the surface properties of the used printing ink, this was expected, but the strength of the correlation is meaningful, displaying the robust relation between the two correlated values for both UV post-treatments.

$\gamma^p$  and  $\Delta cv$  show no correlation for Cosmolight QS printing plate, but very good correlation is present for ACE Digital and Digital MAX printing plates. Increased  $\gamma^p$  for these two printing plates will result with increased coverage values on prints in shadow area.

It can be concluded that coverage values in shadow area can be modified by varying both UVA and UVC post-treatment, influencing  $\gamma^p$  and  $\gamma^d$  of printing plates, but the final effect is dependent on the type of photopolymer material used as a printing plate and used printing ink. In relation to other potentially necessary modifications of printing plate surface properties, one can choose an optimal option of modifying specific component of  $\gamma$  with specific UV post-treatment in order to obtain optimal print quality.

### 5.2.2. Relation of the properties of printing plates and optical density on prints

In order to detect potential connection between optical density ( $D$ ) of solid tonal patch on the print, and the components of  $\gamma$ ,  $r$  values for these two parameters for both UV post-treatments were calculated.

Table 13. presents the correlation between  $D$  on prints and components of  $\gamma$  for printing plates treated with modified UVA post-treatment. One can see that ACE Digital printing plate's  $\gamma$  components show no significant correlation with  $D$ , which means that UVA post-treatment and the changes it causes in  $\gamma^d$  and  $\gamma^p$  cannot be used to purposefully adjust  $D$  on prints. The reason could be that ACE Digital printing plate displays highest  $D$  among tested printing plates, possibly because of the highest ratio of dispersive to polar forces in the printing plate surface (Figure 73.a). Therefore, changes in  $D$ , together with the fact that prints obtained by ACE Digital printing plate obtain the highest ink layer thickness (Figure 74.a), are not as affected by modified UV post-treatments.

Table 13. Calculated  $r$  values for  $D$  on prints and components of  $\gamma$  of photopolymer materials for the set of samples exposed to varied UVA post-treatment

$D$	$\gamma^d$	$\gamma^p$
ACE Digital	-0.26	0.60
Digital MAX	0.82	0.20
Cosmolight QS	-0.64	-0.86

Digital MAX is the only printing plate showing a good correlation of  $D$  and  $\gamma^d$ , visible in Table 13., meaning that the decrease of  $\gamma^d$  results with the decrease of  $D$ , as well. This points to different interactions between printing plates and printing ink used in this research.

On the other hand, for Cosmolight QS printing plates,  $\gamma^p$  dominantly influences  $D$ , values being inversely proportional. This opposite trend when comparing Digital MAX and Cosmolight QS printing plates is interesting. Since both  $\gamma^p$  and  $\gamma^d$  of printing plates change during the UVA post-treatment, their range of changes and their ratio will have an effect of making one of them the dominant component for changing  $D$  on the prints.

Table 14. presents the  $r$  values between components of  $\gamma$  of printing plates treated with varied UVC post-treatment and  $D$ .



Table 14. Calculated  $r$  values for  $D$  on prints and components of  $\gamma$  of photopolymer materials for the set of samples exposed to varied UVC post-treatment

$D$	$\gamma^d$	$\gamma^p$
ACE Digital	-0.37	0.37
Digital MAX	-0.15	-0.73
Cosmolight QS	-0.19	-0.40

It is visible that there is no noticeable correlation for any component of  $\gamma$  and  $D$  on prints, with exception of good negative correlation for  $\gamma^p$  and  $D$  of Digital MAX printing plate. Apparently, the changes in ratios of  $\gamma^p$  and  $\gamma^d$  during the UVC post-treatment do not generally enable the possibility for adjustment of  $D$  on the print in this specific reproduction system.

### 5.2.3. Relation of the properties of printing plates and thickness of printed ink layer

Ink layer thickness is very important characteristic of printed (functional) ink layer. For example, thicker printed layer enables improved electrical conductivity of the functional inks used in printed electronics, while printing of OLEDs requires the thickness of the printed layer to be < 100 nm. If possible to define the influence of printing plate's  $\gamma^p$  and  $\gamma^d$  on this parameter of the print, one could enable simple modification of this qualitative characteristic, especially meaningful in printing of functional layers.

Table 15. displays  $r$  values for printed ink layer thickness ( $d$ ) and the components of  $\gamma$  for printing plates exposed to varied UVA post-treatment. It is visible that very strong correlation is present for  $d$  and  $\gamma^d$ .

Table 15. Calculated  $r$  values  $d$  and components of  $\gamma$  of photopolymer materials for the set of samples with varied UVA post-treatment

$d$	$\gamma^d$	$\gamma^p$
ACE Digital	-0.94	-0.17
Digital MAX	0.94	0.63
Cosmolight QS	0.93	0.70

Changes in  $\gamma^d$  and  $d$  will follow the similar trend for Digital MAX and Cosmolight QS printing plates, while the correlation of  $\gamma^d$  and  $d$  for ACE Digital printing plate displays negative value.

It is important to notice that both Digital MAX and Cosmolight QS printing plates have higher  $\gamma^p$  than ACE Digital printing plate. The influence of  $\gamma$  of ACE Digital printing plate on the deposited ink layer thickness is therefore affected primarily by changes in  $\gamma^d$  which are, during the prolonged UVA post-treatment, specifically connected to the migration of non-polar compounds of low molecular weight to the surface. This was indirectly confirmed by calculations of  $\alpha(t)$  values from the FTIR-ATR spectra (Figure 83.).

For Digital MAX printing plate and Cosmolight QS printing plate, on the other hand, thickness of printed layer will obviously be defined by both  $\gamma^d$  and  $\gamma^p$ .

Table 16. displays  $r$  values of  $d$  and components of  $\gamma$  for printing plates treated with varied UVC post-treatment. There is no significant correlation present, except for very strong

negative correlation of  $d$  and  $\gamma^p$  for ACE Digital printing plate, where increased amount of oxygen with prolonged UVC radiation apparently causes sufficient increase of  $\gamma^p$  to influence  $d$ .

Table 16. Calculated  $r$  values for  $d$  and components of  $\gamma$  of photopolymer materials for the set of samples with varied UVC post-treatment

d	$\gamma^d$	$\gamma^p$
ACE Digital	-0.09	-0.90
Digital MAX	-0.44	-0.21
Cosmolight QS	-0.73	-0.12

There is a fairly good negative correlation present for  $d$  and  $\gamma^d$  of Cosmolight QS printing plate, meaning that, due to the increased range of changes of  $\gamma^d$ , its increase reflected on  $\gamma^{\text{total}}$  will cause the improved wetting of the ink on the printing plate.

Finally, since the influence of the components of  $\gamma$  on  $d$  individually proved as complex,  $r$  values for  $d$  and  $\gamma^{\text{total}}$  were calculated for both UVA and UVC post-treatments (Table 17.)

Table 17. Calculated  $r$  values for  $d$  and  $\gamma$  of photopolymer materials for printing plates exposed to varied UVA and UVC post-treatments

d	$\gamma^{\text{total}}$ (UVA)	$\gamma^{\text{total}}$ (UVC)
ACE Digital	-0.94	-0.27
Digital MAX	0.95	-0.41
Cosmolight QS	0.95	-0.64

After observing Table 17., it can be concluded that the modification of UVA post-treatment will result with good correlation with the changes in ink layer thickness. The sign and strength of the correlation coefficient, however, will depend on the interaction of the ink with the printing plate, the ratio of  $\gamma^p$  and  $\gamma^d$  of the printing plate, as well as on other changes occurring in the surface of the photopolymer material due to the UV post-treatments. However, ink layer thickness on the print is not affected only by the ratio of  $\gamma^p$  and  $\gamma^d$ , or  $\gamma^{\text{total}}$  of the printing plate, but also by the hardness and roughness of the printing plate. Therefore, in order to define the transfer of the printing ink to the printing substrate in the varied UV post-treatment conditions, it is necessary to incorporate the other properties of the printing plate in the model that will define the ink layer thickness on the print.

### **5.3. LS model fitting of the influencing parameters for printing plate and print properties**

In order to perform an integration of the parameters that influence the surface properties of printing plates exposed to varied UVA and UVC post-treatment, a fitting model involving all analysed influencing parameters needed to be constructed.

Specific relations and correlations between each parameter modified by UV post-treatment and its individual impact on  $\gamma^p$  and  $\gamma^d$  of the printing plate, as well as the influence on the print parameters, cannot provide the holistic, quantified description of which parameters are actually causing the changes in the components of  $\gamma$  and print quality, and what are the weights of these parameters.

Therefore, in this chapter, least squares in matrix form are applied as a robust method for the quantification of the parameters influencing printing plate properties, as well as the print properties of interest.

Analysis of the fitting model provided the answers to the following issues:

- The influence of printing plate's roughness on  $\gamma$  and print quality;
- The significance of the integration of oxygen in printing plate's surface for both components of  $\gamma$  (directly and indirectly);
- The influence of the crosslinking degree in the surface of the printing plate monitored by weight loss;
- Significance of the increased hardness of the printing plate, caused by UV post-treatments for the print quality.

### 5.3.1. LS fitting of the printing plate parameters

Least squares (LS) fitting in matrix form was applied for the quantification of the parameters influencing printing plate surface properties, specifically  $\gamma^p$  and  $\gamma^d$ .

It is obvious that the mechanism that influences printing plate's surface properties related to the UV post-treatments is complex.  $r$  values calculated in 5.1. and 5.2. provided the discussion potential for the origin of the changes occurring in the printing plate surface when exposed to UVA and UVC wavelengths, consequently causing the modified properties of the print, as well.

Some presented correlations were very strong, which means that some parameters confidently have a role in the specific changes of the printing plate properties, and can therefore be used to adjust  $\gamma^p$  and  $\gamma^d$  of the printing plate, and in the next step the quality of the prints.

However, very good correlation does not necessarily mean that specific parameter is really significant for the absolute definition of printing plate's surface properties. The case may be that it correlates well, or is influenced by other parameters that are more significant.

LS model fitting in matrix form presents a robust method which was used to obtain the weight coefficients of the parameters influencing printing plate and print properties. For printing plates, parameters incorporated in LS model were:

- $R_a$  – although it does not change significantly with varied UV post-treatments, level of roughness of the surface is in the connection with surface free energy. Furthermore, since tested printing plates had different initial surface roughness, its influence on the surface properties had to be incorporated in the fitting model;
- Weight loss in toluene was incorporated in the model because toluene displayed the most expressed influence on the photopolymer material during the immersion period, causing swelling of up to 180% and weight loss up to 8%. Since toluene's solubility parameters are obviously closest to photopolymer materials' cohesion parameters, weight loss in toluene was chosen as the most relevant parameter for the indirect definition of the influence of changes in the chemical bonds on printing plates' surface properties;
- $\alpha(t)$  for C=O and OH bonds were chosen as indicators of oxygen ratio in the surface, to quantify the influence of the oxygen on the surface free energy of printing plates. Results of  $\alpha(t)$  calculations did not follow the same trend of changes for C=O and OH

bond types in the same sample, meaning that these two bonds are involved in different types of reactions in the photopolymer surface.

All parameters used for the formation of LS model were normalized in order to be comparable. The calculation process included simple matrix algebra, following the procedure for obtaining the normal equation and solving it, thereby obtaining weight coefficients for inputs. The example is given for the calculation of weight coefficients of previously calculated parameters influencing  $\gamma^d$  for printing plate treated with varied UVA post-treatment:

$$A = \begin{matrix} & \begin{matrix} Ra & wl & \alpha(t)_{c=0} & \alpha(t)_{OH} \end{matrix} \\ \begin{bmatrix} 0.811 & 0 & 0 & 0 \\ 0 & 0.807 & 0.519 & 0.495 \\ 0.055 & 0.833 & 0.909 & 0.884 \\ 0.218 & 0.853 & 1 & 0.795 \\ 1 & 1 & 0.567 & 1 \end{bmatrix} & \text{- inputs} \end{matrix}$$

$$b = \begin{matrix} \gamma^d \\ \begin{bmatrix} 0 \\ 1 \\ 0.980 \\ 0.837 \\ 0.604 \end{bmatrix} \end{matrix} \text{ - outputs}$$

System  $Ax = b$  was set,  $x = [u, y, z, w]$  presenting weight coefficients for inputs:

$$\begin{bmatrix} 0.811 & 0 & 0 & 0 \\ 0 & 0.807 & 0.519 & 0.495 \\ 0.055 & 0.833 & 0.909 & 0.884 \\ 0.218 & 0.853 & 1 & 0.795 \\ 1 & 1 & 0.567 & 1 \end{bmatrix} \begin{bmatrix} u \\ y \\ z \\ w \end{bmatrix} = \begin{bmatrix} 0 \\ 1 \\ 0.980 \\ 0.837 \\ 0.604 \end{bmatrix}$$

First,  $B = A^T A$ , and  $c = A^T B$  were calculated:

$$B = \begin{bmatrix} 1.708 & 1.232 & 0.835 & 1.222 \\ 1.232 & 3.074 & 2.597 & 2.815 \\ 0.835 & 2.597 & 2.418 & 2.424 \\ 1.222 & 2.815 & 2.424 & 2.659 \end{bmatrix} \quad c = \begin{bmatrix} 0.840 \\ 2.943 \\ 2.591 \\ 2.632 \end{bmatrix}$$

After that, normal equation  $Bx = c$  was solved, obtaining  $x$  and then calculating  $q$ :

$$x = \begin{bmatrix} -0.112 \\ 1.398 \\ 0.555 \\ -0.945 \end{bmatrix}, \quad q = 0.135$$

Table 18. presents the weight coefficients for the influencing parameters on  $\gamma^p$  and  $\gamma^d$  of ACE Digital printing plate exposed to varied UV post-treatments. It is visible that the changes in  $\gamma^d$  for UVA and UVC post-treatment do not have an entirely same mechanism.

Table 18. Weight coefficients for parameters influencing components of  $\gamma$  for ACE Digital printing plate

Normalized parameters	Weight coefficient for influence on $\gamma^d$ (UVA p.-treatment)	Weight coefficient for influence on $\gamma^p$ (UVA p.-treatment)	Weight coefficient for influence on $\gamma^d$ (UVC p.-treatment)	Weight coefficient for influence on $\gamma^p$ (UVC p.-treatment)
$R_a$	-0.112	0.051	0.004	0.087
Weight loss in toluene	1.398	1.842	0.171	0.312
$\alpha(t)$ for C=O bond	0.555	0.564	1.541	1.242
$\alpha(t)$ for OH bond	-0.945	-1.997	-1.487	-1.717
$q$	0.135	0.684	0.040	0.296

Changes caused by UVA post-treatment are primarily the result of the changes in the crosslinking degree apparent through the weight loss in toluene. In this specific case, increased weight loss as a primary influencing parameter on  $\gamma^d$  for the range of UVA post-treatment suggests that increased solubility in toluene means that  $\gamma^d$  increased, as well. Due to the very low values of  $\gamma^p$  of ACE Digital material, this is possible because the changes in inter- and intra- molecular forces caused by the crosslinking process could result with increased compatibility of cohesion parameters of certain compounds in the material and solubility parameter of toluene.

The incorporation of the oxygen in form of C=O bonds acts on  $\gamma^d$  with positive weight, as well, which indicates that C=O bond plays a role in the crosslinking mechanism. Negative sign of coefficients for  $\alpha(t)$  of OH bonds for printing plates treated with the range of UV post-treatment could be due to the migration of protective non polar compounds to the surface when printing plate is exposed to UV radiation of higher energy.

It is visible that  $R_a$  has a weak influence on the definition of ACE Digital printing plate's surface properties, as well.

Table 19. displays the weight coefficients for the influencing parameters on  $\gamma^p$  and  $\gamma^d$  of Digital MAX printing plate exposed to varied UV post-treatments.

For Digital MAX material, weight coefficients differ significantly from ACE Digital's. For printing plates treated with varied UV post-treatments, OH bond does not affect negatively  $\gamma^d$ .

Since  $\gamma^d$  of Digital MAX material increases throughout the whole range of UVA post-treatment, this indicates that Digital MAX material has a different crosslinking mechanism than ACE Digital. Here, there is an indication that OH bond, as well as C=O bond, has a role in the crosslinking mechanism, since they are both the parameters influencing positively  $\gamma^d$  for whole UV range printing plate samples were exposed to. However, weight loss in toluene displays a negative influence on  $\gamma^d$  for prolonged UVA post-treatment. Since UVA radiation does not result with as expressed photo oxidation of the material as UVC radiation, negative weight of weight loss can be directly related to the increased crosslinking degree resulting with the decreased solubility in toluene.

Furthermore, increased weight loss in toluene for all samples indicates that  $\gamma^p$  increased. This can be assigned to photo oxidation of the material, together with the positive influence of C=O bond on  $\gamma^p$ , and point to the formation of soluble segments as a result of the crosslinking termination. Surface roughness has more impact on  $\gamma^d$  and  $\gamma^p$  than for ACE Digital material, acting with generally negative influence.

Table 19. Weight coefficients for parameters influencing components of  $\gamma$  for Digital MAX printing plate

Normalized parameters	Weight coefficient for influence on $\gamma^d$ (UVA p.-treatment)	Weight coefficient for influence on $\gamma^p$ (UVA p.-treatment)	Weight coefficient for influence on $\gamma^d$ (UVC p.-treatment)	Weight coefficient for influence on $\gamma^p$ (UVC p.-treatment)
<b>R<sub>a</sub></b>	0.318	-0.448	-0.344	-0.975
<b>Weight loss in toluene</b>	-0.419	0.389	0.069	0.696
<b><math>\alpha(t)</math> for C=O bond</b>	0.391	0.679	0.496	-0.203
<b><math>\alpha(t)</math> for OH bond</b>	0.574	0.141	0.914	1.172
<b>q</b>	0.219	0.113	0.185	$5.729 \times 10^{-4}$

In Table 20., one can observe the weight coefficients of parameters influencing  $\gamma^d$  and  $\gamma^p$  of UV post-treated Cosmolight QS printing plate. Here, OH bond generally displays a moderate or strong negative influence on both  $\gamma^d$  and  $\gamma^p$  of UV post-treated material, especially expressed during the prolonged UVC post-treatment. Therefore, it can be concluded that OH bond has a role in the crosslinking termination process, and points to the start of the material degradation after prolonged UV post-treatments. Increased amount of C=O bonds in the surface, on the other hand, is an indicator for the increased  $\gamma^d$  and  $\gamma^p$  for both UVA and UVC post-treatments, either as a segment integrated in the polymer network during one of the crosslinking steps, or as a byproduct of the crosslinking and photo oxidation process.



Table 20. Weight coefficients for parameters influencing components of  $\gamma$  for Cosmolight QS printing plate

Normalized parameters	Weight coefficient for influence on $\gamma^d$ (UVA p.-treatment)	Weight coefficient for influence on $\gamma^p$ (UVA p.-treatment)	Weight coefficient for influence on $\gamma^d$ (UVC p.-treatment)	Weight coefficient for influence on $\gamma^p$ (UVC p.-treatment)
<b>R<sub>a</sub></b>	0.114	0.373	-0.247	0.059
<b>Weight loss in toluene</b>	-0.086	-0.266	-0.118	-0.118
<b><math>\alpha(t)</math> for C=O bond</b>	0.706	0.523	3.308	3.956
<b><math>\alpha(t)</math> for OH bond</b>	0.159	-0.353	-1.799	-3.056
<b>q</b>	0.048	0.213	0.432	0.474

Weight loss does not have the significant weight compared to the dominant influencing parameters. It displays expected negative weight for  $\gamma^d$  for samples treated with both varied UV post-treatments. It is obvious that C=O and OH bonds have the major significance in defining both  $\gamma^p$  and  $\gamma^d$  for both types of UV post-treatments.

Roughness as an influencing parameter displays weak weights for the range of UV post-treatments. The weak negative influence of surface roughness on  $\gamma^d$  for the range of UVC post-treatment indicates that the crosslinking termination and possible start of the material degradation caused by prolonged UVC radiation results with lower roughness.

Figures 87. – 89. present the graphic display of the weight coefficients from Tables 18. – 20.

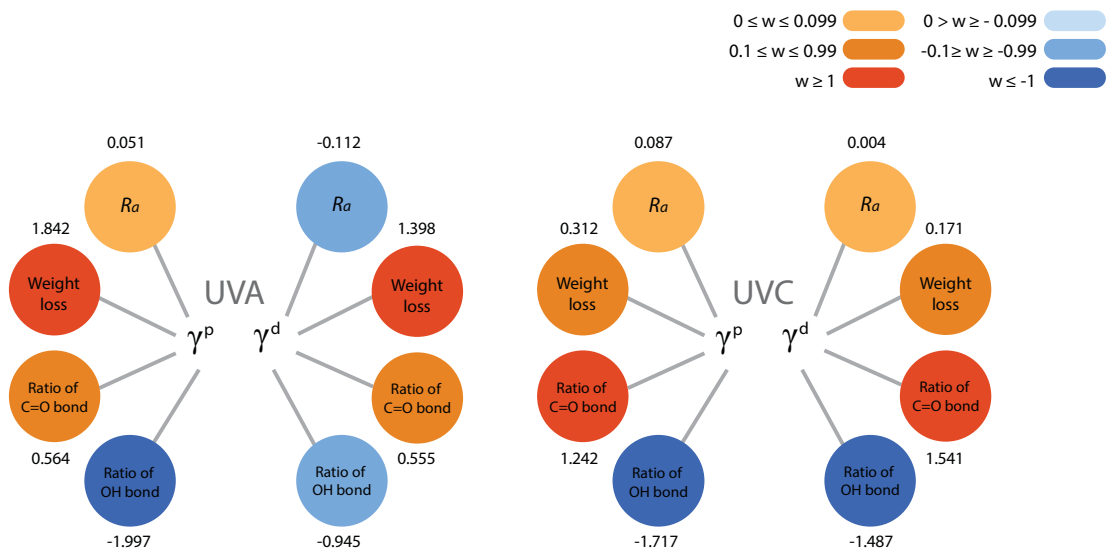


Figure 87. Weight coefficients for the parameters influencing  $\gamma^p$  and  $\gamma^d$  of ACE Digital printing plate

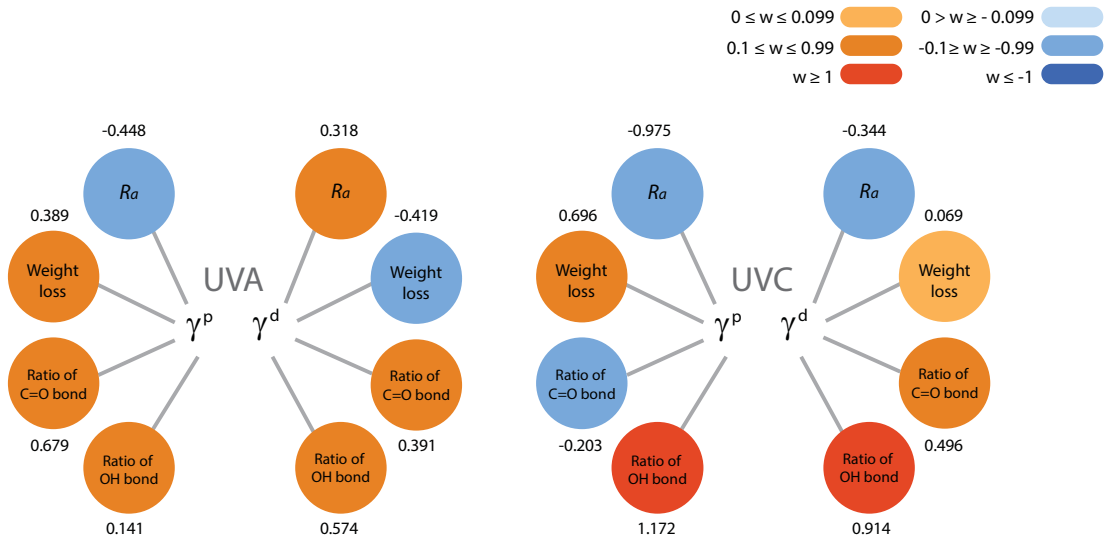


Figure 88. Weight coefficients for the parameters influencing  $\gamma^p$  and  $\gamma^d$  of Digital MAX printing plate

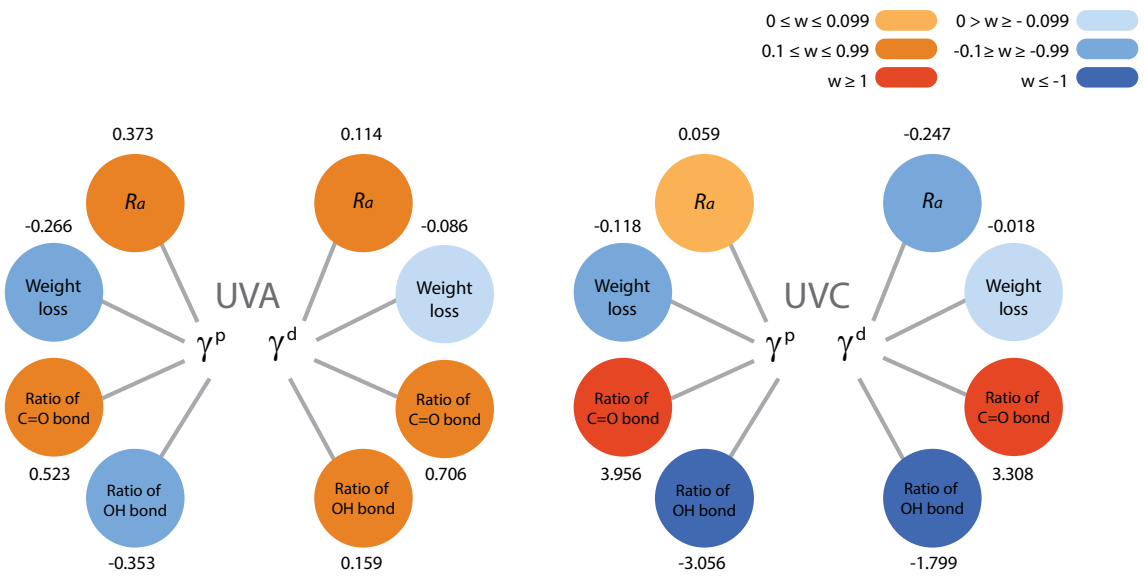


Figure 89. Weight coefficients for the parameters influencing  $\gamma^p$  and  $\gamma^d$  of Cosmolight QS printing plate

### 5.3.2. LS fitting of the print properties

After analyzing the weights of each significant parameter influencing printing plate's surface properties, it was necessary to apply the same calculations for prints obtained by printing plates with modified surfaces.

Optical density ( $D$ ) as an output did not display a good fitting of LS model. It was expected, since optical density showed no significant correlation with  $\gamma^p$  or  $\gamma^d$  of printing plates. Printing ink used in this research was not applied with anilox roller that would ensure that the thickness of the ink layer transferred to and from the printing plate will cause noticeable differences of  $D$  on prints. However, Digital MAX and Cosmolight QS did display a good correlation of the components of  $\gamma$  with  $D$  in UVA and UVC range. This is probably because of the higher hardness of these printing plates compared to ACE Digital (Figure 42.).

Hardness proved to be the significant parameter when modelling the influences on coverage values ( $cv$ ) on prints. Unfortunately, no valid fitting with low  $q$  values could be obtained, either. However, strong correlations of  $cv$  with  $\gamma^p$  and  $\gamma^d$  of UVA and UVC post-treated printing plates presented in Chapter 5.2.1. point to the conclusion that, although their influence on this type of printing ink cannot be precisely quantified,  $\gamma^p$  and  $\gamma^d$  of printing plate can be used to adjust coverage values in shadow area.

Finally, ink layer thickness ( $d$ ) was the most interesting parameter for modelling the influence of the UV post-treatments. Since it is usually adjusted in the printing process by the chosen anilox roller, there is not so much room for the fine adjustment of  $d$  on print in regular reproduction process. If modifying the pressure in order to transfer more ink to the printing substrate, deformations of the printing elements will occur. With modified UV post-treatments for three types of flexographic printing plates analysed in this thesis,  $d$  on prints managed to cover the range from 0.48  $\mu\text{m}$  to 9.97  $\mu\text{m}$  – only by modifying the UV post-treatment process (Figure 74.).

Furthermore,  $d$  displayed a promising correlation with  $\gamma^d$  of printing plates treated with varied UVA post-treatment.

An example of LS model fitting is given by calculation of weight coefficients for prints obtained by UVC post-treated ACE Digital printing plate:

$$A = \begin{matrix} & \begin{matrix} \text{hardness} & \gamma^p & \gamma^d & R_a \end{matrix} \\ \begin{bmatrix} 0 & 0.231 & 0 & 1 \\ 0.375 & 1 & 1 & 0.276 \\ 0.400 & 0.692 & 0.764 & 0.224 \\ 1 & 0 & 0.554 & 0 \\ 1 & 0.077 & 0.252 & 0.268 \end{bmatrix} & \text{- inputs} \end{matrix}$$

$$b = \begin{matrix} d \\ \begin{bmatrix} 1 \\ 0 \\ 0.126 \\ 0.777 \\ 0.961 \end{bmatrix} \end{matrix} \text{ - outputs}$$

System  $Ax = b$ :

$$\begin{bmatrix} 0 & 0.231 & 0 & 1 \\ 0.375 & 1 & 1 & 0.276 \\ 0.400 & 0.692 & 0.764 & 0.224 \\ 1 & 0 & 0.554 & 0 \\ 1 & 0.077 & 0.252 & 0.268 \end{bmatrix} \begin{bmatrix} x \\ y \\ z \\ w \end{bmatrix} = \begin{bmatrix} 1 \\ 0 \\ 0.126 \\ 0.777 \\ 0.961 \end{bmatrix}$$

Calculations of  $B = A^T A$ , and  $c = A^T b$ :

$$B = \begin{bmatrix} 2.300 & 0.729 & 1.487 & 0.460 \\ 0.729 & 1.538 & 1.548 & 0.682 \\ 1.487 & 1.548 & 1.954 & 0.514 \\ 0.461 & 0.682 & 0.514 & 1.198 \end{bmatrix} \quad c = \begin{bmatrix} 1.788 \\ 0.392 \\ 0.769 \\ 1.286 \end{bmatrix}$$

Solution to normal equation  $Bx = c$ :

$$x = \begin{bmatrix} \mathbf{0.648} \\ \mathbf{-0.808} \\ \mathbf{0.228} \\ \mathbf{1.186} \end{bmatrix}, \quad q = \mathbf{0.011}$$

As the influencing parameters, hardness,  $\gamma^p$ ,  $\gamma^d$  and  $R_a$  were chosen. Furthermore, it is important to notice that this fitting model is specific for the printing ink type used in this research. If using the ink of different  $\gamma^p$  and  $\gamma^d$ , weight coefficients would be different.

Table 21. presents weight coefficients of the parameters influencing  $d$  obtained by ACE Digital printing plate.

Table 21. Weight coefficients for parameters influencing  $d$  on prints obtained by ACE Digital printing plate

Normalized parameters	Weight coefficient for influence on $d$ (UVA post-treatment)	Weight coefficient for influence on $d$ (UVC post-treatment)
<b>Hardness</b>	-1.652	0.649
$\gamma^p$	-0.438	-0.808
$\gamma^d$	1.015	0.228
$R_a$	1.039	1.186
<b><math>q</math></b>	0.376	0.011

It was stated before that ACE Digital material possess the specific oxygen protection surface mechanism reflecting in the migration processes of protective, non-polar compounds to the surface of the material when exposed to the influence of the oxygen. This, together with the fact that ACE Digital is the printing plate with lowest hardness (Figure 42.), and is therefore more subject to deformation in the printing process, could disable detailed definition and quantification of the influences on print quality.

Range of UVC post-treatment results with positive influence of  $R_a$  as a primary weight parameter and negative influence of  $\gamma^p$  in the deposition of the specific  $d$ .

This is logical, since increased roughness generally improves ink adsorption, and ACE Digital obtained the highest roughness among three tested printing plates. Furthermore,  $\gamma^p$  of ACE Digital material is almost non-existent (Figure 51.), and obviously, its increase due to the UV post-treatment will benefit the adsorption of this particular ink, transferring the thinner amount of the ink to the substrate.

Table 22. presents weights of the influencing parameters of  $d$  for prints obtained by UV-modified Digital MAX printing plate. Regarding the weight of the parameters of UVA post-treatment range, hardness and  $R_a$  have no significant influence on  $d$ . Here,  $\gamma^d$  is the primary weight factor for influencing  $d$  on print, since the weight of  $\gamma^p$  is also neglectable.

It is shown that  $\gamma^d$  has a positive weight, opposite to UVC post-treatment range. If observing the LS model fitting for influencing parameters on Digital MAX printing plate (Table 19.), one can see that the main difference in weight coefficients for  $\gamma^d$  for ranges of UVA and UVC post-treatment is present for the weight loss, i.e. the indicator of the crosslinking degree.

This means that the changes that occur in the polymer network due to the UVA and UVC post-treatment will have as a consequence different interactions of printing plate with used printing ink in terms of adsorption.

Table 22. Weight coefficients for parameters influencing  $d$  on prints obtained by Digital MAX printing plate

Normalized parameters	Weight coefficient for influence on $d$ (UVA post-treatment)	Weight coefficient for influence on $d$ (UVC post-treatment)
<b>Hardness</b>	0.036	0.080
$\gamma^p$	0.057	0.449
$\gamma^d$	0.773	-0.603
$R_a$	0.023	1.556
<b><math>q</math></b>	0.195	0.235

Although for the UVC post-treatment range,  $R_a$  is the main weight parameter, increased  $\gamma^d$  will result with the decreased  $d$ . This opposite influence than the one caused by UVA post-treatment range could be explained by differences in weights of weight loss of Digital MAX material for UVA and UVC post-treatment range. For the set of samples with modified UVA post-treatment, the lower weight loss points to the increased  $\gamma^d$  (due to the increased crosslinking degree), but for UVC post-treatment range, low positive weight is present for  $\gamma^d$  and weight loss. This suggests that as a result of UVC post-treatment, soluble compounds form on the printing plate surface as a part of the crosslinking process. They will cause the decrease of  $d$  on print due to the different interaction between printing ink and printing plate surface.

In Table 23., one can observe the weight coefficient for influencing parameters of UV post-treated Cosmolight QS printing plate on  $d$ . Range of UVA post-treatment results with negligible influence of  $\gamma^d$ , and setting  $R_a$  as a primary weight parameter, while  $\gamma^p$  has a negative weight.

Since increase of  $\gamma^p$  of Cosmolight QS material exposed to the varied UVA post-treatment is accompanied by increased amount of OH bonds in the surface structure, adsorption of ethanol-based printing ink will be improved, and  $d$  will decrease. Furthermore, for the range of UVC post-treatment,  $\gamma^d$  displays the positive weight in influencing  $d$ . It is not as significant weight as hardness or  $R_a$ , but it is opposite to Digital MAX printing plate.

Hardness is also a relevant parameter for modelling the influences on  $d$  of both UV post-treatments. Cosmolight QS is a printing plate with highest hardness compared to other two used printing plates (Figure 42.). However, increase of the hardness is not as expressed with UVA post-treatment, as for UVC post-treatment.

Table 23. Weight coefficients for parameters influencing  $d$  on prints obtained by Cosmolight QS printing plate

Normalized parameters	Weight coefficient for influence on $d$ (UVA post-treatment)	Weight coefficient for influence on $d$ (UVC post-treatment)
<b>Hardness</b>	0.415	-3.49
$\gamma^p$	-0.534	-0.049
$\gamma^d$	$-1.5 \times 10^{-13}$	2.130
$R_a$	1.119	3.991
<b><math>q</math></b>	$4.73 \times 10^{-15}$	$6.12 \times 10^{-15}$

The increase of hardness caused by UVA post-treatment will still ensure optimal contact between printing plate and printing substrate, while the increase of hardness caused by UVC influences negatively  $d$ , because of the lack of printing plate's elastic deformation during the printing process.  $R_a$  displays a positive weight coefficient, as expected.

After observing the general influences of the parameters on ink layer thickness on the prints, the following can be concluded:

- Hardness of the printing plate is dependent on the components of surface free energy in the determination of the amount of the ink transferred to the printing substrate. Hardness increased to a certain level will, together with improved wetting of the printing ink on the printing plate result with positive influence on the amount of ink transferred to the printing substrate. However, if the hardness of the printing plate is either too low, or increased beyond the recommended range, the contact with the printing substrate will not be optimal;
- $\gamma^p$  and  $\gamma^d$  of the printing plate, as the parameters influencing the ink layer thickness, must be observed jointly. Their ratios need to be adjusted to the used printing ink and its surface tension in order to optimize the ink layer thickness. The changes of the hardness and roughness of the printing plate, which are also occurring due to the varied UV post-treatments, need to be taken into account as well in order to obtain the maximal possible output quality;
- The influence of the roughness of the printing plate during the varied UV post-treatments will depend on the initial level of the printing plate's roughness. However, increased roughness of the printing plate will result with the improved adsorption of the printing ink on the printing plate and therefore increase the ink layer thickness on the print.

Figure 90. presents the graphic display of the weight coefficients from Tables 21. – 23.

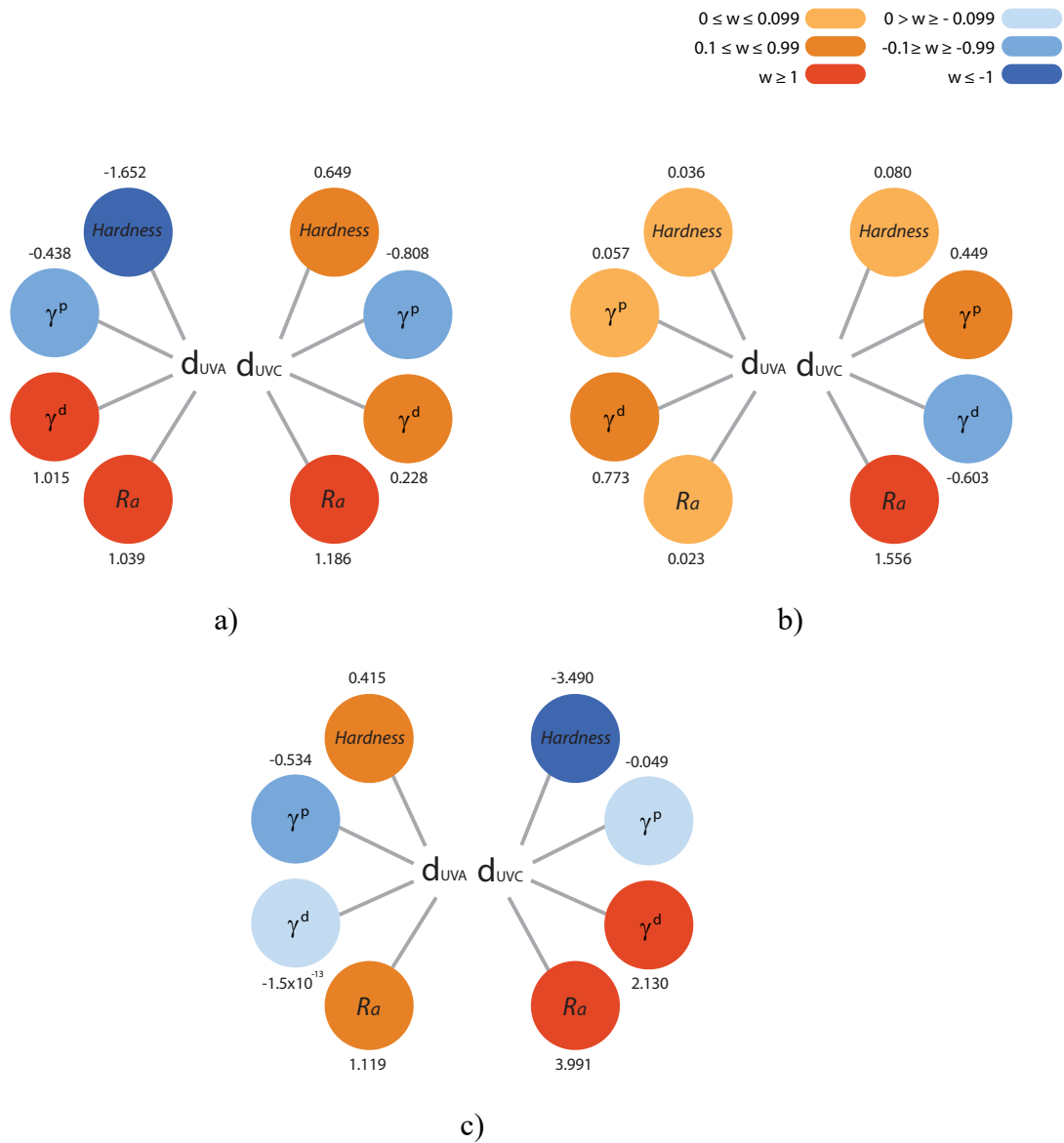


Figure 90. Weight coefficient for the parameters influencing ink layer thickness on prints obtained by:

a) ACE Digital printing plate, b) Digital MAX printing plate, c) Cosmolight QS printing plate



#### **5.4. Neural network as a functional model for estimation of surface properties of photopolymer printing plate**

In the final chapter of this thesis, after performing the measurements and analysis methods in order to define, characterize and obtain the relations between the changes that occur in the photopolymer materials used as a printing plate in flexography, modelling of their surface properties related to UV post-treatments will be conducted by means of a neural network.

Since neural network acts as a “black box” by training, validating and testing the inputs to target the outputs and estimate the behavior of the complex system, the information about the origin of changed printing plate’s surface properties could not be obtained this way. Therefore, before applying modelling by neural network, the influence of UVA and UVC post-treatment needed to be related in detail to the specific properties of printing plates and their influence of the print quality.

After that, when being familiar with the exact needed modification of  $\gamma^p$  and  $\gamma^d$  for obtaining specific result in the printing process and at the same time not damaging printing plate’s surface, neural network can be applied as a quick tool for adjusting the UVA and UVC post-treatment to the desired duration.

This type of modelling could be particularly helpful in the real systems, having in mind that detailed preliminary calculations of  $\gamma$  related to UV post-treatments need to be performed for each type of photopolymer material, in order to get the valid inputs for the neural network.

Neural networks constructed in this thesis were built of an (40x2) matrix as an input layer, presenting the paired durations of UVA and UVC post-treatments. The network had one hidden layer with 6 or 7 nodes, depending on the printing plate type, one output layer, and targets displaying  $\gamma^p$  and  $\gamma^d$  assigned to particular pair of UVA and UVC post-treatment durations. For example, for input of [5, 10], presenting the printing plate sample treated for 5 minutes of UVA post-treatment and 10 minutes of UVC post-treatment, the target was [2.25, 34.68] for ACE Digital printing plate, displaying previously calculated  $\gamma^p$  and  $\gamma^d$ , respectively.

Applied neural network type was “house price estimation” model, used to estimate and predict outputs assigned to multiple variables in inputs. The algorithm used for the network training was Levenberg–Marquardt algorithm used to solve non-linear least squares problem [114].

Neural network will not display the explicit weights of each variable from the input, like LS fitting performed in this research, but it will be able to calculate the outputs for random new inputs not used in training, validation, or testing processes. For all three analysed printing plate types, 75% of the input data were used for the network training, 15% was used for the validation, and 15% for the testing.

Figure 91. presents the distribution of errors obtained by neural network for training, validation and testing of model for estimation of ACE Digital printing plate’s  $\gamma^p$  and  $\gamma^d$ . This neural network was formed with 7 nodes in hidden layer, since it was experimentally shown that this number of nodes results with lowest error and best performance. It is visible in Figure 91. that most of the errors are concentrated around the zero error.

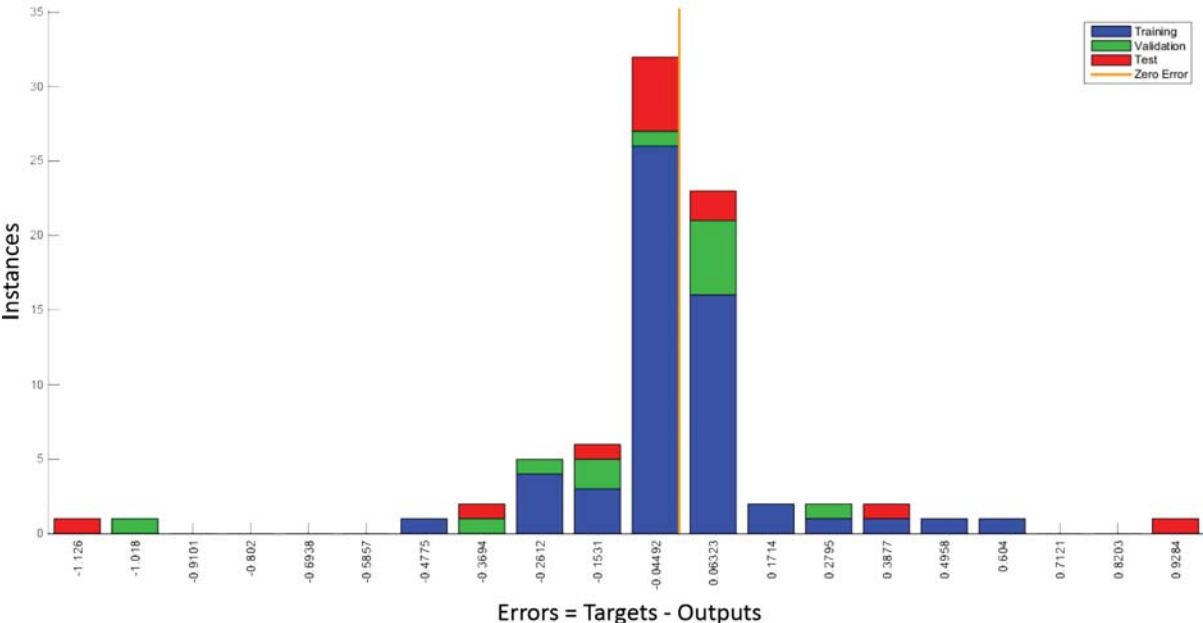


Figure 91. Error histogram for modelling of ACE Digital printing plate surface properties

In Figure 92., where the performance of neural network is displayed, the circled area presents the point at network’s best performance, where the mean squared error (*mse*) reached minimal value of 0.092 at 6<sup>th</sup> iteration. *Mse* measures the average of the squares of the errors, i.e. the difference between the estimator and what is estimated. After the iteration with minimal *mse*, the training continued for 6 more iterations.

Figure 93. displays the regression plots for each phase in the network construction – training, validation and testing, and one plot for all values. It shows the relationship between the outputs of the network and targeted values.

It is visible that the fitting is very good, with almost linear relationship between the outputs and targets ( $R$  values are higher than 0.99). Some points show scattering, which is normal in the real systems and gives the information that some values have poor fits. That is a useful info because it points to the samples/measurements which should be checked.

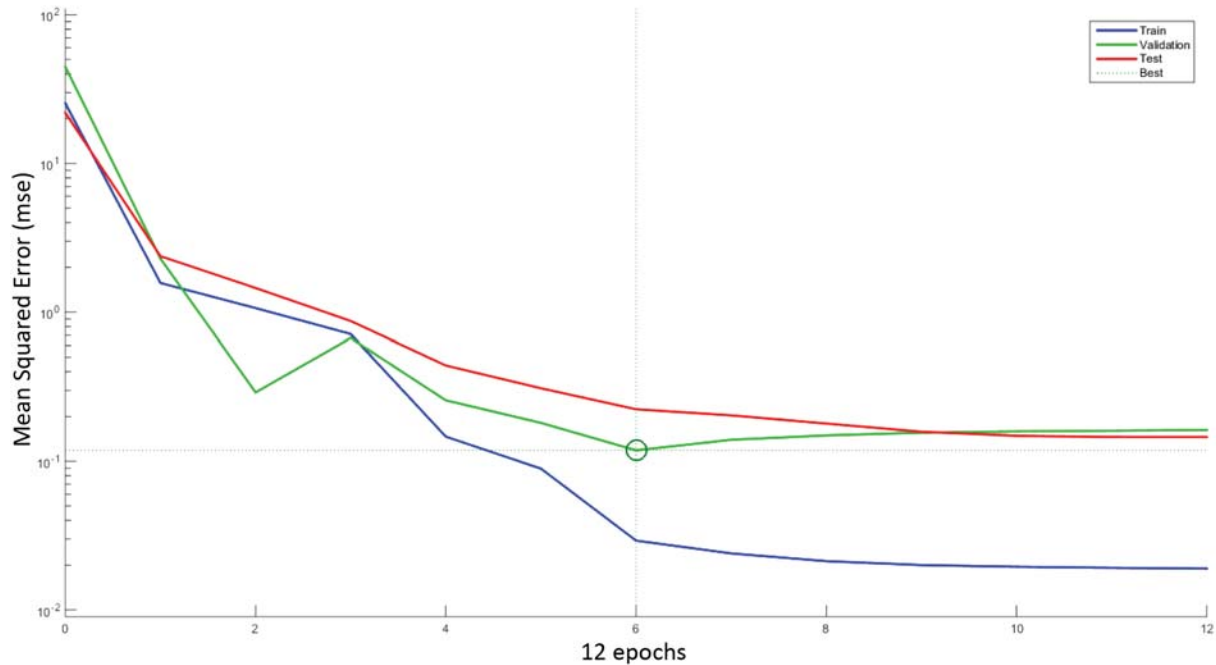


Figure 92. Performance of neural network for estimation of surface properties of ACE Digital printing plate

Overall, modelling of  $\gamma^p$  and  $\gamma^d$  by inputs of the durations of UVA and UVC post-treatment displayed good fitting results for ACE Digital printing plate. In order to demonstrate the actual differences between the targets and the outputs related to  $\gamma^p$  and  $\gamma^d$ , few examples are given (Table 24.):

Table 24. Targets and outputs in neural network for ACE Digital printing plate

Input	Target (mNm <sup>-1</sup> )	Output (mNm <sup>-1</sup> )
[5 min UVA, 10 min UVC]	$\gamma^p = 0.12, \gamma^d = 31.32$	$\gamma^p = 0.13, \gamma^d = 32.15$
[10 min UVA, 10 min UVC]	$\gamma^p = 0.07, \gamma^d = 30.30$	$\gamma^p = 0.12, \gamma^d = 31.96$
[5 min UVA, 20 min UVC]	$\gamma^p = 0.05, \gamma^d = 26.44$	$\gamma^p = 0.04, \gamma^d = 26.12$

Considering the scattering of the results due to the errors of measurements and not complete homogeneity of the printing plate surface, these results are promising. Estimations (outputs)

for  $\gamma^p$  and  $\gamma^d$  ( $\text{mNm}^{-1}$ ) for some random values of inputs of UVA and UVC post-treatment range are:

- [15 min UVA, 5 min UVC] -  $\gamma^p = 0.09$ ,  $\gamma^d = 29.43$ ;
- [5 min UVA, 15 min UVC] -  $\gamma^p = 0.14$ ,  $\gamma^d = 24.39$ ;
- [3 min UVA, 12 min UVC] -  $\gamma^p = 0.14$ ,  $\gamma^d = 25.04$

Furthermore, predictions made by neural network seem to be consistent with the trends of the changes that occurred in the ACE Digital printing plate's surface.

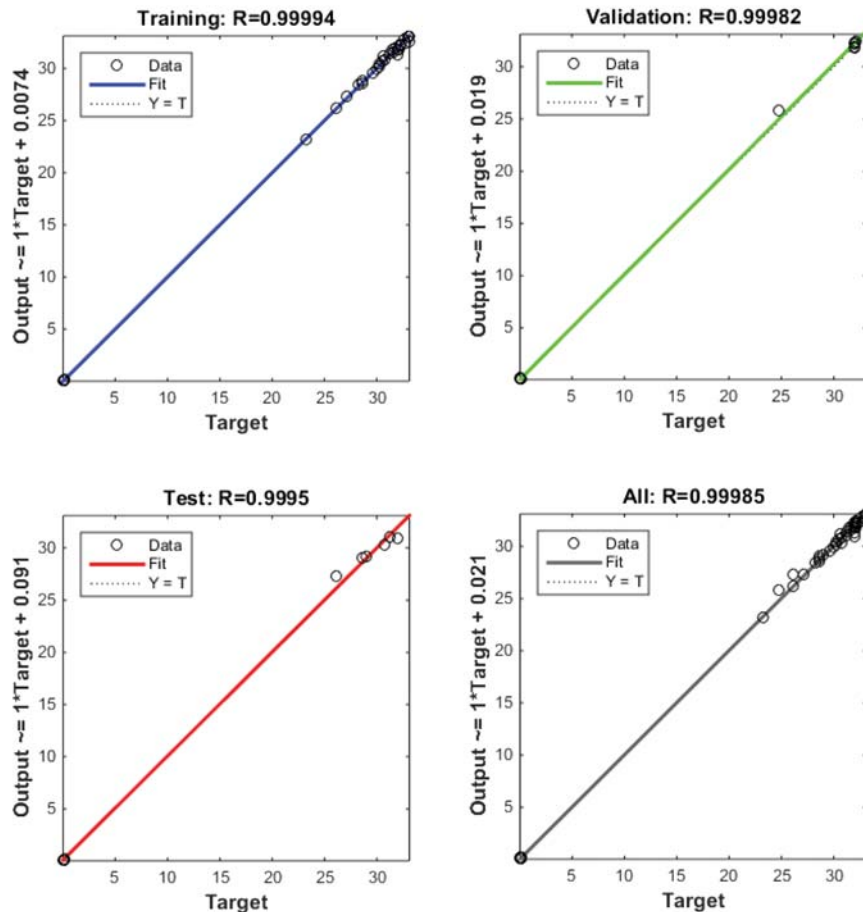


Figure 93. Regression plots of neural network for estimation of surface properties of ACE Digital printing plate

Figures 94. – 96. Present the characteristics of neural network used for estimation of the surface properties of Digital MAX printing plate.

Similar to ACE Digital printing plate, errors presented in Figure 94. are mostly concentrated around the zero error.

For this network, the best results were obtained with 6 nodes in the hidden layer. The best validation performance with minimal *mse* of 0.092 was reached at 9<sup>th</sup> iteration (Figure 95.).

Regression plots presented in Figure 96. show very good fitting, with only few points deviating from the ideal results.  $R$  value is, similar to neural network for ACE Digital, higher than 0.99.

Therefore, this neural network presents the valid model for the estimation of Digital MAX printing plate's  $\gamma^p$  and  $\gamma^d$ .

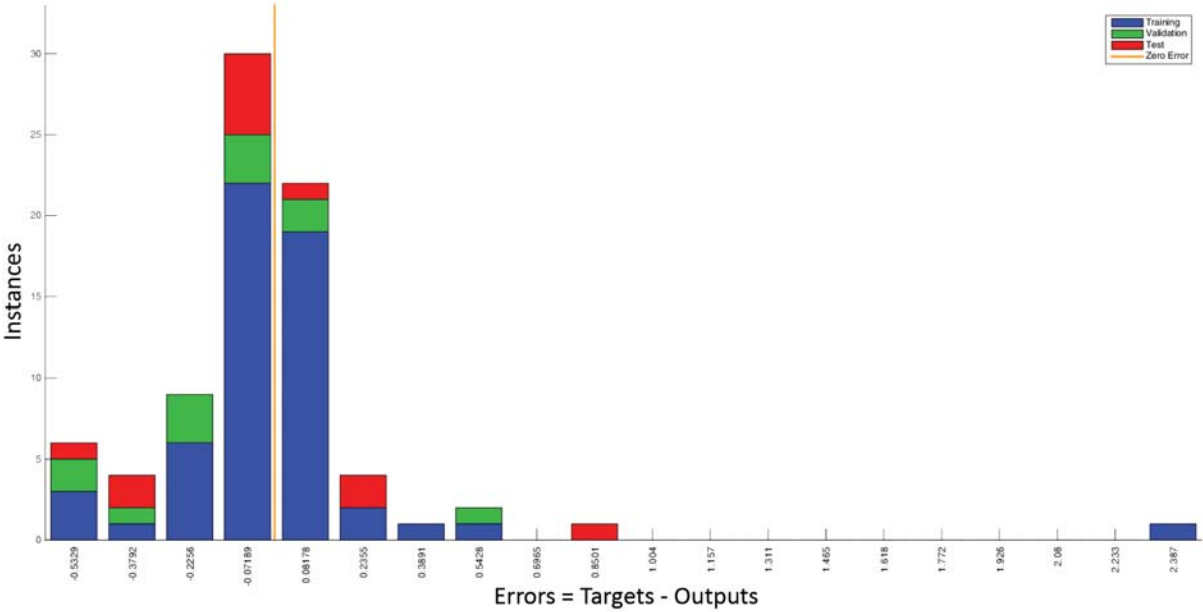


Figure 94. Error histogram for modelling of Digital MAX printing plate surface properties

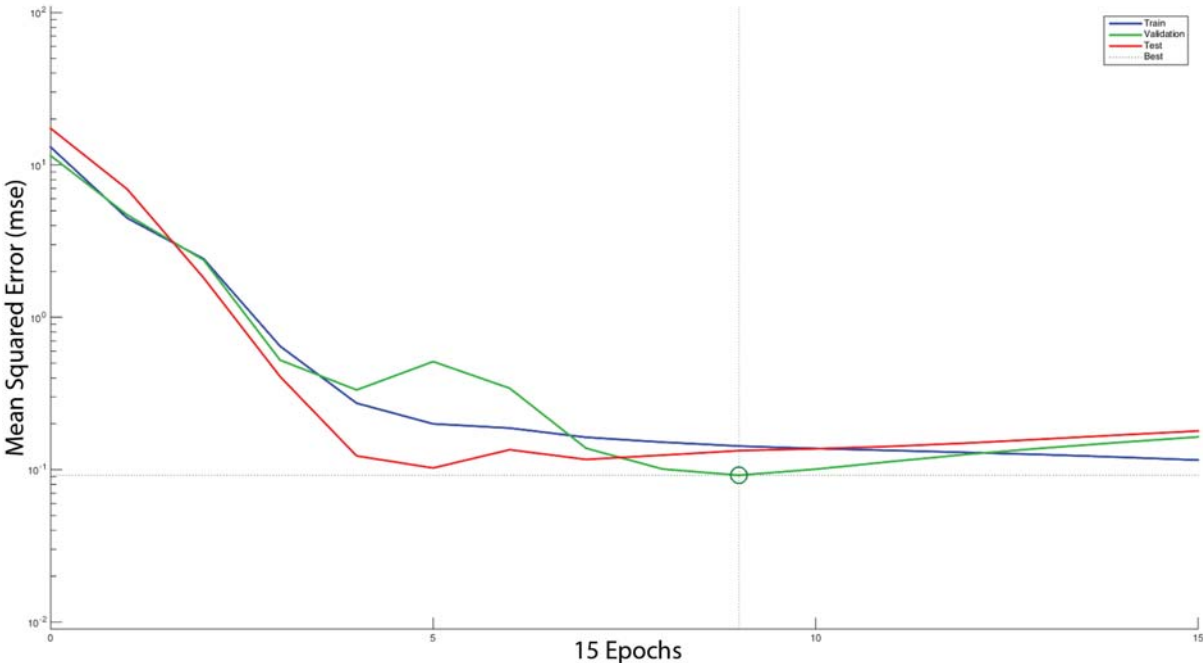


Figure 95. Performance of neural network for estimation of surface properties of Digital MAX printing plate

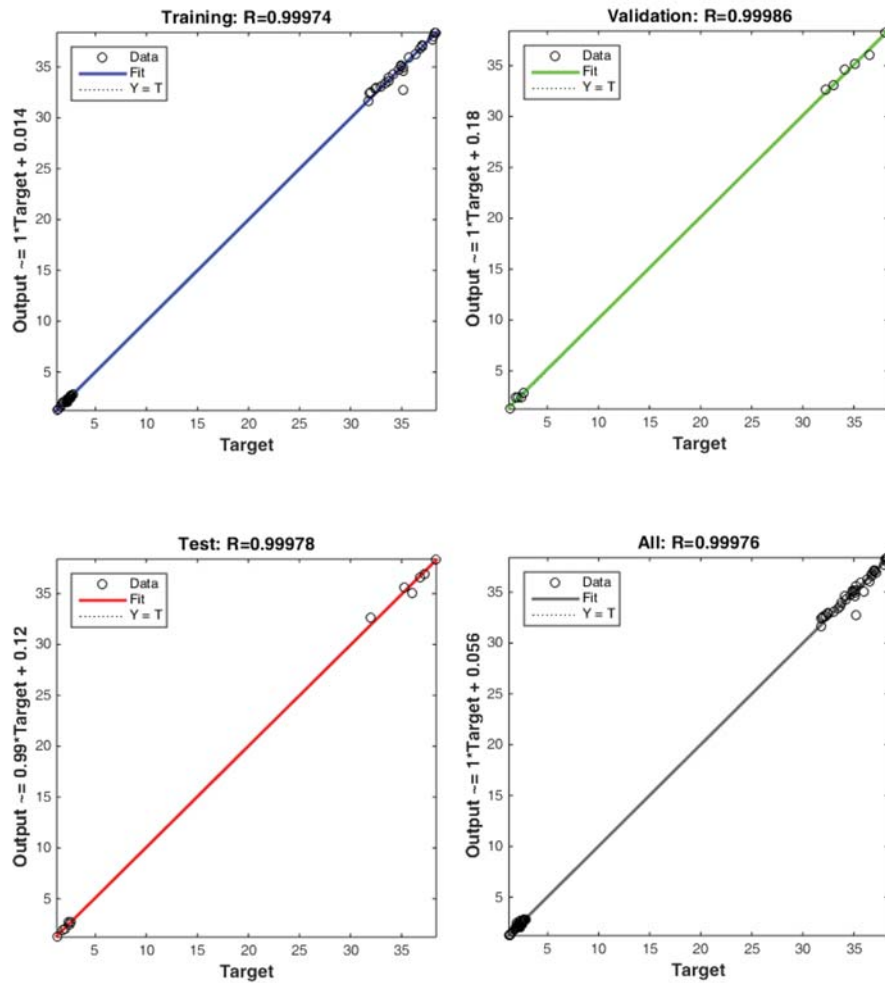


Figure 96. Regression plots of neural network for estimation of surface properties of Digital MAX printing plate

Indeed, checked outputs display similar values to targets (Table 25.)

Table 25. Targets and outputs in neural network for Digital MAX printing plate

Input	Target (mNm <sup>-1</sup> )	Output (mNm <sup>-1</sup> )
[10 min UVA, 5 min UVC]	$\gamma^p = 2.28, \gamma^d = 34.64$	$\gamma^p = 2.25, \gamma^d = 34.68$
[10 min UVA, 10 min UVC]	$\gamma^p = 2.62, \gamma^d = 34.42$	$\gamma^p = 2.72, \gamma^d = 34.08$
[10 min UVA, 20 min UVC]	$\gamma^p = 1.17, \gamma^d = 38.44$	$\gamma^p = 1.25, \gamma^d = 38.32$

Values of outputs calculated from some random inputs are in accordance with the changes of  $\gamma^p$  and  $\gamma^d$  (mNm<sup>-1</sup>) caused by UV post-treatments discussed in this thesis:

- [1 min UVA, 20 min UVC] -  $\gamma^p = 1.15, \gamma^d = 38.36$ ;
- [7 min UVA, 3 min UVC] -  $\gamma^p = 2.03, \gamma^d = 33.19$ ;
- [20 min UVA, 20 min UVC] -  $\gamma^p = 1.66, \gamma^d = 38.34$

Figures 97. – 99. present the error and performance characteristics of neural network applied for estimation of Cosmolight QS printing plate’s surface properties. Errors presented in Figure 97. are less scattered than for other two simulations, but their values are higher.

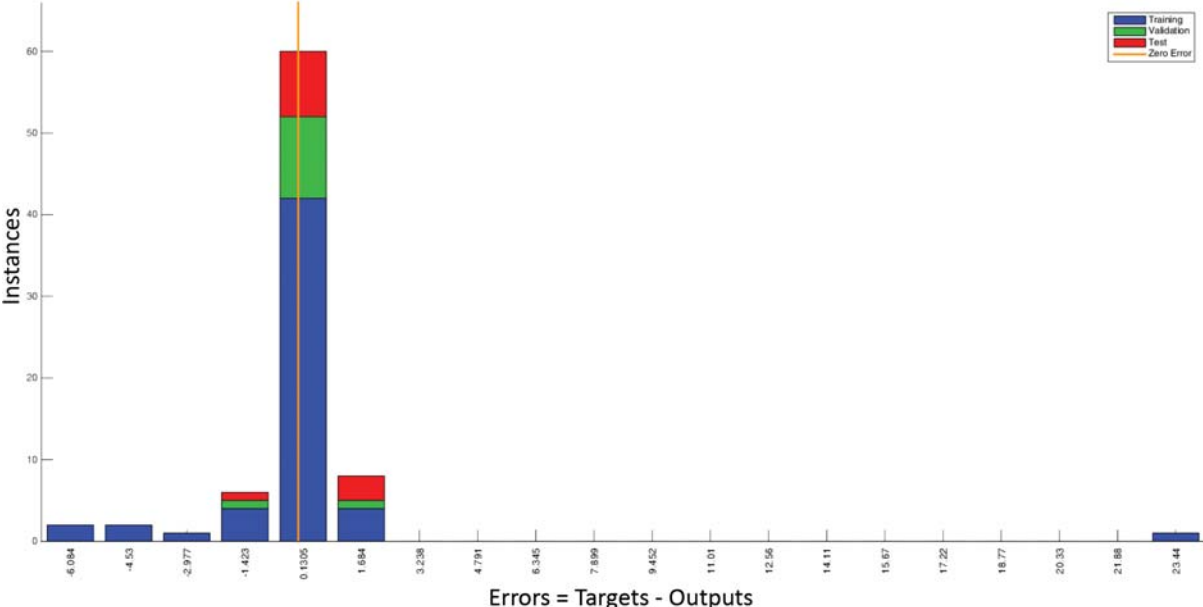


Figure 97. Error histogram for modelling of Cosmolight QS printing plate surface properties

For this neural network, 7 nodes in the hidden layer resulted with the lowest *mse*, 0.275 at 4<sup>th</sup> iteration (Figure 98.).

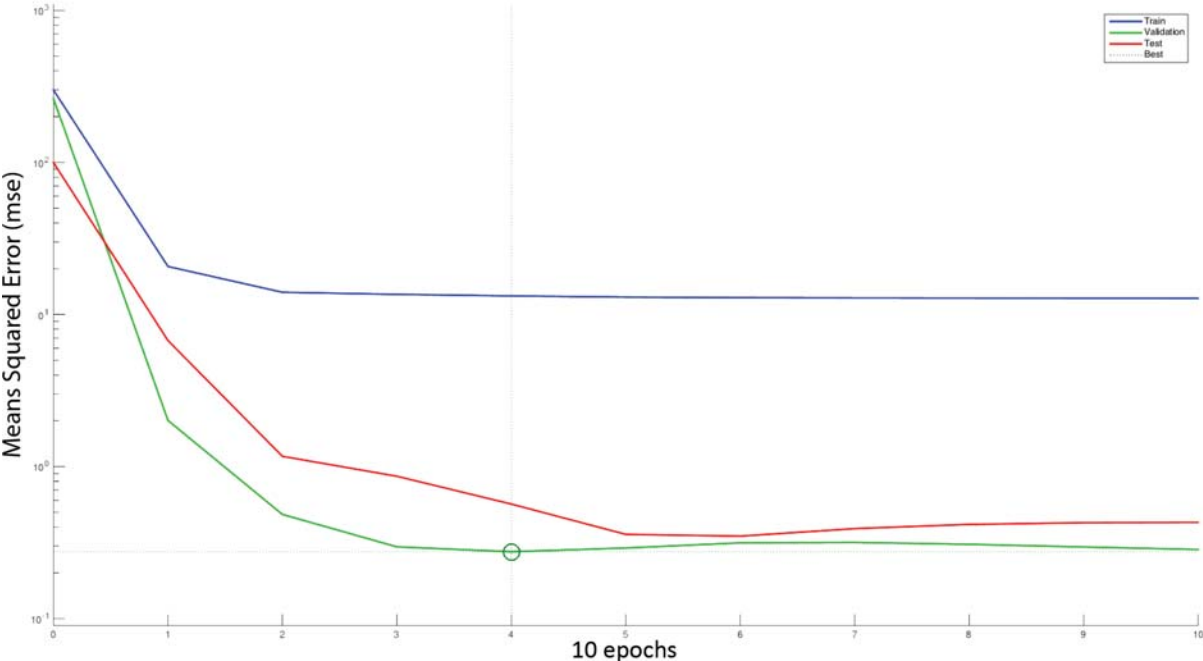


Figure 98. Performance of neural network for estimation of surface properties of Cosmolight QS printing plate

Overall, this neural network displayed the poorest fitting. However, with lowest value of  $R$  (0.948), it is still a good fit.

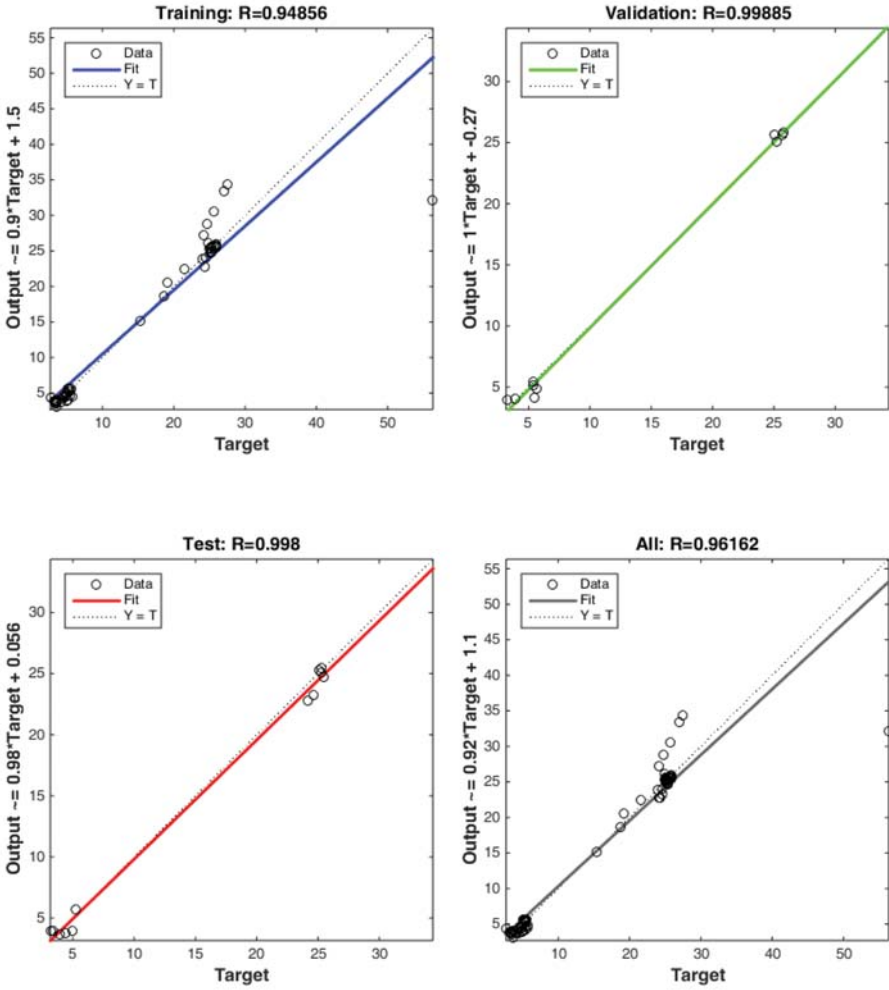


Figure 99. Regression plots of neural network for estimation of surface properties of Cosmolight QS printing plate

This statement is supported by the small differences between targets and tested outputs (Table 26.):

Table 26. Targets and outputs in neural network for Cosmolight QS printing plate

Input	Target (mNm <sup>-1</sup> )	Output (mNm <sup>-1</sup> )
[0 min UVA, 0 min UVC]	$\gamma^p = 1.10, \gamma^d = 15.11$	$\gamma^p = 3.57, \gamma^d = 15.32$
[10 min UVA, 5 min UVC]	$\gamma^p = 3.94, \gamma^d = 24.61$	$\gamma^p = 5.78, \gamma^d = 25.93$
[5 min UVA, 5 min UVC]	$\gamma^p = 3.90, \gamma^d = 24.71$	$\gamma^p = 3.50, \gamma^d = 24.30$



It is visible that the errors are mostly caused by differences in outputs and targets for  $\gamma^p$ . This was expected, since Cosmolight QS did display some inconsistencies in trends of  $\gamma$  with prolonged UV post-treatment due to the start of the material degradation after prolonged UVC post-treatment. In order to improve the fitting, the duration of UVC post-treatment would have to be limited.

Examples for simulated output values of  $\gamma^p$  and  $\gamma^d$  ( $\text{mNm}^{-1}$ ) based on random inputs are:

- [3 min UVA, 3 min UVC] -  $\gamma^p = 3.52$ ,  $\gamma^d = 19.76$ ;
- [7 min UVA, 15 min UVC] -  $\gamma^p = 5.65$ ,  $\gamma^d = 24.53$ ;
- [12 min UVA, 4 min UVC] -  $\gamma^p = 4.16$ ,  $\gamma^d = 28.49$

In conclusion, neural networks proved as a valid tool for modelling of surface properties of photopolymer printing plates related to the modified UVA and UVC post-treatments in the production process.

Performances of three applied neural networks are solid, with high fitting and generally low *mse* values. In order to further improve the performance of the network, more inputs could be added, and the targets that deviate significantly from the outputs can be re-evaluated. If any modifications in printing plate production workflow related to UV post-treatments are being made, neural network can be retrained based on new inputs and be used again.

Neural networks do not display the weights of inputs explicitly, like LS in matrix form applied in this research, but are more applicable and user-friendly in the real systems due to the program support. Neural networks can be used in the flexographic printing plate production as a helpful model for estimation of surface properties of printing plates prior to its production, therefore having the potential to optimize the printing plate production workflow and enable easier “modification-on-demand” of  $\gamma^p$  and  $\gamma^d$  of the printing plate.

## 6. CONCLUSIONS

In this thesis, the properties of three different types of photopolymer flexographic printing plates were analysed in relation to varied exposure to UVA and UVC wavelengths in the post-treatment process of the printing plate production workflow. The aim was to define, interconnect and quantify the changes that occur in chemical, mechanical and surface properties of printing plates during the UV post-treatments, and in the end, to build a functional model of photopolymer printing plate production process, related to modified properties of printing plates.

Since the primary purpose of this research was to retain the functional properties of printing plates in the reproduction process throughout all modifications, all procedures in the printing plate production workflow prior to post-treatment needed to be kept constant and standardized, in order to initially result with functional printing plate. The post-treatment process, as the last step in flexographic printing plate production workflow, is of crucial importance for defining printing plate's surface properties. Furthermore, the post-treatment process is easily alterable in the real systems and is not completely standardized by printing plate manufacturers – its duration is often defined by the recommended range.

Types of photopolymer printing plates analysed in this research were two styrene-diene-based, commonly used solvent-washable LAMS CtP printing plates, and one water-washable LAMS CtP printing plate with still growing share on the market. All printing plate samples were prepared in standard conditions up to the UV post-treatment which was modified, pairing the constant duration of one wavelength type with the other that was varied.

Modified photopolymer printing plate samples were analysed by thermal, chemical, mechanical, optical and spectroscopic methods, and their surface properties were defined and calculated. Prints obtained by modified printing plates were produced in the manufacture-sized, standardized conditions, and their qualitative properties were analysed.

From the results of various measurement, analysis and calculation methods performed in this research, the following conclusions can be made:

- It was proved that the variations of UVA and UVC post-treatment processes result with thermally stable printing plate – thermal degradation even shifts to higher temperatures for some samples exposed to prolonged UV post-treatments due to the increased crosslinking degree in the material;

- It was demonstrated that the two-phase system in the printing plate is generated, as a result of the prolonged UV post-treatments: the surface and the core of photopolymer material. This phenomenon is significant for understanding the influence of UV post-treatment process on the printing plate and print properties. When exposed to UV post-treatments, the core of analysed photopolymer materials undergoes the continued crosslinking process, while the photo oxidation takes place in the surface layer, and results with the start of the degradation by erosion;
- It was proved that the in the dispersive and polar component of the surface free energy of photopolymer materials ( $\gamma^d$  and  $\gamma^p$ ) due to the varied UVA and UVC post-treatments, are primarily caused by oxygen inhibition during the crosslinking propagation and termination. Furthermore, UVA and UVC post-treatments do not result with the same trends of changes in ratios of C=O and OH bonds in the surface layer of different photopolymer materials. This points to different crosslinking propagation and termination mechanisms, as well as to different sensitivity to the oxygen and the potential to modify  $\gamma^d$  or  $\gamma^p$  of printing plate without damaging the surface;
- It was confirmed that the changes in the surface properties ( $\gamma^d$  and  $\gamma^p$ ) of printing plates caused by varied UVA and UVC post-treatment cause the changes in the quality of prints, as well. Coverage values in shadow area, optical density on prints and ink layer thickness display the changes in strong correlations with changed  $\gamma^d$  and  $\gamma^p$ , which demonstrates that UVA and UVC post-treatments can be used as a tool to adjust the print properties to a desired value. Specifically, the range of ink layer thickness with used printing plates, which is often very important feature in functional printing, was expanded from 1-4  $\mu\text{m}$  with recommended duration of UV post-treatments, to 0.5 – 10  $\mu\text{m}$  with variations of UV post-treatments on the printing plates. Therefore, UVA and UVC post-treatments have been specifically recognized as a significant step for obtaining maximal possible quality in the reproduction process;
- It was confirmed that it is possible to quantify the influences of the parameters which have been changed by varied UVA and UVC post-treatments, and are related to printing plate's  $\gamma^d$  and  $\gamma^p$ . Quantification of parameters, by calculating their weights by means of LS model fitting, enabled better understanding of the processes in the printing plate's surface induced by UVA and UVC post-treatments, as well as defined the

primary influencing parameters for the properties of prints obtained by modified printing plates and provided a functional model related to flexographic printing plate production;

- It was proved that neural network is a valid and useful model for estimation of printing plate's  $\gamma^d$  and  $\gamma^p$  modified in the post-treatment process. After the quantification of influencing parameters on printing plate's surface properties, neural network is applicable for finding the durations of UVA and UVC post-treatments where the desired  $\gamma^d$  and  $\gamma^p$  are reached, before performing the post-treatment process.

The hypotheses of this doctoral thesis have therefore been confirmed:

- It is possible to characterize and quantify the influence of the parameters in flexographic printing plate production process by means of spectroscopic, mechanic and optical methods;
- It is possible to define the functional model of flexographic printing plate production by determination of the significant parameters in printing plate production.

## Scientific contribution

The application of various types of measurement and analysis methods in this thesis demonstrated the complexity of the process of defining the surface properties of photopolymer flexographic printing plates and the origin of their changes related to the post-treatment process. The scientific contribution of this thesis, in the field of graphic technology, and in the field of material science, is manifested by:

- The interconnection of the properties of photopolymer materials that change during the exposure to UVA and UVC wavelengths and define dispersive and polar component of the surface free energy of photopolymer materials ( $\gamma^d$  and  $\gamma^p$ ), as well as the properties of the core;
- Detailed and extensive research in graphic technology related to the surface properties of flexographic printing plates, specifically recognizing the UVA and UVC post-treatments as a significant step for obtaining maximal possible quality in the reproduction process. According to available literature, the research in this area, with emphasis on printing plate's post-treatment process, has not been performed yet;
- Definition of printed product's qualitative properties by the modification of printing plate's surface, rather than other parameters in the reproduction process, presents a new approach in optimization of the quality of final product (print);
- Successful application of fitting models which enabled the quantification and estimation of the printing plates' surface properties. Specifically, LS fitting provided a step forward in the analysis of the flexographic photopolymer material's properties in comparison to calculating the correlations, because it provides a holistic approach to analysis of the material's surface properties. Neural network enabled the estimation of photopolymer material's  $\gamma^d$  and  $\gamma^p$  for the specific duration of the defined energy deposition, obtainable prior to the printing plate production;
- Defining the system for fine adjustment of the thickness of deposited ink layer, by modifications of one parameter in printing plate production workflow, i.e. UV post-

treatment. This system for solving the issues in the depositions of (thin) coatings, especially present in printing of functional layers, can be applied in different research and engineering areas.

## **7. REFERENCES**



- [1] H. Kipphan, *Handbook of Print Media*, Springer, Berlin, (2001)
- [2] O. Brajnović, *Adjustment of the photopolymer printing forms to match new qualitative requirements*, Master thesis, Faculty of Graphic Arts, University of Zagreb, (2011)
- [3] J. Page Crouch, *Flexography Primer*, 2nd edition, PIA/GATF Press, Pittsburgh, (1998)
- [4] R. Knoll, *Photopolymerizable flexographic printing elements comprising SIS/SBS mixtures as binder for the production of flexographic printing plates*, Pat. US 6,531,263 B2, (2002)
- [5] Y. Yagci, S. Jockusch, N. J. Turro, *Photoinitiated Polymerization: Advances, Challenges, and Opportunities*, *Macromolecules*, 43, (2010), 6245–6260
- [6] A. Theopold, J. Neumann, D. Massfelder, E. Dörsam, *Effects of solvents on flexographic printing plates*, *Advances in Printing and Media Technology*, Proceedings of the 39th International Research Conference of Iarigai, Ljubljana, (2012)
- [7] R. Bodwell, J. Scharfenberger, *Advancing flexography: The technical path forward*, DuPont Packaging Graphics, (2011.)
- [8] T. Tomašegović, S. Mahović Poljaček, T. Cigula, *Modification of flexographic printing plate's surface properties by variation of UVC finishing*, XI Symposium on Graphic Arts, Pardubice, (2013), 59.
- [9] T.Y. Lee, C.A. Guymon, E. Sonny Jönsson, C.E. Hoyle, *The effect of monomer structure on oxygen inhibition of (meth)acrylates photopolymerisation*, *Polymer*, 45 (2004), Issue 18, 6155–6162
- [10] E. Andzejewska, *Photopolymerization kinetics of multifunctional monomers*, *Progress in Polymer Science*, 26 (2001), Issue 4, 605-665
- [11] S. Mahović Poljaček, T. Cigula, T. Tomašegović. T., *Meeting the quality requirements in flexographic plate making process*, IC2012, Budapest, (2012)
- [12] FIRST, *Flexographic Image Reproduction Specifications & Tolerance*, 3rd edition, Foundation of Flexographic Technical Association, Inc., USA, (2003)
- [13] J. Johnson, *Aspects of flexographic print quality and relationship to some printing parameters*, Doctoral thesis, Faculty of Technology and Science, Karlstad University, Karlstad, (2008)

- [14] G. Cusdin, *Flexography: Principles & Practices 5th ed. Volume 1*, Foundation of Flexographic Technical Association, ASIN B000PZU20I, NY, (1999)
- [15] Kodak DigiCap technology,  
[http://graphics.kodak.com/KodakGCG/uploadedFiles/DigiCapNX\\_WhitePaper.pdf](http://graphics.kodak.com/KodakGCG/uploadedFiles/DigiCapNX_WhitePaper.pdf)
- [16] T. Matsubara, R. Oda, *Block copolymer composition for flexographic printing plates*, Pat. 20,110,308,412, (2011)
- [17] F. Kaoru, H.i Hiroshi, I. Fumio, M. Yoshinobu, S. Sakae, Y. Minoru, *Flexo ink composition*, Pat. US 3912675 A, 1975.
- [18] D.E. Bisset, *The printing ink manual 3. ed*, Northwood Books, London, (1979)
- [19] ISO standard 12647-6, *Graphic technology - Process control for the production of half-tone colour separations, proofs and production prints -Flexographic printing*, (2006)
- [20] C. Andersson, J. Johnson, L. Järnström, *Ultraviolet-induced ageing of flexographic printing plates studied by thermal and structural analysis methods*, Journal of Applied Polymer Science, Volume 112 (2009), Issue 3, pp. 1636–1646
- [21] T. Tomašegović, S. Mahović Poljaček, D. Milčić, *Qualitative Analysis of Coverage Value Transfer in Modern Packaging Printing Workflow*, Proceedings of the 19th IAPRI World Conference on Packaging, Melbourne, (2014), pp. 651-666
- [22] T. Tomašegović, S. Mahović Poljaček, T. Cigula, *Impact of Screen Ruling on the Formation of the Printing Elements on the Flexographic Printing Plate*, Acta graphica, Volume 24 (2013), 1-12
- [23] T. Tomašegović, S. Mahović Poljaček, T. Cigula, M. Gojo, D. Milčić, *Correlation between the lams and printing element area on the flexographic printing plate*, Proceedings of 7th Symposium of Information and Graphic Arts technology, Ljubljana (2014), 43-49
- [24] S. Mahović Poljaček, T. Tomašegović, M. Gojo, *Influence of UV exposure on the surface and mechanical properties of flexographic printing plate*, GRID 2012 Proceedings, Novi Sad: Faculty of Technical Science, (2012), 135-140
- [25] T. Tomašegović, S. Mahović Poljaček, T. Cigula, *Surface properties of flexographic printing plates related to the UVC post-treatment*, Journal of Print and Media Technology Research, Volume 2 (2013), 227-234

- [26] V.V. Krongauz, A.D. Trifunac, *Processes in Photoreactive Polymers*, Springer Science & Business Media, (2013)
- [27] T. Tomašegović, T. Cigula, S. Mahović Poljaček, M. Gojo, *Effect of exposures on the mechanical properties of the liquid photopolymer flexographic printing plate*, Proceedings Matrib 2011, Vela Luka (2011), 495-501
- [28] D. Novaković, D. S. Dedijer, S. Mahović Poljaček, *A model for improving the flexographic printing plate making process*, Technical Gazette 17, (2010), 403-410
- [29] B. Thompson, *Printing Materials: Science and Technology*, 2nd edition, Pira International ( 2004)
- [30] J. Poljak, T. Hudika, S. Mahović Poljaček, M. Gojo, *Printing substrate as a quality parameter in flexography*, Scientific Paperd of University of Pardubice, Ser. A, Volume 19 (2013), 241–248
- [31] J. Coates, *Interpretation of infrared spectra, a practical approach*, In: R.A. Meyers, ed. Encyclopedia of analytical chemistry, Chichester: John Wiley&Sons, (2000), 10815-10837
- [32] D. Galton, D. Bould, T. Claypole, *The effect of surface properties on the printability of flexographic printing plates*, Advances in Printing and Media Technology, Proceedings of the 37th International Research Conference of Iarigai, Montreal, (2010)
- [33] S. Mahović Poljaček, T. Tomašegović, T. Cigula, M. Gojo, D. Milčić, *Formation of the Printing Elements in the Photopolymer Material Used in Flexography*, Key Engineering Materials, Volume 611-612 (2014), 883-891
- [34] AniCAM 3D microscope, [http://www.troika-systems.com/English/\\_downloads/AniCAM-3D\\_Scanning\\_Microscope\\_E.pdf](http://www.troika-systems.com/English/_downloads/AniCAM-3D_Scanning_Microscope_E.pdf)
- [35] G. L. Laurent, *Analysis of the Correlation Between the Print Quality Required in Flexography and the Tolerances in Materials and Paper Manufacturing in Terms of Printability*, Doctoral thesis, Royal Institute of technology, Department of Numerical Analysis and Computer Science, Sweden, (2001)
- [36] MacDermid Digital MAX photopolymer plates, [http://printing.macdermid.com/files/8514/2626/3635/Digital\\_MAX\\_092112.pdf](http://printing.macdermid.com/files/8514/2626/3635/Digital_MAX_092112.pdf)

- [37] Flint ACE Digital photopolymer plates, [http://www.flintgrp.com/en/documents/Printing-Plates/nyloflex/nyloflex\\_ACE\\_EN.pdf](http://www.flintgrp.com/en/documents/Printing-Plates/nyloflex/nyloflex_ACE_EN.pdf)
- [38] Toyobo Cosmolight QS photopolymer plate, [http://www.flexologic.nl/fileadmin/PDF/Toyobo/Cosmoright\\_ENG.pdf](http://www.flexologic.nl/fileadmin/PDF/Toyobo/Cosmoright_ENG.pdf)
- [39] Implementation Guidance for ISO 9001:2008, [http://www.iso.org/iso/06\\_implementation\\_guidance.pdf](http://www.iso.org/iso/06_implementation_guidance.pdf)
- [40] ISO 14001:2004 Environmental management systems - Requirements with guidance for use, [http://www.iso.org/iso/catalogue\\_detail?csnumber=31807](http://www.iso.org/iso/catalogue_detail?csnumber=31807)
- [41] F. Deflorian, L. Fedrizzi, S. Rossi, *Electrochemical impedance spectroscopy and Fourier transform infrared spectroscopy of natural and accelerated weathering of organic coatings*, Corrosion, Volume 54 (1998), Issue 8
- [42] V. Kovačević, S. Lučić Blagojević, M. Leskovic, *Inženjerstvo površina*, Sveučilište u Zagrebu Fakultet kemijskog inženjerstva i tehnologije, (2015)
- [43] M. Sangermano, P. Meier, S. Tzavalas, *Infrared Spectroscopy as a Tool to Monitor Radiation Curing*, Infrared Spectroscopy - Materials Science, Engineering and Technology, ISBN 978-953-51-0537-4, (2012)
- [44] W. R. Herguth, G. Nadeau, *Applications of Scanning Electron Microscopy and Energy Dispersive Spectroscopy (SEM/EDS) To Practical Tribology Problems*, Hergut Laboratories, Inc., (2004)
- [45] INCA Energy, *Energy Dispersive Spectrometry Hardware, The Microanalysis System*, Oxford Instruments, Analytical Ltd., (2009)
- [46] J. Liu, X. J. Zheng, K. Y. Tang, *Study on the gravimetric measurement of the swelling behaviors of polymer films*, Reviews on Advanced Material Science, Volume 33 (2013), 452-458
- [47] M. Batallas, P. Singh, *Evaluation of anticorrosion coatings for high temperature service*, NACE International corrosion conference & expo, (2008)
- [48] B. Bilyeu, *Characterization of cure kinetics and physical properties of a high performance, glass fiber-reinforced epoxy prepreg and a novel fluorin-modified, amine-cured commercial epoxy*, Doctoral thesis, Univeristy of North Texas, (2003)

- [49] S. Thitithanasarn, K. Yamada, U.S. Ishiaku, H. Hamada, *The Effect of Curative Concentration on Thermal and Mechanical Properties of Flexible Epoxy Coated Jute Fabric Reinforced Polyamide 6 Composites*, Open Journal of Composite Materials, Volume 2 (2012)
- [50] F. M. N. Muhammad, S. M. S. Mohd, N. M. Mohamad, A. Nurhaswani, W. A. R. Mohd, A. Yatimah, A. M. Ahmad, *Corrosion and Heat Treatment of Paint Coating Containing Battery Cathode Waste Material-Epoxy Resin in 3.5 wt% Sodium Chloride Solution*, International Journal of Electrochemical Science, Volume 7 (2012)
- [51] V. B. Mišković-Stanković, Z. Ž. Lazarević, Z. M. Kračević-Popović, *Electrochemical properties and thermal stability of epoxy coatings electrodeposited on aluminium and modified aluminium surfaces*, Journal of the Serbian Chemical Society, Volume 66 (2001), Issue 11-12.
- [52] V. Chandra, V. Pandurangadu, T. Subba, *TGA, DSC, DTG Properties of epoxy composites reinforced with feather fibers of 'emu' bird*, International Journal of Innovative Research in Science, Engineering and Technology, Volume 3 (2014), Issue 5.
- [53] D. G. Weldon, *Failure analysis and degree of cure*, JCPL, (2005).
- [54] M.T. Rodríguez, S. J. García, J. J. Gracenea, C. Vitores, J. J. Suay, *Thermal, mechanical, and anticorrosive characterization of an epoxy primer*, Corrosion, Volume 63 (2007), Issue 12
- [55] J. Li, C. S. Jeffcoate, G. P. Bierwagen, D. J. Mills, D. E. Tallman, *Thermal transition effects and electrochemical properties in organic coatings: Part 1 – Initial studies on corrosion protective organic coatings*, Corrosion, Volume 54 (1998), Issue 10
- [56] Dataphysics OCA 30, [http://www.asi-team.com/asi%20team/dataphysics/DataPhysics%20data/OCA30\\_E.pdf](http://www.asi-team.com/asi%20team/dataphysics/DataPhysics%20data/OCA30_E.pdf)
- [57] D. K. Owens, R. C. Wendt, *Estimation of the surface free energy of polymers*, Journal of Applied Polymer Science, Volume 13 (1969), Issue 8, 1741-1747
- [58] C. J. Van Oss, R. F. Giese, Z. Li, K. Murphy, J. Norris, M. K. Chaudhury, R. J. Good, *Contact Angle, Wettability and Adhesion*, VSP, Utrecht, (1993)
- [59] Wyko NT 2000 white light interferometer, <http://erc.ncat.edu/Facilities/Manuals/Wyko.pdf>

- [60] Olympus BX 51 metallurgical microscope,  
<http://www.olympusmicro.com/brochures/pdfs/bx51.pdf>
- [61] X-Rite VipFlex, [https://www.xrite.com/product\\_overview.aspx?ID=797](https://www.xrite.com/product_overview.aspx?ID=797)
- [62] IC Plate II, [https://www.xrite.com/documents/literature/en/L7-413\\_PlateReaders\\_en.pdf](https://www.xrite.com/documents/literature/en/L7-413_PlateReaders_en.pdf)
- [63] X-Rite 939 SpectroDensitometer, [https://www.xrite.com/documents/manuals/en/939-500\\_939\\_Operators\\_Manual\\_en.pdf](https://www.xrite.com/documents/manuals/en/939-500_939_Operators_Manual_en.pdf)
- [64] Ake Björck, *Numerical Methods for Least Squares Problems*, SIAM, ISBN 0898713609, (1996)
- [65] LS in matrix form,  
[http://web.stanford.edu/~mrosenfe/soc\\_meth\\_proj3/matrix\\_OLS\\_NYU\\_notes.pdf](http://web.stanford.edu/~mrosenfe/soc_meth_proj3/matrix_OLS_NYU_notes.pdf)
- [66] B. Yegnanarayana, *Artificial neural networks*, PHI Learning Pvt. Ltd., (2009)
- [67] S. W. Ellacott, J. C. Mason, I. J. Anderson, *Mathematics of Neural Networks: Models, Algorithms and Applications*, Springer Science & Business Media, (1997)
- [68] M. P. Sepe, *Thermal Analysis of Polymers*, iSmithers Rapra Publishing, Volume 8, Number 11, 10-11, (1997)
- [69] H. Ishida, T. Agag, *Handbook of Benzoxazine Resins*, Elsevier, (2011)
- [70] TGA analysis guide,  
[http://www.perkinelmer.com/CMSResources/Images/4474556GDE\\_TGABeginnersGuide.pdf](http://www.perkinelmer.com/CMSResources/Images/4474556GDE_TGABeginnersGuide.pdf)
- [71] F. M. N. Muhammad, S. M. S. Mohd, N. M. Mohamad, A. Nurhaswani, W. A. R. Mohd, A. Yatimah, A. M. Ahmad, *Corrosion and Heat Treatment of Paint Coating Containing Battery Cathode Waste Material-Epoxy Resin in 3.5 wt% Sodium Chloride Solution*, International Journal of Electrochemical Science, Volume 7 (2012), 9633 – 9642
- [72] Analysis of elastomer vulcanizate composition by TG-DTG techniques,  
[http://www.tainstruments.co.jp/application/pdf/Thermal\\_Library/Applications\\_Briefs/TA083.PDF](http://www.tainstruments.co.jp/application/pdf/Thermal_Library/Applications_Briefs/TA083.PDF)
- [73] G. O. Garmong, *Photosensitive polymeric printing medium and water developable printing plates*, Pat. US5348844 A, (1994)

- [74] N. P. Cheremisinoff, P. N. Cheremisinoff, *Handbook of Applied Polymer Processing Technology*, CRC Press, (1996)
- [75] B. A. Miller-Chou, J. L. Koenig, *A review of polymer dissolution*, *Progress in Polymer Science*, Volume 28 (2003), 1223–1270
- [76] C. M. Hansen, *Hansen Solubility Parameters: A User's Handbook*, Second Edition, CRC Press: Boca Raton, (2007)
- [77] M. J. Loadman, *Analysis of Rubber and Rubber-like Polymers*, Springer Science & Business Media, (2012)
- [78] Michael V. Sefton, Edward W. Merrill, *Effect of surface swelling on diffusion on polymers. II. Delamination*, *Journal of Polymer Science: Polymer Chemistry Edition*, Volume 14 (8), (1976), 1829–1838
- [79] H. Zeng, *Polymer Adhesion, Friction, and Lubrication*, John Wiley & Sons, (2013)
- [80] R. A. Wolf, *Plastic Surface Modification: Surface Treatment and Adhesion, Sample Chapter 2: Primary Polymer Adhesion Issues with Inks, Coatings, and Adhesives*, Hanser Publishers, Munich, (2009)
- [81] N. J. Hallab, K. J. Bundy, K. O'Connor, R. L. Moses, *Evaluation of metallic and polymeric biomaterial surface energy and surface roughness characteristics for directed cell adhesion*, *Tissue Engineering*, Volume 7 (1), (2001)
- [82] I. Krásný, I. Kupská, L. Lapčík, *Effect of glow-discharge air plasma treatment on wettability of synthetic polymers*, *Journal of Surface Engineered Materials and Advanced Technology*, Volume 2 (2012), 142-148
- [83] P. Kramer, L. Davis, R. Jones, *Control of Free Radical Reactivity in Photopolymerization of Acrylates*, *Radiotechnology Report*, Volume 4, (2012), 33-41
- [84] F. Cataldo, *The action of ozone on polymers having unconjugated and cross- or linearly conjugated unsaturation: chemistry and technological aspects*, *Polymer Degradation and Stability*, Volume 73 (3), (2001), 511–520
- [85] M. da Conceição Cavalcante Lucena, S. de Aguiar Soares. J. Barbosa Soares, *Characterization and thermal behavior of polymer-modified asphalt*, *Materials Research*, Volume 7 (4), (2004)

- [86] Controlled Radical Polymerization Guide,  
<http://www.sigmaaldrich.com/content/dam/sigma-aldrich/docs/SAJ/Brochure/1/controlled-radical-polymerization-guide.pdf>
- [87] E. Yousif, R. Haddad, *Photodegradation and photostabilization of polymers, especially polystyrene: review*, SpringerPlus, Volume 2, (2013)
- [88] R. Mendelsohna, C. R. Flacha, D. J. Mooreb, *Determination of molecular conformation and permeation in skin via IR spectroscopy, microscopy, and imaging*, Biochimica et Biophysica Acta (BBA) – Biomembranes, Volume 1758 (7), (2006), 923–933
- [89] S. Myhra, J. C. Rivière, *Characterization of Nanostructures*, CRC Press, (2012)
- [90] Kodak NX technology,  
[http://graphics.kodak.com/KodakGCG/uploadedFiles/Products/Computer-to-plate/Flexo\\_CTP/TRENDSETTER\\_NX\\_Imager/Tab\\_Contents/TSNX\\_sellsheet.pdf](http://graphics.kodak.com/KodakGCG/uploadedFiles/Products/Computer-to-plate/Flexo_CTP/TRENDSETTER_NX_Imager/Tab_Contents/TSNX_sellsheet.pdf)
- [91] MacDermid LUX ITP technology,  
[http://printing.macdermid.com/files/5614/2625/6737/LUXITP60\\_Brochure-1.pdf](http://printing.macdermid.com/files/5614/2625/6737/LUXITP60_Brochure-1.pdf)
- [92] L. A. Lindén, J. Jakubiak, *Contraction (shrinkage) in polymerization*, Polimery, Volume 46, (2001), 590 - 595
- [93] Interference and diffraction,  
<http://web.mit.edu/8.02t/www/802TEAL3D/visualizations/coursenotes/modules/guide14.pdf>
- [94] S. Mahović Poljaček, T. Cigula, T. Tomašegović, O. Brajnović, *Meeting the quality requirements in the flexographic plate making process*, International Circular of Graphic Education and Research, Volume 6, (2013)
- [95] B. Havlínová, V. Cicák, V. Brezová, L'. Horňáková, *Water-reducible flexographic printing inks—rheological behaviour and interaction with paper substrates*, Journal of Materials Science, Volume 34 (9), (1999), 2081-2088
- [96] D. Deganello, J.A. Cherry, D.T. Gethin, T.C. Claypole, *Patterning of micro-scale conductive networks using reel-to-reel flexographic printing*, Thin Solid Films, Volume 518(21), (2010), 6113-6116



- [97] J. Baker, D. Deganello, D. Gethin, T. Watson, *Flexographic printing of graphene nanoplatelet ink to replace platinum as counter electrode catalyst in flexible dye sensitised solar cell*, *Materials Research Innovations*, Volume 18 (2), (2014), 86-90
- [98] K. Johansson, P. Lundberg, R. Ryberg, *A Guide to Graphic Print Production*, John Wiley & Sons, (2012)
- [99] M.S. Yusof, T.C. Claypole, D.T. Gethin, A.M. A. Zaidi, *Application of finite elements on non-linear deformation of flexographic photopolymer printing plate*, *Proceedings of the World Congress on Engineering 2008 Vol II*, London, (2008)
- [100] D.C. Bould, T.C. Claypole, M.F.J. Bohan, D.T. Gethin, *Deformation of flexographic printing plates*,  
[http://www.researchgate.net/publication/265084813\\_Deformation\\_of\\_Flexographic\\_Printing\\_Plates](http://www.researchgate.net/publication/265084813_Deformation_of_Flexographic_Printing_Plates)
- [101] R. Olsson, L. Yang, J. van Stam, M. Lestelius, *Effects of ink setting in flexographic printing: Coating polarity and dot gain*, *Nordic Pulp and Paper Research Journal*, Volume 21(5), (2006), 569-574
- [102] J. Izdebska, S. Thomas, *Printing on Polymers: Fundamentals and Applications*, William Andrew, (2015)
- [103] Á. Borbély, R. Szentgyörgyvölgyi, *Colorimetric properties of flexographic printed foils: the effect of impression*, *Óbuda University e-Bulletin*, Volume 2 (1), (2011)
- [104] M. Rentzhog, *Water-based flexographic printing on polymer-coated board*, *Doctoral Thesis*, Royal Institute of Technology, Stockholm, (2006)
- [105] A. Karwa, *Printing studies with conductive inks and exploration of new conducting polymer compositions*, *Master Thesis*, Rochester Institute of Technology, (2006)
- [106] Flexography printing, <http://agpcptech.weebly.com/uploads/1/2/4/2/12423472/unit-3.pdf>
- [107] Cabot, *Specialty Carbon Blacks for Printing Ink Applications*, *Global selection guide*, (2015)
- [108] Surface tension of ethanol,  
[https://www.accudynetest.com/surface\\_tension\\_table.html?sortby=sort\\_st\\_disp](https://www.accudynetest.com/surface_tension_table.html?sortby=sort_st_disp)

- [109] T. R. Crompton, *Polymer Reference Book*, iSmithers Rapra Publishing, Shawbury, (2006)
- [110] Kiran Kambly, *Characterization of curing kinetics and polymerization shrinkage in ceramic-loaded photocurable resins for large area maskless photopolymerization (LAMP)*, Doctoral thesis, Georgia Institute of Technology, (2009)
- [111] L. G. P. Moraes, R. S. F. Rocha, L. M. Menegazzo, E. B. de Araújo, K. Yukimitu, J. C. S. Moraes, *Infrared spectroscopy: A tool for determination of the degree of conversion in dental composites*, Journal of Applied Oral Science, Volume 26 (2), (2008), 145-149
- [112] K. de la Caba, P. Guerrero, I. Mondragon, J. M. Kenny, *Comparative study by DSC and FTIR techniques of an unsaturated polyester resin cured at different temperatures*, Polymer International, Volume 45 (1998), 333-338
- [113] K. Esumi (Ed.), *Polymer Interfaces and Emulsions*, CRC Press, Tokyo, (1999)
- [114] H.P. Gavin, *The Levenberg-Marquardt method for nonlinear least squares curve-fitting problems*, Department of Civil and Environmental Engineering, Duke University, (2015)

# **APPENDIX 1**

**List of figures**

**List of tables**

**List of equations**

**List of identifications**

**List of abbreviations**

## List of figures

**Figure 1.** Flexographic printing plates:

a) rubber flexographic printing plate, b) photopolymer CtP flexographic printing plate

**Figure 2.** Top line – conventional flexographic digital file – 2540 ppi,

bottom line – *HD flexo* digital file – 4000 ppi

**Figure 3.** a) Printing elements on printing plate at 75% coverage (Kodak's SQUARESPOT technology), b) Micro-pattern on flexographic printing element

**Figure 4.** Production of the LAMS-based flexographic printing plate:

a) photopolymeric sheet prepared for the image transfer, b) back-exposure, c) ablation of the LAMS, d) main exposure, e) rinsing, f) drying, g) post-treatment

**Figure 5.** Areas opened on LAMS for: a) 5% and b) 50% nominal coverage value

**Figure 6.** Printing elements on the flexographic printing plate for:

a) 5% and b) 50% nominal coverage value, corresponding to Figure 5.a) and 5.b), respectively

**Figure 7.** 3D display of printing elements of 5% coverage value on flexographic printing plate for: a) magnification of 40x and b) magnification of 200x

**Figure 8.** Influencing parameters in flexography related to printing plate

**Figure 9.** Dependence of printing plate's hardness on main exposure

**Figure 10.** Dependence of contact angle on main exposure

**Figure 11.** Dependence of printing plate's surface energy on main exposure

**Figure 12.** Relation between printing plate's hardness and surface free energy

**Figure 13.** Contact angle of probe liquids on the examined flexographic printing plate samples

**Figure 14.** Surface free energy components of the examined flexographic printing plate samples

**Figure 15.** EDS analysis of the samples with mass portion of carbon (C) and oxygen (O)

**Figure 16.** FTIR analysis of the printing plate sample exposed to UVC radiation for 1 minute

**Figure 17.** FTIR analysis of the printing plate sample exposed to UVC radiation for 14 minutes

**Figure 18.** Topography of flexographic printing elements of 50% coverage value displayed by AniCAM 3D microscope

**Figure 19.** Comparison of the area of openings on LAMS for different bump curves applied in highlights

**Figure 20.** Comparison of the area of the printing elements

for different bump curves applied in highlights

**Figure 21.** Cross-section of printing elements at 1% coverage value with application of bump curve 2BU

**Figure 22.** Cross-section of printing elements at 1% coverage value with application of bump curve 6BU

**Figure 23.** Cross-section of printing elements at 1% coverage value with application of bump curve 10BU

**Figure 24.** 3D display of printing elements of 1% coverage value with application of bump curve 2BU, 6BU and 10BU, respectively

**Figure 25.** Research plan

**Figure 26.** Types of photopolymer printing plates

**Figure 27.** Test image transferred from the digital file to the printing plate

**Figure 28.** Principle of energy-dispersive X-ray spectroscopy

**Figure 29.** Contact angle measurement using sessile drop method

**Figure 30.** Images of fine lines and screen elements of 10% on prints (magnification 50x) obtained by Olympus BX 51

**Figure 31.** 3D image of the photopolymeric printing plate with elements of 5% coverage value

**Figure 32.** Neural network with two hidden layers

**Figure 33.** DSC curves for ACE Digital samples exposed to varied UVA post-treatment

**Figure 34.** DSC curves for ACE Digital samples exposed to varied UVC post-treatment

**Figure 35.** DSC curves for Digital MAX samples exposed to varied UVA post-treatment

**Figure 36.** DSC curves for Digital MAX samples exposed to varied UVC post-treatment

**Figure 37.** DSC curves for Cosmolight QS samples exposed to varied UVA post-treatment

**Figure 38.** DSC curves for Cosmolight QS samples exposed to varied UVC post-treatment

**Figure 39.** TG and DTG curves for ACE Digital photopolymeric samples:

a) non UV post-treated sample, b) 10 min UV post-treatment, c) 20 min UVA post-treatment, d) 20 min UVC post-treatment

**Figure 40.** TG and DTG curves for Digital MAX photopolymeric samples: a) non UV post-treated sample, b) 10 min UV post-treatment, c) 20 min UVA post-treatment, d) 20 min UVC post-treatment

**Figure 41.** TG and DTG curves for Cosmolight QS photopolymeric samples: a) non UV post-treated sample, b) 10 min UV post-treatment, c) 20 min UVA post-treatment, d) 20 min UVC post-treatment

**Figure 42.** Changes of printing plate hardness in dependence on duration of:

a) UVA post-treatment, b) UVC post-treatment

**Figure 43.** Normalized degrees of swelling for UVA post-treated ACE Digital samples immersed in different solvents: a) acetone, b) ethyl acetate, c) toluene

**Figure 44.** Normalized degrees of swelling for UVC post-treated ACE Digital samples immersed in different solvents: a) acetone, b) ethyl acetate, c) toluene

**Figure 45.** Normalized degrees of swelling for UVA post-treated Digital MAX samples immersed in different solvents: a) acetone, b) ethyl acetate, c) toluene

**Figure 46.** Normalized degrees of swelling for UVC post-treated Digital MAX samples immersed in different solvents: a) acetone, b) ethyl acetate, c) toluene

**Figure 47.** Normalized degrees of swelling for UVA post-treated Cosmolight QS samples immersed in different solvents: a) acetone, b) ethyl acetate, c) toluene

**Figure 48.** Normalized degrees of swelling for UVC post-treated Cosmolight QS samples immersed in different solvents: a) acetone, b) ethyl acetate, c) toluene

**Figure 49.**  $R_a$  parameters of printing plate samples exposed with:

a) varied UVA post-treatment, b) varied UVC post-treatment

**Figure 50.** Total surface free energy of printing plate samples exposed with: a) varied UVA post-treatment, b) varied UVC post-treatment

**Figure 51.** Polar component of surface free energy of printing plate samples exposed with: a) varied UVA post-treatment, b) varied UVC post-treatment

**Figure 52.** Dispersive component of surface free energy of printing plate samples exposed with: a) varied UVA post-treatment, b) varied UVC post-treatment

**Figure 53.** FTIR ATR spectra of ACE Digital samples exposed to varied UVA post-treatment

**Figure 54.** FTIR ATR spectra of ACE Digital samples exposed to varied UVC post-treatment

**Figure 55.** FTIR ATR spectra of Digital MAX samples exposed to varied UVA post-treatment

**Figure 56.** FTIR ATR spectra of Digital MAX samples exposed to varied UVC post-treatment

**Figure 57.** FTIR ATR spectra of Cosmolight QS samples exposed to varied UVA post-treatment

**Figure 58.** FTIR ATR spectra of Cosmolight QS samples exposed to varied UVC post-treatment

**Figure 59.** Oxygen ratios in the surface layer of photopolymeric samples exposed to: a) varied UVA post-treatment, b) varied UVC post-treatment

**Figure 60.** 3D scans of printing elements on ACE Digital printing plate at:

a) 5% coverage value, b) 50% coverage value, c) 95% coverage value

**Figure 61.** 3D scans of printing elements on Digital MAX printing plate at:

a) 5% coverage value, b) 50% coverage value, c) 95% coverage value

**Figure 62.** 3D scans of printing elements on Cosmolight QS printing plate at:

a) 5% coverage value, b) 50% coverage value, c) 95% coverage value

**Figure 63.** DFTA control strip

**Figure 64.** 3D scans of fields on DFTA strip transferred to ACE Digital printing plate:

a) field C – 4 px, b) field H – 14 px, c) field P – 30 px

**Figure 65.** 3D scans of fields on DFTA strip transferred to Digital MAX printing plate:

a) field C – 4 px, b) field H – 14 px, c) field P – 30 px

**Figure 66.** 3D scans of fields on DFTA strip transferred to Cosmolight QS printing plate:

a) field C – 4 px, b) field H – 14 px, c) field P – 30 px

**Figure 67.** Lines with nominal width of 20  $\mu\text{m}$  (magnification of 50x) on prints obtained by ACE Digital printing plates exposed to varied UV post-treatments: a) 2 min UVA post-treatment, b) 10 min UV post-treatment, c) 20 min UVA post-treatment, d) 2 min UVC post-treatment, e) 20 min UVC post-treatment

**Figure 68.** Lines with nominal width of 20  $\mu\text{m}$  (magnification of 50x) on prints obtained by Digital MAX printing plates exposed to varied UV post-treatments: a) 2 min UVA post-treatment, b) 10 min UV post-treatment, c) 20 min UVA post-treatment, d) 2 min UVC post-treatment, e) 20 min UVC post-treatment

**Figure 69.** Lines with nominal width of 20  $\mu\text{m}$  (magnification of 50x) on prints obtained by Cosmolight QS printing plates exposed to varied UV post-treatments: a) 2 min UVA post-treatment, b) 10 min UV post-treatment, c) 20 min UVA post-treatment, d) 2 min UVC post-treatment, e) 20 min UVC post-treatment

**Figure 70.** Changes in high coverage area on prints obtained by UV post-treated ACE Digital printing plates: a) with variation of UVA post-treatment, b) with variation of UVC post-treatment

**Figure 71.** Changes in high coverage area on prints obtained by UV post-treated Digital MAX printing plates: a) with variation of UVA post-treatment, b) with variation of UVC post-treatment

**Figure 72.** Changes in high coverage area on prints obtained by UV post-treated Cosmolight QS printing plates: a) with variation of UVA post-treatment, b) with variation of UVC post-treatment

**Figure 73.** Changes of optical density on prints obtained by UV post-treated printing plates:

a) ACE Digital, b) Digital MAX, c) Cosmolight QS

**Figure 74.** Changes of ink layer thickness on prints obtained by UV post-treated printing plates:

a) ACE Digital, b) Digital MAX, c) Cosmolight QS

**Figure 75.** Weight loss of ACE Digital photopolymeric material immersed in different solvents for varied: a) UVA post-treatment, b) UVC post-treatment

**Figure 76.** Weight loss of Digital MAX photopolymeric material immersed in different solvents for varied: a) UVA post-treatment, b) UVC post-treatment

**Figure 77.** Weight loss of Cosmolight QS photopolymeric material immersed in different solvents for varied: a) UVA post-treatment, b) UVC post-treatment

**Figure 78.** Weight loss of photopolymeric materials immersed in acetone for varied:

a) UVA post-treatment, b) UVC post-treatment

**Figure 79.** Weight loss of photopolymeric materials immersed in ethyl acetate for varied:

a) UVA post-treatment, b) UVC post-treatment

**Figure 80.** Weight loss of photopolymeric materials immersed in toluene for varied:

a) UVA post-treatment, b) UVC post-treatment

**Figure 81.** Dependence of  $\gamma^d$  and UV post-treatment durations for:

a) ACE Digital printing plate, b) Digital MAX printing plate, c) Cosmolight QS printing plate

**Figure 82.** Relation between  $R_a$  and components of  $\gamma$  for UVC post-treated Digital MAX

printing plate: a) relation between  $R_a$  and  $\gamma^d$ , b) relation between  $R_a$  and  $\gamma^p$

**Figure 83.**  $\alpha(t)$  for UV post-treated ACE Digital material for: a) C=O bond, b) OH bond

**Figure 84.**  $\alpha(t)$  for UV post-treated Digital MAX material for: a) C=O bond, b) OH bond

**Figure 85.**  $\alpha(t)$  for UV post-treated Cosmolight QS material for: a) C=O bond, b) OH bond

**Figure 86.** Dependence of  $\gamma^p$  and UV post-treatment durations for:

a) ACE Digital printing plate, b) Digital MAX printing plate, c) Cosmolight QS printing plate

**Figure 87.** Weight coefficients for the parameters influencing  $\gamma^p$  and  $\gamma^d$

of ACE Digital printing plate

**Figure 88.** Weight coefficients for the parameters influencing  $\gamma^p$  and  $\gamma^d$

of Digital MAX printing plate

**Figure 89.** Weight coefficients for the parameters influencing  $\gamma^p$  and  $\gamma^d$

of Cosmolight QS printing plate

**Figure 90.** Weight coefficient for the parameters influencing ink layer thickness

on prints obtained by: a) ACE Digital printing plate, b) Digital MAX printing plate,



c) Cosmolight QS printing plate

**Figure 91.** Error histogram for modelling of ACE Digital printing plate surface properties

**Figure 92.** Performance of neural network for estimation  
of surface properties of ACE Digital printing plate

**Figure 93.** Regression plots of neural network for estimation  
of surface properties of ACE Digital printing plate

**Figure 94.** Error histogram for modelling of Digital MAX printing plate surface properties

**Figure 95.** Performance of neural network for estimation  
of surface properties of Digital MAX printing plate

**Figure 96.** Regression plots of neural network for estimation  
of surface properties of Digital MAX printing plate

**Figure 97.** Error histogram for modelling of Cosmolight QS printing plate surface properties

**Figure 98.** Performance of neural network for estimation  
of surface properties of Cosmolight QS printing plate

**Figure 99.** Regression plots of neural network for estimation  
of surface properties of Cosmolight QS printing plate

## List of Tables

**Table 1.** Coverage values on the printing plate and size of openings on LAMS for different bump curve

**Table 2.** Variations of the post-treatments on the samples

**Table 3.** List of materials, devices and software used in the research

**Table 4.** Surface free energy ( $\gamma_{lv}$ ) and their dispersive ( $\gamma_{lv}^d$ ) and polar ( $\gamma_{lv}^p$ ) components for probe liquids

**Table 5.** Characteristics of DSC curves for UV post-treated ACE digital photopolymeric material

**Table 6.** Characteristics of DSC curves for UV post-treated Digital MAX photopolymeric material

**Table 7.** Characteristics of DSC curves for UV post-treated Cosmolight QS photopolymeric material

**Table 8.** Hansen solubility parameters for solvents used in swelling experiments

**Table 9.** Calculated  $r$  values for weight loss and  $\gamma^d$  of photopolymeric materials for the set of samples exposed to varied UVA post-treatment

**Table 10.** Calculated  $r$  values for weight loss and  $\gamma^d$  of photopolymeric materials for the set of samples exposed to varied UVC post-treatment for the set of samples with varied UVC post-treatment

**Table 11.** Calculated  $r$  values for  $\Delta cv$  and components of  $\gamma$  of photopolymeric materials for the set of samples with varied UVA post-treatment

**Table 12.** Calculated  $r$  values for  $\Delta cv$  and components of  $\gamma$  of photopolymeric materials for the set of samples with varied UVC post-treatment

**Table 13.** Calculated  $r$  values for  $D$  on prints and components of  $\gamma$  of photopolymeric materials for the set of samples exposed to varied UVA post-treatment

**Table 14.** Calculated  $r$  values for  $D$  on prints and components of  $\gamma$  of photopolymeric materials for the set of samples exposed to varied UVC post-treatment

**Table 15.** Calculated  $r$  values  $d$  and components of  $\gamma$  of photopolymeric materials for the set of samples with varied UVA post-treatment

**Table 16.** Calculated  $r$  values for  $d$  and components of  $\gamma$  of photopolymeric materials for the set of samples with varied UVC post-treatment

**Table 17.** Calculated  $r$  values for  $d$  and  $\gamma$  of photopolymeric materials for printing plates exposed to varied UVA and UVC post-treatments

**Table 18.** Weight coefficients for parameters influencing components of  $\gamma$  for ACE Digital printing plate

**Table 19.** Weight coefficients for parameters influencing components of  $\gamma$  for Digital MAX printing plate

**Table 20.** Weight coefficients for parameters influencing components of  $\gamma$  for Cosmolight QS printing plate

**Table 21.** Weight coefficients for parameters influencing  $d$  on prints obtained by ACE Digital printing plate

**Table 22.** Weight coefficients for parameters influencing  $d$  on prints obtained by Digital MAX printing plate

**Table 23.** Weight coefficients for parameters influencing  $d$  on prints obtained by Cosmolight QS printing plate

**Table 24.** Targets and outputs in neural network for ACE Digital printing plate

**Table 25.** Targets and outputs in neural network for Digital MAX printing plate

**Table 26.** Targets and outputs in neural network for Digital MAX printing plate

## List of equations

- (1) Activation of photo initiator
- (2) Initiation of crosslinking
- (3) Crosslinking propagation
- (4) Crosslinking termination
- (5) Normalized degree of swelling
- (6) Surface free energy
- (7) Least squares fitting
- (8) Quadratic adjustment in least squares fitting
- (9) Quality of quadratic adjustment
- (10) Pearson product-moment correlation coefficient
- (11) Relative oxygen ratio
- (12) Difference of sums of coverage values

## List of identifications

$\gamma_s$	surface free energy of solid
$\gamma_l$	surface free energy of liquid
$\gamma^d$	dispersive component of surface free energy
$\gamma^p$	polar component of surface free energy
$\gamma^{\text{total}}$	total surface free energy
$\gamma_{lv}$	surface free energy of probe liquid
$\gamma_{lv}^d$	dispersive surface free energy of probe liquid
$\gamma_{lv}^p$	polar surface free energy of probe liquid
$M_t$	normalized swell ratio
$\delta t$	total Hildebrand parameter
$\delta d$	dispersion component
$\delta p$	polar component
$\delta h$	hydrogen bonding component
$R_a$	arithmetic average of the roughness profile
$cv$	coverage value
$\Delta cv$	difference between sum of coverage values
$D$	optical density
$d$	thickness of printed layer
$\alpha(t)$	relative oxygen ratio
$r$	correlation coefficient
$q$	quality of adjustment

## List of abbreviations

<b>CtP</b>	Computer to Plate
<b>lpi</b>	lines per inch
<b>ppx</b>	pixels per inch
<b>SBS</b>	styrene-butadiene-styrene
<b>SIS</b>	styrene-isoprene-styrene
<b>LAMS</b>	Laser Ablation Mask Layer
<b>TIL</b>	Thermal Imaging Layer
<b>FTIR ATR</b>	Fourier transform infrared spectroscopy – attenuated total reflectance
<b>DSC</b>	differential scanning calorimetry
<b>TGA</b>	thermogravimetric analysis
<b>EDS</b>	energy-dispersive X-ray spectroscopy
<b>TG</b>	thermogravimetric (curve)
<b>DTG</b>	derivative thermogravimetric (curve)
<b>LS</b>	least squares
<b>mse</b>	mean squared error

## **APPENDIX 2**

**ACE Digital printing plate – material safety data sheet**

**Digital MAX printing plate – material safety data sheet**

**Cosmolight QS printing plate – material safety data sheet**

This safety information covers the product groups designated

**nyloflex® ACE Digital**  
**nyloflex® ACT Digital**  
**nyloflex® ART Digital**  
**nyloflex® FAB Digital**  
**nyloflex® FAC Digital**  
**nyloflex® FAH Digital**  
**nyloflex® Gold A Digital**  
**nyloflex® Seal F Digital**

## 1. Product information

<b>Manufacturer</b>	Flint Group Germany GmbH 70466 Stuttgart, Germany	<b>Solubility</b>	Molecular-dispersion-soluble in all common washout solutions for flexo plates, tetrachloro-ethylene and hydrocarbon mixtures.
<b>Supplied as</b>	Products of a specified size with a photosensitive layer.	<b>Flammability</b>	Not classified as flammable, but combustible. Dangerous decomposition products: carbon monoxide, carbon dioxide.
<b>Composition</b>	Photosensitive layer of styrene diene elastomers, polymerizable low-molecular-weight acrylates, plasticizers, photo-initiators, stabilizers and dyestuffs.	<b>pH value</b>	Photopolymer layer: neutral
<b>Density</b>	Approx. 1 (without base)		
<b>Evaporation rate</b>	not applicable		
<b>Boiling point</b>	not applicable		
<b>Thermal decomposition</b>	None when used properly. Decomposition starts at 200 °C with occurrence of organic decomposition products.		

## 2. Regulations for handling and transport

- No hazardous material as defined by transport regulations
- Declaration:  
Not subject to compulsory declaration under the German Hazardous Substances Ordinance (Gefahrstoffverordnung), since product.

## 3. Safety-relevant information

- The photopolymerizable layer contains acrylates and methacrylates. Acrylates and methacrylates may have sensitizing effects; acrylates may irritate the respiratory system. Contact of the photopolymerizable layer with the eyes should be avoided.
- The exhaust air generated in lasering must be extracted to prevent it from escaping into machine interior and working surroundings. The operating instructions for the laser must always be observed.
- The used wash-out solutions contain the constituents of the photopolymer layer in dissolved form. As far as handling the washout solution is concerned, please consult the relevant safety data sheets.



## 4. Workplace safety

- Printing plates** Do not touch the unexposed photopolymer layer!  
Wear protective gloves!  
Do not eat, drink, smoke during work. Use only in well-ventilated areas.
- Washout solution** Observe the precautionary measures usual when working with chemicals and solvents:
- **Wear protective goggles!**
  - **Wear protective gloves!**
  - **Protect your skin with cream!**
  - **Ensure adequate ventilation of the workrooms!**
  - **Also consult the safety data sheet for the particular washout solution used!**
- In case of skin contact** Clean the wetted areas of the skin with soap and water. Apply protective skin cream.
- Prophylaxis** Apply protective skin cream to skin.

Used washout solution contains the constituents of the photopolymer layer at maximally 4 % weight in dissolved form, and therefore may be subject to compulsory declaration under the German Hazardous Substances Ordinance (Gefahrstoffverordnung). The safety data sheet on the washout solution in question must be observed.

If the protective measures described above are observed, then on the basis of experience thus far and of all information available, no adverse effects on health are to be expected from working with the above-mentioned product groups.

## 5. First-aid measures

- Clothing** Remove wetted clothing.
- Skin** Wash thoroughly with soap and water.
- Accidental swallowing** If you have swallowed any, rinse your mouth out immediately and drink large amounts of water, seek medical aid.
- Eyes** Rinse thoroughly for 15 minutes under running water with eyelids held apart, then have eyes checked by an ophthalmologist.

## 6. Information on waste disposal

Entrust disposal of waste only to a company qualified for it.

The used and thoroughly exposed plates must be disposed of in accordance with the local regulations.

For disposal, the following waste codes are suggested, which apply in EU countries. In each case, however, the decision must be made in consultation with the waste disposal company.

### nyloflex® on plastic base:

- |             |                |                            |
|-------------|----------------|----------------------------|
| EAK: 120105 | Type of waste: | Pieces of plastic material |
| EAK: 200106 | Type of waste: | Other plastics             |

### nyloflex® on aluminium base:

- |             |                |           |
|-------------|----------------|-----------|
| EAK: 170402 | Type of waste: | Aluminium |
|-------------|----------------|-----------|

When disposing of the used washout solutions, observe legal regulations.



## SAFETY DATA SHEET

---

### 1 - IDENTIFICATION OF THE SUBSTANCE/PREPARATION AND OF THE COMPANY/UNDERTAKING

#### Identification of the substance or preparation:

Name: Digital MAX – Photopolymer Plate

Product code: not assigned

#### Company/undertaking identification:

MacDermid Printing Solutions

Phillip Lee Drive SW, Atlanta , GA, 30336 USA

Phone 404-696-4565

www.macdermid.com/printing

**Emergency telephone: 404-696-4565**

---

### 2 - IDENTIFICATION OF HAZARDS

#### NFPA Rating

**0 Health**                      **1 Flammability**  
**0 Reactivity**                      **Other**

(0 = Insignificant, 1 = Slight, 2 = Moderate, 3 = High and 4 = Extreme)

Chemical Name	CAS #	Weight %	OSHA PEL	ACGIH TLV
Styrenic copolymer with plasticizer	Proprietary	78-92%	NE	NE
Acrylic Esters	Proprietary	4 -14 %	NE	NE
Photoinitiator	Proprietary	1 – 4%	NE	NE
BHT	128-37-0	< 5%	NE	NE

**Physical State** Solid red tinted photopolymer plate between two polyester films (one transparent and one black, non-transparent). Mild odor.

#### Potential acute health effects

**Inhalation**                      None under normal use  
**Ingestion**                      None under normal use  
**Skin**                              None under normal use  
**Eyes**                              None under normal use

#### Potential chronic health effects

**Ingestion**                      None under normal use  
**Skin**                              None under normal use. Repeated or prolonged contact may cause skin sensitization.  
The use of rubber gloves is recommended during the handling of plates.  
**Eyes**                              None under normal use

---

### 3 - COMPOSITION/INFORMATION ON INGREDIENTS

#### **Hazardous substances present on their own:**

(present in the preparation at a sufficient concentration to give it the toxicological characteristics it would have in a 100% pure state)  
None

**Other substances representing a hazard: Not applicable**

**Substances present at a concentration below the minimum danger threshold: Not applicable**

**Other substances with occupational exposure limits: Not applicable**

---

### 4 - FIRST AID MEASURES

Contact a physician in all cases of exposure . First Responders should provide for their own safety prior to rendering assistance.

<b>Eyes</b>	None under normal use. Material is combustible. Combustion results in products of incomplete combustion.
<b>Skin</b>	None under normal use. <b>Repeated or prolonged contact may cause skin sensitization. The use of rubber gloves is recommended during the handling of plates.</b> Material is combustible. Combustion results in products of incomplete combustion.
<b>Ingestion</b>	None under normal use. Material is combustible. Combustion results in products of incomplete combustion.
<b>Inhalation</b>	None under normal use. Material is combustible. Combustion results in products of incomplete combustion.
<b>Caution</b>	None under normal use. Material is combustible. Combustion results in products of incomplete combustion. Use supplied air respirator to fight large fires

---

## 5 - FIRE-FIGHTING MEASURES

<b>Flash Point</b>	Not applicable
<b>Extinguishing Media</b>	Water, carbon dioxide, standard fire extinguishers suitable for combustible solids
<b>Unusual Fire &amp; Explosion Hazards</b>	Material is combustible. Combustion results in products of incomplete combustion. Use supplied air respirator to fight large fires

---

## 6 - ACCIDENTAL RELEASE MEASURES

**In case of Transportation Accidents, call the following 24 hour telephone number :**

<b>USA</b>	CHEMTREC (1-800-424-9300)
<b>International</b>	(To be Determined)

**SPILL CONTROL AND RECOVERY** Material is a solid. No spill control is required.

Due to more restrictive waste disposal regulations, NEVER dispose of material until you check your appropriate local, state, & federal regulations for requirements. Spills may REQUIRE notification to FEDERAL, STATE and/or LOCAL AUTHORITIES.

---

## 7 - HANDLING AND STORAGE

<b>STORAGE TEMPERATURE</b>	Ambient. Best to store below 100 °F to retain product quality.
<b>PROPER STORAGE CONDITIONS AND WARNINGS</b>	Protect from particulate contamination of the surface. Store away from sunlight.
<b>SPECIAL HANDLING DURING USE</b>	Wear heat resistant gloves when handling hot plates. Wear chemical resistant gloves when handling developed plates before drying. Safety glasses may be required when developing plates.

---

## 8 - EXPOSURE CONTROLS/PERSONAL PROTECTION

**OSHA/HCS status** OSHA HAZARD COMMUNICATION RULE, 29 CFR 1910.1200:  
Based on our evaluation, the following ingredients in this product are subject to this rule:

Not a hazardous material regulated by OSHA or HCS

<b>RESPIRATORY PROTECTION</b>	None required during normal use. Note precautions in fire fighting.
<b>VENTILATION</b>	None required during normal use.
<b>PROTECTIVE EQUIPMENT</b>	None required during normal use. Note precautions in fire fighting.

These are general recommendations to provide a safe level of protection for various material handling conditions . Consult with your Safety Professional /Industrial Hygienist for specific information regarding applications at your facility.

---

## 9 - Physical and Chemical Properties

<b>Density</b>	0.98 g / cubic centimeter	<b>Appearance/ Physical state</b>	Photopolymer plate / solid
<b>Specific Gravity</b>	N / A	<b>pH</b>	N / A
<b>Freezing Point</b>	N / A	<b>Flash Point</b>	N / A
<b>Vapor Pressure</b>	N / A	<b>Volatile %</b>	N / A
<b>Boiling Point</b>	N / A	<b>Melting Point</b>	N / A
<b>Chemical Oxygen Demand (COD)</b>	N / A	<b>Biological Oxygen Demand (BOD)</b>	N / A
<b>Solubility in water</b>	N / A	<b>Color/Odor/Odor threshold</b>	Red tint / mild odor / not established

NOTE : These physical properties are typical values for this product .

---

## 10 - STABILITY AND REACTIVITY

<b>INCOMPATIBILITY</b>	None during normal use.
<b>HAZARD DECOMPOSITION</b>	When combusted, releases products of incomplete combustion. Thermal decomposition above 400°F
<b>PRODUCTS STABILITY</b>	Stable.
<b>HAZARDOUS POLYMERIZATION</b>	None.

---

## 11 - TOXICOLOGY INFORMATION

**TOXICITY STUDIES :** Toxicity studies have not been conducted on this product . However toxicity literature surveys have been conducted on the ingredient(s) in section 2. The results are as follows:

**ACUTE ORAL TOXICITY** Material is a solid with no known toxicity.

**ACUTE DERMAL TOXICITY** Material is a solid with no known toxicity.

**ACUTE RESPIRATORY TOXICITY** Material is a solid with no known toxicity.

**HAZARD REVIEW (THR)** Material is a solid with no known toxicity.

**Listed as suspected carcinogen by :**

IARC NO

NTP NO

OSHA NO

---

## 12 - ECOLOGICAL INFORMATION

**Ecotoxicity:** None known

---

## 13 - DISPOSAL CONSIDERATIONS

Refer to Section 7: Handling and Storage and Section 8: Exposure controls / Personal Protection for additional handling information and protection of employees .

---

## 14 - TRANSPORTATION INFORMATION

**Not Regulated.**

## 15 – REGULATORY INFORMATION

The following regulations apply to this product.

### **FEDERAL REGULATIONS Not Regulated**

### **STATE REGULATIONS**

#### CALIFORNIA PROPOSITION 65

This product contains ingredient(s) listed on California Prop 65 suspected carcinogen list

#### MICHIGAN CRITICAL MATERIALS

This product does not contain ingredient(s) listed on the Michigan Critical Material Register.

### **EUROPEAN UNION Not Regulated**

---

## 16- OTHER INFORMATION

Prepared by MacDermid's Safety & Regulatory Compliance Department, based upon publicly available reference information. To the best of our knowledge the information contained herein is correct. All chemicals may present unknown health hazards and should be used with caution. Although certain hazards are described herein, we cannot guarantee that these are the only hazards which exist. Final determination of suitability of the chemical is the sole responsibility of the user. Users of any chemical should satisfy themselves that the conditions and methods of use assure that the chemical is used safely. NO REPRESENTATIONS OR WARRANTIES, EITHER EXPRESSED OR IMPLIED, OF MERCHANTABILITY, FITNESS FOR A PARTICULAR PURPOSE OR ANY OTHER NATURE ARE MADE HERE UNDER WITH RESPECT TO THE INFORMATION CONTAINED HEREIN OR THE CHEMICAL TO WHICH THE INFORMATION REFERS.



## Safety Data Sheet

### 1 PRODUCT AND COMPANY IDENTIFICATION

Product Name	Photopolymer printing plate "Cosmolight"
Product Code	QS
Supplier	TOYOBO Co., Ltd.
Address	2-8 Dojima Hama 2-chome, Kita-Ku OSAKA 530-8230 JAPAN Photo-Functional Materials Dept.
Telephone No.	+81-6-6348-3059 (9am -6pm Japan Standard Time Mon-Fri)
Fax No.	+81-6-6348-3099
Recommended use and restrictions on use	Printing Materials, Sign Plates, etc.

### 2 HAZARD IDENTIFICATION

Important Hazards	Eye contact or skin contact with the material may cause some irritation. The material contains small amount of hazardous ingredients or the ingredients of insufficient investigation of hazards. Flammable with the existence of ignition sources
Specific Hazards	Prolonged inhalation of fumes or gases generated from the material may cause headache, respiratory irritation.

#### GHS classification

##### Physical and Chemical Hazards

Explosives	Not applicable
Combustible/flammable gases	Not applicable
Combustible/flammable aerosols	Not applicable
Combustion-supporting/oxidizing gases	Not applicable
Gases under pressure	Not applicable
Flammable liquids	Not applicable
Combustible solids	Not classified
Self-reactive substances and mixtures	Classification not possible
Pyrophoric liquids	Not applicable
Pyrophoric solids	Not classified
Self-heating substances and mixtures	Classification not possible
Substances and mixtures which, in contact with water emit flammable gases	Not classified
Oxidizing liquids	Not applicable
Oxidizing solids	Not classified
Organic peroxides	Not classified
Corrosive to metals	Not classified

##### Health Hazards

Acute toxicity (Oral)	Category 5
Acute toxicity (Dermal)	Classification not possible
Acute toxicity (Gases)	Classification not possible



## Safety Data Sheet

### 2 HAZARD IDENTIFICATION (Continued.)

Acute toxicity (Vapors)	Classification not possible
Acute toxicity (Dusts)	Classification not possible
Acute toxicity (Mists)	Classification not possible
Skin corrosion/irritation	Not classified
Serious eye damage/eye irritation	Not classified
Respiratory or skin sensitization	Classification not possible
Germ cell mutagenicity	Not classified
Carcinogenicity	Classification not possible
Reproductive toxicity	Classification not possible
Specific Target Organ Toxicity (Single Exposure)	Classification not possible
Specific Target Organ Toxicity (Repeated Exposure)	Classification not possible
Aspiration hazard	Classification not possible
Environmental Hazards	
Hazards to the aquatic environment (Acute)	Classification not possible
Hazards to the aquatic environment (Chronic)	Classification not possible
GHS label elements	
Pictogram or Symbol:	Not required
Signal word:	Warning
Hazard statement:	May be harmful if swallowed. (oral)
Precautionary statement:	(Prevention)
	•Wear protective equipments.
	•Use with adequate ventilation or local exhaust system.
	•Wash hands thoroughly after handling.
	(Response)
	•Inhalation: In case of irritation, remove victim to fresh air and await recovery. Seek immediate medical attention if irritation persists.
	•Skin Contact: Wash the affected area thoroughly with water and soap. Seek medical attention if necessary.
	•Eye Contact: Immediately flush eyes with plenty of clean water for at least 15 minutes. Seek medical attention if irritation persists.
	•Ingestion: Rinse mouth with water. Seek immediate medical attention if indisposition persists.
	(Storage)
	•Keep the packages flat, and not vertical. Pay attention not to fall them down.
	•Store plates in a cool (< 25°C) and dry location. Put and store all the unexposed plates into the particular masking bag.
	(Disposal)
	•Dispose of in accordance with all applicable local and national laws/regulations.



## Safety Data Sheet

### 3 COMPOSITION / INFORMATION ON INGREDIENTS

Chemical Product	Article		
Chemical Identity	Water dispersive photo-sensitive resin		
Chemical Name	Conc.	Chemical formula	CAS No.
Synthetic rubber	48%	Trade secret	-
Liquid rubber	32%	Trade secret	-
Polyurethane-methacrylate compounds	13%	Trade secret	-
Derivative of Acrylates	5%	Trade secret	-
Photo-initiator and other additives	2%	Trade secret	-
Carbon black	< 1.0%	-	-
Toluene	< 0.1%	C6H5CH3	108-88-3

### 4 FIRST-AID MEASURES

Inhalation	In case of irritation, remove victim to fresh air and await recovery. Seek immediate medical attention if irritation persists.
Skin Contact	Wash the affected area thoroughly with water and soap. Seek medical attention if necessary.
Eye Contact	Immediately flush eyes with plenty of clean water for at least 15 minutes. Seek medical attention if irritation persists.
Ingestion	Rinse mouth with water. Seek immediate medical attention if indisposition persists.

### 5 FIRE-FIGHTING MEASURES

Extinguishing Media	Water Spray, Carbon Dioxide, Dry Chemical Powder
Specific Hazards	When burning, this product may emit harmful gas as carbon monoxide, nitrogen oxides, etc.
Specific Methods	Extinguish the fire from windward by water or carbon dioxide.
Protection of Firefighters	In case of a big fire, wear self-contained breathing apparatus and protective clothing.

### 6 ACCIDENTAL RELEASE MEASURES

Personal Precautions	If the material contacts the body, wash the affected area thoroughly with water and soap. Wash-out solution remained on the skin may cause some irritation.
Environmental Precautions	The unexposed plate is dispersive in water, that may pollute environment.
Methods for Cleaning up	Carefully pick up and collect the dropped plates. Wipe the area with a cloth containing soapy water to remove any adherent material. Remove all the spilt wash-out solution with absorbent.





## Safety Data Sheet

### 7 HANDLING AND STORAGE

#### HANDLING

Technical Measures	Wash hands thoroughly after handling. Pay attention not to contact skin and eyes with the plate material. Wear protective equipments.
Precautions	Use with adequate ventilation or local exhaust system. Do not inhale fumes and gases. Do not contact skin and eyes with the wash-out solution.
Safe Handling Advice	Handle with care not to get hurt to hands with outer case or edge of the plate.

#### STORAGE

Technical Measures	Keep the packages flat, and not vertical. Pay attention not to fall them down.
Incompatible Products	Strong oxidizing materials Keep away from alkali and toluene in which the material is soluble.
Storage Conditions	Store plates in a cool (< 25°C) and dry location, away from sources of intense heat and ignition. Put and store all the unexposed plates into the particular masking bag.
Packaging Materials	Masking bag or corrugated board package

### 8 EXPOSURE CONTROLS / PERSONAL PROTECTION

#### ENGINEERING

Use with adequate ventilation or local exhaust system. Ensure eyewash/safety shower stations are available near areas where the material is used.

#### MEASURES

#### Control Parameters: Toluene

ACGIH TLV-TWA	50ppm (skin)
OSHA PEL-TWA	200ppm
NIOSH PEL-TWA	100ppm
MSHA TWA	100ppm (skin)

#### PERSONAL PROTECTIVE EQUIPMENT

Respiratory Protection	Suitable gas mask
Hand Protection	Impervious rubber or plastic gloves
Eye Protection	Safety glasses, goggles or face shield
Skin and Body Protection	Impervious clothing

### 9 PHYSICAL AND CHEMICAL PROPERTIES

Physical State	Yellowish transparent solid sheet
Odor	Slightly sweet odor
pH	Not available
Melting Point	Not available
Flash Point	Not available
Explosion Properties	None
Relative density	1.0
Solubility	Soluble in alkali and toluene
Autoignition point	Not available
Decomposition point	Not available



## Safety Data Sheet

### 10 STABILITY AND REACTIVITY

Stability	Stable at ambient temperature
Possible Hazardous Reactions	Flammable with the existence of ignition sources
Conditions to Avoid	High temperature, ignition sources, direct sun-light
Material to Avoid	Strong oxidizers
Hazardous Decomposition Products	When burning, this product may emit harmful gas as carbon monoxide, nitrogen oxides, etc.

### 11 TOXICOLOGICAL INFORMATION

Acute toxicity (Oral)	Oral-Rat LDLo: > 2,000mg/kg
Skin corrosion/irritation	No irritation potential to the rabbit skin
Serious eye damage /eye irritation	No irritation potential to the eyes of rabbits
Mutagenicity	No mutagenicity under the Ames test

### 12 ECOLOGICAL INFORMATION

Mobility	Unexposed plate and washed-out solution are dispersive in water, and are possible to diffuse in watercourse.
----------	--

### 13 DISPOSAL CONSIDERATIONS

Waste from Residues	Dispose of in accordance with all applicable local and national laws/regulations.
Contaminated Packaging	Dispose of as well as the material.

### 14 TRANSPORT INFORMATION

International Regulations	
UN Classification Number	Not classified
Specific Precautionary	Keep it dry and handle with care.

### 15 REGULATORY INFORMATION

Follow all the laws and regulations in your country.

### 16 OTHER INFORMATION

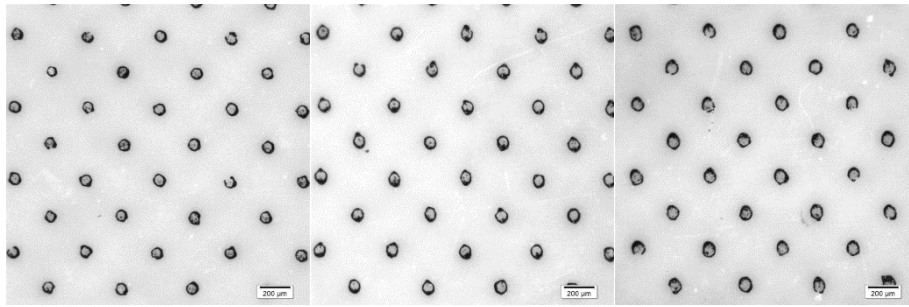
Notice	The information in this SDS, to the best of our knowledge, is accurate and correct. However, TOYOBO makes no warranty and assumes no liability whatsoever in connection with any use of this information. The SDS is subject to revision as new information becomes available.
--------	--

# APPENDIX 3

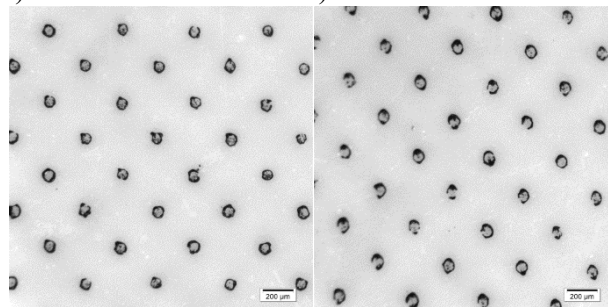
*(Chapter 4.3.2.)*

**Printed elements in highlight area**

**(1% and 10% nominal coverage value)**



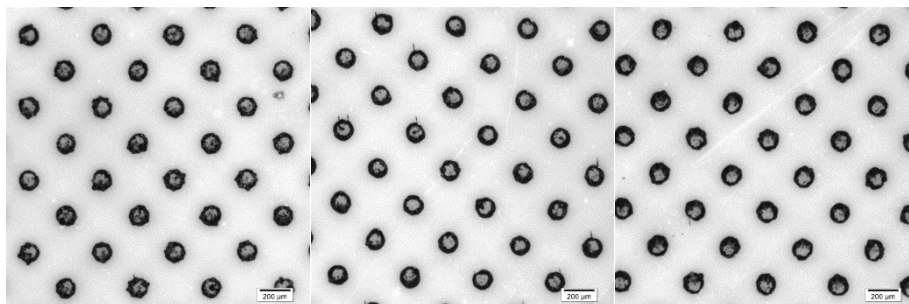
a) b) c)



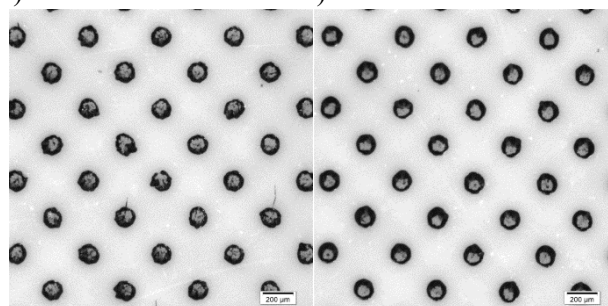
d) e)

Printed elements of 1% nominal coverage value obtained by ACE Digital printing plate at 50x magnification:

a) 2 min UVA, b) 2 min UVC, c) 10 min UVA, d) 20 min UVA, e) 20 min UVC



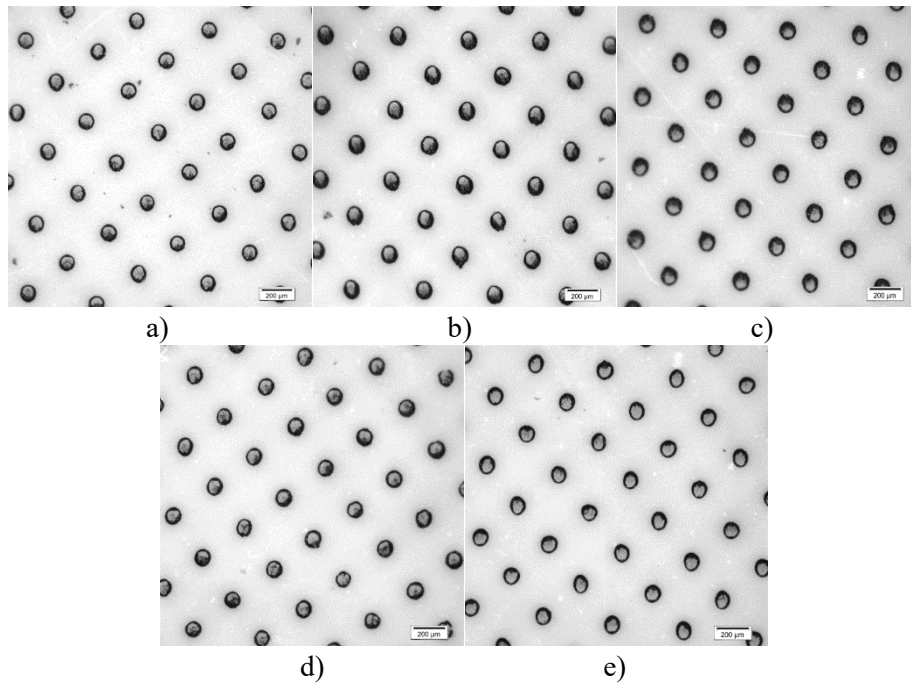
a) b) c)



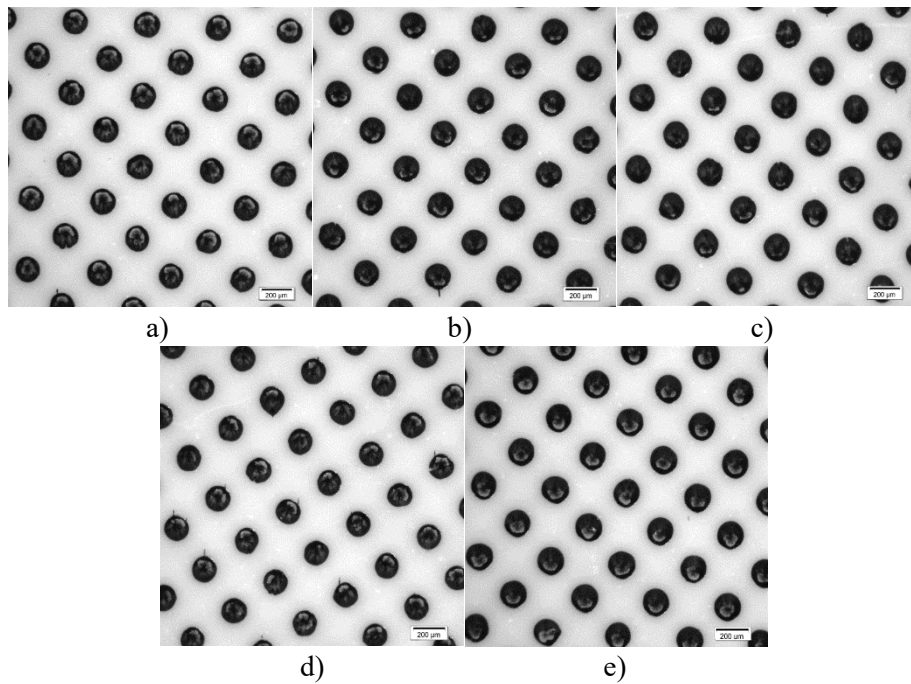
d) e)

Printed elements of 10% nominal coverage value obtained by ACE Digital printing plate at 50x magnification:

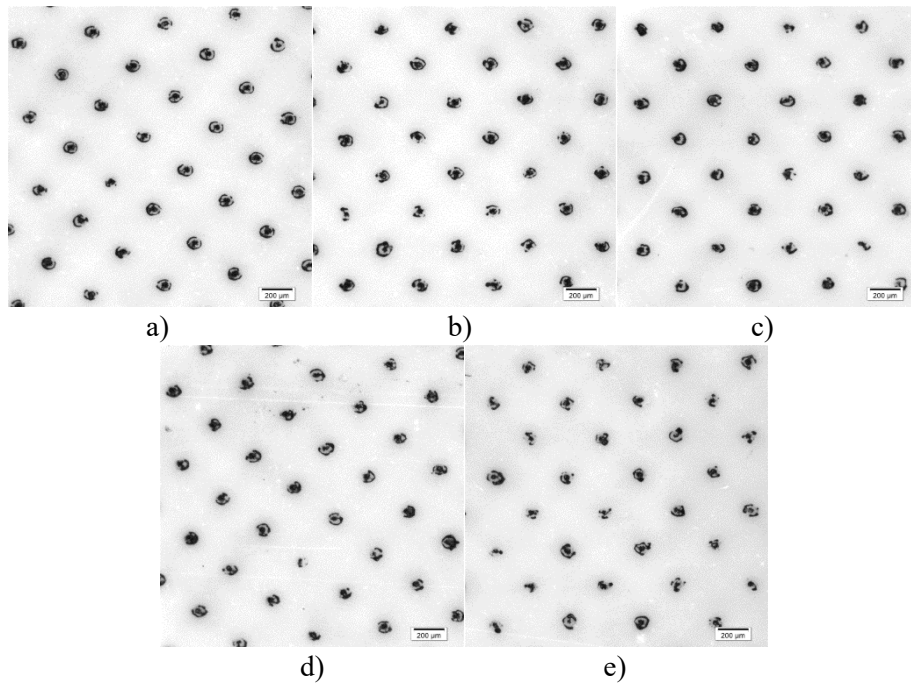
a) 2 min UVA, b) 2 min UVC, c) 10 min UVA, d) 20 min UVA, e) 20 min UVC



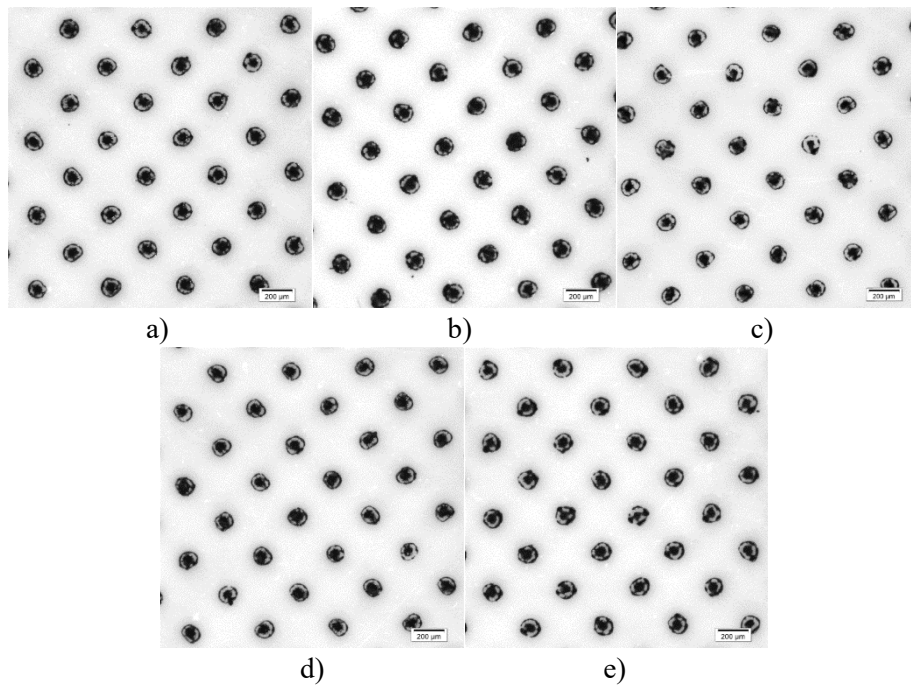
Printed elements of 1% nominal coverage value obtained by Digital MAX printing plate at 50x magnification:  
 a) 2 min UVA, b) 2 min UVC, c) 10 min UVA, d) 20 min UVA, e) 20 min UVC



Printed elements of 10% nominal coverage value obtained by Digital MAX printing plate at 50x magnification:  
 a) 2 min UVA, b) 2 min UVC, c) 10 min UVA, d) 20 min UVA, e) 20 min UVC



Printed elements of 1% nominal coverage value obtained by Cosmolight QS printing plate at 50x magnification:  
 a) 2 min UVA, b) 2 min UVC, c) 10 min UVA, d) 20 min UVA, e) 20 min UVC



Printed elements of 10% nominal coverage value obtained by Cosmolight QS printing plate at 50x magnification:  
 a) 2 min UVA, b) 2 min UVC, c) 10 min UVA, d) 20 min UVA, e) 20 min UVC

# APPENDIX 4

**Modification of surface properties of photopolymer printing plate  
by UV-ozone treatment**

## **Abstract**

In the fast-paced technology development in graphic industry, modern flexography has found its domain mostly in the packaging and functional printing. Due to the new qualitative requirements, workflows and materials used in flexography had to be updated and improved. The application of digitally controlled processes and procedures has taken the place of the analogue production, together with the new methods of material processing and improvements of the materials themselves.

This report focuses on the functional modification of photopolymer flexographic printing plate's properties with the aim of achieving optimal output quality. During the transfer of the printing ink from the anilox to the printing plate and then to the printing substrate, surface properties of the printing plate highly influence the quality of the print. Therefore, surface properties of the printing plate should be compatible with the used printing ink and the printing substrate, which is especially important when using new formulations of functional inks and experimenting with different printing substrates and applications.

In this research, several types of photopolymer flexographic printing plates with differences in composition and processing technology were exposed to the UV-ozone treatment in order to modify the surface properties of the photopolymer material. Preliminary experiment was performed in order to adjust the duration of the UV-ozone treatment to the period where no visible damage would appear on the surface of the printing plates. Results have displayed the significant changes in surface free energy of the photopolymer material when the printing plates were exposed to the UV-ozone for periods up to 5 minutes. However, depending on the main composition of the printing plate, trends of the changes differed. Fourier-transform infrared spectroscopy – attenuated total reflectance (FTIR-ATR) and white light interferometry implied that the changes in surface free energy were caused primarily by changes in chemical composition, with no considerable influence of the changes in roughness parameters of the printing plate. In order to analyse the quality of the prints produced with UV-ozoned flexographic printing plates, test prints were produced with UV-ozoned MacDermid LUX ITP 60 printing plate. Prints produced with printing plates with longer UV-ozone treatment have displayed the decreased optical density of the printed ink layer, as well as the qualitative changes in the reproduction of fine printed elements.

Performed research proved that the functional modification of flexographic printing plates with the aim of improving the print quality is possible. UV-ozone treatment is a procedure where the printing plate is exposed to significantly higher energy than with conventional UVA and UVC tubes. Therefore, the duration of the UV-ozone treatment must be precisely adjusted in order to maximize the quality of the print, while at the same time maintaining printing plate's functionality.

**Keywords:** flexography, printing plate, photopolymer, UV-ozone, surface free energy.



## 1. Background

Flexography is a printing technique mostly used in packaging and functional printing. Flexographic printing plates are made of photopolymer materials, formulated to meet mechanical and qualitative requirements in the graphic reproduction process. In the significant part of its domain, flexography is competing with gravure printing. In past few years, there have been some gains in share over gravure printing because of the greater flexibility of the prepress in the flexography, as well as for the jobs with shorter run lengths, frequent design changes and special functional applications [1].

Many parameters influence the quality of the final product in flexography: photopolymer material used for the printing plate production [2], quality of the file adjustment, type of the anilox roller, type of the tape placed under the printing plate to adjust the elastic deformation of the printing plate, properties of the printing ink and printing substrate, control of the printing process, and a set of parameters associated with the printing plate production [3].

Flexographic printing process has achieved significant improvements in the quality of the printed product. The automation of the printing process ensured better control over the output. Printing ink and anilox technology improved in quality as well, but the main improvements have been made in the area of printing plates and imaging methods [1, 4].

New formulations of photopolymer materials (Fig.1.) enabled production of smaller dots on the printing plates, in some cases even being able to eliminate the bump curve. This resulted with the higher quality of the prints in the highlight area and expanded gamut. Photopolymer materials used nowadays have the increased resistivity to solvents and ozone, and are compatible with solvent-based, water-based and UV-curable inks. Furthermore, new technologies in the flexographic printing plate processing workflow enabled the production of “flat-top” dots [4]. However, the debate about superiority of this shape of printing element over the conventional, “bullet-shaped” dots, exists.



*Fig.1. MacDermid LUX ITP 5% dots at 150 lpi*

(source: <http://www.paperandprint.com/flexotech/features/flexo-2014/june-2014/04-06-14-hi-tech-plates.aspx#.VUtBHfVhBc>)

Furthermore, new formulations of photopolymer materials used in flexographic printing plate production enabled increased ecological sustainability in the processing. Water-washable printing plates eliminated the use of the volatile organic solvents from the printing plate production process [5,

6, 7]. Mechanical (chemistry-free) process of engraving the polymer material in the printing plate production was re-introduced to flexography as well.

In the graphic reproduction process, the transfer of the printing ink from the anilox to the printing plate and finally to the printing substrate depends on the surface properties of the used materials. Since the printing plate is in the middle of the ink transfer chain, its surface free energy ( $\gamma$ ) must be adequate to achieve the optimal transfer of the printing ink from the anilox to the printing substrate [8, 9].

Improvements of the flexographic printing plate's surface properties in the past several years have been made, as well. Patterned textures have been applied to the surface of the printing elements on the printing plate in the plate making process [10, 11]. Surface of the printing plate roughened in this way enables better adsorption of the printing ink to the printing plate, and better transfer of the ink to the printing substrate, reducing the fingering. However, flexographic printing plate manufacturers have several approaches to the cause-effect relation of the surface properties of the printing plate and the quality of the print. An illustrated example of the effect of the  $\gamma$  on the adsorption of the printing ink can be seen in Fig. 2.

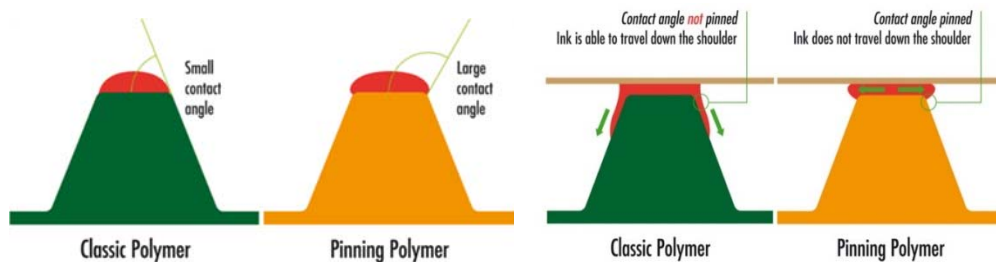
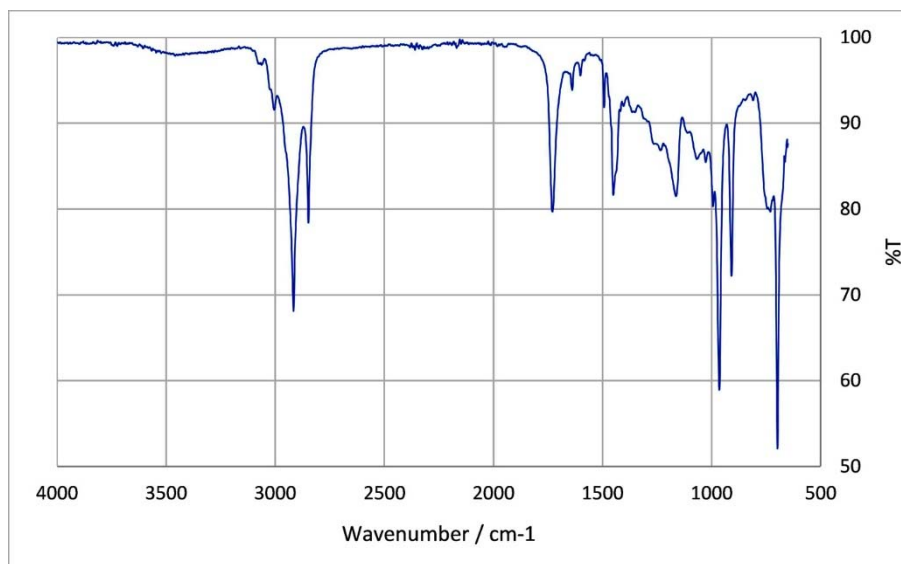


Fig.2. Asahi's Pinning TOP technology

(source: <http://www.duomedia.com/news/7385/>)

Furthermore,  $\gamma$  of the printing plate can be modified in the standard printing plate production workflow if needed, during the post-treatment process [12]. Previous research [12, 13] has indicated that UVA and UVC post-treatments influence printing plate's physico-chemical surface characteristics by changing the components of  $\gamma$  of the photopolymer material. This could result with either improved or negative influence on the transfer of the printing ink from the anilox to the printing plate and from the plate to the printing substrate.

EDS analysis showed that the changes in contact angles of probe liquids and  $\gamma$  are caused by the increase of oxygen concentration in the surface layer of the printing plate, while FTIR-ATR (Fig.3.) analysis pointed specifically to the increased ratio of carbonyl and hydroxyl bonds [13]. Therefore, duration and intensity of the post-treatment process must be strictly adjusted and regularly monitored.



*Fig.3. FTIR-ATR spectra of photopolymer printing plate sample*

Apart from  $\gamma$ , UVA and UVC post-treatment can modify hardness [14] and roughness of the photopolymer material, as well.

Modifications of the printing plate's properties during the UV post-treatment depend on the type of the photopolymer material and should be performed in the printing plate production workflow in accordance with the type of the used printing ink and printing substrate.

Since standards in flexography are mainly focused on the process control concerning screen ruling and parameters connected to process colours, printing substrates and dot gain [15], further analysis and experiments are yet to be performed when considering the influences of the printing plate quality on the graphic reproduction process.

The aim of this research is to determine the influence of the printing plate's surface modification, precisely, the influence of UV-ozone treatment, on the surface properties of the printing plate and the quality of the prints.

## **2. Experimental settings**

### **2.1. Materials and methods**

In this research, five types of the CtP flexographic printing plates with thickness of 1.14 mm, from four different manufacturers were used: Toyobo Cosmolight QS, Flint ACE Digital, DuPont DPR, MacDermid DMAX and MacDermid LUX ITP 60. Printing plates used in this research were produced in the standard conditions suggested by the printing plate manufacturer. The aim was to determine the effect of the UV-ozone on the surface properties of different photopolymer materials, as well as their

resistivity to the treatment and the overall quality of the photopolymer materials' performance during the formation of the printing elements on the printing plate.

Therefore, two sets of samples for each type of printing plate were made:

- fields with 100% surface coverage;
- samples with applied control elements which consisted of different fine elements, control elements and strips, as well as control wedges with halftones (from 1% - 100% coverage value) (Fig.4.).

Motives were transferred on all printing plate samples with the application of the same compensation curve – FlexoSync 56. PET was used as a printing substrate.

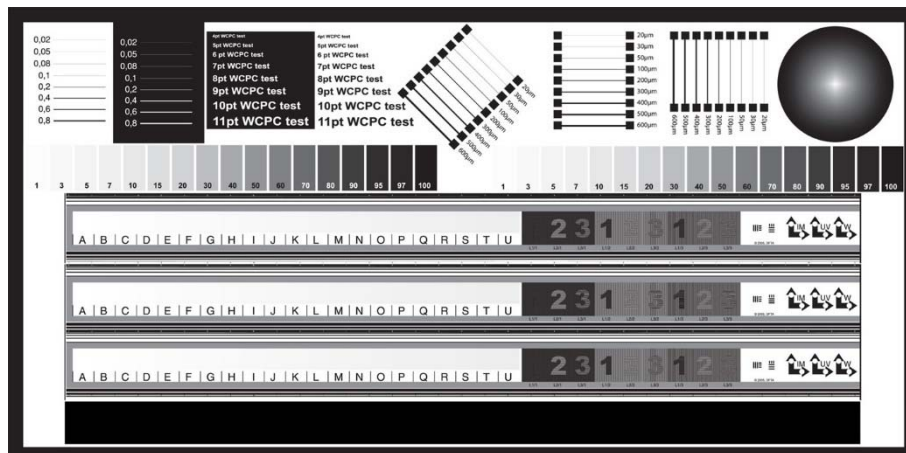


*Fig.4. Set of control elements on tested printing plates*

In order to adjust the duration of the UV-ozone treatment, preliminary test was performed on ASAHI AFP TSP printing plate. UV-ozone treatment was performed in NOVA SCAN PSD Pro Series Digital UV Ozone System. UV lamps in NOVA SCAN PSD generate UV light at wavelengths of 185 nm and 254 nm. NOVA SCAN PSD produces O<sub>3</sub> and provides molecular excitation [16]. After determining the duration of the treatment with first visible damage on the printing plate (5 minutes), samples used in this research were exposed to the treatment, as well.

All samples of printing plates were treated by UV-ozone up to 5 minutes (0.5, 1, 1.5, 2, 3 and 5 minutes). Several methods were used to analyse the changes of the sample surfaces:

1. Visual analysis of samples was performed by means of the white light interferometry on WYKO NT - 2000 White Light Interferometer, which was also used to calculate the roughness parameters of the printing plate surface. WYKO NT- 2000 is used to profile objects (structures) by using interferometry. The profiles and surfaces of the structures can be measured without contacting the sample, which can greatly minimize the chance of destroying the fragile structures. Software support for WYKO NT – 2000 was used to calculate the width of printed fine lines, surface coverage and ink layer thickness and volume on the prints [17].

2. AniCAM 3D microscope was used to obtain the 3D images of printing elements of different sizes and cross-section of printing elements in order to assess the formation of the printing elements on each plate type (Fig. 5.). The AniCAM 3D Scanning Microscope is the capturing device for measuring flexographic printing plates, anilox rollers and gravure printing cylinders. The internal high-tech motors can be stepped in fractions of a micron. The 3D images are generated from a number of photos taken at a different focus depths. The software combines the sharp parts of each image and creates the 3D representation of the substrate. The depth, opening, volume, dot shape and profile of the observed element can be analysed [18].



*Fig.5. AniCAM 3D microscope*

(source: <http://www.providentgrp.com/troika/>)



*Fig.6. IGT F1 unit*

(source: <http://www.idd.tu-darmstadt.de/>)

3. On the printing plate samples, contact angles of different probe liquids were measured by means of Fibro DAT 1100 Dynamic Contact Angle Measuring System. Contact angles of the probe liquids are the parameters which are then used to calculate the surface energy of the solid samples. Three probe liquids of known surface energy were used for the measurements: water, glycerol and diiodomethane. Contact angle was measured using sessile drop method, five times on each sample, on the different parts of the printing plate. The shape of the probe liquid drops was a spherical cap, and the volume of the drops was 4  $\mu\text{l}$ . All measurements of the contact angles on the samples were performed in the same moment after the drop touched the photopolymer surface, and the average value was calculated [19, 20]. After that, mean value of the contact angle for each sample was calculated and  $\gamma$  of printing plates was obtained using the OWRK method, by means of the OCA20 software support. OWRK (Owens-Wendt-Rabel and Kaelble) method is applicable for polymer, aluminium and coatings characterization [20, 21].

4. FTIR-ATR analysis was performed by means of Perkin Elmer Spectrum One system in order to identify the chemical changes in the surface of the UV-ozoned samples. Attenuated Total Reflectance (ATR) is today the most widely used FTIR-ATR sampling tool. ATR generally allows qualitative or quantitative analysis of samples with little or no sample preparation [22].

5. IGT F1 unit (Fig.6.) and Cooper Sheet Fed Flexo Press were used to produce the test prints with UV-ozoned samples of MacDermid LUX ITP 60 printing plate. IGT F1 is a device for testing different types of aniloxes/printing plates/printing inks/printing substrates. It can simulate the speed

and the pressure of the printing machines, on laboratory scale. Cooper Sheet Fed Flexo Press is a single colour printing machine for flexography, where the flexographic printing system can be tested throughout the complete printing process with all adjustments in the steps.

6. Gretag Spectrolino Reflective Spectrophotometer was used to measure the optical density of the ink on test prints. Gretag Spectrolino is a colour measurement instrument which can operate in reflection and transmission mode. Colour and paper samples, as well as transparencies, colour charts and monitors can be measured [23].

## 2.2. Preliminary test

The aim of this research was to perform the functional modification of printing plate's surface properties. This means that the the duration of the UV-ozone treatment had to be adjusted in a way that it does not damage the surface of the photopolymer material. Since previous research [13] showed that the regular UV post-treatment has a significant influence on the surface properties of the printing plate, initial duration of the UV-ozone treatment was set up to 10 minutes. For the purpose of the preliminary experiment, ASAHI AFP TSP with pinning top technology was used because of its relatively low initial calculated  $\gamma$  ( $31.45 \text{ mNm}^{-1}$ ). Images of printing plate's surface after different exposures to UV-ozone, obtained by white light interferometry, are presented in Fig.7.

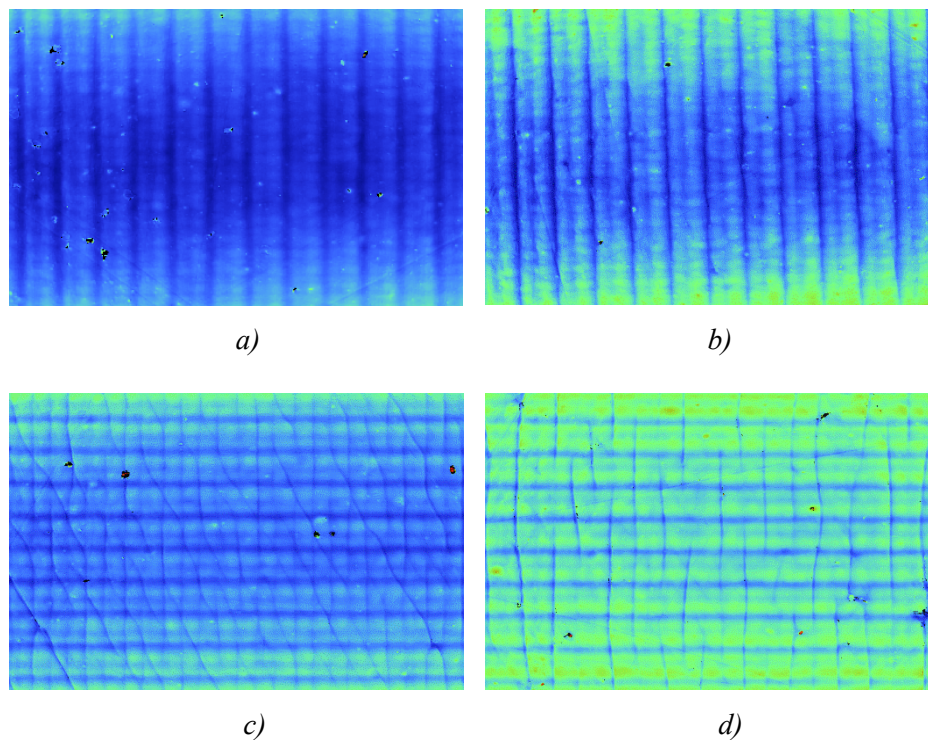


*Fig.7. Surface of ASAHI AFP TSP printing plate exposed to UV-ozone for  
a) 0.5 min, b) 3 min, c) 5 min, d) 10 min*



One can see that the visible signs of the damage on the surface appear after 5 minutes of UV-ozone treatment. Since ozone has the destructive influence on the photopolymer material, the degradation of the surface starts to take the effect. It was therefore decided that the samples tested in this research will be exposed to the UV-ozone treatment for periods up to 5 minutes.

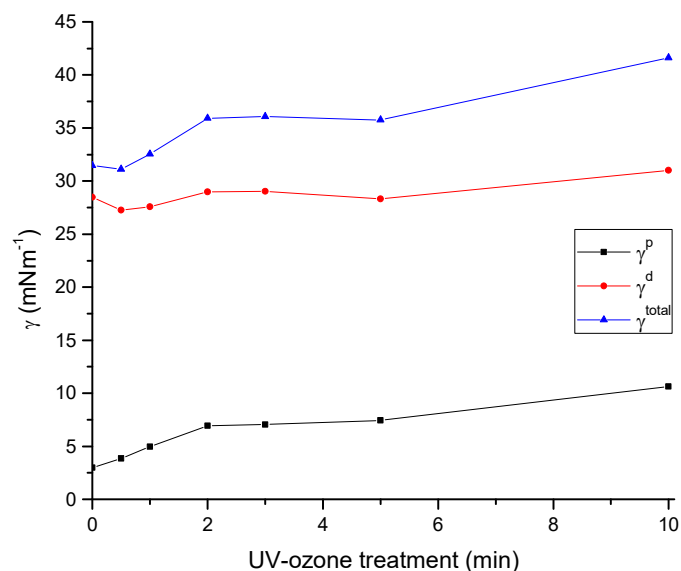


Fig. 8.  $\gamma$  of the UV-ozoned Asahi ASAHI AFP TSP printing plates

Results of  $\gamma$  calculation are displayed in Fig. 8. The overall surface free energy ( $\gamma^{total}$ ) increases from 31.45 mNm<sup>-1</sup> before the UV-ozone treatment to 41.63 mNm<sup>-1</sup> after 10 minutes of the treatment. However, it is interesting to discuss the increase of the polar component ( $\gamma^p$ ) and dispersive component ( $\gamma^d$ ) of the surface free energy.  $\gamma^d$ , which is primarily the result of the intermolecular forces in the material (van der Waals forces) and the increase of the roughness, increases from 28.48 mNm<sup>-1</sup> before the UV-ozone treatment to 31 mNm<sup>-1</sup> after 10 minutes of the treatment. Since the increase of the dispersive forces in polymers can be caused by increase of the degree of crosslinking, as well as the increase of the adhesion forces due to the higher roughness [24, 25], this suggests that further crosslinking in the material, even after the printing plate was processed in standard conditions, can still occur. White light measurements didn't show the significant changes in the roughness of the samples. These results were not considered because of the changes in surface topography due to the damage.

$\gamma^p$  for the treated samples increases from 2.98 mNm<sup>-1</sup> to 10.63 mNm<sup>-1</sup>. This corresponds to the previous research results and the effect of the UV treatments on the flexographic printing plate, where the oxygen integrates in the plate's surface [26]. The ratio of the oxygen in the surface of the photopolymer material increases with the intensity of the UV treatment, which is significantly higher than the intensity of the regular UV exposures. Therefore, the UV-ozone has the higher impact on  $\gamma^p$  than the regular UVA and UVC post treatments.

In order to test the permanence of the changes in the printing plate's surface, UV-ozoned samples were stored away from the light for two weeks. After that, contact angles of the defined probe liquids were measured, and  $\gamma$  and its components were calculated again. The results didn't deviate from the previous. Therefore, one can conclude that the UV-ozone treatment has a permanent effect on printing plate's  $\gamma$ , the same as the regular UV post-treatments applied in the printing plate processing.

### 3. Results and discussion

#### 3.1. Influence of the UV-ozone on the surface of printing plates

##### 3.1.1. White light interferometry of UV-ozoned photopolymer surfaces

Results of the surface scanning by means of the white light interferometry are presented in Fig.9. – Fig.13. No physical damage is visible on the surfaces of printing plates. Slight differences in surface topography between samples not exposed to UV-ozone and those exposed to the UV-ozone can be noticed in Fig.10.

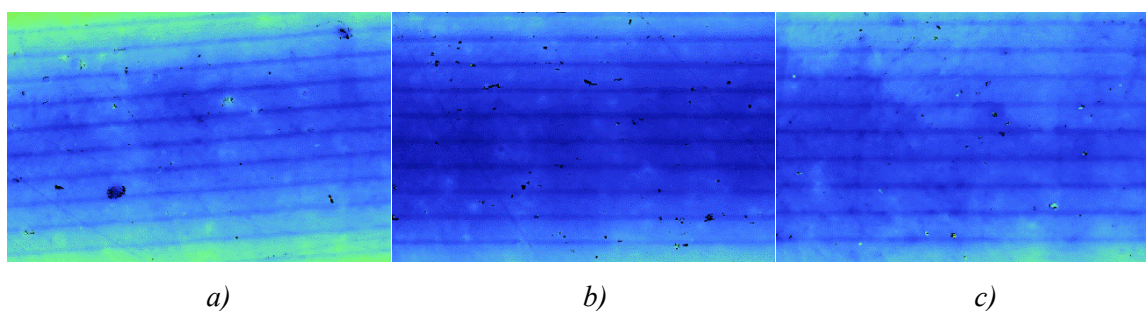


*Fig.9. Surfaces of the UV-ozoned DuPont DPR printing plates exposed for:*

*a) 0 minutes, b) 2 minutes, c) 5 minutes*

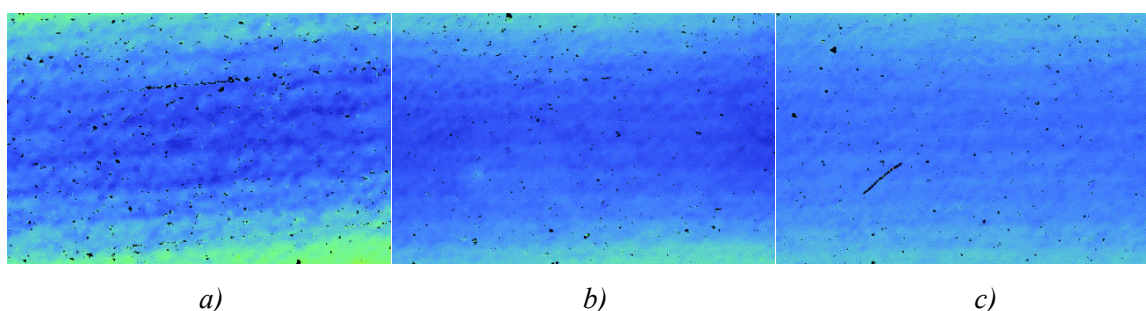


*Fig.10. Surfaces of the UV-ozoned FLINT ACE Digital printing plates exposed for:*

*a) 0 minutes, b) 2 minutes, c) 5 minutes*



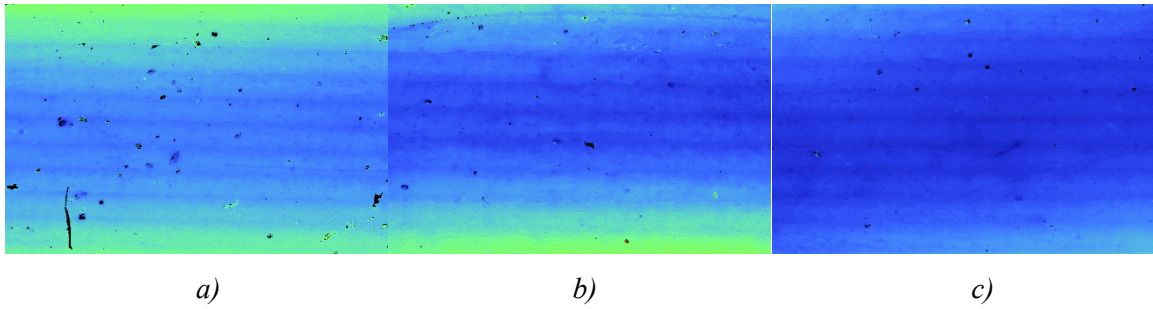


Fig.11. Surfaces of the UV-ozoned MacDermid DMAX printing plates exposed for:  
a) 0 minutes, b) 2 minutes, c) 5 minutes

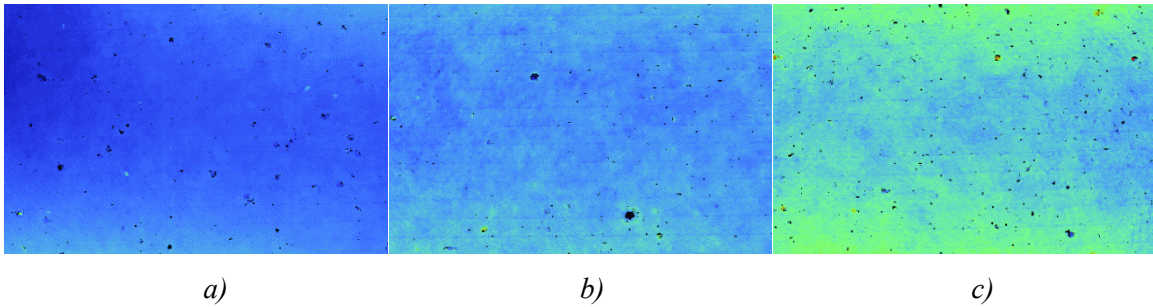


Fig.12. Surfaces of the UV-ozoned Toyobo Cosmolight printing plates exposed for:  
a) 0 minutes, b) 2 minutes, c) 5 minutes

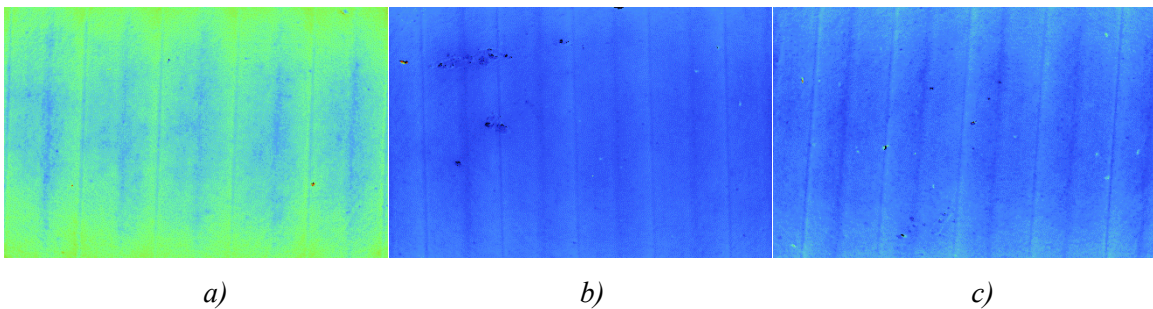


Fig.13. Surfaces of the UV-ozoned MacDermid LUX ITP 60 printing plates exposed for:  
a) 0 minutes, b) 2 minutes, c) 5 minutes

### 3.1.2. Surface free energy of the UV-ozoned photopolymer surfaces

Results of the  $\gamma$  calculations are presented in Fig.14.

The differences in initial  $\gamma$  of the samples are expressed between LUX ITP 60 plate ( $43.37 \text{ mNm}^{-1}$ ) and the other samples (range between  $29 \text{ mNm}^{-1}$  and  $32 \text{ mNm}^{-1}$ , except for the DMAX plate with the initial  $\gamma$  of  $37.11 \text{ mNm}^{-1}$ ).

While all printing plate samples show the increased  $\gamma^{\text{total}}$  with prolonged UV-ozone treatment,  $\gamma^{\text{p}}$  and  $\gamma^{\text{d}}$  display different trends for different samples. DPR sample displayed highest resistivity to the UV-ozone treatment. In Table 1. one can see the differences between  $\gamma^{\text{p}}$  and  $\gamma^{\text{d}}$  for the samples that were not UV-ozoned and the samples exposed to 5 minutes of the treatment.

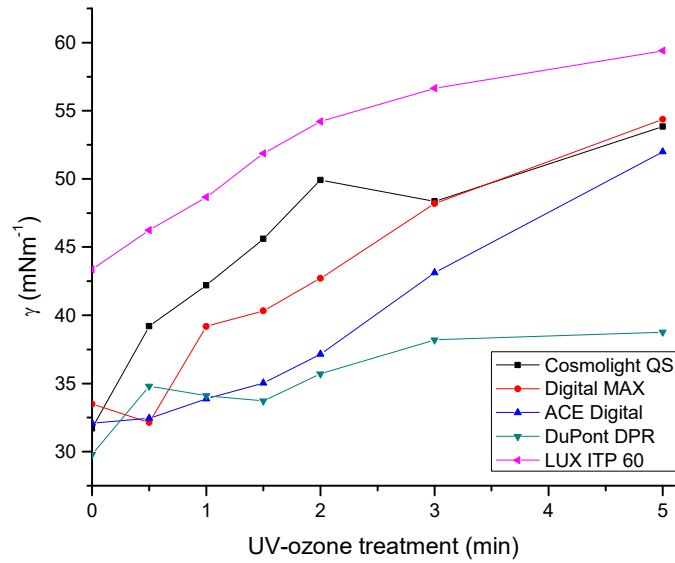


Fig.14.  $\gamma^{\text{total}}$  of UV-ozoned printing plate samples

Table 1. Changes in  $\gamma^{\text{p}}$  and  $\gamma^{\text{d}}$  of UV-ozoned printing plate samples

Sample	Initial $\gamma^{\text{p}}$	$\gamma^{\text{p}}$ after 5 minutes of UV-ozone treatment	Initial $\gamma^{\text{d}}$	$\gamma^{\text{d}}$ after 5 minutes of UV-ozone treatment
<b>Cosmolight QS</b>	5.78 ↗	32.74	25.93 ↘	21.10
<b>DMAX</b>	2.72 ↗	18.13	36.35	36.25
<b>ACE Digital</b>	0.12 ↗	18.07	31.77 ↗	33.91
<b>DPR</b>	0.57 ↗	8.76	29.22	30.01
<b>LUX ITP 60</b>	6.55 ↗	23.13	36.32	36.26

It is visible that  $\gamma^{\text{p}}$  primarily influences the increase of the overall values for all samples. The reason for this is the integration of the oxygen in the surface layer of the photopolymer material during the UV-ozone treatment, common to the UV treatments in the printing plate processing. DPR sample has therefore showed the highest resistivity to the treatment.

Furthermore, it is worth to mention that the ACE sample displayed the decrease of the  $\gamma^{\text{p}}$  up to 1 minute of the UV-ozone treatment, after which  $\gamma^{\text{p}}$  started to increase. Some printing plates (especially if composed of styrene-isoprene-styrene copolymer, as ACE) have the ozone-protection waxes added to their composition [27]. When exposed to increased temperature and the ozone, the waxes migrate to the surface of the photopolymer material, forming the “protection layer”. Since the waxes are composed of non-polar hydrocarbon chains, the increase of  $\gamma^{\text{d}}$ , as well as decrease of  $\gamma^{\text{p}}$ , occurs.

However, after 1 minute of the UV-ozone treatment,  $\gamma^{\text{d}}$  on ACE sample decreased for cca. 5 mNm<sup>-1</sup>, and after that both  $\gamma^{\text{p}}$  and  $\gamma^{\text{d}}$  started to increase. This indicates that the ozone-protection works when

the plate is exposed to lower intensity of the UV radiation, such as regular UVC tubes used in the post treatment of the flexographic plates.

UV-ozone treatment did not result with the significant changes in  $\gamma^d$ , except for the Cosmolight QS and ACE Digital samples. The decrease in  $\gamma^d$  on Cosmolight QS samples points to the weaker intermolecular bonds with the prolonged UV-ozone treatment and the start of the material degradation despite the absent of visible damage of the surface. This was apparent during the handling of the samples after UV-ozone treatment, when the photopolymer material cracked easily when exposed to mechanical straining. Cosmolight QS is a polyurethane-based water-washable printing plate, while other types of tested plates are made of styrene-diene based materials. Other samples displayed the slight increase of  $\gamma^d$  with shorter exposures to UV-ozone treatment. However, after periods of 3 and 5 minutes of the exposure,  $\gamma^d$  started to decrease back to the initial values before the UV-ozone treatment. The increase of  $\gamma^d$  can be the result of the further crosslinking in the photopolymer material, and the following decrease can be the consequence of the termination of the crosslinking process, breakage of the chains and start of the material degradation [28, 29].

ACE sample showed the overall increase of the  $\gamma^d$ , which could, due to its styrene-isoprene-styrene-based composition, be the result of the activation of ozone-protection layer and/or further crosslinking due to the treatment.

### 3.1.3. Roughness of the UV-ozoned photopolymer surfaces

Since the changes in surface roughness could influence  $\gamma^d$  due to the changes in adhesion forces,  $R_a$  parameters were measured by means of the white light interferometry for all samples. They are presented in Fig.15.  $\Delta R_a$  presents the difference in roughness parameter  $R_a$  between each UV-ozoned sample and initial, non UV-ozoned sample.

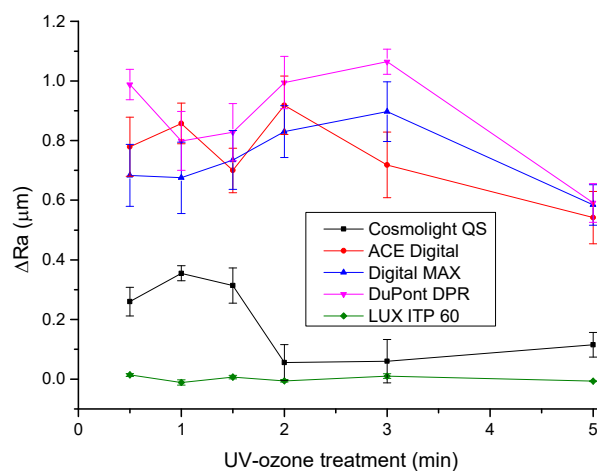


Fig.15. Changes in  $R_a$  parameter of UV-ozoned printing plate samples

The results of  $\gamma$  calculations displayed no considerable changes in  $\gamma^d$  (Table 1.), which indicates that the changes of the roughness on this level (highest  $R_a$  of 1.18  $\mu\text{m}$  was measured on DPR sample) do not have a distinct impact on the printing plate's surface properties. Furthermore, surface of the flexographic printing plate is not entirely uniform, with some defects present, as well as the "pattern" imprinted into plate's surface in the production process (visible in Fig.9 – Fig.13). Because of these reasons, the results of the surface roughness measurement could not be correctly fitted and presented with a trendline.

In Fig.15. one can see that the LUX ITP 60 sample displays the lowest deviation from the initial  $R_a$  when exposed to the UV-ozone treatment. ACE Digital, DMAX and DPR samples show higher deviations in  $R_a$  compared to other samples – for ACE Digital the changes in roughness are even visible on the images obtained by white light interferometry (Fig.10). Generally, one can notice that the surface roughness of the samples increases when they are exposed to the UV-ozone treatment. However, if roughness is to be the parameter which will influence the printing plate's surface properties and increase the adhesion of the printing ink, special patterns (for example, Kodak's DigiCap) should be applied onto printing plate's surface in the plate production workflow.

### **3.2. Analysis of MacDermid LUX ITP 60 printing plate and test prints**

#### **3.2.1. Surface free energy components of MacDermid LUX ITP 60 printing plate**

$\gamma$  of all tested printing plate samples were displayed in Fig.14. and Table 1. However, a set of MacDermid LUX ITP 60 printing plate samples was received by MacDermid Printing Solutions to test the performance in the printing process when plate was exposed to the UV-ozone treatment, as well. Therefore, as LUX ITP 60 was not analysed by FTIR-ATR spectroscopy when exposed to the UV treatments prior to this research, FTIR-ATR analysis was performed in the framework of this report. The FTIR-ATR spectra of the flexographic printing plate explains the main reasons for the changes in  $\gamma$ . Therefore, before the results of FTIR-ATR analysis,  $\gamma$  and its components for LUX ITP 60 are graphically presented in Fig.16.

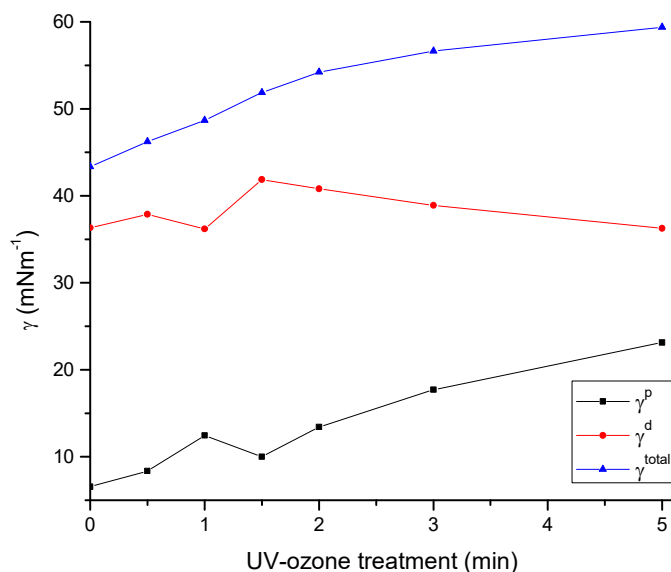


Fig.16. Surface free energy of UV-ozoned LUX ITP 60 printing plate samples

As previously discussed, the main reason for the increase of  $\gamma^{total}$  of the flexographic printing plate after the UV treatments is the increase of  $\gamma^p$ . This is visible in Fig.16., as  $\gamma^d$  does not change distinctively throughout the variation in UV-ozone treatment.  $\gamma^p$ , on the other hand, increases progressively from 6.55 mNm<sup>-1</sup> to 23.13 mNm<sup>-1</sup>.  $\gamma^{total}$  increases from 43.37 mNm<sup>-1</sup> for non-treated printing plate sample up to 59.40 mNm<sup>-1</sup> for the sample treated with the UV-ozone for 5 minutes.

### 3.2.2. FTIR-ATR analysis of MacDermid LUX ITP 60 printing plate

In Fig.17., the FTIR-ATR spectra of the UV-ozoned LUX ITP 60 printing plates are presented. The differences between samples are displayed in several absorption areas.

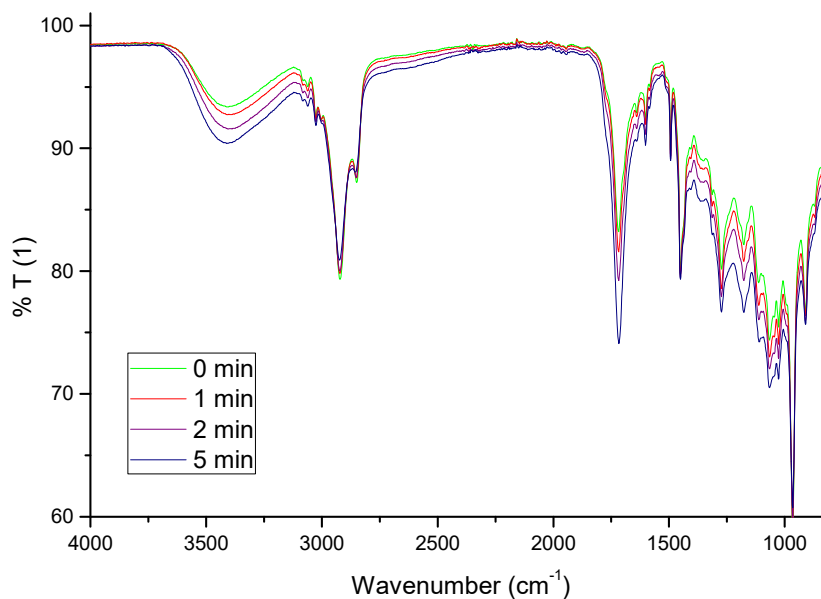


Fig.17. FTIR-ATR spectra of UV-ozoned LUX ITP 60 printing plate samples

It is important to mention that the changes in absorption frequencies below  $1500\text{ cm}^{-1}$  are not easily interpreted. The area in FTIR-ATR absorption frequencies between  $500\text{ cm}^{-1}$  and  $1500\text{ cm}^{-1}$  is called “fingerprint region”. This is the area where the complicated series of absorption may occur due to the different bending vibrations within the molecule. Furthermore, if the detailed composition of the material is not known, the certain interpretation of the fingerprint area becomes even more difficult. Solvent-washable flexographic printing plates are usually composed of styrene diene elastomers (more than 70% of the mass portion), polymerizable low-molecular-weight acrylates, plasticizers, photo-initiators, stabilizers and dyes. Styrene-butadiene-styrene, styrene-isoprene-styrene, or the mixture of both copolymer types can be used [27, 30].

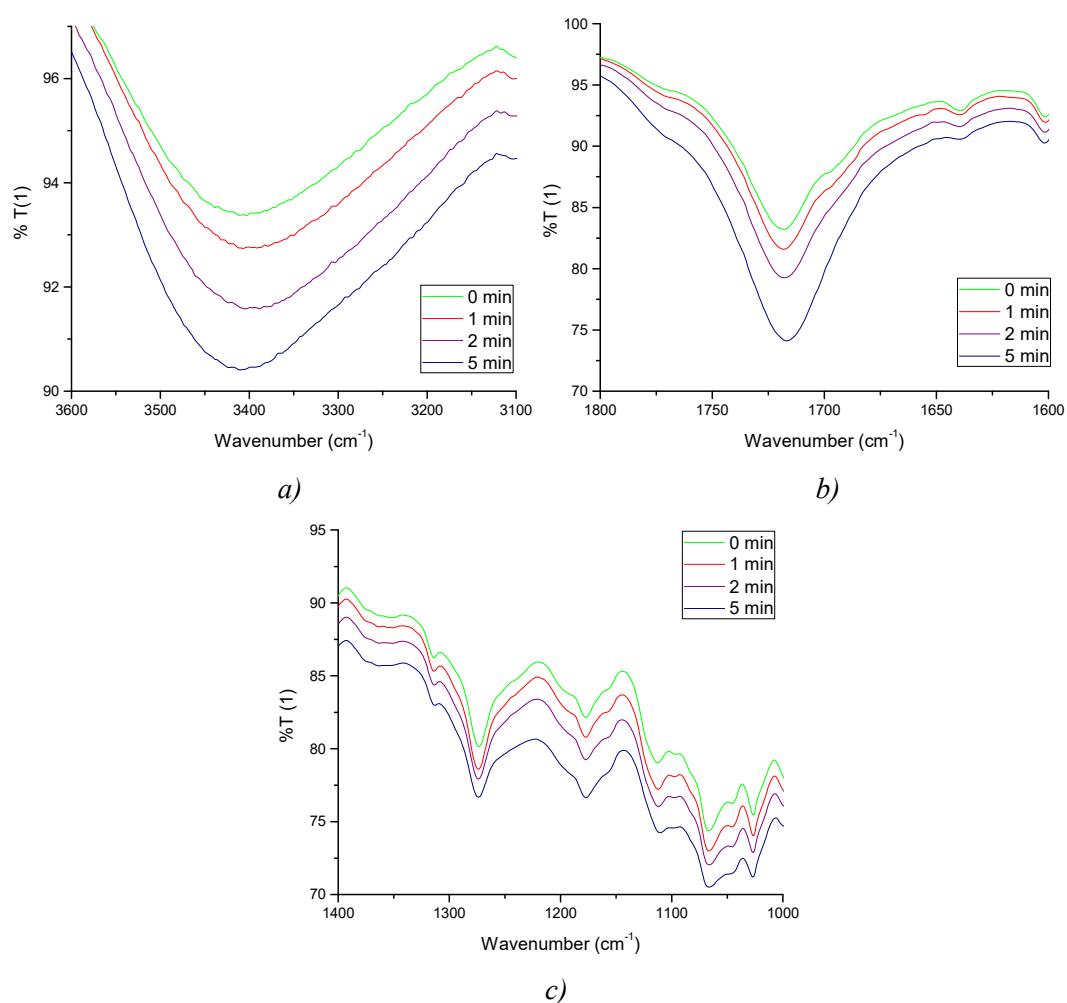


Fig.18. Changes in FTIR-ATR spectra of UV-ozoned samples in areas between:  
a)  $3200 - 3500\text{ cm}^{-1}$ , b)  $1700 - 1740\text{ cm}^{-1}$ , c)  $1000 - 1400\text{ cm}^{-1}$

Water-washable printing plates can have polyurethane-methacrylate compounds added to their structure, as well [31]. Knowing the basic composition, one can interpret the changes in FTIR-ATR spectra in the wavenumber area higher than  $1500\text{ cm}^{-1}$ .

The differences in FTIR-ATR spectra of the samples are expressed in three main areas:  $3200 - 3500\text{ cm}^{-1}$ ,  $1700 - 1740\text{ cm}^{-1}$  and between  $1000$  and  $1400\text{ cm}^{-1}$  in the fingerprint area. Decrease of the

transmittance in area between  $3200 - 3500 \text{ cm}^{-1}$  (Fig.18.a) presents the stretching vibrations of the hydroxyl (O-H) bond, and therefore the increased amount of hydroxyl bonds in the photopolymer material. The decreased transmittance of the samples is consistent with the increase of the duration of the UV-ozone treatment. This can be directly connected to the increase of  $\gamma^p$ , due to the changes of the photopolymer surface in form of increased amount of polar bonds. Similar interpretation is valid for the area between  $1700 \text{ cm}^{-1}$  and  $1740 \text{ cm}^{-1}$  (Fig.18.b). This area corresponds to the carbonyl (C=O) bond, and is responsible for the increase of  $\gamma^p$ , as well [32].

Finally, the changes in the transmittance are present in the fingerprint area, too. Their interpretation could not be confidently precise, but the changes in the area of  $1350 - 1450 \text{ cm}^{-1}$  could correspond to the in-plane O-H bending, as well as the vibration of different types of bonds between carbon and hydrogen. This would point to the changes in the molecular structure of the carbohydrate chains in the photopolymer material. Region from  $1000 - 1300 \text{ cm}^{-1}$  could correspond to the carbon-oxygen (C-O) bond [32].

### 3.2.3. Test prints

#### 3.2.3.1. White light interferometry and analysis of fine lines on test prints

Test prints of the motive (Fig.4) transferred to MacDermid LUX ITP 60 printing plate were produced by means of IGT F1 unit and the Cooper press. Several parameters were measured on test prints: width of the fine lines, ink film thickness, optical density of black UV-curable cationic flexo printing ink and coverage values of the halftones from 1% - 100%. All parameters were measured and monitored in dependence on the duration of UV-ozone treatment.

Width of the fine lines on the prints produced by Cooper press was measured by means of the software support of WYKO NT 2000 (Fig.19.). Results of the measurements are displayed in Fig.20.



Fig.19. Cross section and width of the printed fine line measured by white light interferometry



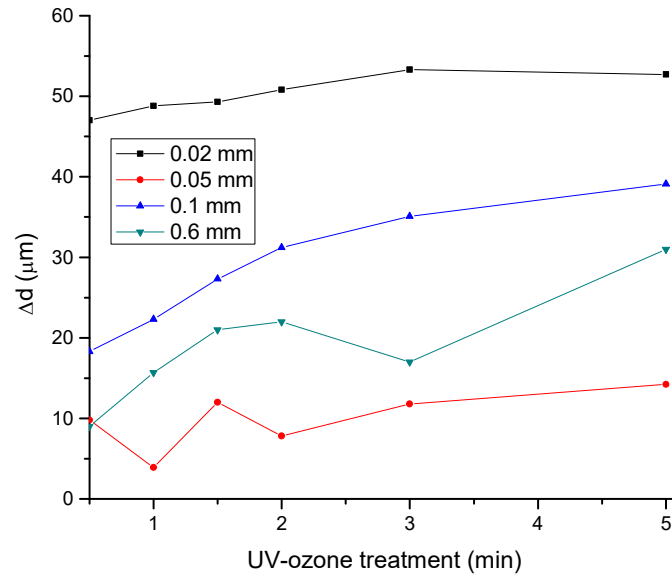
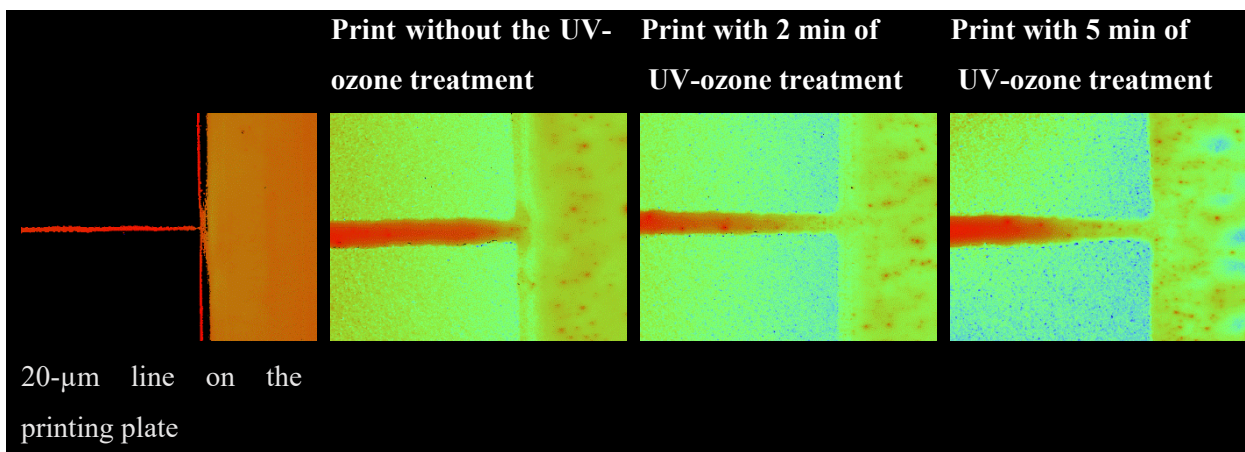


Fig.20. Width of the fine lines printed with UV-ozone treated plates

$\Delta d$  presents the difference between width of the line on prints produced without the UV-ozone treatment and the width of the line on the print produced with each duration of UV-ozone treatment (lines are labeled on the legend by their initial width on the print without the UV-ozone treatment). The measurement results have shown that the width of the lines reduces with increased duration of UV-ozone treatment. Previous research [14] showed that the UV treatment increases the hardness of the flexographic printing plate due to the further crosslinking and changes in the chemical bonds in the photopolymer material. Indeed, hardness of MacDermid LUX ITP 60 printing plate samples was measured by Shore A hardness tester, and the results showed the increase in hardness for approx. 4 Shore A between the non UV-ozoned sample and the sample UV-ozoned for 5 minutes. Therefore, printing elements on the plate become more stable and deformed less in the printing process. Furthermore, the difference between the prints made with non UV-ozoned and UV-ozoned fine lines is more expressed for the thinnest line (0.195 mm). This could be a helpful recommendation for solving the issues of dot gain on fine printing elements in flexography.

Table 2. Images of the motive used in printed electronics





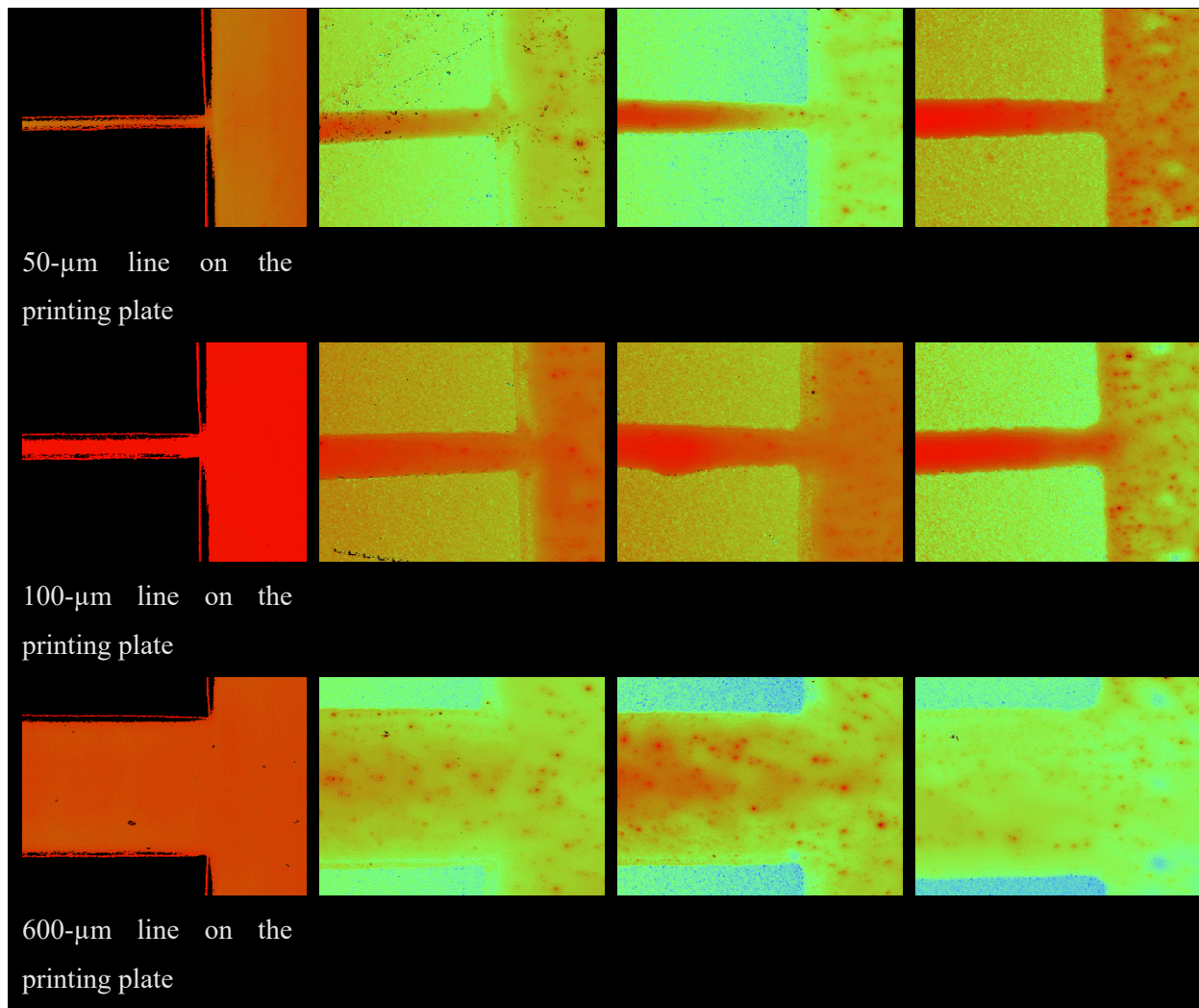
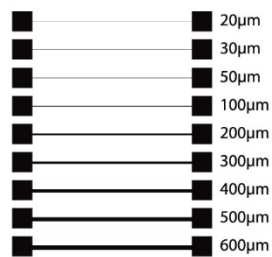


Table 2. presents the comparison of the magnified motive composed of fine line connected to the square field, usually used in printed electronics (Fig.21.), on the printing plate and prints. Images were obtained by WYKO NT 2000. Printing of this type of motive can be problematic because of the deformation of the printing plate. The results are usually either correctly printed line, but poor quality of the connection between the line and square area, or vice versa. This could result with problems in conductivity when printing conductors and other electronic components.



*Fig.21. Motive for testing print quality in printed electronics*

It is visible that the area of the connection of line and square improves both in the uniformity of the ink layer on the line, and the area of the connection between the elements with prolonged UV-ozone treatment. However, because of the general decrease of the ink film thickness (3.2.3.3.), UV-ozone treatment should be properly adjusted to obtain both improvement in the print quality and needed thickness of the ink layer important in printed electronics domain.

**3.2.3.2. Surface coverage of halftones on test prints**

The same trend of printing ink transfer in dependence on the UV-ozone treatment presented in 3.2.3.1. is visible in Fig.22. for the halftone reproduction. Images of the halftones were obtained by the WYKO NT 2000 and coverage values were calculated in the interferometer’s software support. Due to the changes of the mechanical properties of the photopolymer material caused by UV-ozone treatment, dot gain is less expressed with prolonged duration of the UV-ozone treatment. FlexoSync 56 compensation curve was applied to all samples of printing plates, but due to the features of laboratory printing process, dot gain is higher than expected. Nevertheless, UV-ozone treatment with the duration of 5 minutes decreased the coverage from 90% to 80%, on the field with 50% nominal coverage value. Therefore, depending on the printing ink and the type of printing substrate, one can experiment with UV treatments and use them as a tool for lowering the dot gain.

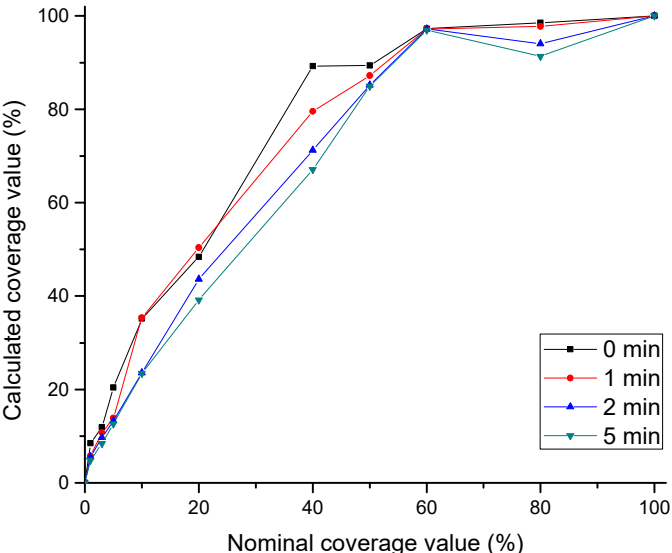


Fig.22. Coverage values of halftones on prints produced with UV-ozone treated plates

**3.2.3.3. Ink layer volume, thickness, and optical density on test prints**

In Fig.23. one can see the results of ink volume calculations on the halftone area, expressed in  $\mu\text{m}^3$  per area of  $1 \text{ mm}^2$ . Similar to the results of coverage value calculations, the volume of the ink on the

halftone prints decreases with the prolonged UV-ozone treatment. These results are in conformity with other results of analysis of the prints, presented in Fig.24 and Fig.25.

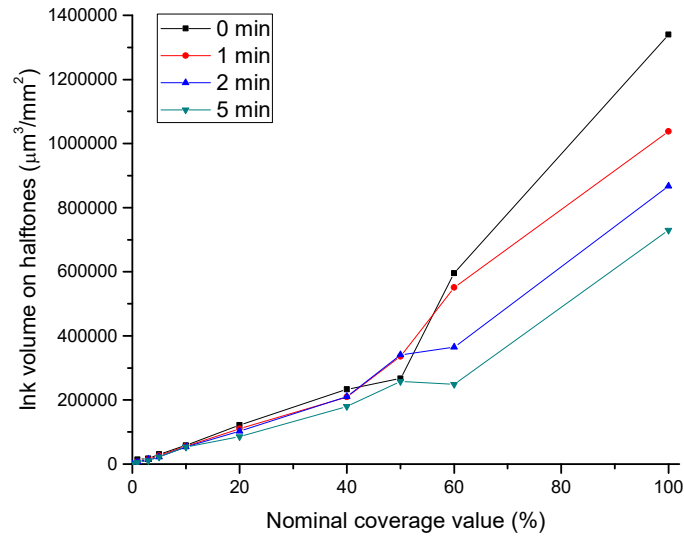


Fig.23. Ink volume on halftones on prints produced with UV-ozone treated plates

Pressure in the printing process adjusted to the hardness of the printing plate, the type of the printing ink and the printing substrate is an easily alterable parameter. However, ink film thickness on the print in specific printing system is essentially the effect of the anilox type used in the reproduction process. The results presented in Fig.24. (obtained by means of WYKO NT 2000) showed that the ink film thickness on the print can be changed by the UV-ozone treatment, as well.

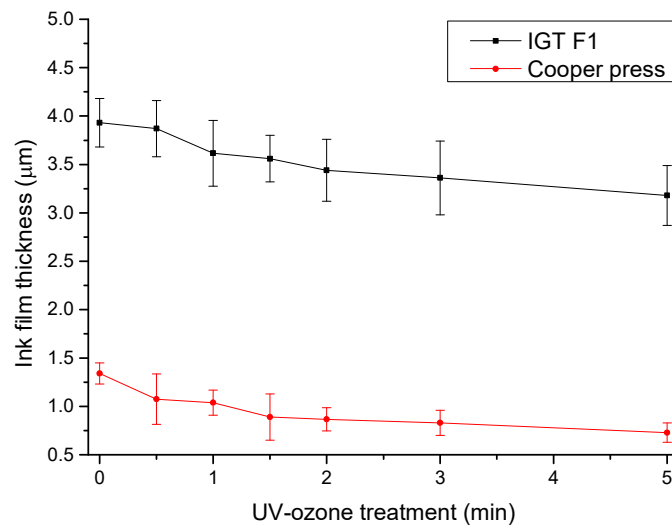


Fig.24. Ink film thickness on prints produced with UV-ozone treated plates

Although initial ink film thicknesses were different, the same trend of the decrease of the ink film thickness is visible on prints produced both by IGT F1 and Cooper press. Ink film thickness decreases from 3.93 µm to 3.18 µm on prints produced by IGT F1, and from 1.34 µm to 0.73 µm on prints produced by Cooper press. Hardness of the printing plate is not the only parameter that influences the thickness of the ink film on the print (and the dot gain). Changes in  $\gamma$  that occurred on the printing

plates due to the UV-ozone treatment result with the lower contact angle of the UV-curable cationic ink used in this research. This means that the thinner layer of the printing ink is present on the printing plate during the printing process (due to the improved wetting), and therefore even thinner layer transferred to the printing substrate.

In Fig.25. one can see the changes in optical density of 100% coverage values of the printing ink layer as a result of the UV-ozone treatment.

It is interesting to compare Fig.24. and Fig.25. Optical density of ink film on prints produced by IGT F1 is not affected by the decrease of the ink film thickness, even with decrease of the thickness to 3.18  $\mu\text{m}$ .

Prints produced by Cooper press have the initial ink thickness of 1.34  $\mu\text{m}$ . Further decrease of the ink film thickness as a result of the UV-ozone treatment affects the optical density of the prints. It decreases from 2.21 for non UV-ozoned sample to 1.5 after 5 minutes of UV-ozone treatment. Correlation coefficient between the ink film thickness and optical density in dependence on the UV-ozone treatment for Cooper press-printed samples is 0.9296. The correlation between the ink film thickness and optical density will be different for different colours and types of the printing inks. However, if modifying  $\gamma$  of the printing plate, one should check the optical density, especially if expecting to print a thin layer - in order to achieve the optimal quality of the print.

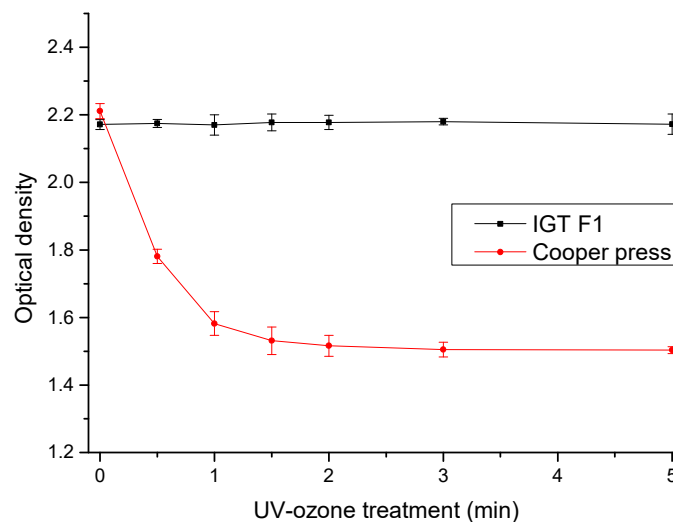
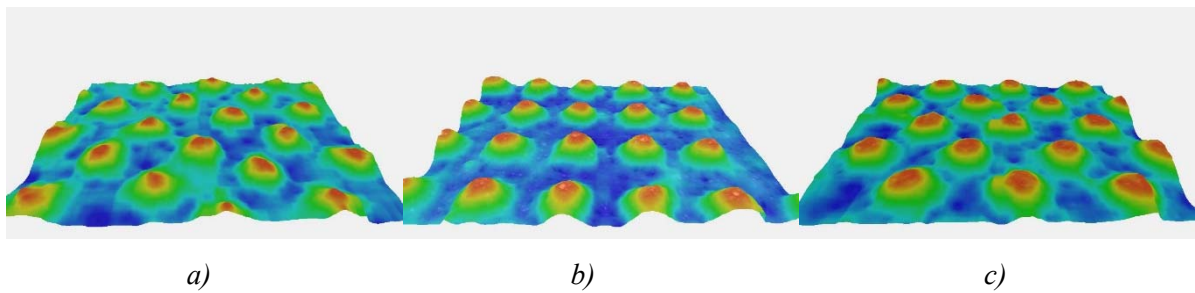


Fig.25. Optical density of the ink film on prints produced with UV-ozone treated plates

### 3.3. Formation of the printing elements in photopolymer material

Variety of photopolymer materials are used in the composition of different flexographic printing plates. Results presented in this section are emphasizing the effect of the formation of the printing elements in photopolymer material on the print quality (especially in highlight area) during the printing plate processing, before the UV post treatments.

Images presented in Fig.26. - Fig.31. were obtained by AniCAM 3D microscope. Fields of 5%, 50% and 95% surface coverage were scanned in order to compare the surface of the halftones on different printing plates.



*Fig.26. 3D scans of 5% coverage value on:*

*a) DuPont DPR sample, b) MacDermid LUX ITP 60 sample, c) Toyobo Cosmolight QS sample*

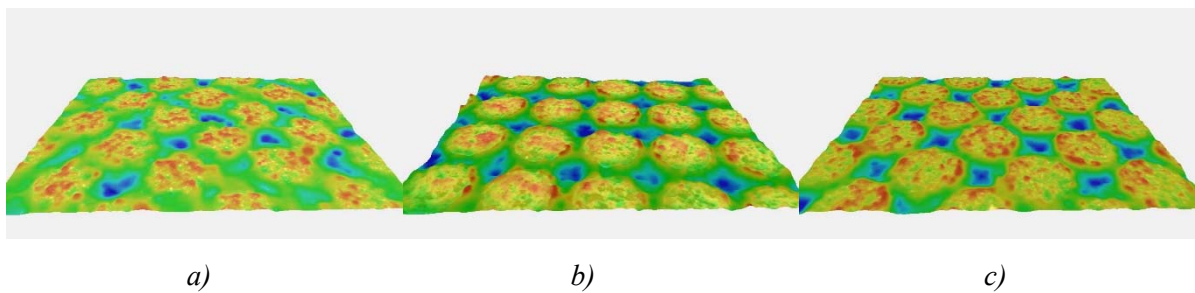


*Fig.27. 3D scans of 50% coverage value on:*

*a) DuPont DPR sample, b) MacDermid LUX ITP 60 sample, c) Toyobo Cosmolight QS sample*

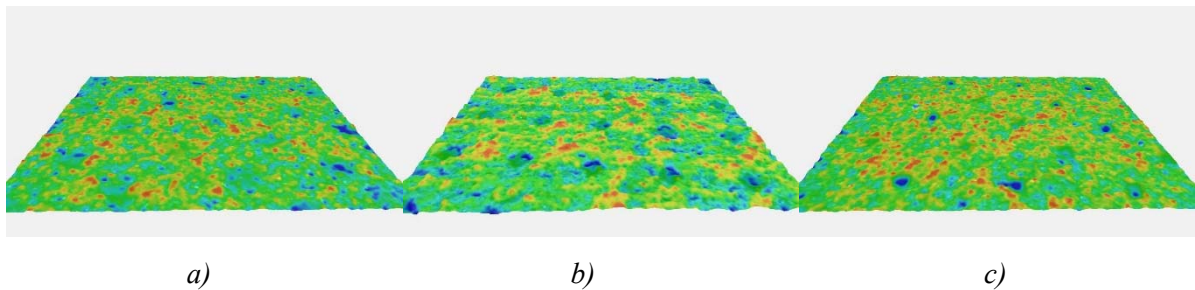


*Fig.28. 3D scans of 95% coverage value on:*

*a) DuPont DPR sample, b) MacDermid LUX ITP 60 sample, c) Toyobo Cosmolight QS sample*

Despite the same compensation curve applied to all printing plate samples, one can notice the differences in the shape and sizes of the printing element tops on the 5% surface coverage area. The shape of the printing element top is influenced by the oxygen inhibition in the main exposure process, and the size (area) of the printing element is then determined by the bump curve, adjusted to the each type of photopolymer specifically.

In Fig.27.a), the difference in topography of the printing elements in the area of 50% coverage is visible, as well. With the increase of the coverage value, visual differences on the surface become less apparent.



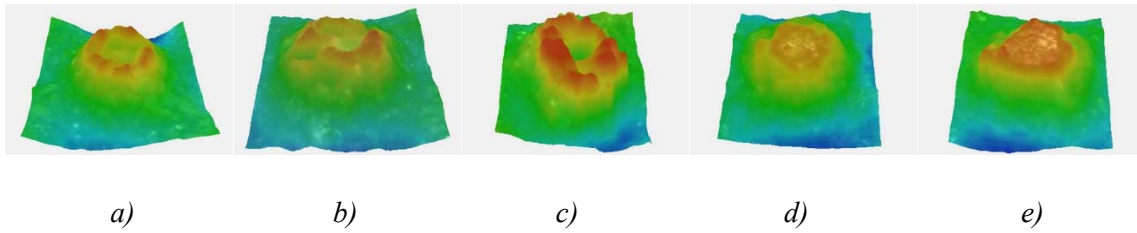


Fig.29 3D scans of C field on DFTA wedge of:

- a) DuPont DPR sample, b) FLINT ACE Digital, c) MacDermid LUX ITP 60 sample,  
d) MacDermid DMAX, e) Toyobo Cosmolight QS sample

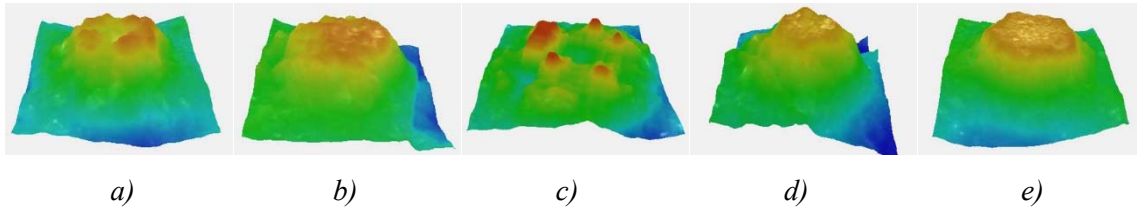


Fig.30. 3D scans of H field on DFTA wedge of:

- a) DuPont DPR sample, b) FLINT ACE Digital, c) MacDermid LUX ITP 60 sample,  
d) MacDermid DMAX, e) Toyobo Cosmolight QS sample

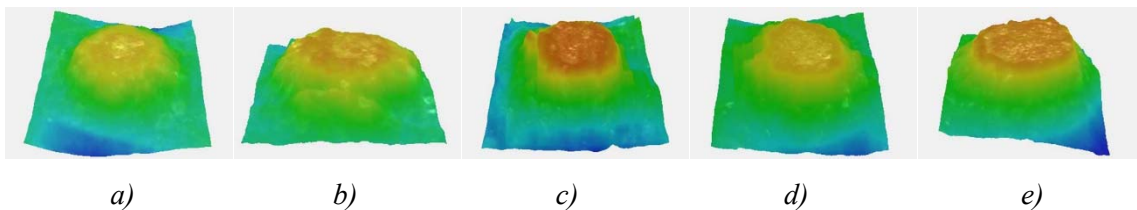


Fig.31. 3D scans of P field on DFTA wedge of:

- a) DuPont DPR sample, b) FLINT ACE Digital, c) MacDermid LUX ITP 60 sample,  
d) MacDermid DMAX, e) Toyobo Cosmolight QS sample

In order to observe the printing elements formed in the highlight area, selected elements of DFTA control strip used to analyse the shape of small elements were scanned with AniCAM 3D microscope. Fig.29. displays the field C on DFTA wedge, which was supposed to be the first field with stable and correctly formed printing elements after the application of correction curves. It corresponds to the area of 4 pixels ablated on mask layer of the plate by means of the laser.

However, it is visible that not all the elements formed with a correct shape. The similar situation is apparent in Fig.30., as well (Field H corresponds to the area of 14 pixels ablated on the mask layer on the printing plate). Several printing elements (Fig.29. a), b), c) and Fig.30. a), c) have formed with the higher edge than the inside area of the element top. This occurrence is often connected to the relaxation after the compression of the photopolymer material for printing plates produced by technology that includes the oxygen-protection layer attached to the plate before and during the

exposure (for example, Kodak NX technology with TIL film, MacDermid LUX technology). However, printing plate samples in Fig.29. – Fig.31. a) and b) were not produced using that type of technology. Furthermore, in Fig.30. one can see mostly flat-top, correctly formed elements (field P corresponds to 30 pixels ablated on the mask layer of the printing plate). Besides that, photopolymers usually contract during the crosslinking process. Therefore, the reason for the incorrectly formed elements on field C and H could be the diffraction of light passing through the ablated areas of small dimensions in combination with lower sensitivity of those photopolymer materials to the UV radiation [33].

It can be concluded that there are many sets of interdependent parameters influencing the printing plate's quality – from the start of the printing plate production to the applied post treatments. However, when given a specific printing plate, one can improve some of its properties and adjust them to the specific needs of the graphic reproduction system. At the same time, careful monitoring of the changes of other parameters connected to the printing plate that influence the quality of the final product should take place, as well.

#### **4. Conclusion and future steps**

The aim of this research was to modify the surface properties of photopolymer flexographic printing plates by means of the UV-ozone treatment in order to influence the properties of the print. At the same time, printing plate needed to retain its functional properties.

After the preliminary experiment, the duration of the UV-ozone treatment for tested printing plates was set to periods up to 5 minutes. The treatment proved to influence the following properties of printing plates and test prints:

1. Topography of the printing plate surface – after the exposure of the printing plates to the UV-ozone treatment, surface roughness increased on most types of the tested printing plates. The roughness varied throughout the changes in duration of the UV-ozone treatment, but generally remained increased compared to the roughness of non UV-ozone treated samples. The changes in roughness can be the result of chemical changes in photopolymer material such as further crosslinking of the molecules. Furthermore, visible mechanical damage can appear on the printing plate surface as a result of the long exposure to the UV-ozone treatment.
2.  $\gamma$  of the printing plate – all tested printing plates displayed a significant increase in  $\gamma$  after the UV-ozone treatment. The average difference in  $\gamma^{\text{total}}$  between non-exposed samples and samples exposed to the UV-ozone treatment for 5 minutes was  $15 \text{ mNm}^{-1}$ . Some samples showed higher resistivity to the treatment than the others. The main reason for these changes was the increase of  $\gamma^{\text{p}}$ . This increase was

the result of integration of the oxygen in the composition of the photopolymer material, which was proved by FTIR-ATR analysis.  $\gamma^d$  started to increase with shorter exposures to UV-ozone treatment, but on some samples it decreased after the longer exposure. This points to the start of the degradation of the photopolymer material as a result of the longer exposures to the UV-ozone treatment. Variations in roughness parameters did not display the distinct impact on the  $\gamma$ .

3. Properties of the test prints – the UV-ozone treatment of the printing plates resulted with the changes in width of the fine lines on test prints, surface coverage of the halftones, thickness of the ink layer on the test prints and optical density of the ink layer. Width of the fine lines decreased after the UV-ozone treatment, which was caused by the increased mechanical stability of the printing elements. This improvement, in combination with the decrease of the ink layer thickness as a consequence of the UV-ozone treatment, resulted with lower dot gain on the halftones. Due to the improved wetting on the printing plate, thinner layer of the printing ink is transferred to the printing substrate in the reproduction process. Optical density of the ink layer on the printing substrate decreased on the prints with thinner initial ink film, as well. Therefore, when adjusting the duration of UV-ozone treatment, one should compromise between the mechanical stability of the printing elements, dot gain and optical density.

As an addition, formation of the printing elements in the photopolymer material during the regular main exposure in the printing plate production workflow was analysed, as well. 3D displays of the printing elements have shown the differences in the shape of the printing element tops in highlight area. Even after the application of bump and compensation curves, some of the first stable printing elements were not formed correctly. This occurrence can be the result of the light source properties during the crosslinking process and the level of sensitivity of the photopolymer material to UV radiation. Therefore, a room for the further improvement in the area of the regular exposure processes in flexography exists.

Future steps in the research of the UV treatments and their effects on flexographic printing plates and prints include testing the influence of the surface modification on the behavior of the printing plate in higher run-length systems. Interconnected mechanical, thermal and chemical properties of post-treated printing plates and their effects on the print quality should be tested both in the reproduction process, and in laboratory. Some laboratory test should include the TGA, DSC, EDS and swelling analysis in order to obtain better understanding of the changes that occur in the photopolymer material due to the UV treatments and try to predict the behavior of the treated printing plate in the graphic reproduction process. Future research should include more types of flexographic printing plates in order to expand the knowledge about the properties of different photopolymer materials and influence of different plate production technologies in flexography. Specifically, different exposure systems in the plate production workflow (conventional LAMS technology, lamination technologies, high-energy pre-



exposure technologies) should be analysed, with emphasis on the troubleshooting of the element formation in the highlight area.

Since the quality of the print depends on the various parameters in the printing process, different types of printing substrates, inks and aniloxes should be tested in the assessment of the influence of UV treatments on the flexographic reproduction process. The possibilities for expanding the research on the influence of this type of flexographic printing plate treatment on the graphic reproduction process are wide. With each new technology of the printing plate production on the market, some qualitative properties of the flexographic prints increase, providing the new opportunities for the application of flexography in printing industry. This research targeted some possibilities for further improvement of high quality flexographic products in existing systems, with the aim of expanding the further potential for application of flexography in printing industry.

## **5. Acknowledgements**

*I would like to thank Welsh Centre for Printing and Coating for inviting me to spend three months at Swansea University as a visiting researcher, and British Scholarship Trust for funding my visit. Furthermore, I would like to offer my special gratitude to MacDermid Printing Solutions and Rotoplast d.o.o. for providing the samples used in this research. My special thanks are extended to the staff of WCPC – Prof. Tim Claypole, Ms Christine Hammet, Dr. David Beynon, Dr. Davide Deganello, Dr. Youmna Mouhamad, Ms Sakulrat Foulston and the other members of the research team for providing me all the help, support and advice; to Prof. Sanja Mahović Poljaček, my supervisor, for encouraging me to apply for this internship, advising me and helping me with my research and Prof. Mladen Lovreček, for the help with organization of my visit.*

## 6. References

- [1] Bodwell R., Scharfenberger J., *Advancing flexography: The technical path forward*, DuPont Packaging Graphics, 2011.
- [2] Matsubara, T., Oda, R., 2011. *Block copolymer composition for flexographic printing plates*, Pat. 20,110,308,412
- [3] Mahović Poljaček, S., Cigula, T., Tomašegović, T., Brajnović, O. *Meeting the Quality Requirements in the Flexographic Plate Making Process*, International Circular of Graphic Education and Research, No. 6, 2013.
- [4] [http://www.fppa.net/events/2012convention/2\\_round\\_flat\\_why\\_when.pdf](http://www.fppa.net/events/2012convention/2_round_flat_why_when.pdf)
- [5] <http://andersonvreeland.com/portfolio/digital-cosmolight-water-wash-plates>
- [6] [http://www.asahi-photoproducts.com/Datasheet/Plates/Eng/AWP\\_leaflet.pdf](http://www.asahi-photoproducts.com/Datasheet/Plates/Eng/AWP_leaflet.pdf)
- [7] <http://www.flintgrp.com/en/products/Printing-Plates/nyloflex/sprint.php>
- [8] Mahović Poljaček, S., Cigula, T., Tomašegović, T., *Meeting the quality requirements in flexographic plate making process*, IC2012, Budapest, Hungary, 2012.
- [9] Page Crouch, J., *Flexography Primer*, 2nd edition, PIA/GATF Press, Pittsburgh, 2005.
- [10] [http://graphics.kodak.com/KodakGCG/uploadedFiles/DigiCapNX\\_WhitePaper.pdf](http://graphics.kodak.com/KodakGCG/uploadedFiles/DigiCapNX_WhitePaper.pdf)
- [11] <http://www.preplate.com/PixelPlusNextFlatop.html>
- [12] Mahović Poljaček, S., Tomšegović, T., Cigula, T., Milčić, D. *Application of FTIR in structural analysis of flexographic printing plate*, IC 2014 Conference proceedings, Athens, Greece, 2014.
- [13] Tomašegović, T., Mahović Poljaček, S., Cigula, T. *Surface properties of flexographic printing plates related to UVC post-treatment*, Journal of Print and Media Technology Research, 4-2013, 227-234
- [14] Mahović Poljaček, S., Tomašegović, T., Gojo, M. *Influence of UV exposure on the surface and mechanical properties of flexographic printing plate*, GRID 2012 Proceedings / Novaković, Dragoljub (ur.), Novi Sad, 2012.
- [15] ISO standard 12647-6, *Graphic technology - Process control for the production of half-tone colour separations, proofs and production prints - Flexographic printing*, 2006.
- [16] <http://microfluidics.cnsi.ucsb.edu/tools/Novascan%20UV-Ozone%20cleaner%20user%20guide.pdf>
- [17] <http://erc.ncat.edu/Facilities/Manuals/Wyko.pdf>
- [18] [http://www.troika-systems.com/English/\\_downloads/AniCAM-3D\\_Scanning\\_Microscope\\_E.pdf](http://www.troika-systems.com/English/_downloads/AniCAM-3D_Scanning_Microscope_E.pdf)
- [19] DataPhysics Instruments GmbH, *Operating manual OCA*, 2006.
- [20] Owens, D. K., Wendt, R. C., *Estimation of the surface free energy of polymers*, Journal of Applied Polymer Science, Volume 13, Issue 8, 1969.
- [21] Application Note #5: *Surface free energy - Background, calculation and examples by using contact angle measurements*, Attension, Espoo, Finland

- [22] [http://www.utoronto.ca/~traceslab/ATR\\_FTIR.pdf](http://www.utoronto.ca/~traceslab/ATR_FTIR.pdf)
- [23] [http://www.xrite.com/documents/literature/gmb/en/100\\_spectrolino\\_brochure\\_en.pdf](http://www.xrite.com/documents/literature/gmb/en/100_spectrolino_brochure_en.pdf)
- [24] <https://books.google.co.uk/books?id=ZzmtGEHCC9MC&printsec=frontcover#v=onepage&q&f=false>
- [25] Chun-Wei Fan, Shih-Chin Lee, *Surface Free Energy Effects in Sputter-Deposited W<sub>N</sub>x Films*, Materials Transactions, Vol. 48, No. 9, 2007.
- [26] Lee, T.Y., Guymon, C.A., Sonny Jönsson, E., Hoyle, C.E., *The effect of monomer structure on oxygen inhibition of (meth)acrylates photopolymerization*, Polymer, Volume 45, Issue 18, Elsevier, 2004.
- [27] Knöll, R. *Photopolymerizable flexographic printing elements comprising SIS/SBS mixtures as binder for the production of flexographic printing plates*, Pat. US 6531263 B2, 2003.
- [28] Kronberg, B., Holmberg, K., Lindman, B. *Surface Chemistry of Surfactants and Polymers*, Wiley, 2014.
- [29] Andersson, C., Johnson, J., Järnström, L., *Ultraviolet-induced ageing of flexographic printing plates studied by thermal and structural analysis methods*, Journal of Applied Polymer Science, Volume 112, Issue 3, 2009.
- [30] Mayenez, C., Muijldermans, X. *Flexographic printing plates from photocurable elastomer compositions*, pat. EP 0696761 B1, 1998.
- [31] *Toyobo Safety data sheet no. 391F*
- [32] Coates, J., *Interpretation of infrared spectra, a practical approach*, Encyclopedia of analytical chemistry, R.A. Meyers (Ed.), John Wiley&Sons Ltd., Chichester, 2000.
- [33] <http://web.mit.edu/8.02t/www/802TEAL3D/visualizations/coursenotes/modules/guide14.pdf>

## CURRICULUM VITAE

---

<b>Name and surname:</b>	Tamara Tomašegović
<b>Date and place of birth:</b>	30. April 1987., Zagreb
<b>Citizenship:</b>	Croatian
<b>Education:</b>	2005. Graduated from XV Gymnasium, Zagreb  2008. BSc in Graphic technology, University of Zagreb Faculty of Graphic Arts  2010. M. Eng. in Graphic technology, University of Zagreb Faculty of Graphic Arts
<b>Work experience:</b>	2010. – research fellow/assistant at University of Zagreb Faculty of Graphic Arts
<b>Area of scientific interest:</b>	<ul style="list-style-type: none"><li>▪ reproduction processes in graphic technology</li><li>▪ standardization and measurement of printing plates</li><li>▪ materials in printing plate production</li><li>▪ surfaces and interfaces</li></ul>
<b>Foreign languages:</b>	English, German
<b>Scholarships, awards:</b>	<ul style="list-style-type: none"><li>▪ British Scholarship Trust grant for mobility to Swansea, United Kingdom for period of 3 months (2015.)</li><li>▪ award for the best author of the XI Symposium on Graphic Arts, Pardubice (2013.)</li><li>▪ fellowship from City of Zagreb for especially talented students during the second year of graduate study</li><li>▪ fellowship from University of Zagreb, for 100 best students, during the first year of graduate study</li><li>▪ Rector's award for paper <i>Effect of the developing solution on the wetting of offset printing plate's nonprinting areas</i> (2009.)</li><li>▪ 1<sup>st</sup> place won in category „Printing“ at PDP Convention, 14. - 16. May 2009., Novi Sad</li><li>▪ fellowship from Ministry of Science, Education and Sport for especially talented students throughout the whole period of undergraduate study</li></ul>

---

## LIST OF PUBLISHED SCIENTIFIC RESEARCH

### Master thesis

EIS as a method for the analysis of nonprinting surface on the offset printing plates, University of Zagreb Faculty of Graphic Arts, 2010.

### Journal articles in CC journals

**Tomašegović, Tamara;** Beynon, David; Claypole, Tim; Mahović Poljaček, Sanja. *Tailoring the properties of deposited thin coating and print features in flexography by application of UV-ozone treatment*. Journal of coatings technology and research, (2016) (accepted for publication).

**Tomašegović, Tamara;** Mahović Poljaček, Sanja; Leskovac, Mirela. *UVA and UVC modification of photo polymeric surface and application for flexographic deposition of thin coatings*. Journal of applied polymer science, 133 (2016) 24, 5764-5775.

### Scientific papers in other journals

Hoffmann-Walbeck, Thomas; Riegel, Sebastian; Tuchel, Benedikt; Mahović Poljaček, Sanja; Cigula, Tomislav; **Tomašegović, Tamara**. *Quality Assurance of Process Free Thermal Plates*. Acta graphica 26 (2015), 3, 31-37.

Mahović Poljaček, Sanja; **Tomašegović, Tamara;** Cigula, Tomislav; Gojo, Miroslav; Milčić, Diana. *Formation of the Printing Elements in the Photopolymer Material Used in Flexography*. Key Engineering Materials 611-612 (2014), 883-891.

**Tomašegović, Tamara;** Mahović Poljaček, Sanja; Cigula, Tomislav. *Impact of Screen Ruling on the Formation of the Printing Elements on the Flexographic Printing Plate*. Acta graphica 24 (2013); 1-12.

**Tomašegović, Tamara;** Mahović Poljaček, Sanja; Cigula, Tomislav. *Surface properties of flexographic printing plates related to UVC post-treatment*. Journal of Print and Media Technology Research 2 (2013), 4, 227-233.

**Tomašegović, Tamara;** Žitinski Elias, Paula Yadranka; Baračić, Marina; Mrvac, Nikola. *E-learning and Evaluation in Modern Educational System*. US-China Education Review 8 (2011), No. 2, 198-203.

## Professional papers in other journals

Mahović Poljaček, Sanja; Cigula, Tomislav; Hoffmann-Walbeck, Thomas; **Tomašegović, Tamara**; Riegel, Sebastian. *Processless offset printing plates*. Journal of graphic engineering and design 6 (2015), 1; 23-27.

## Scientific conference papers with international peer-review

Cigula, Tomislav; Mahović Poljaček, Sanja; Hoffmann-Walbeck, Thomas; Veljačić, Domagoj; **Tomašegović, Tamara**. *Consistency of the development process of the processless offset printing plates*. International Conference MATRIB 2015 Materials, Wear, Recycling Proceedings, Ćorić D., Žmak I., Editors. Vela Luka (2015), 99-104.

Cigula, Tomislav; Mahović Poljaček, Sanja; **Tomašegović, Tamara**; Milčić, Diana. *The influence of the printing plate's temperature on its wetting properties*. 5<sup>th</sup> International joint conference on environmental and light industry technologies proceedings, Borbely A., Editor. Budapest (2015), 202-206.

Donevski, Davor; Milčić, Diana; Banić, Dubravko; Poljaček Mahović Sanja; **Tomašegović, Tamara**. *Approaches to linearization in ICC profiles*. 46<sup>th</sup> Annual International Conference on Graphic Arts and Media Technology, Management and Education conference proceedings, Politis A. E., Gatsou C., Editors. Athens (2014), 179-183.

**Tomašegović, Tamara**; Mahović Poljaček, Sanja; Cigula, Tomislav; Gojo, Miroslav; Milčić, Diana. *Correlation between the lams and printing element area on the flexographic printing plate*. Proceeding, 7<sup>th</sup> Symposium of Information and Graphic Arts technology, Blaznik B., Editor. Ljubljana (2014), 43-49.

**Tomašegović, Tamara**; Mahović Poljaček, Sanja; Milčić, Diana. *Qualitative Analysis of Coverage Value Transfer in Modern Packaging Printing Workflow*. Responsible Packaging for a Global Market - Proceedings of the 19<sup>th</sup> IAPRI World Conference on Packaging, Sek M.A., Rouillard V., Bigger S.W., Editors. Melbourne (2014), 651-666.

Cigula, Tomislav; Mahović Poljaček, Sanja; **Tomašegović, Tamara**; Gojo, Miroslav. *The offset printing plate characteristics related to developing process*. Conference Proceedings MATRIB 2013, Alar, Ž., Jakovljević, S., Editors. Zagreb (2013), 84-89.

Cigula, Tomislav; **Tomašegović, Tamara**; Mahović Poljaček, Sanja; Gojo, Miroslav. *Transfer of the coverage values on the processless printing plate depending on the screen ruling*. 4<sup>th</sup> International Joint Conference on Environmental and Light Industry Technologies, Borbely Á., Editor. Budapest (2013), 374-377.

Cigula, Tomislav; Poljak, Jelena; Peko, Vedrana; **Tomašegović, Tamara**. *Sodium metasilicate solutions as a developer for CtCP offset printing plates*. GRID 2012 Proceedings, Novaković, D., Editor. Novi Sad (2012), 115-120.

Mahović Poljaček, Sanja; **Tomašegović, Tamara**; Gojo Miroslav. *Influence of UV exposure on the surface and mechanical properties of flexographic printing plate*. GRID 2012 Proceedings, Novaković D., Editors. Novi Sad (2012), 135-140.

Cigula, Tomislav; Mahović Poljaček, Sanja; **Tomašegović, Tamara**. *Characterization of the silver halide printing plate's surface properties*. Proceedings of the 43<sup>rd</sup> conference of the International Circle of Educational Institutes for Graphic Arts Technology and Management. Norrköping (2011), 111-118.

**Tomašegović, Tamara**; Cigula, Tomislav; Mahović Poljaček Sanja; Gojo, Miroslav. *Comparison of different measuring systems for printing plate's coverage values evaluation*. Printing future days proceedings 2011, Baumann R. R., Editor. Chemnitz (2011), 39-44.

**Tomašegović, Tamara**; Cigula, Tomislav; Mahović Poljaček, Sanja; Gojo, Miroslav. *Effect of exposures on the mechanical properties of the liquid photopolymer flexographic printing plate*. Conference Proceedings MATRIB 2011, Schauerl Z., Šolić S., Editors. Vela Luka (2011), 495-501.

**Tomašegović, Tamara**; Cigula, Tomislav; Mahović Poljaček, Sanja; Gojo, Miroslav. *Wetting of CtP offset plate as a function of developing process*. Proceedings, 22<sup>nd</sup> International DAAAM Symposium: Intelligent Manufacturing & Automation: Power of Knowledge and Creativity, Katalinić B., Editors. Vienna (2011), 0019-0020

Žitinski Elias, Paula Yadranka; Baračić, Marina; **Tomašegović, Tamara**; Mrvac, Nikola. *E-learning and evaluation in modern educational system*. Proceedings of INTED 2010 Conference, Valencia (2010), 1152-1157.

**Tomašegović, Tamara**; Žitinski Elias, Paula Yadranka; Baračić Marina; Cigula, Tomislav. *Influence of the printing media on the properties of fountain solution*. Proceedings of the 13<sup>th</sup> International conference of printing, design and graphic, Bolanča Z., Editors. Senj (2009), 245-248.

Žitinski Elias, Paula Yadranka; **Tomašegović, Tamara**; Modrić, Damir. *Modelling of dispersion and reflection of light on paper surface*. Annals of DAAAM for 2008 & Proceedings of the 19<sup>th</sup> International DAAAM Symposium Vol 19, No1, Katalinić B., Editor. Trnava (2008), 1557-1558.

### **Other refereed conference papers**

Cigula, Tomislav; Mahović Poljaček, Sanja; **Tomašegović, Tamara**; Gojo, Miroslav. *Dynamic contact angle as a method in graphic materials characterization*. Proceedings, 7<sup>th</sup> International Symposium on Graphic Engineering and Design GRID 2014, Novaković, Dragoljub, Editor. Novi Sad (2014), 87-91.

Hudika, Tomislav; **Tomašegović, Tamara**; Mahović Poljaček, Sanja. Offset printing plates: alternative method for quality control. GRID 2012 Proceedings, Novaković D., Editors. Novi Sad (2012), 129-133.

**Tomašegović, Tamara**; Mahović Poljaček, Sanja; Cigula, Tomislav; Gojo, Miroslav. *Adjustment of flexographic printing plate to meet qualitative requirements*. Conference Proceedings MATRIB 2012, Alar Ž., Jakovljević S., Editors. Vela Luka (2012), 331-336.

#### **Non-refereed conference paper**

Mahović Poljaček, Sanja; **Tomašegović, Tamara**; Cigula, Tomislav; Milčić, Diana. *Application of FTIR in structural analysis of flexographic printing plate*. 46<sup>th</sup> Annual International Conference on Graphic Arts and Media Technology, Management and Education conference proceedings, Politis A. E., Gatsou C., Editors. Athens (2014), 133-141.

#### **Abstracts in Book of abstracts**

**Tomašegović, Tamara**; Mahović Poljaček, Sanja; Cigula, Tomislav. *Modification of flexographic printing plate's surface properties by variation of UVC finishing*. Conference proceedings XI Symposium on Graphic Arts. Pardubice (2013), 59-59.